The molecular basis for oocyst wall formation in *Eimeria maxima*

by

Kelly Mai
B. Sc. (Biological and Biomedical Sciences)

A thesis submitted for the degree of Doctor of Philosophy

Institute for the Biotechnology of Infectious Diseases
University of Technology, Sydney
Australia

2008

CERTIFICATE OF AUTHORSHIP

I certify that this thesis has not previously submitted for any degree and is not being submitted as part of candidature for any other degree. I also certify that the thesis has been written by me and that any help that I have received in preparing this thesis, and all sources used, have been acknowledged in the thesis.

Production Note:
Signature removed prior to publication.

Kelly Mai

ACHNOWLEDGEMENTS

I would like to firstly acknowledge Dr Martin Shirley from Institute for Animal Health that provided *E. tenella* oocysts; and Per Thebo from National Veterinary Institute, Uppsala, Sweden to supply sporulated *E. maxima* oocysts for this project.

I would like to express my appreciation to our collaborators, David DeSouza and Professor Malcolm McConville, at the University of Melbourne for their excellent expertise in compositional analyses of oocyst walls by gas chromatography and mass spectrometry. To Dr Xuecheng Zhang, Dr Zhi-Ping Feng and Professor Ray Norton, (from Walter and Eliza Hall Institute of Medical Research), a special thanks for their assistance in structural analysis by 1D-NMR and for the constructive advice in the field of the research. I would also like to sincerely thank Professor David Ferguson at the University of Oxford for his enthusiasm and for the time he devoted to produce beautiful EM images of oocyst walls. To Dr Catherine Luxford and Dr Michael Davies at Heart Research Institute, thank you so much for the help with dityrosine measurement by HPLC.

Special thanks to Andrew Mynott and Dr Paul Curmi at the University of New South Wales for enabling me to use their CD spectrometer and for their time and guidance to teach me how to operate the spectrometer.

Thank you to all staff and students from IBID such as Michael Johnson, Matt Padula, Scott Minns, Christopher Weir, Kate Miller, Cameron Jennings and Joyce Tao for their help in the lab in general. I would also like to recognize the contribution of Jan Slapeta, Iveta Slapeta and Robert Walker in particular their assistance with animal work (oocyst harvest from caeca and faeces) especially Jan for his effort and constructive advice to this project. I would also like to thank Dr Ying Lei for her speedy revision of my thesis and Dr Marilyn Katrib for her advice in thesis preparation.

I would like to sincerely thank my supervisors Associate Professor Nick Smith, Dr Sabina Belli and Professor Michael Wallach for their supervision, advice, encouragement and

support throughout the course of my PhD especially Nick for his expert guidance, and valuable advice in preparing my thesis. This work would not have been possible without his support.

I would like to express my gratitude to RIRDC (Rural Industries Research & Development Corporation) for funding this project in which I received PhD scholarship award and also for giving me a great opportunity to attend the workshop (host by Poultry CRC) in Brisbane 2004.

Finally, special thanks to my parents, Tony and Erica, and sister, Joyce, and brothers, Miller and David, for their love, support both financially and mentally, and encouragement throughout the highs and lows of my PhD.

PAPERS PRESENTED AT SCIENTIFIC CONFERENCES

Mai, K., Belli, SI., Ferguson, D.J.P., Luxford, C., Davies, M.J., Slapeta, J., and Smith, N.C. (2006) Tyrosine oxidation in the development of eimerian oocysts. 2006 ASP & ARC/NHMRC Research Network for Parasitology Annual Conference Legends Hotel, Surfers Paradise, Gold Coast, Queensland, Australia, July.

Mai, K., Belli, S., Wallach, M.G. and Smith, N.C. (2004) Dityrosine mediated protein crosslinks in a 56 kDa gametocyte protein from *Eimeria maxima*. Australian Society for Parasitology Annual Meeting Esplanade Hotel, Fremantle, Perth, Australia, September 2004.

Belli, S.I., **Mai, K.**, Ferguson, D.J.P., Luxford, C., Davies, M.J., Wallach, M.G. and Smith, N.C. (2004) Molecular Architecture of the Oocyst Wall of the Apicomplexan Parasite *Eimeria maxima*, Lorne Conference of Protein Structure and Function, Lorne, Australia.

TABLE OF CONTENTS

LIST OF ABBREVIATIONS

aa	amino acids
AGRF	Australian Genome Research Facility
APGA	affinity purified gametocyte antigens
APx	*Arthromyces* peroxidase
3'AT	3'-amino-1, 2, 4-triazole
BCIP/NBT	5-bromo-4-chloro-3-indolyl phosphate/nitro blue tetrazolium
BSTFA	*N, O-bis*(trimethylsilyl)trifluoroacetamide
bp	base pairs
BSA	bovine serum albumin
CD	circular dichroism
COWP	*Crptosporidium* oocyst wall protein
DAPI	4, 6-diamidino-2-phenylindole
DEAE	diethylaminoethyl
DNA	deoxyribonucleic acid
DOPA	3, 4-dihydroxyphenylalanine
ECL	Enhanced chemiluminescence
EDTA	ethylenediaminetetraacetic acid
EIA	enzyme immunoassay
ELISA	enzyme-linked immunosorbent assay
EmGam56	56 kDa gametocyte antigen from *E. maxima*
EmGam82	82 kDa gametocyte antigen from *E. maxima*
ExPASy	Expert Protein Analysis System
g	centrifugal force (gravity)
GC	gas chromatography
GLC	gas-liquid chromatography
hr	hour(s)
HPLC	high-pressured liquid chromatography
HRPO	horseradish peroxidase
I (or IL)	inner layer of oocyst walls

IPTG	isopropyl-b-thiogalactopyranoside
IUPs	intrinsically unstructured proteins
kDa	kilodalton
LB Amp medium	Luri-Bertani medium containing 100 μg/ml ampicillin
LB Amp plate	Luri-Bertani plate containing 100 μg/ml ampicillin
LB medium	Luria-Bertani medium
lpm	litre per minute
M	molar
mA	milliampere(s)
min	minute(s)
ml	milliliter
μl	microlitre
μm	micrometre
mM	millimoles per litre
MPx	myeloperoxidase
MS	mass spectrometry
NCS	normal chicken serum
1D-NMR	one-dimensional nuclear magnetic resonance
O (or OW)	oocyst walls
OD	optical density
O (or OL)	outer layer of oocyst walls
O/N	over night
PAGE	polyacrylamine gel electrophoresis
PBS	phosphate buffered saline
PCR	polymerase chain reaction
PDB	protein data bank
PEG	poly(ethylene glycerol)
pETEmGam56.102-225	gene encoding for a truncated form of EmGam56
pETEmGam56.102-225	a truncated form of EmGam56
PG	polysaccharide granules
PH	phenylhydrazine hydrochloride

ppm	parts per million
PVDF	polyvinylidene fluoride
RIA	radioimmunoassay
rpm	revolutions per minute
RNN	recursive neural network
RT	retention time
r56	gene encoding for a recombinant form of EmGam56
r56	a recombinant form of EmGam56
S	sporocyst walls
SDS	sodium dodecyl sulfate
SDS-PAGE	sodium dodecyl sulfate polacrylamide gel electrophoresis
SHA	salicylhydroxamic acid
SpW	sporocyst walls
S/O	sporulated oocysts
TBE	tris borate/EDTA
TBS	tri-buffered saline
t-BHP	*tertiary*-butylhydroperoxide
TCA	trichloroacetic acid
TE	tris/EDTA
TEM	Transmission Electron Microscopy
TMCS	trimethylchlorosilane
TMS	trimethylsilyl
Tris	tris[hydroxymethyl]aminomethane
U/O	unsporulated oocysts
UV	ultraviolet
W or WFB	wall forming bodies
W1 or WFB1	wall forming bodies type 1
W2 or WFB2	wall forming bodies type 2

LIST OF FIGURES

LIST OF TABLES

ABSTRACT

Eimeria is a genus of protozoa within the Apicomplexa, a phylum that includes *Plasmodium* species (which cause malaria) and *Toxoplasma gondii* (which cause foetal abnormalities and encephalitis), and many other species of parasites. *Eimeria* belongs to the subclass Coccidia, and a defining characteristic of this group is their transmission from host to host via oocysts that contaminate food and water. The resilient oocyst wall protects the parasites as they are excreted in the host's faeces and in the outside world, allowing them to survive for several months between hosts. It is formed from the contents of specialised organelles – wall forming bodies – found in the macrogametocyte stage of the parasites.

Two proteins, EmGam56 and EmGam82, from the wall forming bodies of *Eimeria maxima* have been studied intensively in recent years (see Belli *et al.,* 2006). Both are processed and/or degraded into smaller tyrosine-rich polypeptides (from 8 to 33 kDa) and incorporated into the oocyst wall. The tyrosine richness of these proteins and the presence of dityrosine in the oocyst wall has led to the proposal that dityrosine cross-linking of these proteins forms a matrix that is crucial component for oocyst wall formation (Belli *et al.,* 2006). The aims of this thesis are to:

[1] deduce the biochemical composition of the oocyst walls using gas chromatography (GC) and mass spectrometry (MS);

[2] determine the structural features of EmGam56 using bioinformatics, circular dichroism (CD), and one-dimensional nuclear magnetic resonance (1D-NMR);

[3] demonstrate that peroxidase-catalysed dityrosine crosslinks can be induced to form between truncated forms of EmGam56.

GC and MS revealed that the *Eimeria* oocyst wall is composed mainly of proteins (>90%) with small amount of lipids (1.4-7.6%) and carbohydrates (0.3-2.0%). There is little difference between the unsporulated and sporulated oocyst walls of *E. tenella* and *E. maxima*. Thus, the structure of proteins like EmGam56 is key to understanding how oocyst walls are constructed.

Bioinformatic analyses indicated that EmGam56 is an intrinsically unstructured protein (IUP), dominated by random coils (52-70%), with some α-helices (28-43%) but few β-sheets (1-11%); this was confirmed by CD and 1D-NMR. Furthermore, the structural integrity of the protein under extreme temperatures (boiling for 40 minutes) and pH (pH 1.3-11) indicated its IUP nature. The intrinsic lack of structure in EmGam56 could facilitate its incorporation into the oocyst wall in two ways: first, IUPs are highly susceptible to proteolysis, explaining the several differently-sized oocyst wall proteins derived from EmGam56; and, second, the flexibility of IUPs could facilitate cross-linking between these tyrosine-rich derivatives.

Peroxidases are key to the formation of dityrosine bonds (see Belli *et al.,* 2006 for a review). An *in vitro* cross-linking assay was developed using a recombinant 42 kDa truncation of EmGam56. The protein was exposed to various peroxidases and peroxides, the formation of polymers was followed by Western blotting, and the formation of dityrosines was determined by HPLC. Peroxidases from plants or fungi, but not mammals, catalysed rapid formation of polymers. No peroxidase has yet been found in the incompletely annotated *E. tenella* genome database but peroxidase activity has been detected in the wall forming bodies (Belli *et al.,* 2006). Therefore, future searches for *Eimeria* peroxidases should focus on plant-like homologous.

The results presented in this thesis support the proposal that dityrosine bonding between proteins is an important factor in the formation of the oocyst wall of coccidian parasites and are consistent with the hypothesis that antibodies stimulated by vaccination with EmGam56 and related proteins could prevent formation of oocysts.

Chapter One
Introduction

1.1 *Eimeria*

Eimeria is a genus of parasitic protozoa that belongs to the subclass, Coccidia, within the phylum Apicomplexa. The phylum Apicomplexa comprises many parasites of medical and veterinary importance including the causative agents of malaria, *Plasmodium,* the zoonotic organisms, *Cryptosporidium* and *Toxoplasma,* and many *Eimeria* species, which are responsible for the intestinal disease, coccidiosis, in poultry (Obata, 2000).

The number of *Eimeria* species that exist in any given host is controversial. For example, Levine and Ivens (1965) catalogued 204 species of *Eimeria* in rodents but they estimated a total of 45,000 species would be found in this genus. The more important and widely accepted species of *Eimeria* with their particular hosts are shown in Table 1.1 (Cox, 1993). Different species of *Eimeria* infect different hosts. They are often restricted to a certain host species and parasitize specific organ systems or particular types of cells and even in a specific location within the cells (Obata, 2000). Most of them inhabit the intestinal tracts of vertebrates but a few are found in the liver and kidneys. Some of them are major pathogens of domesticated animals.

There are seven *Eimeria* species that cause disease in chickens: *Eimeria necatrix, Eimeria tenella, Eimeria maxima, Eimeria brunetti, Eimeria mitis, Eimeria acervulina and Eimeria praecox* (Shirley, 1986). The characteristics of each *Eimeria* species differ with respect to pathogenicity, site of infection, prevalence and immunogenicity (Rose and Long, 1980). The pathogenicity of *Eimeria* species varies from slightly to highly pathogenic. *E. mitis* and *E. praecox,* for example, cause mild infections resulting in reduced growth rate and feed utilisation but without causing mortality in chickens (Williams, 1998) whereas *E. necatrix* and *E. tenella* lead to severe infections with symptoms that include a bloody diarrhoea,

sloughing of epithelium, blood loss, shock syndrome and even death (Vermeulen *et al.*, 2001). *Eimeria tenella* is the most pathogenic among these seven species. It parasitizes epithelial cells of the caeca and destroys tissues, resulting in high mortality rate in young birds (Obata, 2000).

Table 1.1 Important *Eimeria* species with their respective hosts (Cox, 1993)

Host	*Species*	*Host*	*Species*
Chickens	*E. acervulina*	Sheep	*E. crandallis*
	E. brunetti		*E. ovina*
	E. maxima		*E. ovinoidalis*
	E. mitis		*E. arloingi*
	E. necatrix		*E. ninakohlyakimovae*
	E. praecox		
	E. tenella	Pigs	*E. debliecki*
Turkeys	*E. meleagrimitis*	Horses	*E. leukarti*
	E. adenoeides		
		Rabbits	*E. flavescens*
Geese	*E. anseris*		*E. intestinalis*
	E. nocens		*E. stiedai*
	E. truncata		
		Rats	*E. nieschulzi*
Ducks	*E. danailova*		
		Mice	*E. falciformis*
Cattle	*E. bovis*		*E. vermiformis*
	E. zuernii		

All seven *Eimeria* species are ubiquitous. At least six species (*E. acervulina, E. maxima, E. mitis, E. praecox, E. tenella* and *E. brunetti*) may occur concurrently on a farm (Williams *et al*, 1996), with their oocysts appearing in the litter samples during the first 6 weeks of the life of a flock. *Eimeria maxima* and *E. acervulina* are the most prevalent species (Razmi and Kalideri, 2000). They infect the duodenum and the small intestine (duodenum loop and jejunum), respectively. Severe infection of these parasites causes weight loss, poor feed conversion and death (Long, 1973). A summary of broad characteristics of *Eimeria* species of chickens is shown in Table 1.2.

The immunogenicity of *Eimeria* species varies from moderate to highly immunogenic (Table 1.2). *E. maxima* is highly immunogenic; it has been shown that chickens infected with a single oocyst of *E. maxima* are at least partially immune even to challenge with 4×10^5 oocysts (Lee and Fernando, 1978). However, *E. mitis*, *E. necatrix* and *E. tenella* are only moderately immunogenic (Long, 1973). For example, it has been shown that to enable *E. mitis* to provide protection against challenge, a series of increasing immunising doses (10^3-10^5) is needed and chickens only become immune by the sixth dose (Fitz-Coy and Edgar, 1989).

Table 1.2 Pathogenicity, site of infection and immunogenicity of *Eimeria* species that infect chickens (Adapted from Long, 1973)

Species	Pathogenicity	Site of Infection	Immunogenicity
E. acervulina	++	small intestine (duodenal loop and jejunum)	++
E. brunetti	+++	small intestine	++++
E. maxima	+++	small intestine (duodenum)	++++
E. mitis	++	small intestine	++
E. necatrix	++++	small intestine	++
E. praecox	+	small intestine (duodenal loop)	++++
E. tenella	++++	caeca	++

++++= very pathogenic/immunogenic; +++ or ++= moderately pathogenic/immunogenic; += slightly pathogenic/immunogenic.

1.2 Life cycle of *Eimeria* species

Eimeria species are obligatory intracellular for most of their life cycle. The life cycle has three major phases: schizogony, gametogony and sporogony (Figure 1.1). Schizogony and gametogony occur within the host whereas sporogony is exogenous (Obata, 2000). When infective sporulated oocysts are ingested by chickens, the oocyst wall is broken by the

grinding process in the bird's gizzard and sporozoites are released from sporocysts. This process is aided by pancreatic enzyme, trypsin, bile salt and CO_2 (Allen and Fetterer, 2002; Jeurissen, *et al.*, 1996). Sporozoites then infect the gut epithelium of the host, where they replicate and develop into merozoites. With the rupture of epithelial cells, the motile merozoites enter a new cell and repeat the asexual life cycle. This phase of the asexual life cycle is called schizogony. This cycle can be repeated several times with a large number of merozoites being produced, resulting in significant damage to the intestine.

After two to five generations of asexual development, it is believed that the merozoites develop into male or female gametocytes (Jeurissen *et al.*, 1996). The male gametocytes divide into microgametes and female gametocytes develop into macrogametes. A zygote is produced when a microgamete fuses with a macrogamete. The zygote produces a cyst wall and becomes an oocyst, which ruptures from the intestinal cells and passes out in the faeces as an unsporulated oocyst (Obata, 2000).

Sporogony (or sporulation) is the stage where the transformation of unsporulated oocysts into sporulated oocysts takes place. The sporulation process requires oxygen and appropriate conditions of moisture and warmth (Williams, 1998). A sporulated oocyst contains four sporocysts, each of which has two sporozoites (Figure 1.2). The double layer oocyst wall allows *Eimeria* to survive harsh conditions in the external environment (Obata, 2000). For example, the oocysts are resistant to climatic change and remain infective for long periods (Jeurissen *et al.*, 1996), facilitating transmission, which occurs as a result of ingestion of oocysts.

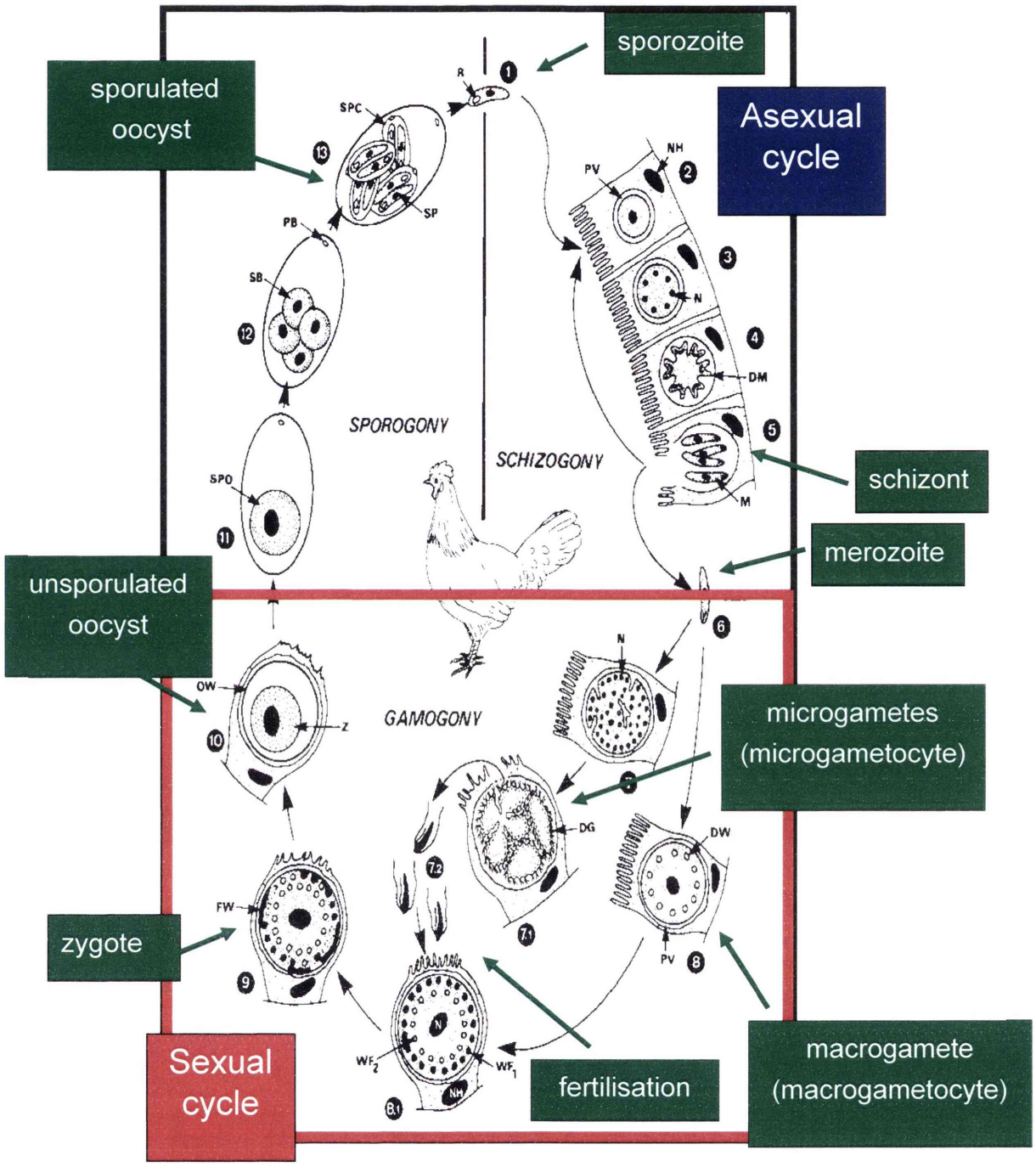

Figure 1.1 Life cycle of *Eimeria* species (modified from Melhorn, 1988). Infection begins with the ingestion of sporulated oocysts. Sporozoites are released from the sporocysts contained within the oocysts and rapidly invade cells of the gut, where they divide asexually (schizogony) forming schizonts. Merozoites escape from the intestinal cells and rapidly re-invade new cells, reiterating the asexual cycle. After a pre-programmed number of asexual cycles, the merozoites differentiate into either microgametocytes or macrogametocytes. Microgametocytes are flagellated and motile that fertilize the sedentary, intracellular macrogametocytes. A wall forms around the resulting zygotes, which are excreted in the faeces of the host as unsporulated oocysts and, in the right temperature and humidity, these divide into four sporocysts (sporulation), each of which contains two sporozoites.

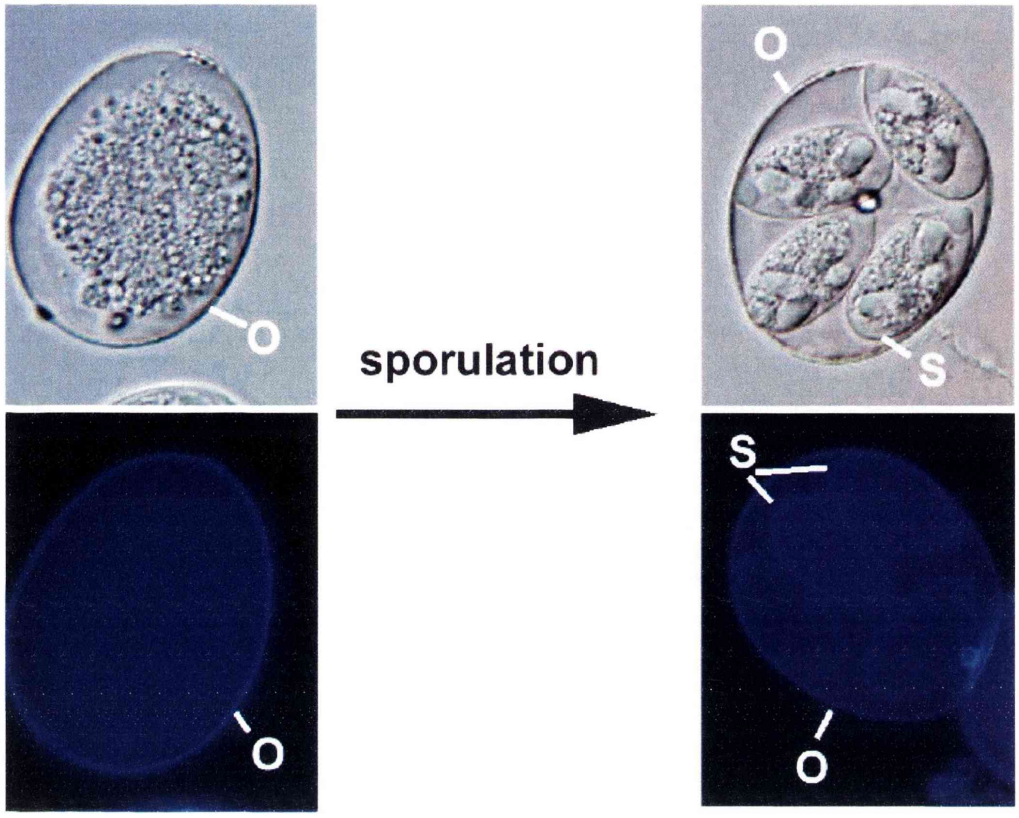

Figure 1.2 Structure of an unsporulated (left) and a sporulated (right) oocyst from *Eimeria maxima* showing UV autofluoresence in blue (Belli *et al.*, 2006). A sporulated oocyst contains four sporocysts, each of which has two sporozoites. O= oocyst walls. S= sporocyst walls.

1.3 Poultry Coccidiosis

Coccidiosis is one of the most important diseases in the poultry industry worldwide. As indicated above, transmission of *Eimera* is via the faecal-oral route (Cox, 1993). The intensive rearing conditions, characteristic of the modern poultry industry, facilitate transmission of *Eimeria* because chickens are in direct contact with contaminated faeces in the floor litter. Coccidiosis results in a reduced production of poultry meat and egg with considerable economic loss. For example, the total cost of coccidial infections in chickens in 1995 in the United Kingdom was estimated to be at least £38.5 million of which 80.6% was due to the effects on mortality, weight gain and feed conversion and 17.5% was due to

the cost of chemoprophylaxis and therapy (Williams, 1999). In the United States, coccidiosis results in a loss of at least US $800 million per year for commercial chicken producers (Williams, 1998).

Several approaches have been taken to control coccidiosis, such as improving hygiene in poultry houses, the use of coccidiostats and the administration of vaccines. Routine cleaning of broiler houses avoids the build up of oocysts in the flock and prevents the spread of infections. However some infective oocysts can still survive any practical cleaning procedure (Vermeulen *et al.*, 2001). In addition, they have a very high reproductive potential and oocysts are easily disseminated into the poultry house environment. Therefore, chemoprophylactic "in-feed" medication is used to reduce the risk of contracting an infection.

1.4 Chemoprophylaxis to control coccidiosis

Coccidiostats or anticoccidials are the drugs used to prevent and control coccidiosis in chickens. These drugs have been used since the 1940s. The advantages of using coccidiostats via feed are convenience, saving in labour time, cost effectiveness and ease of administration. The drugs are classified into two groups based on their modes of action: (i) chemicals that inhibit metabolic pathways of the parasite; (ii) polyether ionophores that alter ion transporter and disrupt osmotic balance (Table 1.3). The extensive use of anticoccidials has resulted in the selection for drug-resistant parasites, which has reduced the efficacy of many currently used drugs. For example, resistance to anticoccidials has been reported in sulphonamides, amprolium, nitrofurazone, nicarbazin, clopidol, monensin, narasin, lasalocid, salinomycin, and so on (Chapman, 1993; 1999; Stephan *et al.*, 1997; Allen and Fetterer, 2002).

Table 1.3 Mode of action of anticoccidial agents and their efficacy

Drug	Year of Launch	Modes of Action	Efficacy
Inhibition of parasite metabolic pathways			
Quinolones [a]	1968	Inhibition of mitochondrial respiration with a point block between ubiquinone and cytochrome b.	xxx
Clopidol [b]	1968	Inhibition of mitochondrial function	xxx
Robenidine [c]	1972	Inhibition of oxidative phosphorylation in mitochondria.	xxx
Clopidol/methyl benzoquate [d]	1984	Inhibition of electron transport and oxidative phosphorylation, presumably inhibition of pyrimidine biosynthesis at the dihydro-orotate-dehydrogenase step.	xxx
Toltrazuril [e]	1987	Inhibition of NADH oxidase and succinate cytochrome reductase in mitochondria	xxx
Diclazuril	1993	Unknown	xxx
Sulphonamides [f]	1945	Inhibition of folic acid metabolism	xx
Nicarbazin [g]	1956	Inhibition of dihydropteroate synthase	xxx
Amprolium [h]	1960	Inhibition of thiamine transport across cell membrane	xx
Amprolium/sulphonamide/ Ethopabate [d]	1963	Inhibition of thiamine transport, folic acid metabolism and dihydropteroate synthase	xxx
Arpinocide	1980	Inhibition of hypoxanhine and guanine uptake into infected eukaryotic cells.	xxx
Polyether Ionophores			
Semduramycin[i], Monensin [j], Salinomycin, Lasalocid, Maduramycin	1971	Destruction of membrane integrity, destruction of transport membrane ion gradients, formation of complexes with Na+, increase Na+/K+ ATPase activity, depletion of amylopectin stores, rapid influx of water, swelling of cells, vacuolization and destruction of intracellular structures.	xxx

xxx= high efficacy; xx= partial efficacy; x= low efficacy.

a (Wang, 1975); b (Challey and Jeffers, 1973); c (Lee and Millard, 1972); d (Salisch, 1989); e (Harder and Haberkorn, 1989); f (Wang *et al.*, 1975); g (Dougherty, 1974); h (James, 1980); i (McKenzie *et al.*, 1993); j (Smith and Galloway, 1983).

Moreover, a concern over residual drug in meat is an issue. It has been demonstrated that chickens medicated with diclazuril were protected for several days after withdrawal of medication, apparently because of compound residues in the intestinal mucosa (McDougald and Seibert, 1998).

The continued sustainability of chemoprophylaxis is questionable. Developing a new anticoccidial drug is possible, however, it is time consuming and requires a lot of money. The expenditure for the commercial development of a new anticoccidial drug is approximately US $50 to 100 million and it may take 15 years from discovery of a new compound to introduction of a new product (Williams, 1998). Progress of the development of a new anticoccidial drug is slow and there has been no new class of anticoccidial drug available in the market for many years. Nevertheless, potential new drug targets such as PW2, a novel peptide possessing *in vitro* activity against *E. acervulina* and *E. tenella* sporozoites (Silva *et al.*, 2002), via enzymes of the sporozoite mannitol cycle and trophozoite histone deacetylase (Schmatz, 1997; Allocco *et al.*, 1999; Snelling *et al.*, 2007) have been identified recently.

1.5 Live vaccines against coccidiosis

Vaccination is an alternative means that can be used to control coccidiosis. Although the immune mechanisms governing resistance to infection with *Eimeria* species are still not completely understood, it is clear that chickens that are deliberately infected with low numbers of *Eimeria* species for two to three consecutive infections are able to develop protective immunity (Joyner and Norton, 1973; Long *et al.*, 1986). The development of all currently used live vaccines is based on this principle and there are several live vaccines that are commercially available (Table 1.4). Live vaccines can be divided into two

categories: (i) wild type virulent strains; (ii) attenuated strains of *Eimeria* species. Immunocox™ and Coccivac™ are the most widely used examples of the wild type virulent parasite vaccines and each contains a variable number of parasite strains. The number of virulent strains in these two vaccines depends on their formulation and region of application (Lee, 1987). Each of Immunocox™ and Coccivac™ comes in two different types of vaccines (Immunocox C1, Immunocox C2 and Coccivac B, Coccivac D, respectively). Immunocox C1 is composed of wild type virulent strains of *E. acervulina*, *E. tenella*, *E. maxima* and *E. necatrix*. It is administered by spraying on feed whereas Coccivac B (which contains virulent strains of *E. acervulina*, *E. tenella*, *E. maxima* and *E. mivati*) can be administered in drinking water or by spraying on birds (Vermeulen *et al.*, 2001). The disadvantage of the live virulent vaccines is the risk of disease - some birds may die after vaccination due to the fact that not all birds are equally exposed to the parasites (Williams, 1994), some receiving large infectious doses.

Paracox™ and Livacox™ are composed of live attenuated parasites. Attenuated lines of *Eimeria* parasites can be obtained by repeated selection for early development of oocysts (precocious lines) or serial passage through embryonated eggs, which are inoculated with sporozoites (Long, 1972; Jeffers, 1975). Paracox™ and Livacox™ contain different combinations of attenuated *Eimeria* species (Table 1.4). In general, Paracox™ has more attenuated *Eimeria* species than Livacox™. Thus, Paracox™ contains precocious lines (sporulated oocysts) of seven *Eimeria* species (shown in Table 1.4), and it can stimulate immunity to each of these parasites independently (Williams, 1992) thus protecting birds against infections of these seven species. Livacox™ D contains two *Eimeria* species, *E. acervulina* and *E. tenella* resulting in a limited protection of birds. However, a potential drawback of these precocious vaccines is the loss of immunogenicity of the line without

stability of the attenuation (Williams, 1992). In addition, it is relatively more difficult and costly to produce attenuated lines of all seven *Eimeria* species (especially in Paracox™) and this form of coccidiosis control is not likely to be accepted by broiler industries (Williams, 1992) since these vaccines are less cost-effective than other anticoccidial controls (eg. anticoccidial drugs). However, Paracox 5, which contains fewer species and strains and is manufactured via a simpler, less exacting protocol, may ultimately prove cost-efficient for broilers, especially if EU moves to outlaw in-feed medication for poultry proceed.

Table 1.4 Commercially available vaccines against chicken coccidiosis (Vermeulen *et al.*, 2001)

Trade name	**Attenuated**	**Ionophore tolerance**	**Species[a]**	**Application[b]**	**Manufacturer**
Coccivac D	No	No	A, T, M, N, B, P, H, Miv	DW	Schering plough
Coccivac B	No	No	A, T, M, Miv	DW/SB	Schering plough
Immucox C1	No	No	A, T, M, N	DW/G	Vetech labs
Immucox C2	No	No	A, T, M, N, B, Mi, P	DW	Vetech labs
Paracox	Yes	No	A, T, M2, N, B, Mi, P	DW	Schering plough
Paracox 5	Yes	No	A, T, M2, Mi	SF	Schering plough
Livacox D	Yes	No	A, T	DW	Biopharm
Livacox T	Yes	No	A, T, M	DW	Biopharm
NovilisCOXATM	No	Yes	A, T, M2	DW/SB	Intervet

[a] Species: *E. acervulina* (A), *E. tenella* (T), *E. maxima* (M), *E. necatrix* (N), *E. brunetti* (B), *E. mitis* (Mi), *E. mivati* (Miv), *E. hagani* (H), *E. praecox* (P). M2 means two antigenically different strains of *E. maxima.*

[b] Applications: drinking water (DW), spray on birds (SB), spray on feed (SF), oral gel (G).

1.6 Subunit vaccines against coccidiosis

A subunit vaccine is a vaccine that comprises part of or complete molecules of protective antigens produced from specific developmental stage from the parasite. Several attempts have been made to develop subunit vaccines against *Eimeria* based almost exclusively on antigens from the asexual (sporozoite and merozite) stages of the parasite but have been

essentially unsuccessful, providing, at best, only partial protection against infection (reviewed in depth by Jenkins, 1998; Vermeulen, 1998). CoxAbic®, a vaccine that includes native proteins from the sexual stage (macrogametocytes) of the parasite, however, has experienced some success and is the only commercially available subunit vaccine against coccidiosis. It is composed of, principally, two antigens from the macrogametocytes of *E. maxima* with molecular weights of 56 (EmGam56), 82 (EmGam82), though a 230 kDa gametocyte protein is also present (Wallach, 2002). The vaccine operates on the principle of transmission blocking immunity and therefore, aims to control coccidiosis by reducing the number of contaminating oocysts in the environment, hence preventing the incidence of disease (Wallach *et al.*, 1995). It has been shown that the antibodies produced in response to this vaccine can effectively block the transmission of parasites (Wallach, 1997). Since less oocysts pass out in the faeces, the chance and the number of oocysts being ingested by other chickens is greatly reduced, therefore preventing further spread of the parasite.

CoxAbic® is administrated to breeding hens and takes advantage of the phenomenon of maternal immunity. It has been shown that breeding hens can transfer parasite-specific IgG (immunoglobulin G), via the egg yolk, providing protection to offspring chicks against various *Eimeria* species (Smith *et al.*, 1994a, b; Wallach *et al.*, 1994; 1995). Administration of CoxAbic® to breeding hens not only provides immediate protection to chicks but is also cost-effective; since immunisation of one hen can lead to the protection of over 100 chicks, this greatly reduces the cost of vaccination (Wallach, 1997). In addition, immunisation of birds with CoxAbic® does not carry the risk of disease, which could happen when using live vaccines. CoxAbic®'s efficacy has been tested in the laboratory, in floor pen trials, and in extensive field trials conducted in several countries spanning four continents (Michael, 2002).

The antigens found in CoxAbic® are destined for incorporation into the oocyst wall of *Eimeria* (see Belli *et al.,* 2006, for a review). This has prompted considerable research into the molecular basis for oocyst wall formation (summarized below). The oocyst wall serves as a barrier to protect parasites from harsh external environment; it ensures the survival of oocysts both in the intestines of the host, whilst being passaged in the faeces, and in external environment upon oocyst excretion from the host, thus facilitating the transmission of parasites from host to host. The parasites would not be able to survive without the oocyst wall.

1.7 Oocyst biogenesis

The oocyst wall of *Eimeria* is formed from the contents of specific organelles, wall forming bodies, found exclusively in the macrogametes (Scholtyseck, 1973; Pittilo and Ball, 1980; Ferguson *et al.*, 2003; Figure 1.3). There are two types of wall forming bodies: wall forming bodies type 1 (WFB1 or W1) and wall forming bodies type 2 (WFB2 or W2) and both of them are involved in the oocyst wall formation in *Eimeria* (Scholtyseck *et al.*, 1969; Scholtyseck, 1973; Pittilo and Ball, 1980; Ferguson *et al.*, 2003; Belli *et al.*, 2006).

In the early stages of macrogamete biogenesis, the macrogametocyte contains a nucleus and nucleolus located in the centre with numerous small granules in cytoplasm known as early wall forming bodies (Figure 1.3 a), which stain positively with four antibodies: anti-APGA (antibodies to affinity purified gametocyte antigens; Figure 1.3 d), anti-EmGam56, anti-EmGam82 and anti-EmGam230 antibodies (antibodies to 56, 82 and 230 kDa gametocyte antigens of *E. maxima*, respectively; Ferguson *et al.*, 2003). The early wall forming bodies differentiate into WFB2, followed by WFB1, which are seen in the early/mid- and mid-stage of development, respectively (Figure 1.3 b and e, respectively).

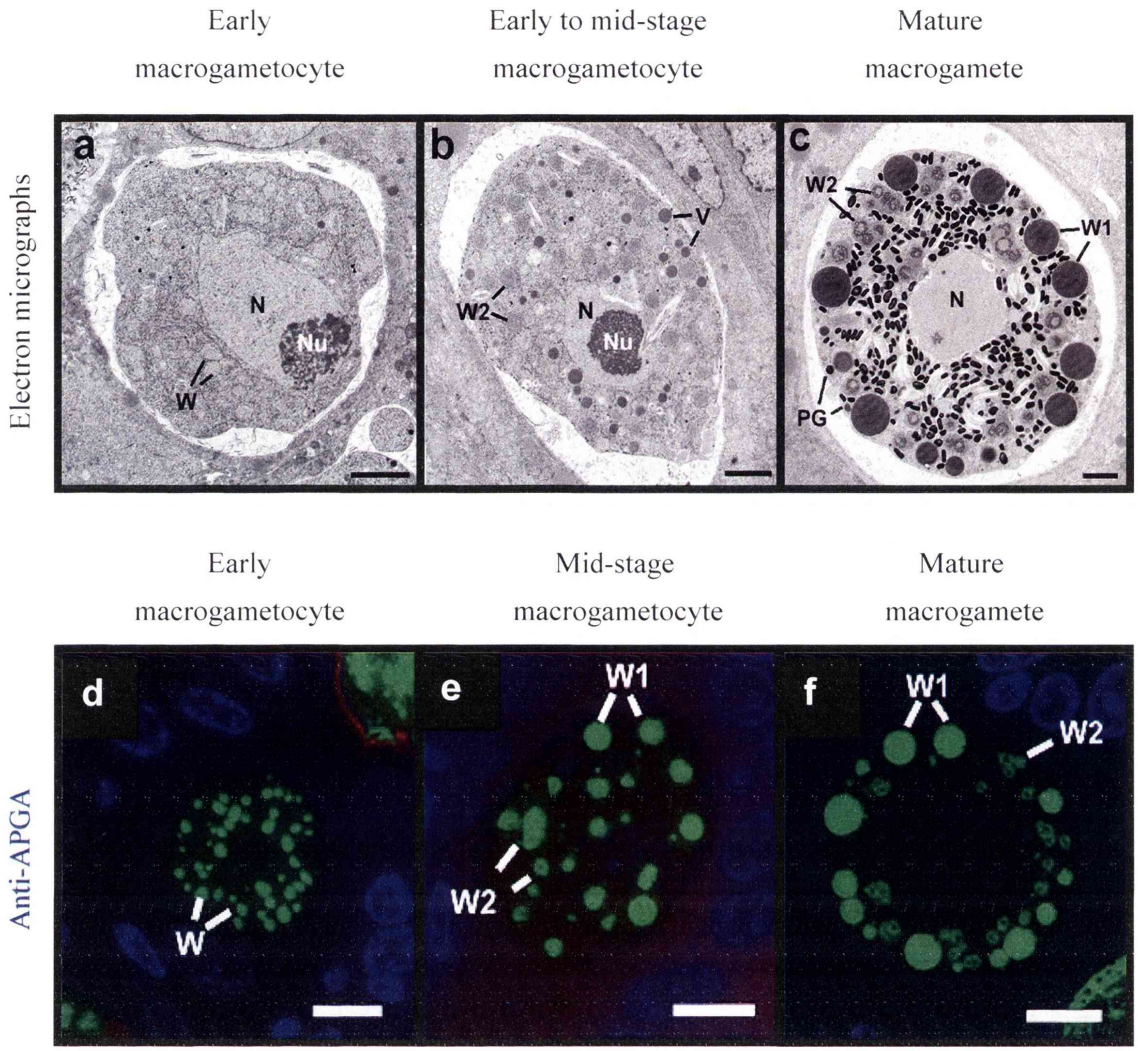

Figure 1.3 Electron micrographs of developing and mature macrogametocytes (a-c); and plastic embedded sections (d-f) of developing and mature macrogametocytes that have been immuno-labelled with anti-APGA antibodies and visualized with fluoresceine isothiocyanate with DAPI counterstaining (Ferguson *et al.*, 2003). W= wall forming bodies. W1= wall forming bodies type 1. W2= wall forming bodies type 2. V= veil forming bodies. N= nucleus. Nu= nucleolus. PG= polysaccharide granules. I= inner layer of the oocyst wall. O= outer layer of the oocyst wall. Bars represent 2 μm (a-c) or 5 μm (d-f).

Along with WFB2, development of veil forming bodies also occurs in the early to mid-stage of macrogametocyte biogenesis (Figure 1.3 b). In the mature macrogametocyte, WFB1 locate in the periphery of the parasite inter-mixed with WFB2. A large number of polysaccharide granules are also seen in the cytoplasm of the mature macrogametocyte (Figure 1.3 c). Both WFB1 and WFB2 stain positively with anti-APGA antibodies (Figure 1.3 f).

The veil forming bodies have lucent vacuoled appearance, are secreted during macrogemete maturation, and are responsible for the formation of outer veil (a membrane like structure located on the surface of outer layer of the oocyst wall) in *E. maxima* (Ferguson *et al.*, 2003). The outer veil of *E. maxima* stains positively with anti-*T. gondii* microneme protein 4 antibodies (anti-TgMIC4 are antibodies to the apple domains of *Toxoplasma gondii* microneme protein 4, which is associated with oocyst wall formation in *Toxoplasma gondii*) suggesting that the veil is composed of MIC4-like proteins and the structure of the veil is preserved between coccidia (Ferguson *et al.*, 2000; 2003). The veil is lost when oocysts are excreted from host (Ferguson *et al.*, 1975; Pittilo and Ball, 1980); therefore it is thought that the outer veil plays no role in protection of parasites during either passage out of the host or in the external environment (Belli *et al.*, 2006). Its precise role of veil is still unknown; though it seems possible that it provides a temporary "frame" under which the oocyst wall is assembled. This idea is supported by the fact that the veil remains in place throughout the entire intracellular development phase of the oocyst (Pittilo and Ball, 1980).

WFB1 in mature macrogametocytes are electron-dense, osmiophilic in nature and have a round-shaped structure (Pittilo and Ball, 1979; Ferguson *et al.*, 2003; Belli *et al.*, 2006;

Figure 1.3 c). They are located in the periphery of the parasite and have long been thought to contain mucoproteins, mucopolysaccharides and glycoproteins (McLaren, 1969; Scholtyseck, 1973). The size of WFB is species-specific. For example, WFB1 are larger than WFB2 in *E. tenella*, *E. maxima*, *E. stieda* and *E. perforans* whereas in *E. bovis* and *E. falciformis*, the reverse is true (Scholtyseck, 1973). WFB2 are less electron dense than WFB1, have a less distinct structure (Ryley, 1973; Scholtyseck, 1973), and are located within rough endoplasmic reticulum (Pittilo and Ball, 1979; Ferguson *et al.*, 2003; Figure 1.3 c). The contents of WFB1 are responsible for the formation of the outer layer of the oocyst wall in *Eimeria*, whereas the inner layer of the oocyst wall is derived from the contents of WFB2 (Pittilo and Ball, 1980; Ferguson *et al.*, 2003).

As mentioned earlier (Section 1.2), once fertilized by a microgamete, a macrogamete develops into a zygote. The oocyst wall starts to form shortly afterwards with WFB1 aligning beneath the limiting membrane of the zygote cytoplasm (Pittilo and Ball, 1980). A recent study (Ferguson *et al.*, 2003) of oocyst wall formation in *E. maxima* using immuno-cytochemistry with anti-APGA antibodies adds substantial and compelling evidence to support the mechanism of oocyst wall formation originally proposed by Pittilo and Ball in 1980. Thus, Ferguson *et al.* showed that oocyst wall formation is a sequential release of: [1] the contents of the veil forming bodies; [2] WFB1; and [3] WFB2. It is thought that this mechanism may be controlled at the level of the rough endoplasmic reticulum/Golgi apparatus (Ferguson *et al.*, 2003). Thus, in the mature macrogametocyte or zygote, after the veil has been laid down, WFB1 and WFB2 relocate to the periphery of the parasite and both of them are recognized by anti-APGA antibodies (Figure 1.4 a). WFB1 quickly disaggregate and appear to fuse together at the surface of the parasite (Figure 1.4 b) ultimately forming the outer layer of the oocyst wall (Figure 1.4 c-d). Shortly after WFB1

form the outer layer, WFB2 also disaggregate and spread out, fusing beneath the outer layer (Figure 1.4 c-d) and create the inner layer of the oocyst wall (Figure 1.4 e). The newly formed oocyst contains a large central nucleus, a number of polysaccharide storage granules containing amylopectin and lipid droplets (Pittilo and Ball, 1980).

Initially, the outer layer of the oocyst wall may be as thick as 500-600 nm but, as the development of oocyst wall progresses, the outer layer is compacted to ~200 nm. An inner zone of approximately 40 nm separates the outer and inner layers, the latter layer also ultimately being ~40 nm thick (Ferguson *et al.,* 2003). The fact that anti-APGA antibodies recognize WFB1, WFB2 and the outer and inner layers of the oocyst wall suggests that the oocyst wall is composed of the proteins contained in APGA. The precise composition of the oocyst wall has been controversial for many years. Though there is some agreement that it is composed of a mixture of protein, lipid and carbohydrate, there is considerable conjecture about the relative contributions of each of these metabolites to the overall composition of the wall and, additionally, whether the compositions of the inner and outer layers of the walls are similar or not (see Monné and Hőnig, 1954; Nyberg *et al.*, 1968; Nyberg and Knapp, 1970; Ryley, 1973; Belli *et al.*, 2006). This is discussed (and re-evaluated) in detail in Chapter 3 of this thesis.

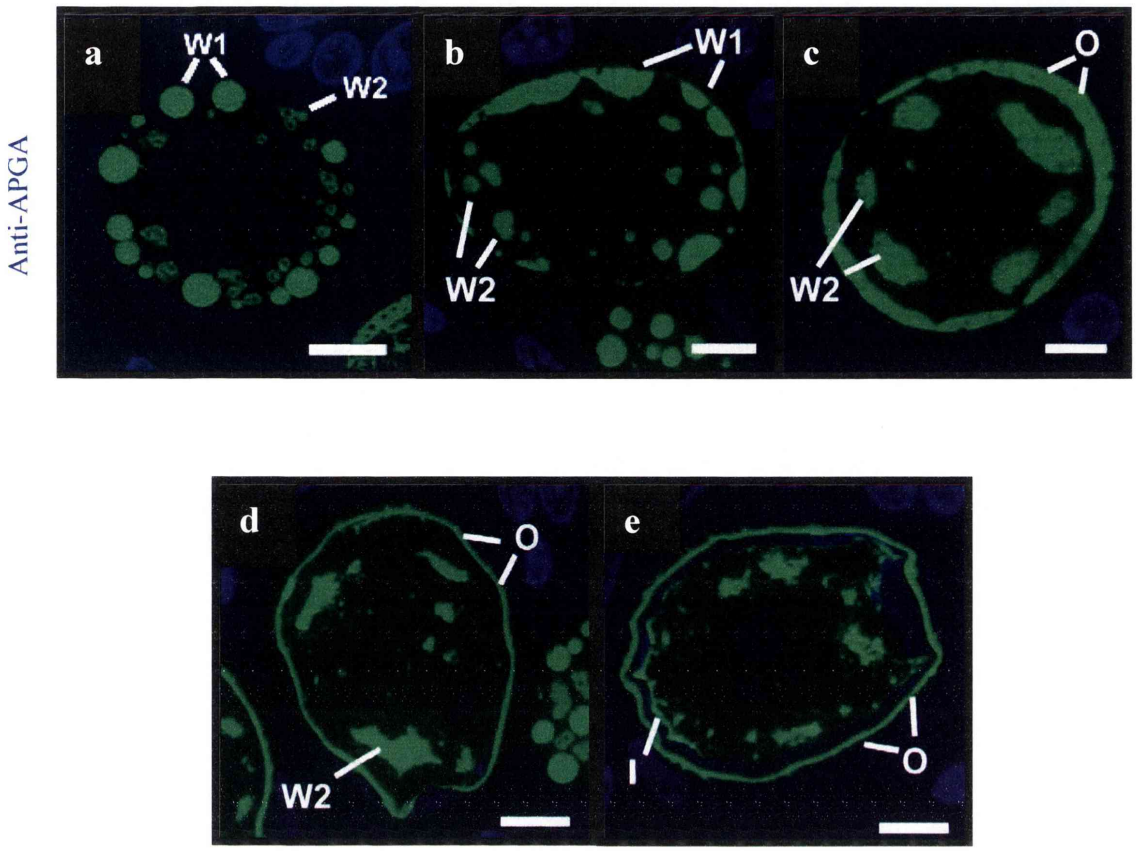

Figure 1.4 Plastic embedded sections showing the various stages of oocyst wall formation in organisms that have been immuno-labelled with anti-APGA antibodies and visualized with fluoresceine isothiocyanate and DAPI counterstaining (Ferguson *et al.*, 2003). Wall forming bodies type 1 (W1) and type 2 (W2) in a mature macrogametocyte were recognized by anti-APGA antibodies (a). W1 disaggregate and fuse together at the surface of the parasite (b) forming the outer layer of the oocyst wall (c). Shortly after the formation of the outer layer, W2 also disaggregate and spread out, fusing beneath the outer layer (d) and create the inner layer of the oocyst wall (e). W= wall forming bodies. W1= wall forming bodies type 1. W2= wall forming bodies type 2. I= inner layer of the oocyst wall. O= outer layer of the oocyst wall. Bars represent 5 μm.

1.8 EmGam56 and EmGam82 are precursor proteins involved in oocyst wall formation

EmGam56 and EmGam82 have been well characterized and they exist, in part, as soluble, globular proteins within the macrogametocyte of the parasite suggesting that they may be hydrophilic (Belli *et al.*, 2002a). Both of them are acidic in nature with predicted isoelectric points (pI) 4.81 and 5.16 for EmGam56 and EmGam82, respectively (Belli *et al.*, 2002b; 2003a). They are developmentally regulated: the expression of *EmGam56* is first detected at 120 hours post infection whereas *EmGam82* appears at 130 hours post infection (Belli *et al.*, 2002b; 2003a).

As alluded to above, EmGam56 and EmGam82 reside within the wall forming bodies of macrogametocytes (Belli *et al.*, 2002b; 2003a) and are believed to play a role in oocyst wall formation. The evidence for this is as follows: (1) a monoclonal antibody to EmGam56 (1E11-11) recognizes the wall forming bodies in macrogametocytes, the wall of unsporulated and sporulated oocysts and outer wall of the sporocysts (Belli *et al.*, 2002b); (2) anti-APGA antibodies react with WFB1, WFB2, the outer and inner layers of the oocyst wall in *E. maxima* (Ferguson *et al.*, 2003); and (3) antibodies to recombinant versions of EmGam56 and EmGam82 recognise WFB2 in macrogametocytes and the inner layer of oocyst wall in *E. maxima* (Belli *et al.*, 2003a; Ferguson *et al.*, 2003). Belli *et al.* (2003b) have demonstrated that neither EmGam56 nor EmGam82 are incorporated into the oocyst wall intact. Rather, they are processed or degraded into smaller polypeptides: wp33 (a 33 kDa wall protein) and wp12 (a 12 kDa wall protein) from EmGam56; and wp8 (an 8 kDa wall protein) and wp10 (a 10 kDa wall protein) from EmGam82 (Belli *et al.*, 2003b). All of these proteins are unusually rich in tyrosine (Belli *et al.*, 2003b), as are other oocyst wall proteins identified in *E. tenella* and *E. acervulina* (Eschenbacher *et al.*, 1996).

The discovery of these tyrosine-rich proteins in the oocyst wall of *Eimeria* prompted the proposition that the formation of dityrosine crosslinks between these proteins is integral to wall formation (Belli *et al.,* 2003b; 2006). There is good evidence to support this proposal: autofluorescence of intact oocysts (Figure 1.2), developing oocysts and purified oocyst wall fragments under UV light at 330-350 nm, is indicative of the presence of dityrosine, a dimer of tyrosine (Figure 1.5), produced by oxidation of tyrosine, and emitting a characteristic blue fluorescence at 330-350 nm (Belli *et al.,* 2003b; 2006). In addition, amino acid analysis of oocyst extracts by high-pressure liquid chromatography (HPLC) shows that oocyst extracts contain very high concentrations of dityrosine and DOPA (another oxidation product of tyrosine; Belli *et al.,* 2003b; 2006). Further support for this proposal exists in the fact that peroxidase activity localizes highly specifically to the WFBs and developing oocyst wall of *Eimeria*; peroxidase and/or DOPA oxidase are often associated with the oxidation of tyrosine and the consequent formation of dityrosine crosslinks between proteins (Belli *et al.,* 2006). The role of dityrosine bond formation in the construction of the oocyst wall of *Eimeria* is discussed in more detail in Chapter 6 of this thesis but, in short, the reaction proceeds via the following reaction:

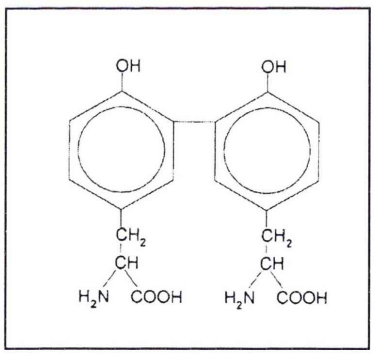

Figure 1.5 Structure of dityrosine (Smail *et al.*, 1995).

1.9 Project aims

The overall goal of the research conducted for this thesis is to add to the body of knowledge describing the molecular basis for the formation of the oocyst wall of parasites of the genus, *Eimeria,* in the phylum Apicomplexa. The specific aims are to:

[1] deduce the biochemical composition of the oocyst walls of unsporulated and sporulated oocysts of *E. tenella* and *E. maxima* using gas chromatography (GC) and mass spectrometry (MS);

[2] determine the structural features of one of the key protein components of the oocyst wall, EmGam56, using bioinformatics, circular dichroism (CD), and one-dimensional nuclear magnetic resonance (1D-NMR);

[3] demonstrate that dityrosine crosslinks can be induced to form between truncated forms of EmGam56, in the presence of peroxides and DOPA oxidase or peroxidases.

Chapter Two

Materials and Methods

2.1 Materials

2.1.1 General chemicals

All chemicals used throughout this study were of analytical grade.

- Acetic acid (Amresco, USA), acetone (Sigma-Aldrich), acrylamide (Bio-Rad Laboratories, USA), agarose (Amresco, U.S.A), alkaline phosphatase substrate (SIGMAFAST™ BCIP®/NBT; Sigma), ampicillin (Amresco, Australia), 3'-amino-1, 2, 4-triazole (Sigma, Australia)
- Bacteriological agar (DIFCO Laboratories, USA), bovine serum albumin (CSL Limited, Australia), bromophenol blue (Sigma, USA), BSTFA + 1% TMCS (PIERCE, USA)
- Calcium chloride (AJAX chemicals, Australia), chloroform (Amresco, USA), coomassie Brilliant Blue R250 (Sigma)
- Diethylaminoethyl cellulose (Whatman, UK), dNTP (Fisher Biotech, Australia), diploma skim milk powder (Bonlac Foods, Australia)
- Ethanol (Merck Pty Ltd, Australia), ethidium bromide (Fluka BioChemika), ethylene diamine tetra-acetic acid (Amresco, U.S.A)
- Glucose, glycine (BDH, Australia), glutaraldehyde solution, glycerol (Sigma-Aldrich)
- Hemoglobin from bovine blood (Sigma), heptadecanoic acid (Fluka, Australia), hexamethyldisilazane (PIERCE, Australia), hexamethylene tetramine (Riedel-de Haën), hydrochloric acid (Chem Supply Pty Ltd, Australia), hydrogen peroxide solution (Riedel-de Haën)
- Imidazole (Sigma-Aldrich, Australia)
- Lead citrate (Fluka), isopropyl-b-thiogalactopyranoside (Austal, Australia)
- Nickel sulfate (Aldrich, Australia)
- Mercaptoacetic acid (Aldrich), methanol (Merck Pty Ltd, Australia), methoxyamine hydrochloride in pyridine (Sigma)
- Osmium tetroxide (Sigma-Aldrich)
- Phenol (Amresco, U.S.A), phenylhydrazine hydrochloride, p-nitrophenyl phosphate, potassium chloride, potassium dichromate, pyridine (Sigma), propylene oxide (Fluka), PEG (Sigma-Aldrich);

- Salicylhydroxamic acid (Aldrich), *scyllo*-inositol, silver nitrate, silver methenamine, sodium azide, sodium chlorite, sodium dodecyl sulfate, sodium phosphate dibasic, sodium thiosulfate, sucrose (Sigma), sodium borohydride, sodium carbonate monohydrate, sodium deoxycholate, sodium tetraborate decahydrate (Sigma-Aldrich), sodium hypochlorite (APS, Australia), Spurr's epoxy resin (Fluka)
- TCA (Riedel-de Haën), *tertiary*-butylhydroperoxide, trizma base (Sigma-Aldrich), TMCS (PIERCE, Australia), tryptone (DIFCO Laboratories, USA), Tween 20 (ICN Chemical Inc, USA), trypsin 250 (DIFCO Laboratories, USA)
- Yeast extract (DIFCO Laboratories, USA)
- Uranyl acetate (Fluka)
- Xylene cyanol (Sigma, USA)

2.1.2 Miscellaneous materials

- PVDF protein transfer membrane (Pall, USA)
- Polymon mesh – 10 and 17 μm, (Swiss Bolting Company, Switzerland)
- Stainless steel laboratory test sieves, 1 mm and 0.25 mm gauge (Endecotts, UK)
- 96 well plates (Nunclon™ Surface, Denmark), 96 well flat-bottomed EIA/RIA plates (Costar)
- Minisart single use filter unit – 0.45 μm (Satorius, Germany)
- Vivaspin500, 3000 Da MWCO(Vivascience, Germany)

2.1.3 General solutions and growth media

- Luria-Bertani medium pH 7.0: 1% tryptone, 0.5% yeast extract, 0.5% sodium chloride.
- LB agar: LB medium with 1.5% agar
- Coomassie Blue solution: 0.2% Coomassie Brilliant Blue R250, 50% methanol, 10% glacial acetic acid
- Destaining solution: 12% ethanol, 7% glacial acetic acid
- Milton-2 solution: 2% sodium hypochloride, 16.5% sodium chloride.

- Phosphate buffered saline pH 7.4: 0.14 M sodium chloride, 2.68 mM potassium chloride, 10.14 mM sodium phosphate dibasic, 1.76 M potassium dihydrogen orthophosphate.
- SDS electrophoresis buffer 1x: 25 mM Tris, 190 mM glycine, 0.1% SDS
- SDS-PAGE sample buffer 1x: 62 mM Tris-HCl pH6.8, 10% glycerol, 2.3% SDS, 5% β-mercaptoethanol, 0.5% bromophenol blue
- Sodium phosphate buffer pH 6.8 (0.1 M): 0.463 M Na_2HPO_4, 0.537 M NaH_2PO_4
- SOC medium: 2% tryptone, 0.5% yeast extract, 10 mM sodium chloride, 2.5 mM potassium chloride. 10 mM magnesium chloride, 10 mM magnesium sulfate, and 20 mM glucose.
- TBE electrophoresis buffer: 0.089 M Tris, 0.089 M borate, 0.002 M EDTA
- TBS: 10 mM Tirs-HCl pH 7.5, 150 mM NaCl
- TE buffer: 10 mM Tris-HCl pH8.0, 1 mM EDTA
- Transfer buffer: 25 mM Trizma® base, 192 mM glycine, 20% methanol
- Triton solution: 20 mM Tris-HCl pH 7.5, 500 mM NaCl, 0.05% Tween-20, 0.2% Triton (Tx-100)

2.1.4 Commercial kits and columns

- Champion™ pET Directional TOPO® Expression Kits (Invitrogen™, Australia)
- HiTrap™ Chelating HP Column (Amersham Biosciences, Australia)
- Disposable PD-10 Desalting Column (GE Healthcare, Australia)
- QIAquick® Gel Extraction Kit (QIAGEN, Australia)
- QIAquick® PCR Purification Kit (QIAGEN, Australia)
- QIAGEN PlasmidAmp Kit (QIAGEN, Australia)

2.1.5 Molecular weight markers

- 100 bp ladder (Pharmacia, Sweden)
- 1 kb DNA ladder (Promega, USA)
- BenchMark™ protein ladder (Invitrogen™, Australia)
- BenchMark™ pre-stained protein ladder (Invitrogen™, Australia)
- SeeBlue® Plus 2 pre-stained protein ladder (Invitrogen™, Australia)

2.1.6 Antibodies

- Anti-chicken and anti-mouse IgG (whole molecule) alkaline phosphatase conjugates (Sigma, USA)
- Anti-mouse IgG (whole molecule) horseradish peroxidase conjugates (Sigma, USA)
- Mouse anti-pentahis antibodies (QIAGEN, USA)
- Mouse or chicken anti-recombinant 56 kDa antibodies (provided by Abic Ltd, Israel)
- Chicken anti-APGA serum (provided by Abic Ltd, Israel)

2.1.7 Enzymes

- alpha-amylase from barely malt (Sigma, Australia)
- Catalase from bovine liver (Sigma, Australia)
- Lysozyme from chicken egg white (Sigma, Australia)
- Myeloperoxidase from human leukocytes (Sigma, Australia)
- Peroxidase from *Arthromyces ramosus* (Sigma, Australia)
- Peroxidase from Horseradish (Fluka, Australia)
- P*fu* DNA polymerase (Fermantas, Australia)
- *Taq* DNA polymerase (Fisher Biotech, Australia)
- Tyrosinase from mushroom (Sigma, USA)

2.1.8 Bacterial strains for expression

- *E. Coli* strain TOP10 Genotype: F^+, *mcr*A Δ(*mrr-hsd*RMS-*mcr*BC) ϕ80 *lacZ*ΔM15 Δ*lac*X74 *deo*R *rec*A1 *ara*D139 Δ(*ara-leu*)7697 *gal*U *gal*K *rps*L *end*A1 *nup*G; provided with the Xpress™ System Protein Expression TrcHis (Invitrogen™, USA)
- *E. Coli* strain BL21 Star™ (DE3) Genotype: F^+ *omp*T *hsdS*$_B$ (r_B-m_B-) *gal dcm rne131* (DE3); provided with Champion™ pET Directional TOPO® Expression Kits (Invitrogen™, Australia)

2.1.9 Animal strains

The Australorp strain of domestic chicken was used throughout this project. Chickens (one day-old) were provided by Barter and Sons Pty Ltd, Huntingwood, NSW, Australia. They were housed in the Gore Hill Research Laboratories, initially under heat lamps for the first 2 weeks of their life, and then at 21°C on a 12 hour light/dark cycle with free access to food

(unmedicated standard layer mash, Gordon's Specialty Stockfeed, Yanderra, NSW, Australia) and water.

2.1.10 Parasites

The Houghton strains of *Eimeria maxima* and *Eimeria tenella* were used throughout this project. Sporulated *Eimeria maxima* oocysts were originally supplied by Per Thebo, the National Veterinary Institute, Uppsala, Sweden and *E. tenella* by Dr Martin Shirley, Institute for Animal Health. They were subsequently passaged regularly through Australorp chickens at the Gore Hill Research Laboratories

2.2 Methods

2.2.1 Parasite preparation

2.2.1.1 *E. maxima* oocyst harvest from faeces

The protocol used here was adopted from Shirley (1995). Birds (3-4 weeks old) were infected orally with $5x10^3$ *E. maxima* sporulated oocysts. Faeces collected at day 6, 7 and 8 post-infection were transferred to a beaker containing tap water (3 parts of water to 1 part of faeces), followed by homogenization using an industrial strength blender (Townson & Mercer Pty. Ltd) for 20 seconds. The homogenate was filtered, sequentially, through a 1 mm and then a 0.25 mm sterile, stainless steel laboratory sieve to remove large particles of faecal debris. The flow through was collected and centrifuged in sterile bottles at 3,000 rpm, for 10 minutes at room temperature. The pellet was then resuspended in saturated saline and centrifuged at 1,000 rpm, for 5 minutes at room temperature. Oocysts floating on the supernatant were collected and filtered through a 0.25 mm sterile, stainless steel laboratory sieve, followed by a 10 μm polymon mesh. The oocysts retained on the mesh were washed with water for three times to eliminate salt. The oocysts were then transferred to a clean tube and centrifuged at 3,500 rpm for 10 minutes. The purified oocysts were either stored at -80°C as unsporulated oocysts or sporulated in 2% potassium dichromate at 28°C for 3-4 days until 90% sporulation was observed.

2.2.1.2 *E. tenella* oocyst harvest from caeca

The protocol used here was adopted from Shirley (1995). Birds (3-4 weeks old) were infected orally with $2.5x10^3$ *E. tenella* sporulated oocysts. Caeca removed after 134 hours post-infection were cut open longitudinally. The caecal contents were scraped away from the tissue and transferred to a sterile beaker containing PBS (pH 7.0). The scrapings were homogenised in a blender (using full power for approximately 30 seconds) and then transferred to a sterile beaker. Trypsin was added to 1.5% of the total volume to degrade connective tissue and the homogenate was incubated at 41°C in a water bath for 90 minutes with constant swirling. The homogenate was then filtered through a double layer cheese cloth to capture large particles of host contaminants such as fat and host tissues, followed by centrifugation at 2000 rpm for 12 minutes at 4°C. The supernatant was discarded and the pellet was resuspended in PBS (pH 7.0), followed by centrifugation at 2000 rpm for 12 minutes. This step was repeated three times. The oocysts (in pellet) were either incubated at 28°C in a water bath for 72 hours to induce sporulation or stored at -80°C as unsporulated oocysts.

2.2.1.3 Sodium hypochlorite treatment of oocysts

Oocysts were bleached routinely to eliminate contaminants such as faecal or caecal material, bacteria and other microorganisms according to Shirley (1995). However, half population of oocysts was not processed as unbleached samples for subsequent comparison. The oocysts (approximately 5 ml pellet) were resuspended in 48 ml of cold Milton-2 solution (2% sodium hypochlorite, 16.5% sodium chloride) and left on ice for 10 minutes with occasional gentle shaking. 2 ml of sterile distilled water was carefully layered on top of the suspension. The sample was centrifuged at 1500 rpm for 7 minutes either at 4 °C for unsporulated oocysts, or at room temperature for sporulated oocysts. Oocysts floating on top of the tube (formed a white layer) were collected and transferred to a clean falcon tube, which was topped up to 50 ml with sterile distilled water. The oocysts were centrifuged at 2500 rpm for 5 minutes and supernatant was discarded and pellet was resuspended in 50 ml with sterile distilled water and centrifuged again. This washing step was repeated for three times to wash away residual bleach in the sample. The yield of the oocysts was estimated using a haemocytometer and the oocysts were stored in aliquots at -80°C.

2.2.2 Isolation of oocyst walls from intact oocysts

Oocyst walls were isolated according to Stotish *et al.* (1978). 10^7 bleached or unbleached oocysts were resuspended in distilled water (two volume of pellet size) and suspension was sonicated on ice at 45-50 W for 10 seconds, power output at 8 (Sonicator® 300 Ultrasonic Liquid Processor, MISONIX) with 30 seconds break between each interval. Oocyst breakage was monitored by microscopic examination and the sonication was repeated until no intact oocysts were seen or at least greater than 99% of oocyst breakage was observed. The lysate was then centrifuged at 10,000 g for 10 minutes at 4°C, followed by two washes in distilled water. The pellet was resuspended in ten volumes of 1 M sucrose (sterile filtered) and centrifuged at 2500 g for 15 minutes at 4°C. This step was repeated five times to ensure the elimination of internal contents of the parasite. The pellet was then washed in 10 volumes of distilled water and centrifuged at 10,000 g for 10 minutes at 4°C. The washing and centrifugation step was repeated five times to eliminate residual sucrose in the sample. The purified oocyst walls were stored as $2x10^6$ aliquots at -80°C until needed.

2.2.3 Elimination of polysaccharide granule contamination from oocyst wall preparation

Oocyst walls ($2x10^6$) were resuspended in 100 µl distilled water and treated with either alpha-amylase or heat treatment according to the protocol from Ryley (1973) with modification. For enzyme treatment, alpha-amylase was added to a final concentration of 0.5 mg/ml and 1 mg/ml for comparison and samples were incubated at 20°C over night (O/N). On the next day the samples were centrifuged at 10,000 g for 10 minutes at 4°C and supernatant was discarded and pellet was washed in distilled water. The washing step was repeated three times. For heat treatment, the oocyst walls were boiled for 5 and 10 minutes using dry block heater (Thermoline, Australia) for comparison. The effect of alpha-amylase and heat treatment on elimination of polysaccharide granules was investigated under microscopic examination and iodine test (iodine lights up polysaccharides granules; Edgar *et al.*, 1944). The results were further confirmed by Transmission Electron Microscopy (TEM).

2.2.4 Examination of the oocyst walls by Transmission Electron Microscopy (TEM)

The oocyst walls (prepared from bleached or unbleached oocysts) were examined by TEM according to Ferguson *et al.* (2003) with the help from Professor David Ferguson at University of Oxford. Each sample of oocyst wall fragments was centrifuged and the pellets were fixed in 4% glutaraldehyde in 0.1 M phosphate buffer. The pellets were post-fixed in 1% osmium tetroxide in phosphate buffer, dehydrated in absolute ethanol, treated with propylene oxide and embedded in Spurr's epoxy resin. Thin sections of oocyst walls were then mounted on copper grids and stained with uranyl acetate and lead citrate for routine electron microscopy. In additon, certain sections were mounted on formvar-coated gold grids and stained with silver methenamine. The sections were floated on drops of a freshly prepared and filtered mixture containing silver nitrate and hexamethylene tetramine in a borax-based buffer pH 9.2. Sections were stained in the dark at 40°C for 60 minutes and washed in water prior to examination. In both cases, sections were examined in a Jeol 1200EX TEM.

2.2.5 Preparation of oocyst walls for compositional analysis

2.2.5.1 Methanolysis

Compositional analysis of oocyst walls was carried out according to McConville *et al.* (1990) with the help from David DeSouza and Professor Malcolm McConville at the University of Melbourne. Oocyst walls (10^6) were resuspended in 50 µl of 1:1 chloroform:methanol and transferred into a clean glass capillary tube with one end flame sealed. 10 nmoles of heptadecanoic acid (C17:0) was added to the capillary tube as an internal standard for subsequent quantification of metabolites. The sample was then dried *in vacuo* at 50°C. This step was repeated again in the presence of methanol to enable the complete removal of H_2O. 50 µl of methanolic HCl (0.5 M HCl in methanol) was added to each capillary tube and sealed under vacuum. The sample was then incubated at 80°C O/N. Following methanolysis, the sample was cut open and the acid was neutralized by the addition of 10 µl pyridine. The neutralized solution was then transferred to a GC-MS vial insert and dried *in vacuo*. 50 µl of trimethylsilyl (MSTFA + 1% TMCS) reagent was added to the tube, which was gently flicked to ensure the sample was well mixed. The sample was then transferred into an insert

vial of autosampler vials for compositional analyses (such as carbohydrates and lipids) by Gas Chromatography (GC) (Agilent 6890N GC) and Mass Spectrometry (MS) (Agilent 5973 Mass Selective Detector). Internal standards were included in the analyses to confirm the accuracy of the method (see Appendices).

2.2.5.2 Acid hydrolysis

Compositional analysis of oocyst walls was carried out according to McConville *et al.* (1990) with the help from David DeSouza and Professor Malcolm McConville at the University of Melbourne. Oocyst walls (10^6) were resuspended in 100 µl of 1:1 chloroform:methanol and transferred into GC-MS vial insert containing 1 nmole of *scyllo*-inositol as an internal control for subsequent quantification of metabolites. The sample was dried *in vacuo* at 55°. The vial was then transferred into a reactivial containing 200 µl 6N HCl, followed by evacuation under nitrogen. The sample was capped immediately to prevent oxidation by air and incubated at 110°C over night. The vial insert was then placed into GC-MS vial and the residual HCl was evaporated under nitrogen. Vial contents were then incubated for 2 hours at room temperature in 20 µl pyridine to allow resuspension and neutralization of HCl contaminants. 20 µl BSTFA+1% TMCS was added to enable TMS derivatisation and the reaction was carried out at 80°C for 30 minutes. The amino acid composition of the oocyst wall proteins was analyzed by GC (Agilent 6890N GC) and MS (Agilent 5973 Mass Selective Detector). Internal standards were included in the analyses to confirm the accuracy of the method (see Appendices).

2.2.6 Extraction of oocyst wall proteins by NaOH

Oocyst wall proteins were extracted using the method described by Meyers *et al.* (1998) with the help from David DeSouza and Professor Malcolm McConville at the University of Melbourne. Oocyst walls (10^6) were resuspended in 100 µl of 1 M NaOH, followed by boiling for 10 minutes to solubilize the wall proteins. The lysate was then cooled down at room temperature for 10 minutes. 20 µl of 5M HCl was added to neutralize the lysate, which was then brought up to 1 ml by the addition of 880 µl PBS. Absorbance at 230 nm and 260 nm was measured using a spectrophotometer (GeneQuant, Amersham Biosciences) and protein concentration was calculated using the following equation: [Protein] = $(183 \times A_{230})$ -

($75.8xA_{280}$) (Meyers *et al.* 1998). Internal standards were included in the analyses to confirm the accuracy of the method (see Appendices).

2.2.7 Bioinformatic analysis of protein sequence of EmGam56

2.2.7.1 Secondary structure predictions on EmGam56

Disorder predictions for EmGam56 was performed using bioinformatic programs such as PSIPRED, APSSP2, SSpro, GOR4, HNN and SOPMA, which can be accessed via the web sites shown in Table 2.1. The amino acid sequence of EmGam56 was submitted to perform the prediction. These programs can predict secondary structures including alpha-helix, beta sheets, and random coils. The results are presented with secondary structure prediction assigned to each amino residue.

2.2.7.2 Disorder predictions on EmGam56

Structural analysis of EmGam56 was performed using bioinformatics programs such as FoldIndex©, IUPred, RONN, DISPROT and DisEMBL™, which are web servers for remote and automatic data processing by accessing website address shown in Table 2.2. The accuracy of these disorder predictions seems to be fairly high (Obradovic *et al.*, 2003; 2005; Thomson *et al.*, 2003; Ward *et al.*, 2004; Yang *et al.*, 2005) that allow the assignment of structured versus unstructured, fold versus unfold, regions with whether there is a disorder region in a protein under native physiological conditions. Protein sequence of EmGam56 was imported into a window of each web server (see Table 2.2) and then submitted the request for disorder or intrinsically unfolded predictions. The results were received electronically and presented in a graph indicating disorder probability or tendency of disorder predictions on EmGam56 with disorder tendency assigned in each amino acid residue.

Table 2.1 Secondary structure predictors used for prediction on EmGam56

Secondary structure predictors	Description of secondary structure predictions/Web site address	References
APSSP2	It is an advanced version of PSSP server which predicts secondary structure of proteins from their amino acid sequence, based on neural network approach. APSSP2 has high accuracy of predictions with 82.9% of Q3 (a three state prediction) score. http://imtech.res.in/raghava/apssp/	Raghava, 2002
SSpro	It is based on the use of ensembles of one-dimensional recursive neural network (1D-RNN) architectures using methods directly on PDB (protein data bank) training set, PSI-BLAST (Position Specific Iterated - BLAST) profile including all homologous proteins. http://www.igb.uci.edu/servers/psss.html	Cheng *et al.*, 2005a
GOR4	It is an advanced version of the predictor, GOR, based on the information theory which was developed previously by Garnier *et al.*, 1978. GOR4 uses all possible pair frequencies within a window of 17 amino acid residues. After crossvalidation on a data base of 267 proteins, the version IV of GOR has a mean accuracy of 64.4% for Q3. http://npsa-pbil.ibcp.fr/.	Garnier *et al.*, 1996 Garnier *et al.*, 1978
HNN	It is based on the idea of discrimination which assesses on an open biological sequence processing problem: the problem of globular protein secondary structure prediction. The discrimination task is performed with an introduction of a hierarchical and modular approach in which combination is used at an intermediate level. http://npsa-pbil.ibcp.fr/.	Guermeur, 1997
PSIPRED	The method (version 2) incorporates two feed-forward neural networks which perform an analysis on output obtained from PSI-BLAST. It includes a new algorithm that further increases prediction accuracy. PSIPRED is capable of achieving an average Q_3 score of nearly 78%. http://bioinf.cs.ucl.ac.uk/psipred/	Jones, 1999; McGuffin *et al.*, 2000
SOPMA	It is an improved version of SOPM (self-optimized prediction method) which predicts all the sequences of a set of aligned proteins belonging to the same family. It correctly predicts 69.5% of amino acids for a three-state description of the secondary structure in a whole database containing 126 chains of non-homologous proteins. http://npsa-pbil.ibcp.fr/.	Geourjon and Deléage, 1995

Table 2.2 Protein disorder predictors used for disorder prediction on EmGam56

Protein disorder predictors	Description of disorder prediction/ Web site address	References
DisEMBL™	It is based on the artificial neural networks trained for predicting several definitions of disorder (criteria for assigning disorder are loops/coils, hot loops with a high degree of mobility, and missing coordinates in X-ray structure). http://dis.embl.de/	Linding *et al.*, 2003a Iakoucheva and Dunker, 2003
DISPROT	It is based on the lack of a fixed 3D structure along the entire protein as well as the proteins that have local regions lacking a fixed 3D structure. http://www.ist.temple.edu/disprot/predictor.php	Obradovic *et al.*, 2003; Obradovic *et al.*, 2005
DISpro	A disorder residue is defined as any residue for which no coordinates exist in the corresponding PDB (protein data bank) file. This method involves the use of evolutionary information in the form of files, predicted secondary structure and relatively solvent accessibility, and 1D-recursive neural network. http://www.ics.uci.edu/~baldig/diso.	Cheng *et al.*, 2005b
FoldIndex©	It is based on the average hydrophobicity of amino acids and on the absolute value of net charge of the sequences. http://bioportal.weizmann.ac.il/fldbin/findex	Prilusky *et al.*, 2005
IUPred	It is based on the estimation of the capacity of polypeptides to form stabilizing contacts (pairwise energy content). http://iupred.enzim.hu/	Dosztanyi *et al.*, 2005
RONN	It is based on the extension of bio-basis function neural network method, a sequence alignment technique originally developed for the detection of protease cleavage sites. http://www.strubi.ox.ac.uk/RONN	Yang *et al.*, 2005 Thomson *et al.*, 2003

2.2.8 Generation of recombinant constructs

2.2.8.1 DNA amplification by PCR

The recombinant construct containing DNA fragments encoding amino acids 102-225 of *EmGam56* (Figure 2.1) was generated according to the method described in Sambrook and Russell (2001). DNA was amplified by PCR using PTC-200 Peltier Thermal Cycler DNA Engine (MJ Research). Each reaction contained 1 µl of DNA template (50 ng of 56pET25b containing DNA fragment corresponding to 172-1127 bp of *EmGam56* gene which had been engineered in an expression vector, pET25b by Dr Sabina Belli, University of Technology, Sydney, unpublished data), 1 µl of 10 µM gene-specific forward primer, 1 µl of 10 µM gene-specific reverse primer (oligonucleotide primers were synthesized by Sigma Genosys Australia Pty Ltd, see Figure 2.1), 5 µl of 2 mM dNTP, 5 µl of 10x P*fu* Buffer with $MgSO_4$, and 0.4 µl of 2.5 u/µl P*fu* DNA polymerase – a high fidelity polymerase recommended for use with blunt end PCR cloning (Fermentas) and sterile distilled water to a total volume of 50 µl. The reaction was carried out as follows: initial denaturation at 95°C for 5 minutes, denaturation at 95°C for 30 seconds, primer annealing at 55°C for 1 minute (annealing temperature varied slightly from each reaction for optimal amplification), extension at 72°C for 90 seconds and the whole cycle was repeated 35 times with a final extension at 72°C for 10 minutes.

2.2.8.2 Agarose gel electrophoresis

PCR products (5 µl) were separated on 1% agarose gels in the presence of blue/orange 6x DNA loading dye (0.25% bromophenol blue, 0.25% xylene cyanol FF, 30% glycerol) according to the method described in Sambrook and Russell, (2001). The gel containing ethidium bromide was run at 100 V for 1 hour. The DNA fragments were visualized on an ultraviolet light transilluminator and photo-documented using a Kodak imaging system.

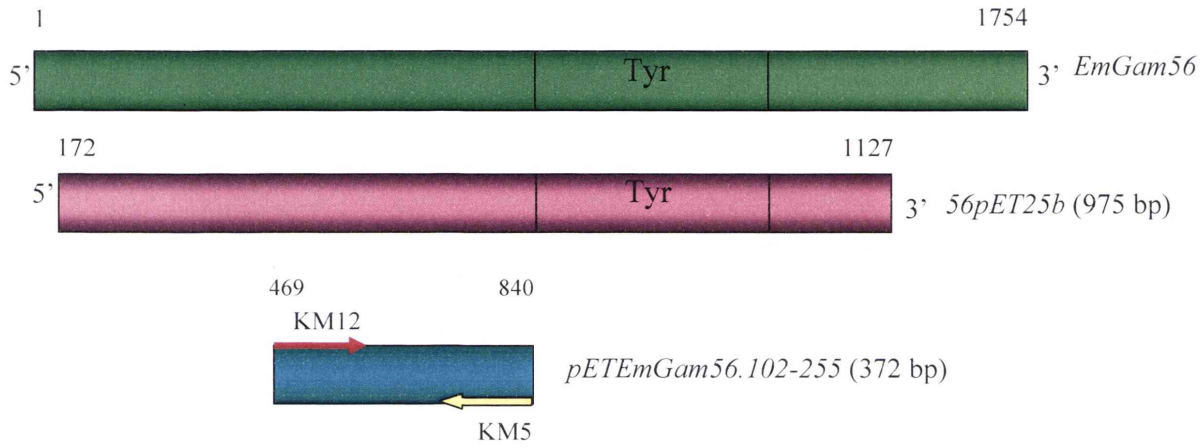

DNA template	Primer sets	Targeted region on EmGam56
56pET25b	KM12/KM5	469-840 bps (102-225 a.a.)

Primer name	Primer direction	Sequences (5' to 3')
KM5	reverse	GCTCCTGCCCTTTCTGCCCATATTT
KM12	forward	CACCATGTCCAACAGAATGAACGCTGCCATG

Figure 2.1 Strategy used to generate DNA fragment encoding amino acids 102-255 of *EmGam56*. 56pET25b, kindly provided by Dr Sabina Belli (University of Technology, Sydney), containing DNA fragment encoding for amino acids 24-338 (corresponding to 172-1127 bp of *EmGam56* gene) served as the parent construct for DNA amplification of the region, amino acids 102-225, by PCR. The DNA fragment encoding amino acids 102-225 was amplified from the parent construct, 56pET25b, using specific primer sets (KM5 and KM12, arrows represent primers). The truncated fragment was designated *pETEmGam56.102-255* with expected size shown in the bracket. The number in bp represents the location in the gene that the truncated DNA fragment maps. For example, the DNA fragment *pETEmGam56.102-255* is in 469-840 bp of the *EmGam56*. Tyr represents tyrosine rich region in *EmGam56* or *r56*.

2.2.8.3 Gel extraction

PCR products were separated by agarose gel electrophoresis and the DNA fragments of interest were excised from the gels with a clean scalpel blade and then gel purified using a QIAquick® Gel Extraction Kit (QIAGEN) according to the manufacturer's instructions. The DNA fragments were recovered in 30 µl of sterile distilled water and stored at -20°C.

2.2.8.4 Ligation

The purified DNA fragment from section 2.2.8.3 was cloned into the pET101/D-TOPO® vector according to the manufacturer's instructions (Champion™ pET101 directional TOPO® expression kit, Invitrogen™). Each reaction contained 1 µl of DNA (~5 ng), 0.5 µl of salt solution (provided from the kit), 0.5 µl of pET101/D-TOPO® vector and sterile distilled water to a total volume of 3µl. The reaction was carried out at room temperature for 5 - 10 minutes and the recombinant construct was then transformed into competent bacterial cells otherwise stored at -20°C until needed.

2.2.8.5 Transformation

The ligation mix prepared from section 2.2.8.4 was added to *E. coli* TOP10 competent cells (Invitrogen™) and incubated on ice for 10 minutes with a gentle swirl using pipette tips, followed by heat shock at 42°C for 30 seconds according to the manufacturer's instructions (Champion™ pET101 directional TOPO® expression kit, Invitrogen™). Samples were left on ice immediately after heat shock. SOC medium (250 µl) was then added and incubated at 37°C for 1 hour with shaking at 200 rpm. Different volume of culture was plated onto LB Amp plates (LB agar containing 100 µg/µl ampicillin) for the selection of transformants. The plate was then incubated at 37°C O/N. A number of transformants were selected for colony PCR.

2.2.8.6 Colony PCR

Colony PCR was performed to ensure the DNA was correctly inserted in the constructs following the method described by Sambrook and Russell (2001). Several colonies were picked randomly using a sterile toothpick, from LB Amp plates that contained ampicillin-resistant transformants prepared as described in section 2.2.8.5. A short streak of each colony

was made onto a new LB Amp plate and then dipped in 50 µl of 10 mM Tris-HCl pH 7.4 in an Eppendorf tube. Cells were lysed by boiling for 5 minutes. The lysate was left on ice to cool down for approximately 10 minutes. Each reaction contained 5 µl of lysate, 5 µl of 25 mM $MgCl_2$ (Fisher Biotech, Australia), 5 µl of 2 mM dNTP (Fisher Biotech, Australia), 5 µl of 10x *Taq** DNA polymerase buffer (Fisher Biotech, Australia) , 1 µl of 10 µM T7 or gene-specific forward primer, 1 µl of 10 µM T7term or gene-specific reverse primer (T7 and T7term are vector specific primers, supplied from Champion™ pET Directional TOPO® Expression Kit, Invitrogen™; see Table 2.3), 0.2 µl of *Taq** DNA polymerase (5.5 units/µl, Fisher Biotech, Australia), and sterile distilled water to a total volume of 50 µl. The thermal cycling for the PCR reaction was performed using an initial denaturation at 95°C for 3 minutes, a denaturation at 95°C for 30 seconds, a primer annealing at 55°C for 30 seconds, a extension step at 72°C for 90 seconds and 30 repeats of cycles with a final extension step at 72°C for 10 minutes. Amplification products were analyzed by gel electrophoresis as described in section 2.2.8.2. Constructs containing correct size of DNA insert were selected for subsequent plasmid preparation.

Vector specific primers	Primer direction	Sequences
T7	forward	5'-TAATACGACTCA-3'
T7term	reverse	5'-GCTAGTTATTGCTCAGCGG-3'

Table 2.3 Vector specific primer pairs used for Colony PCR and DNA sequencing.

2.2.8.7 Plasmid preparation

A single colony that contained the correct size of DNA insert was used to inoculate 4 ml of LB Amp medium, and the culture was incubated at 37°C O/N with shaking at 200 rpm. The next day, plasmid was isolated from 6 ml of O/N culture using QIAprep® Spin Miniprep Kit (QIAGEN) according to the manufacturer's instructions. The purified plasmid was recovered in 30 µl of sterile distilled water and stored at –20°C.

2.2.8.8 DNA sequencing

DNA sequencing was carried out to verify that the recombinant constructs contained the correct sequence of DNA insert. Each sample contained ~400 ng of plasmids (prepared from section 2.2.8.7), 6.4 pmoles of each vector-specific forward primer (T7) or reverse primer (T7term) and sterile distilled water in a total volume of 10 µl. The samples were sent to AGRF (Australian Genome Research Facility, Queensland) for automatic double-stranded sequencing of plasmids using dideoxy dye-terminator chemistry and ABI automated sequencers. DNA was sequenced in both forward and reverse directions. The consensus sequences were obtained by aligning sequenced DNA fragments to *EmGam56* using AssemblyLIGN™ (Oxford Molecular Ltd) software.

2.2.9 Expression of recombinant proteins

Cultures of *E. coli* strain Top10 cells containing 56pTrcHisb (as described previously by Belli *et al.*, 2002a) were used to produce the full-length r56 protein. The recombinant protein, r56, arising from this construct is recognized by the antibodies to the native protein, EmGam56, and therefore maintains its antigenicity and immunogenicity (Belli *et al.*, 2004). The protocol used here was adapted from Belli *et al.* (2004) with minor modification. Basically, an overnight culture of 56pTrcHis in *E. coli* Top10 was grown (150 ml of LB Amp medium at 37°C with agitation at 200 rpm O/N). The next day, LB Amp medium (5 liters) was inoculated with 100 ml of the O/N culture and incubated at 37°C with shaking until the cell density reached mid-log phase (wavelength of 600 nm (OD600) = 0.5-0.6). The culture was chemically induced by addition of IPTG to a final concentration of 1 mM and incubated at 37°C for 3 hours. The cell pellet was harvested by centrifugation at 4000 rpm for 30 minutes at 4°C.

E. coli strain BL21 Star™ cells containing the recombinant construct pETEmGam56.102-225 with the correct DNA sequence were grown in 10 ml of LB Amp medium at 37°C with agitation at 200 rpm O/N. On the next day LB Amp medium (20 ml) was inoculated with 100 µl of O/N culture and incubated at 30°C with shaking until the cell density - OD600 was 0.5-0.6. Half of the culture was then chemically induced with IPTG to a final concentration of 1 mM for protein expression and the other half contained no IPTG which served as a control

for the expression. The culture was induced with 1 mM IPTG for 3 hours at 30°C. An aliquot (1 ml) was taken from each sample and pellet was harvested by centrifugation at 12,000 g for 5 minutes. The supernatant was discarded and the pellets were stored at -20°C until required.

Conditions for optimal protein expression of pETEmGam56.102-225 were investigated. All procedures were the same as above except the temperature, IPTG concentrations and induction time. The recombinant protein was expressed at different temperatures such as 25°C and 30°C with either 0.1 mM IPTG or 1 mM IPTG induction for different time points: 0.5, 1, 2 and 3 hours. The culture was transferred to falcon tubes and centrifuged at 4,000 rpm for 25 minutes at 4°C. The supernatant was discarded and pellet stored at -20°C until required.

2.2.10 Purification of recombinant proteins

Recombinant proteins r56 and pETEmGam56.102-225 were purified from the pellet using a HiTrap™ chelating HP column (Amersham Biosciences, Australia) according to the protocol described by Belli *et al.* (2004) with minor modification. The pellet (500 ml) was resuspended in 40 ml of 10 mM imidazole and lysozyme was added to a final concentration of 5 mg/ml to lyse cells. The suspension was left on ice for 30 minutes followed by sonication on ice at a power 40-50 W, six times 20 seconds with a few minutes rest on ice between each interval. The lysate was centrifuged at 10,000 g for 30 minutes at 4°C. The supernatant was filtered through a 0.45 μm filter unit (Sartorius, Germany) to eliminate cell debris or aggregated matter before loading onto a 5 ml chelating HP column which was pre-charged with $NiSO_4$. The column was washed with a gradient of imidazole, from 20 mM, 100 mM, 150 mM up to 300 mM, to flush away non-specific binding of bacterial proteins to the column and flow through was also collected to monitor the purification. The recombinant proteins were eluted in 500 mM imidazole (five times 5 ml fractions or 1 ml fractions depending on the staring culture volume) and the protein concentration from each fraction was measured using a Bio-Rad protein assay based on the Bradford dye-binding method. The purified proteins were desalted and buffer-exchanged in 0.25 M sodium borate buffer pH 8.35 for r56 or 50 mM sodium phosphate buffer pH 6.8 for pETEmGam56.102-225 using a PD-10 desalting column (GE Healthcare, Australia). The recombinant protein

pETEmGam56.102-225 was then concentrated using a centricon, Vivaspin500, (Vivascience, Germany) according to the manufacture's instructions. The purified proteins were stored at -20°C until needed.

2.2.11 Ion exchange chromatography

The recombinant protein pETEmGam56.102-225 from section 2.2.10 was further purified using anion exchange chromatography according to the protocol described by Witcombe *et al.* (2003) with minor modification. Briefly, the column was prepared using approximately 1 g (2 ml) of DEAE cellulose anion exchange resin which was previously incubated in the following solutions: distilled water for 30 minutes; 40 mM Tris-HCl pH 7.4 for 15 minutes; 0.6 M NaCl in 40 mM Tris-HCl pH 7.4 for 15 minutes and then 40 mM Tris-HCl pH 7.4 for 15 minutes (which allows the swelling of beads and buffer exchange of the resin). The resin was transferred to a 1 cm (diameter) by 15 cm (length) column and equilibrated with 10x column volume of 40 mM Tris-HCl pH 7.4 at a flow rate of 0.5 ml/min. pETEmGam56.102-225 (~100 μg) were loaded onto the column and 5 ml of 40 mM Tris-HCl pH 7.4 was added to flush away unbounded proteins. Flow through was collected for monitoring the purification. The protein elution was performed with a gradient of 100-600 mM NaCl in 40 mM Tris-HCl pH 7.4 at a flow rate of 0.5 ml/min. Fractions were collected in four times 0.5 ml aliquots for each concentration of NaCl solutions. The purified fractions were analysed by SDS-PAGE, followed by silver staining as described below.

2.2.12 SDS-PAGE

Pellets (1 ml culture) prepared from section 2.2.9 to 2.2.11 were resuspend in 100 μl of 1x SDS-PAGE sample buffer and boiled for 3 minutes, followed by centrifugation at 12,000 g for 2 minutes to remove insoluble or aggregated matters. Proteins from supernatant (10 μl) and protein markers (5 μl) were separated on an 18% polyacrylamide gel according to the protocol described by Laemmli (1970). The gel was run in 1x SDS-PAGE running buffer at 50 mA until the dye front reached the bottom of the gel. Proteins were visualized either by silver staining or coomassie blue staining (for 1 hour followed by destaining until the proteins of interest were visible and the background was clear).

2.2.13 Silver staining

Proteins from section 2.2.11 were visualized by silver staining according to the instruction outlined in Amersham Pharmacia silver staining kit. Gels were soaked in fixative 1 (50% ethanol, 10% acetic acid) for 30 minutes and then in fixative 2 (5% ethanol, 1% acetic acid) for 15 minutes with shaking followed by three times washes in distilled water for 5 minutes. The gel was soaked in 0.2 mg/ml of $Na_2S_2O_3$ for 1 minute then three times washes in distilled water for 20 seconds followed by silver staining solution (2 mg/ml $AgNO_3$, 0.06% formaldehyde) for 20 minutes. The gel was then washed in distilled water as above and then developed in a solution containing 60 mg/ml of Na_2CO_3, 0.004 mg/ml of $Na_2S_2O_3$, 0.02% formaldehyde for 5 minutes or until protein bands were visualized. The reaction was stopped in 5% acetic acid and the gels were either left in distilled water or dried on cellophane, which had been soaked previously in 8 M PEG for 2 hours.

2.2.14 Immunoblotting

Proteins were transferred to PVDF membrane (Millipore, USA) for 2 hours at 100 V in the presence of transfer buffer using protocols published previously (Harlow and Lane, 1988). The membranes were blocked either in 5% skim milk/PBS (5g skim milk powder per 100 ml of PBS) or 3% BSA/TBS (3g BSA per 100 ml of TBS; for blots probed with mouse anti-pentahis antibodies - a recommended blocking buffer for anti-his antibodies to avoid strong background - QIAexpress Detection and Assay Handbook, QIAGEN) at 4°C O/N. The membranes were incubated with a primary antibody (chicken or mouse anti-recombinant 56 kDa antibodies or chicken anti-APGA serum; Wallach *et al.*, 1990) diluted in 5% milk/PBS or 3% BSA/TBS on a rotating wheel for 1-2 hours at room temperature, followed by three times washes with 0.03% Tween-20/PBS (for the membrane blocked with 5% skim milk/PBS) or Triton solution (0.05% Tween-20, 0.2% Tx-100 in TBS; for the membrane blocked with 3% BSA/TBS) for 30 minutes. The membranes were then incubated with a secondary antibody, followed by another three washes as described above. The membranes were developed in the presence of an alkaline phosphatase substrate, Sigma Fast™ BCIP®/NBT, for several minutes or until the protein bands of interest were visible and then rinsed in water to stop the chromogenic reaction.

2.2.15 ELISA

The protocol used here was adopted from Smith *et al.* (1994) with a minor modification. Ninety-six well flat-bottomed EIA/RIA plates (Costar) were coated with 100 ng of recombinant protein pETEmGam56.102-225 prepared in ELISA buffer 1 (0.1 M carbonate/bicarbonate buffer pH 9.6, 0.02% NaN_3) O/N at 4°C. On the next day plates were emptied and washed in wash buffer (0.03% Tween-20/PBS), followed by incubation with 3% skim milk power in PBS for 1 hour at room temperature to block non-specific binding sites. Wells in plates were emptied and washed three times in wash buffer. 100 µl of chicken (or mouse) anti-recombinant 56 kDa or chicken anti-APGA serum diluted in ELISA buffer 2 (0.3 % Tween-20, 0.02% NaN_3, 0.05% bovine hemoglobin in PBS; 1:100 dilution) were added to the corresponding wells and incubated at 37°C for 2 hours. The plates were washed as above, followed by incubation with 100 µl of anti-chicken or anti-mouse IgG alkaline phosphatase conjugated antibodies (Sigma) diluted in ELISA buffer 2 at 37°C for 2 hours. The plates were washed as above and 100 µl of substrate (1 mg/ml p-nitrophenyl phosphate) diluted in ELISA buffer 3 (0.1 M carbonate/bicarbonate buffer pH 9.8, 2 mM $MgCl_2$) was added and incubated at 37°C for 10-15 minutes. The optical densities were measured at 405 nm after 10-15 minutes incubation.

2.2.16 Secondary structure analysis of pETEmGam56.102-225 by CD

The recombinant protein, pETEmGam56.102-225, (at a concentration of 0.2 mg/ml), previously desalted and buffer exchanged in 50 mM sodium phosphate buffer pH 6.8, was used for this analysis. The protein was centrifuged at 12,000 g for 3 minutes to remove any aggregated matter and 200 µl of the supernatant was loaded into a cell (Starma Pty Ltd, Australia) with a path length of 1 mm. Secondary structure of the recombinant protein was determined by circular dichroism (CD) according to Feng *et al.* (2005) with the help from Andrew Mynott and Dr Paul Curmi at the University of New South Wales. The spectrum was recorded at a wavelength range of 190 to 260 nm under nitrogen gas at a flow rate of 5 lpm using a Jasco Model J-800 spectropolarimeter. A control sample containing 50 mM sodium phosphate buffer pH 6.8 was also analyzed by CD as a blank (background) for this experiment. Each analysis accumulated three scans and spectrum was presented as an

average of these scans. Three analyses were carried out and the spectrum representing the 50 mM sodium phosphate buffer was subtracted from that of pETEmGam56.102-225.

2.2.17 Structural analysis of pETEmGam56.102-225 by 1D-NMR

Purified pETEmGam56.102-225 was desalted using a PD-10 column and then eluted in 3.5 ml of 50 mM sodium phosphate buffer pH 6.8. The sample for 1D-NMR was concentrated using a centrifugation concentrator (Vivaspin500 with a 3,000 Da molecular weight cut-off), followed by centrifugation at 15,000 g for 10 minutes and the final protein concentration was ~1.5 mg/ml. Structural analysis of the recombinant protein by 1D-NMR was carried out according to Feng *et al.* (2005) with the help from Dr Xuecheng Zhang, Dr Zhi-Ping Feng and Professor Ray Norton at the Walter and Eliza Hall Institute of Medical Research. Before the NMR spectrum was recorded, 5% D_2O was added and then the sample was spun at 16,000 xg for 10 minutes to remove precipitation of proteins or aggregated matter. 1D NMR spectrum was recorded on a Burker DRX600 spectrometer at 298 K and processed using TOPSPIN (Version 1.3, Bruker Biospin).

2.2.18 *In vitro* crosslinking of r56

Purified r56 proteins from section 2.2.10 were used for *in vitro* crosslinking assays by modifying a protocol described by Malencik and Anderson (1996). Each sample contained: 5 μg of r56 proteins; 0.1, 0.2 or 0.25 μg of exogenous peroxidase such as horseradish peroxidase (HRPO), arthromyces peroxidase (APx) or myeloperoxidase (MPx); and 1% v/v *tertiary*-butylhydroperoxide (*t*-BHP; final concentration) in a total volume of 100 μl. The reaction was carried out in 0.25 M sodium borate buffer pH 8.35 at 37°C in a water bath for 0, 5, 10, 20, 30, 40, 50 or 60 minutes. Samples in the absence of peroxidase or peroxide were also included as negative controls for this experiment.

For dityrosine measurement, each sample contained 120 μg of r56 proteins, 6 μg of peroxidase (HRPO, APx or MPx) and 30.5 μl of *t*-BHP or 100 μl of H_2O_2 (peroxide in a final concentration of 1%) in a total volume of 3 ml. The reaction was carried out at 37°C in a water bath for 50 minutes. The crosslinked proteins were analyzed by immunoblotting,

followed by ECL using mouse anti-recombinant 56 kDa antibodies (mouse anti-r56 antibodies).

The effect of the three inhibitors, salicylhydroxamic acid (SHA), phenylhydrazine hydrochloride (PH) and 3'-amino-1, 2, 4-triazole (3'AT), on r56 crosslinking was also investigated. All crosslinking samples were prepared as described above and the inhibitors (SHA, PH, or 3'AT) were added to the sample at a concentration range from 0.1 mM, 0.5 mM, 1 mM, 1.5 mM up to 2 mM. Samples without inhibitors were also included as negative controls for this study. The samples were analyzed by immunoblotting, followed by ECL using mouse anti-r56 antibodies.

Purified r56 (5 μg) from section 2.2.10 was also treated with catalase to a final concentration of 0.05 mg/ml in order to eliminate endogenous peroxide in the sample (catalase catalyzes decomposition of hydrogen peroxide into water and oxygen). The reaction was carried out at 37°C for 50 minutes The sample was then left on ice for 10 minutes to cool down and crosslinking assays were performed as described above using APx and *t*-BHP. The crosslinked proteins were analyzed by immunoblotting, followed by ECL using mouse anti-r56 antibodies.

2.2.19 Detection of high molecular weight oligomers by ECL

Crosslinked samples prepared from section 2.2.18 were analyzed by immunoblotting (ECL). 20 μl of 4x SDS-PAGE sample buffer was added to a crosslinked sample (100 μl) and boiled for 3 minutes followed by centrifugation at 12, 000 g for 2 minutes at room temperature. 20 μl of each sample and 5 μl of pre-stained protein ladder (Invitrogen™) were separated on a 12% polyacrylamide gel as described in section 2.2.12. The proteins from the gel were then transferred to a PVDF membrane as described in section 2.2.14. The membrane was blocked in 5% skim milk/PBS over night at 4°C. The next day, mouse anti-r56 antibodies diluted in 5% skim milk/PBS (1 in 1000 dilution) were used to probe the membrane on a rotating wheel for 1-2 hours at room temperature. The membrane was washed with three changes of 0.03% Tween-20/PBS for 30 minutes, and then incubated with a secondary antibody, anti-mouse IgG horseradish peroxidase conjugate (diluted in 5% skim milk/PBS; 1 in 1000 dilution),

followed by another three washes as above. The membrane was soaked in ECL reagent mix (ECL reagent 1 and 2 in a ratio of 1 to 1; GE Healthcare, Australia) for 1 minute and then the membrane was exposed for 1, 3 or 5 minutes (or until the protein bands of interest were visible) using ChemiDoc system according to the instructions of the manufacturer, Bio-Rad.

2.2.20 Detection of dityrosine by HPLC

Dityrosine from protein samples was measured by HPLC according to Belli *et al.* (2003b) with the assistance from Dr Cathy Luxford and Dr Michael Davies at Heart Research Institute, Sydney. Protein samples were transferred to brown glass autosampler vials and treated with 1 mg of sodium borohydride per ml, 0.03% sodium deoxycholate, and 50% (w/v) TCA, followed by centrifugation at 4,000 g for 2 minutes. The pellets were washed twice with cold acetone and freeze-dried. The vials were then transferred to Pico-Tag reaction vials containing 1 ml of 6 M HCl and 50 µl of mercaptoacetic acid, followed by evacuation to remove oxygen in the sample. The samples were then incubated at 110°C for 16 hours to hydrolyze proteins. The hydrolysate was then freeze-dried and redissolved in 200 µl of distilled water. The samples were then injected into a Sorbax octydecyl silane column with a flow rate of 1 ml/min. Standards such as *p*-tyrosine, *m*-tyrosine, *o*-tyrosine, and dityrosine were also analyzed by HPLC to monitor the separation. The presence of dityrosine was detected by serial UV-visible and fluorescence detectors. Quantification of dityrosines was performed by measuring fluorescence at an excitation wavelength of 280 nm and an emission wavelength of 320 nm whereas parent-tyrosines (p-tyr) were quantified by UV absorbance. This was done by comparing peak areas of protein samples to an appropriate standard curves/peaks constructed with authentic materials. The level of dityrosine expressed in a ratio of dityrosine over p-tyrosine (millimole of dityrosine per mole of p-tyrosine) was the average of four measurements (n= 4) with errors representing standard deviation.

Chapter Three

The Composition of the Oocyst Walls of *Eimeria tenella* and *Eimeria maxima*

3.1 Introduction

The oocyst wall of *Eimeria* protects it from potentially harsh conditions encountered during excretion in the faeces of the host and in the external environment; it helps ensure the survival and successful transmission of these parasites. It is generally agreed that the oocyst wall of *Eimeria* consists of two layers (an inner layer or endocyst and an outer layer or ectocyst) containing lipids and glycoproteins. However, the descriptions of the structure of the oocyst wall, and its biochemical composition, reported in the literature are quite discrepant; even the effect of sodium hypochlorite treatment on the oocyst wall of *E. maxima* and *E. tenella* appears controversial.

The first serious microscopic examination of the oocyst wall (of *E. maxima*) was conducted by Monné and Hőnig (1954), who used a number of destructive treatments that led them to conclude that the outer layer of the oocyst wall contained mainly quinone-tanned proteins without lipids because the outer layer reacted with ammoniacal silver nitrate solution (an indication of quinones). They also noted that the outer layer was stripped off upon exposure to sodium hypochlorite, whereas the structure of the inner layer remained unchanged, leading them to conclude that the inner layer consisted of a lipid-protein matrix; they believed that lipids were firmly bound to proteins, thus protecting the inner layer against the disintegrating effect of sodium hypochlorite.

The first biochemical examination of the oocyst walls was carried out by Ryley in 1973 using *E. tenella.* Ryley also noted that the ectocyst was removed by sodium hypochlorite and found that it contained carbohydrates and proteins, with high proline content, whereas the endocyst consisted of 1.5% carbohydrates, 30% lipids and 70% proteins. The lipid in the endocyst was extractable in chloroform and appeared to be a mixture of "waxes" containing very small amounts of nitrogen and phosphorus (Ryley, 1973). However, there are some limitations in this report: first, it showed no experimental work (analyses) in detail; and, second, it did not document the metabolites detected in the endocyst.

The most recent biochemical analysis of the oocyst wall was conducted by Stotish *et al.* in 1978 using unsporulated oocysts isolated from the caeca of chickens infected with *E. tenella.* These researchers proposed that lipids were concentrated in the outer layer whereas the inner layer was composed of mainly glycoproteins. In addition, compositional analysis of the oocyst wall by gas-liquid chromatography and SDS-PAGE electrophoresis indicated that it was 19% carbohydrates, 14% lipids and 67% peptides (Stotish *et al.*, 1978). Lipids identified from the walls included a number of fatty alcohols, steroids and fatty acids such as docosanol, tetracosanol, hexacosanol, myristate, palmitate, stearate, oleate, linoleate, and phospholipids. Protein content in the oocyst wall consisted of a repeating subunit of ~10 kDa. Four carbohydrates - mannose, galactose, glucose and hexosamine – were detected. However, some doubts surround the validity of these conclusions because Stotish *et al.* noted that sodium hypochlorite treatment *did not* affect the structure of the oocyst walls from *E. tenella* unsporulated oocysts since the oocyst wall remained intact (bi-layered) and this was a major basis for their conclusion that lipids are concentrated in the outer layer of the wall (since lipids would be expected to give some protection against stripping by sodium hypochlorite). In direct contradiction to the observations of Stotish *et al.* it has been shown that sodium hypochlorite treatment *does* have an effect on the structure of the oocyst wall in both *E. maxima* and *E. tenella* - the outer layer is stripped off (Monné and Hőnig, 1954; Nyberg *et al.*, 1968; Nyberg and Knapp, 1970; Ryley, 1973; Belli *et al.*, 2006). Therefore, the biochemical compositions assigned to the two layers of the oocyst wall of *E. tenella* by Stotish *et al.* could be erroneous and need to be reinvestigated using more reliable, sensitive modern methods.

The research described in this chapter aims to:
(1) investigate the effect of sodium hypochlorite on the oocyst walls of *E. tenella* and *E. maxima* sporulated and unsporulated oocysts, confirming the purity of isolated wall preparations (ie, freedom from contamination with internal oocyst contents or extraneous matter) and the presence of one or two layers by transmission electron microscopy (TEM); and (2) determine the oocyst wall composition of sporulated and unsporulated oocysts of *E. tenella* and *E. maxima* using the latest gas chromatography (GC) and mass spectrometry (MS) protocols (GC plus MS is more accurate than GC alone – as used by

Stotish *et al.* – because the MS step confirms the identity of any metabolites identified by GC and thereby eliminates false positives).

A flow chart for the experimental approach followed in this chapter is presented as Figure 3.1. Briefly, oocyst walls were isolated from sporulated or unsporulated oocysts by sonication and density sucrose centrifugation, as originally described by Stotish *et al.* (1978). The oocyst walls were then hydrolyzed by one of two methods, methanolysis and acid hydrolysis, followed by GC and MS, in parallel with examination of the oocyst walls by TEM to confirm the presence or absence of bi-layered walls.

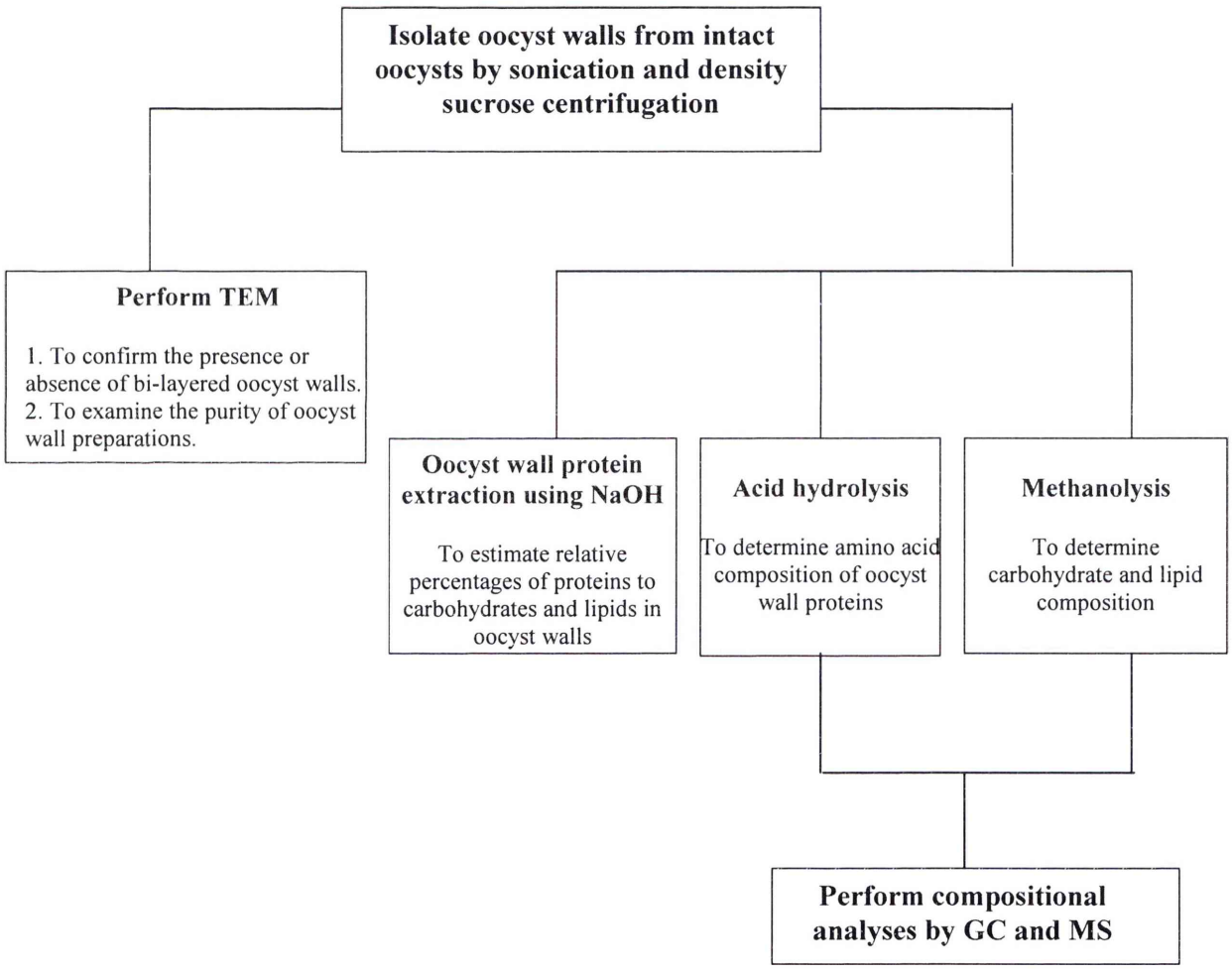

Figure 3.1 Experimental plans for the study carried out in this chapter.

3.2 Microscopic and TEM examination of oocyst walls prepared as per Stotish *et al.* (1978) revealed contamination with polysaccharide granules

Oocysts of *E. tenella* and *E. maxima* were purified as described in Chapter 2, Section 2.2.1. Half the population of the oocysts was bleached and the other half left unbleached. Oocyst walls were isolated from the intact oocysts according to the protocol of Stotish *et al.* (1978) by sonication and density sucrose centrifugation as described in Chapter 2, Section 2.2.2. The natural blue UV autofluorescence of oocysts (Figure 3.2 B) was used to monitor purification and integrity of the oocyst wall preparations.

Sonication caused the lysis of oocysts as shown in Figure 3.2 C and D. The purified oocyst walls appeared as long strips under bright field (Figure 3.2 E and G) and autofluoresced blue under UV light (Figure 3.2 F and H). When oocyst walls were examined under higher magnification (100x), small non-fluorescent particles were observed (Figure 3.2 G and H), which could be contaminants from the internal contents of the oocysts. The oocyst walls were, therefore further analyzed by TEM, which allows visualization of samples down to nanometers. The TEM images confirmed that the oocyst walls appeared as long strips (Figure 3.3 B) but also identified some in spiral form (Figure 3.3 C and D). The contaminants observed under light microscopy could be identified as polysaccharide granules (PG) by TEM (personal communication, Professor David Ferguson, University of Oxford) because of their characteristic round shaped structure (Figure 3.3 A-D).

Contamination with polysaccharide granules appears likely to be due to adherence of the granules to the oocyst walls (Figure 3.3 C, see areas highlighted with arrows) and, hence, they were co-purified with the walls by sucrose centrifugation. Polysaccharide granule contamination would interfere with compositional analyses of the oocyst walls. Therefore, methods to eliminate polysaccharide granules, without altering the structure of oocyst walls, were investigated.

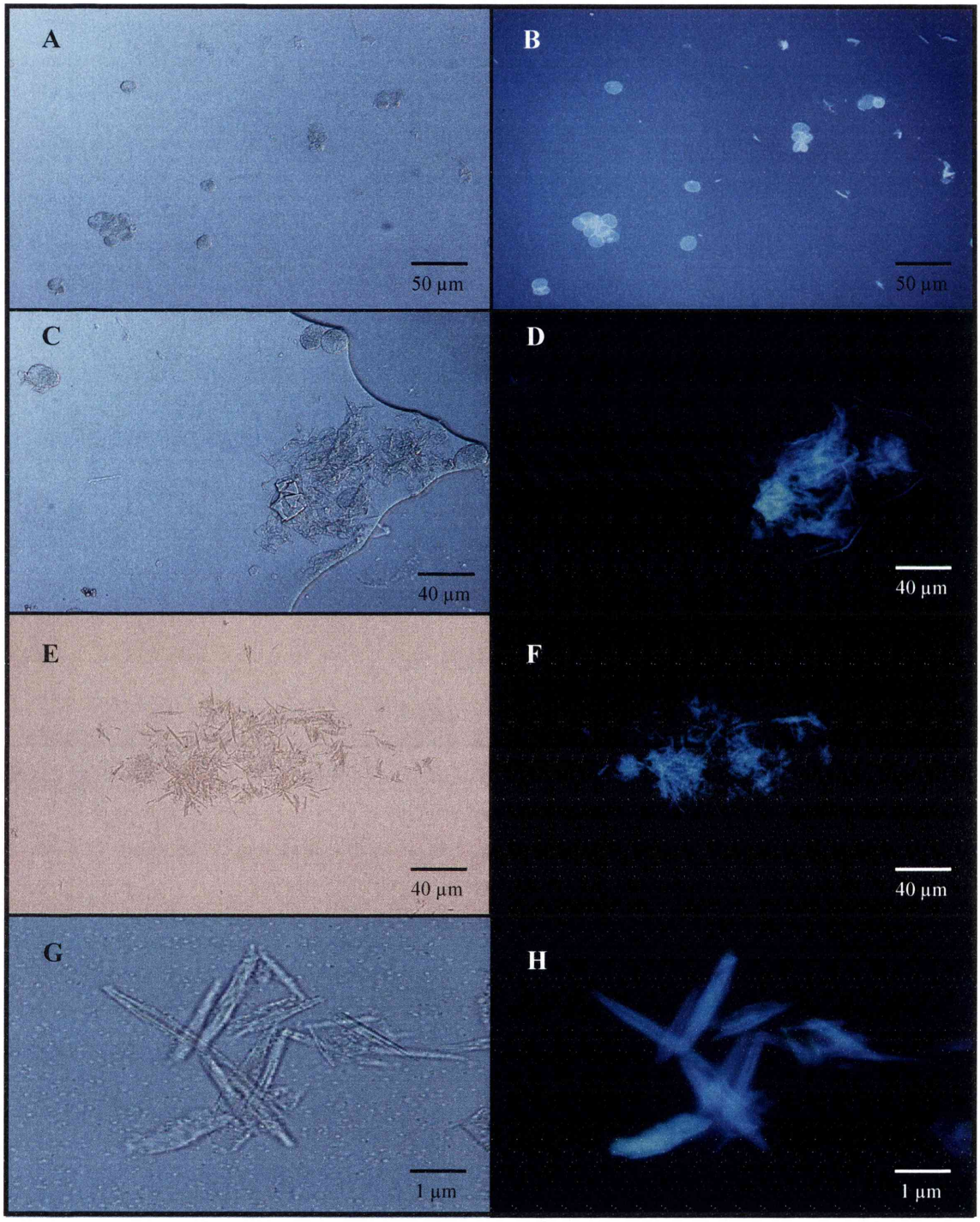

Figure 3.2 Microscopic examination of oocyst walls before and after purification by density sucrose centrifugation. *E. maxima* bleached unsporulated oocysts under bright field (A) and UV light (B) in 20 x magnification. Lysed oocysts after sonication under bright field (C) and UV light (D) in 40x magnification. Purified oocyst walls after sucrose centrifugation under bright field (E) and UV light (F) in 40x magnification; (G) and (H) in 100x magnification.

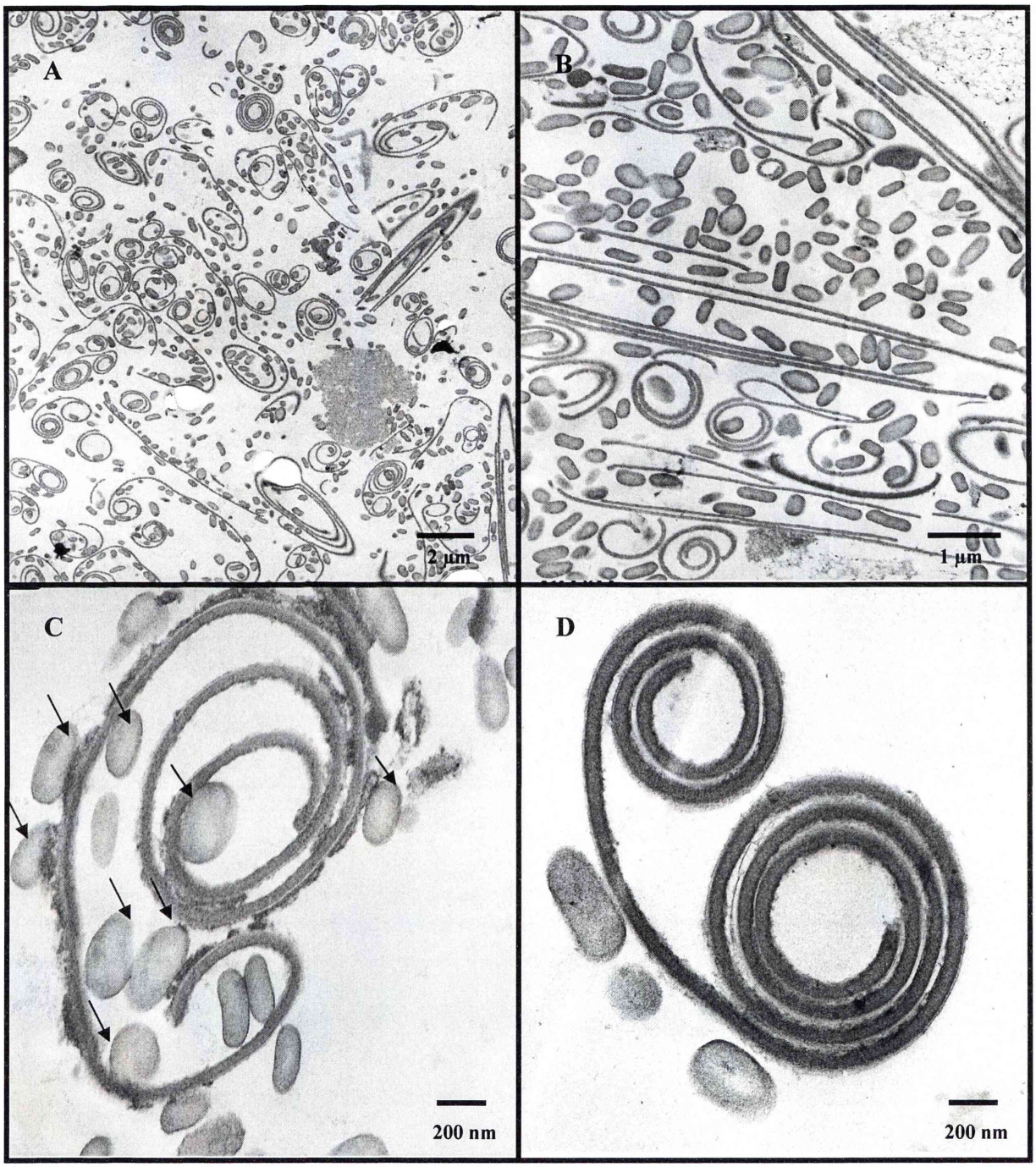

Figure 3.3 Electron microscopic images of purified oocyst walls from *E. maxima* bleached unsporulated oocysts. Oocyst walls under lower magnification (A and B) and higher magnification (C and D). The round shaped structures present in the oocyst wall preparations (A, B, C and D) are polysaccharide granules (as highlighted in C with arrows).

3.3 Elimination of polysaccharide granules from oocyst wall preparations

Polysaccharide granules found in the oocysts of apicomplexan parasites such as *Eimeria*, *Toxoplasma* and *Crytosporidium* are well known to be composed almost exclusively of amylopectin, a highly branched polysaccharide found commonly in plants (Ryley *et al.*, 1969; Coppin *et al.*, 2003; Harris *et al.*, 2004). Amylopectin is one of two components of starch, and exists as a polymer consisting entirely of glucose monomers joined by alpha-1, 4, linkages (Ryley *et al.*, 1969). Two methods for hydrolysis of polysaccharide granules - heat and enzyme treatment (using alpha-amylase) - were investigated.

The optimal time for heat treatment and the optimal concentration of alpha-amylase for the hydrolysis of polysaccharide granules were investigated. Briefly, the oocyst walls isolated from $2x10^6$ *E. maxima* unsporulated oocysts were resuspended in 100 µl of distilled water and boiled for 5 minutes and 10 minutes for comparison (as described in more detail in Chapter 2, Section 2.2.3). For enzyme treatment, alpha-amylase (from barley malt purchased from Sigma, one unit of alpha-amylase will liberate 1 mg of maltose from starch in 3 min at pH 6.9 at 20°C) was added to a final concentration of 0.5 mg/ml and 1 mg/ml for comparison (as described in more detail in Chapter 2, Section 2.2.3). A negative control contained the same amount of oocyst walls without heat treatment or in the absence of alpha-amylase. The oocyst walls were examined by TEM and light microscopy.

Polysaccharide granules were hydrolyzed by heat treatment as indicated by the loss of their distinctive shape (Figure 3.4 C and D). However, the oocyst walls appeared to adhere to each other, perhaps due to the stickiness of the hydrolyzed polysaccharide granules in the sample boiled for 5 minutes (Figure 3.4 C, area with arrows). Even after increasing the boiling time to 10 minutes, contamination with polysaccharide granules was still observed in the oocyst wall preparations (Figure 3.4 D). Hence, heat treatment failed to remove polysaccharide granules from oocyst wall preparations.

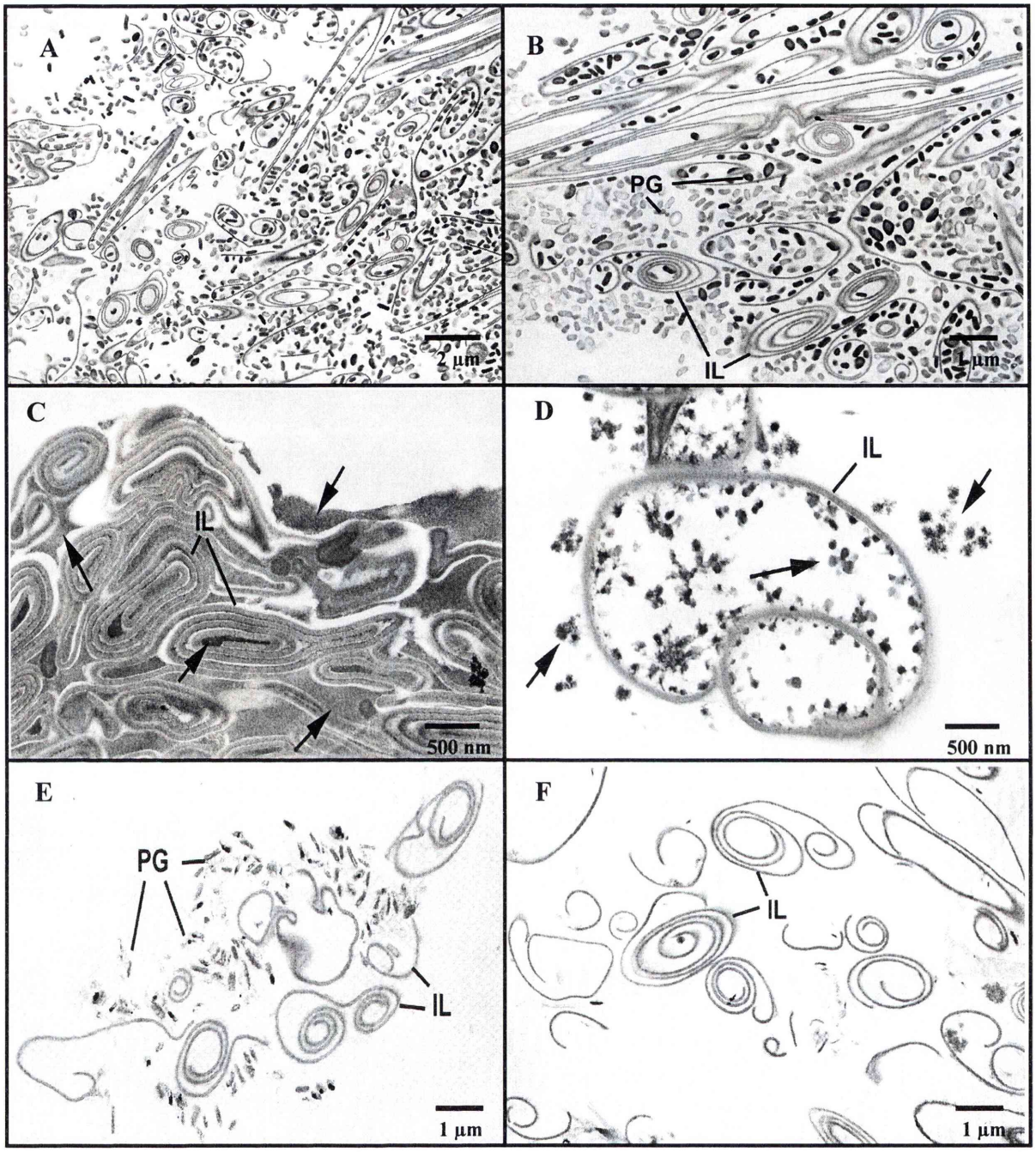

Figure 3.4 Electron microscopic images of heat and alpha-amylase treated oocyst walls prepared from *E. maxima* bleached unsporulated oocysts. Each sample contained oocyst walls equivalent to $2x10^6$ *E. maxima* unsporulated oocysts in the absence of heat treatment or alpha-amylase (A and B); heat treated wall preparations either boiled for 5 minutes (C) or 10 minutes (D); treated with alpha-amylase to a final concentration of 0.5 mg/ml (E) or 1 mg/ml (F). PG= polysaccharide granules. IL= inner layer of oocyst walls. Arrows indicate hydrolyzed polysaccharide granules, which in (C) appear to have glued the oocyst walls together.

In contrast, when alpha-amylase was added to the oocyst walls, polysaccharide granules were reduced remarkably, as shown in the sample treated with 0.5 mg/ml alpha-amylase (Figure 3.4 E and Figure 3.5 B) and, more especially, in the sample treated with 1 mg/ml alpha-amylase (Figure 3.4 F and Figure 3.5 C). Examination by light and UV microscopy confirmed the characteristic blue autofluorescence of the purified oocyst walls after alpha-amylase treatment (Figure 3.5 D), indicating that the basic chemical structure of the walls was not significantly altered by the treatment.

There were some residual undigested polysaccharide granules observed in the sample treated with 0.5 mg/ml alpha-amylase (Figure 3.4 E and Figure 3.5 B, highlighted by arrows), suggesting that the higher concentration (1 mg/ml) is a better choice to degrade polysaccharide granules in the given amount of the oocyst walls.

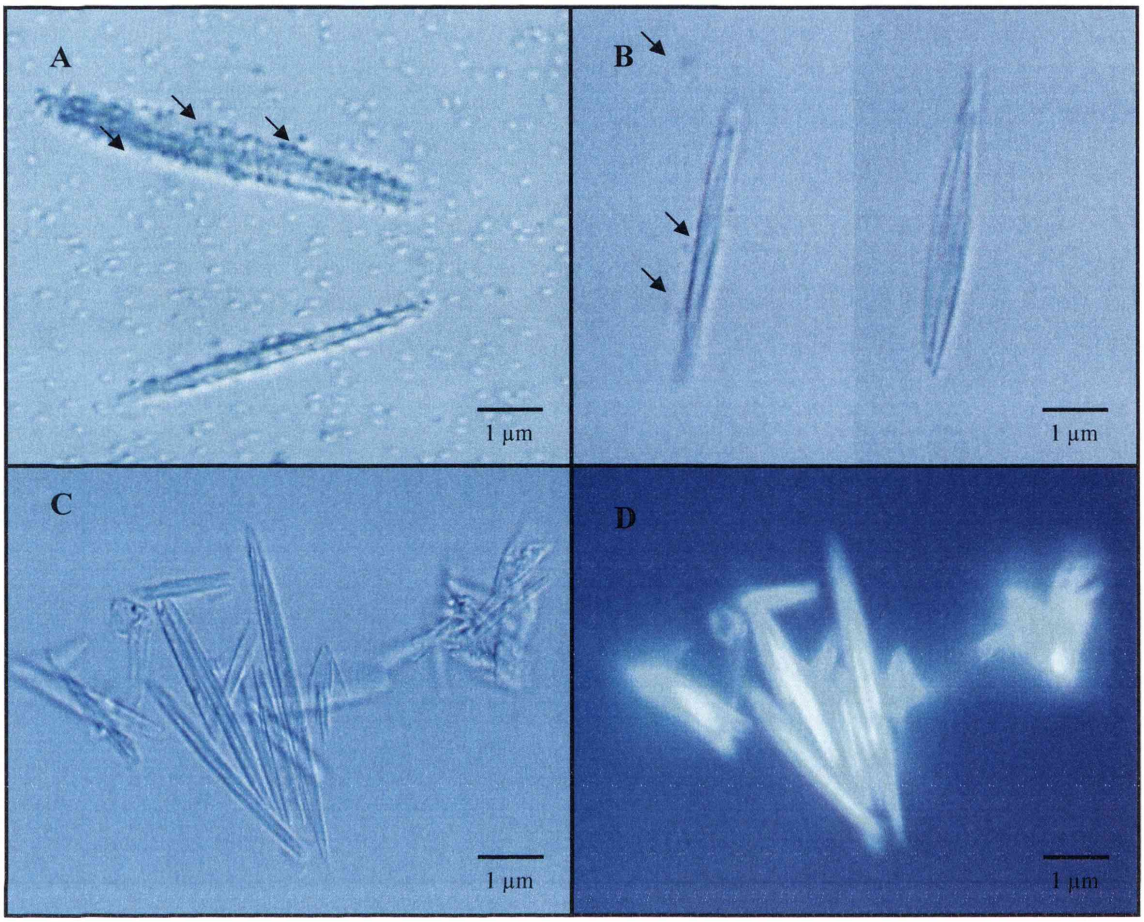

Figure 3.5 Microscopic images of alpha-amylase treated oocyst walls from *E. maxima* bleached unsporulated oocysts. Oocysts walls in the absence of alpha-amylase (A); treated with alpha-amylase to a final concentration of 0.5 mg/ml (B) and 1 mg/ml (C= bright field; D= under UV light). Iodine was added to each sample, followed by microscopic examination under 100x magnifications. Polysaccharide granules lit up by iodine were abundant throughout the sample (A). Area with arrows indicates polysaccharide granules.

3.4 The effect of sodium hypochlorite on the bi-layered structure of the oocyst wall

The oocyst walls prepared from *E. tenella* and *E. maxima* sporulated and unsporulated oocysts were examined by TEM as described in Chapter 2, Section 2.2.4 to confirm the presence of the inner and/or outer layers of the oocyst walls. The outer layer of the oocyst walls (both *E. tenella* and *E. maxima*) appeared electron-dense, with a roughened appearance on the outer surface, and the inner layer was electron-lucent, observations that are consistent with those of Ferguson *et al.* (2003). In general, the oocyst walls from unbleached samples remained intact (retaining a bi-layered structure) whereas in bleached samples, only the inner layer was seen (Figure 3.6), confirming the observations that bleaching does strip the outer layer of oocyst walls (Monné and Hőnig, 1954; Nyberg *et al.*, 1968; Nyberg and Knapp, 1970; Ryley, 1973; Belli *et al.*, 2006). There was a single exception to this pattern; walls prepared from a sample of bleached *E. tenella* sporulated oocysts remained intact as a bi-layered structure (Figure 3.6 B). This was not always observed and the reason for this exception is not known. However, this exceptional sample proved very useful in subsequent comparisons of wall composition.

3.5 Oocyst walls of *E. tenella* and *E. maxima* are composed of lipids, carbohydrates and proteins

The purified oocyst walls from the various bleached samples of *E. tenella* and *E. maxima* were hydrolyzed using two methods, methanolysis (0.5 M HCl in methanol) and acid hydrolysis (6N HCl), as described in Chapter 2, Section 2.2.5. The hydrolysates of the oocyst walls were then analyzed by GC and MS to determine the levels of carbohydrates and lipids within the oocyst walls. Some samples were also extracted with NaOH to allow determination of relative levels of proteins to lipids and carbohydrates in the samples. Unfortunately, unbleached samples could not be analysed due to the presence of various contaminants that were incompatible with the machinery and would, in any case, distort the analyses.

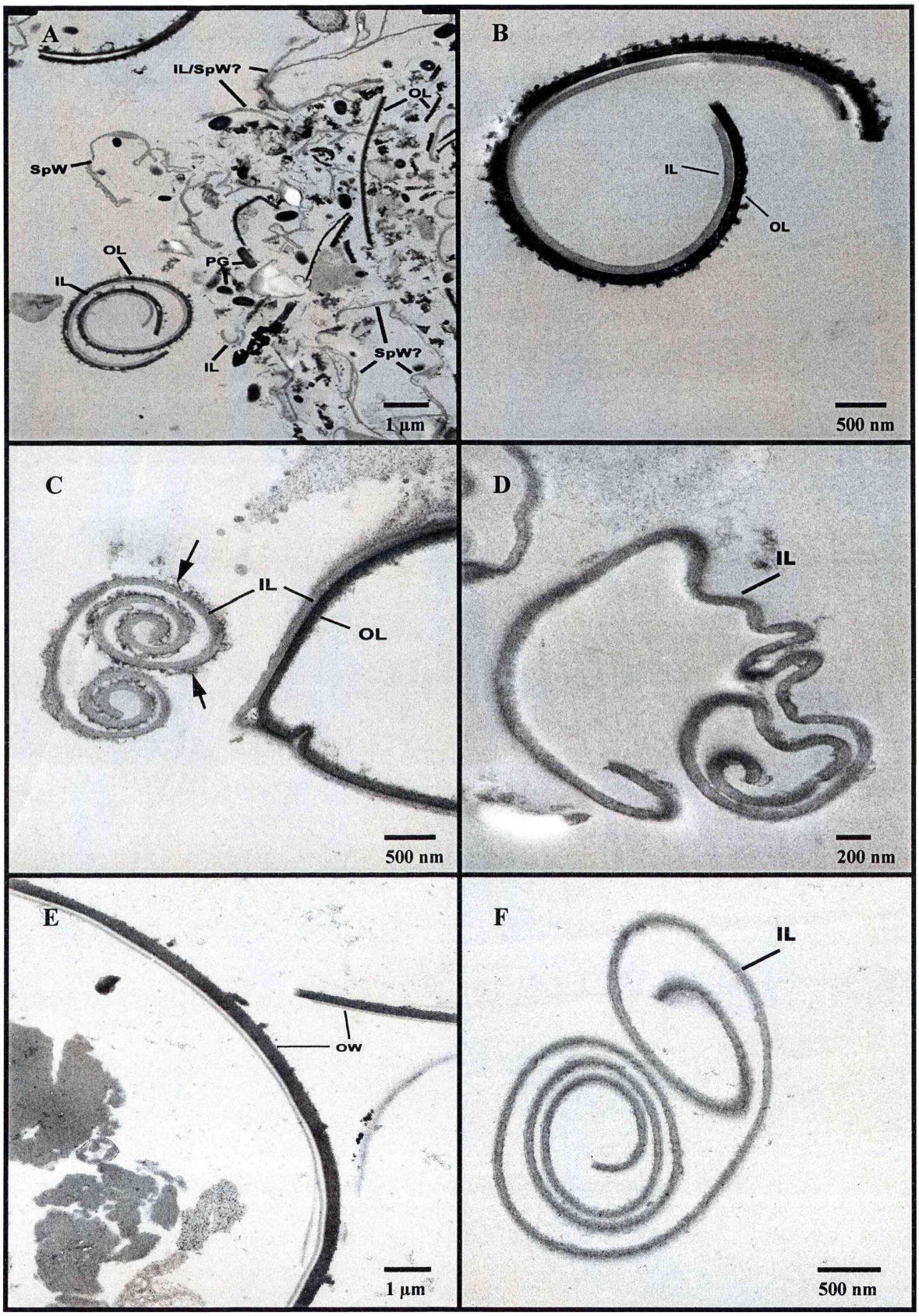

Figure 3.6 Electron microscopic images of oocyst wall preparations from *E. tenella* and *E. maxima* (Continued…).

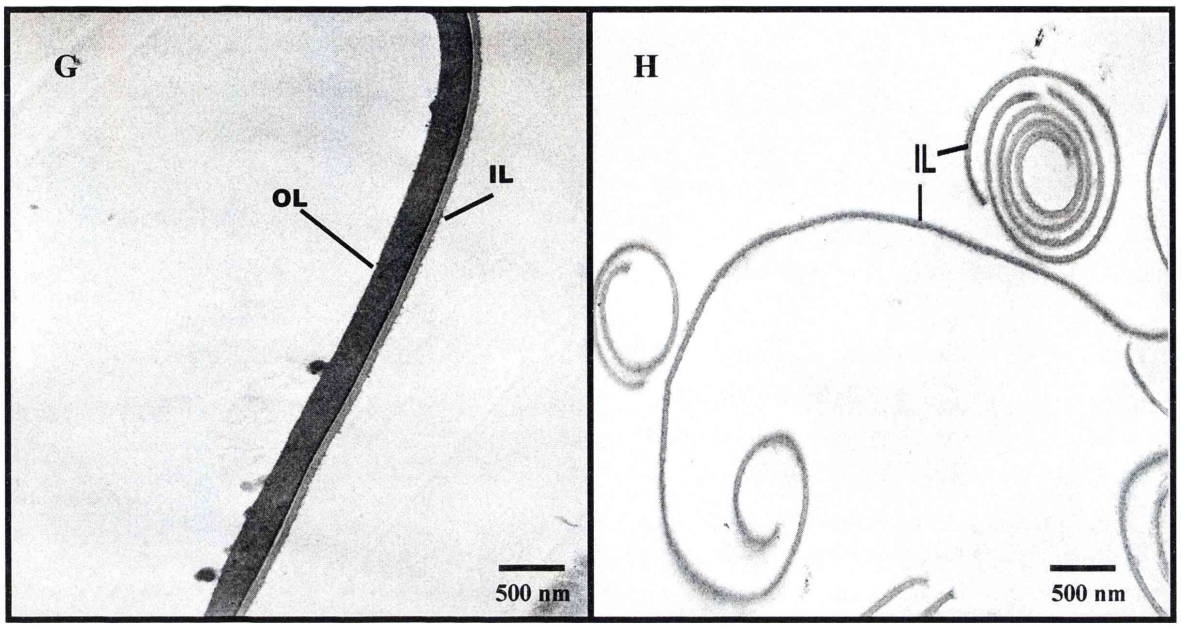

Figure 3.6 Electron microscopic images of oocyst wall preparations from *E. tenella* and *E. maxima* unbleached versus bleached sporulated versus unsporulated oocysts. A and B = *E. tenella* unbleached and bleached sporulated oocyst walls, respectively. C and D = *E. tenella* unbleached and bleached unsporulated oocyst walls, respectively. E and F = *E. maxima* unbleached and bleached sporulated oocyst walls, respectively. G and H = *E. maxima* unbleached and bleached unsporulated oocyst walls, respectively. OL= outer layer of oocyst wall. IL= inner layer of oocyst wall. PG= polysaccharide granules. SpW= sporocyst walls. OW= oocyst walls.

The concentration of carbohydrates and lipids was determined from GC and MS profiles (reproduced in the appendices of this thesis) and protein concentration was determined as described in Chapter 2, Section 2.2.6. The oocyst wall contents were then converted into percentage contributions (by weight in μg). These analyses revealed remarkable similarities between all the samples (Table 3.1 A and B). Thus, the compositions, on a percentage w/w basis, for carbohydrate, lipid and protein were contained in relatively narrow ranges of 0.6-2.0% carbohydrate, 1.4-7.6% lipid and 90.4-98.3% protein, for unsporulated or sporulated oocysts, from *E. tenella* or *E. maxima.* It is perhaps noteworthy, however, that the lower values for carbohydrates and lipids were seen in the sporulated oocyst samples from both *E. tenella* and *E. maxima.* This indicates that the single bilayered oocyst wall sample (the sporulated oocysts of *E. tenella*) did not exhibit a distinctly different composition than the single layered sporulated oocyst wall sample from *E. maxima.* In contrast to these results, however, the percentages of carbohydrate, lipid and protein reported by Stotish *et al.* (1978) for unsporulated oocysts of *E. tenella* are radically different with only 67% protein and 19% carbohydrate and 14% lipid being recorded (Table 3.1 C).

Analysis of 6N HCl hydrolysates of the oocyst walls of *E. tenella* and *E. maxima* revealed that essentially all twenty amino acids are present in the walls of sporulated and unsporulated oocysts as, indeed, they are in EmGam56 and EmGam82 though, in some sample runs, certain lower abundance amino acids were not detected (such as histidine and cystine; see appendices for profiles). The percentage contribution of each individual amino acid to the total protein content of the oocyst wall could not be determined with certainty. This is due to a problem with derivatisation of wall samples. For example, multiple peaks (instead of one consistent peak) representing each of amino acids glycine, serine, phenylalanine and tyrosine were seen from GC and MS profiles of all wall samples due to the presence of either one, two or three trimethylsilyl residues. Thus, these amino acids could not be quantified accurately.

However, a limited qualitative comparison of five of the more abundant amino acids, isoleucine (Ile), aspartic acid (Asp), valine (Val), proline (Pro) and arginine (Arg) was possible by assigning Ile a standardized value of 1.0 and presenting the other four amino acids as a ratio of this (Table 3.2). It is important to not over interpret this data; it provides a limited snapshot of the relative order of abundance of these five amino acids but the ratio values presented probably do not very precisely reflect their abundance. When examined in this way, the relative abundance of the amino acids is similar in all the samples, whether *E. tenella* or *E. maxima,* unsporulated or sporulated oocysts, and is in the order Ala>Pro>Val>Asp>Ile. The only slight exception to this is the sporulated oocyst sample of *E. maxima,* where Asp and Val are reversed, but marginally. The results of Stotish *et al.* (1978) are in accord with these observations (Table 3.2). In the cases of full length EmGam56 or EmGam82, Pro is more abundant than Ala, however, the predicted composition of the recombinant EmGam56, which lacks the proline-rich C-terminal of the full length protein, has the same order of abundance – ie, Ala>Pro>Val>Asp>Ile – as the analysed oocyst wall samples (Table 3.2).

Table 3.1 Summary of oocyst wall contents in percentages of metabolites (w/w) from oocyst walls prepared from 10^6 *E. tenella* sporulated and unsporulated oocysts (A), *E. maxima* sporulated and unsporulated oocysts (B) and *E. tenella* unsporulated oocysts from Stotish *et al.* (1978) (C). S/O= sporulated oocysts. U/O= unsporulated oocysts.

A. *E. tenella* oocyst walls % of metabolites (w/w)			
Metabolites / Samples	**Carbohydrates**	**Lipids**	**Proteins**
Walls from S/O	0.6%	1.6%	97.8%
Walls from U/O	1%	4.4%	94.6%
B. *E. maxima* oocyst walls			
Metabolites / Samples	**Carbohydrates**	**Lipids**	**Proteins**
Walls from S/O	0.3%	1.4%	98.3%
Walls from U/O	2.0%	7.6%	90.4%
C. *E. tenella* from Stotish *et al.* (1978)			
Metabolites / Samples	**Carbohydrates**	**Lipids**	**Proteins**
Walls from U/O	19%	14%	67%

Table 3.2 Summary of amino acid compositions of oocyst wall proteins prepared from 10^6 *E. tenella* sporulated and unsporulated oocysts (A), *E. maxima* sporulated and unsporulated oocysts (B), *E. tenella* unsporulated oocysts from Stotish *et al.* (1978) (C) and gametocyte antigens from *E. maxima* (D). S/O = sporulated oocysts. U/O = unsporulated oocysts. The amino acids (Ala, Val, Pro, Ile and Asp) are presented in simplified ratio standardised against Ile, which receives a standardised value of 1.

Amino acid composition of oocyst wall proteins of *E. tenella* and *E. maxima*					
Amino acid residue / Samples	Ile	Asp	Val	Pro	Ala
A. *E. tenella* oocyst walls					
Walls from S/O	1	2.0	3.6	4.3	5.8
Walls from U/O	1	1.3	6.1	7.3	7.3
B. *E. maxima* oocyst walls					
Walls from S/O	1	2.1	1.4	2.2	2.8
Walls from U/O	1	0.7	1.4	2.3	3.0
C. *E. tenella* from Stotish *et al.* (1978)					
Walls from U/O	1	3.6	9.2	11	11
D. Gametocyte antigens from *E. maxima**					
EmGam56	1	1.7	2.2	6.7	4.2
r56[#]	1	2.3	2.5	4.4	4.7
EmGam82	1	2.1	4.5	8.9	8.0

*Protein sequence of EmGam56 and EmGam82 were extracted from Belli *et al.*, 2002a; [#]r56 represents a recombinant version of EmGam56, lacking the proline-rich C-terminal region.

The lipid composition of the oocyst walls of *E. tenella* and *E. maxima* was determined by methanolysis (in 0.5M HCl in methanol), followed by GC and MS analysis (profiles reproduced in the appendices of this thesis). Sporulated oocysts of both species contained a number of fatty acids (saponifiable lipids) including palmitic acid (C16:0), stearic acid (C18:0), oleic acid (C18:1), linoleic acid (C18:2), behenic acid (C22:0), lignoceric acid (C24:0) (Table 3.3 A and B). Non-saponifiable lipids such as cholestadiene, cholestane, and cholesterol were also detected. Most of these were present in a similar w/w percentage in the two species except that the bilayered *E. tenella* sample was comprised of 44.7% oleic acid whereas the *E. maxima* sample was only 19.5% oleic acid. The *E. tenella* sample also had higher quantities of palmitic acid (13.2% versus 5.9% in *E. maxima).* In apparent compensation of these differences, walls from *E. tenella* sporulated oocysts had lower relative percentages of linoleic acid (2.1% in *E. tenella* versus 8.2% in *E. maxima*), lignoceric acid (1.8% versus 5.4%) and, especially, cholestane (3.5% versus 11.0%) and cholesterol (12.1% versus 24.2%) than the *E. maxima* sporulated oocyst walls.

The levels of lipids in unsporulated oocysts of *E. tenella* and *E. maxima* were quite similar to each other (Table 3.3 A and B) but differed from the sporulated wall samples in that they totally lacked linoleic acid. The relative levels of oleic acid in the unsporulated oocyst samples resembled that seen in the *E. maxima* sporulated oocyst sample and, so, were also different from the levels apparent in the bilayered *E. tenella* sporulated oocyst sample.

The data from Stotish *et al.* (1978) for lipid composition of unsporulated oocyst walls of *E. tenella* (Table 3.3 C) did not resemble the observations made here using GC and MS. First, the samples analysed by Stotish *et al.* (1978) contained no behenic acid, lignoceric acid, cholestadiene or cholestane. Second, Stotish *et al.* (1978) reported the presence of myristate and phospholipids, as well as several fatty alcohols (docosanol, tetracosanol, hexacosanol, octacosanol and triacosanol) not detected here; Stotish *et al.* (1978) reported hexacosanol and phospholipids as being especially abundant (Table 3.3 C).

Table 3.3 Summary of metabolites of lipids in percentages from oocyst walls prepared from 10^6 *E. tenella* sporulated and unsporulated oocysts (A), *E. maxima* sporulated and unsporulated oocysts (B) and *E. tenella* unsporulated oocysts from Stotish *et al.* (1978) (C). S/O = sporulated oocysts. U/O = unsporulated oocysts. Metabolites for fatty acids in blue and pink represent high and low abundances, respectively. Metabolites for nonsaponifiable lipids in green represent high abundance.

A. *E. tenella* oocyst walls % of metabolites (w/w)		
Samples / Lipids	Walls from S/O	Walls from U/O
Palmitic acid (C16:0)	13.2%	13.3%
Stearic acid (C18:0)	13.7%	22.2%
Oleic acid (C18:1)	44.7%	16.1%
Linoleic acid (C18:2)	2.1%	0
Behenic acid (C22:0)	4.5%	9.8%
Lignoceric acid (C24:0)	1.8%	2.9%
Cholestadiene	4.4%	7.2%
Cholestane	3.5%	16.7%
Cholesterol	12.1%	11.8%

Table 3.3 (Continued...) Summary of metabolites of lipids in percentages from oocyst walls prepared from 10^6 *E. tenella* sporulated and unsporulated oocysts (A), *E. maxima* sporulated and unsporulated oocysts (B) and *E. tenella* unsporulated oocysts from Stotish *et al.* (1978) (C). S/O = sporulated oocysts. U/O = unsporulated oocysts. Metabolites for fatty acids in blue and pink represent high and low abundances, respectively. Metabolites for nonsaponifiable lipids in green represent high abundance.

B. *E. maxima* oocyst walls		
Samples / Lipids	Walls from S/O	Walls from U/O
Palmitic acid (C16:0)	5.9%	11.7%
Stearic acid (C18:0)	14.4%	21.4%
Oleic cid (C18:1)	19.5%	18.4%
Linoleic acid (C18:2)	8.2%	0
Behenic acid (C22:0)	6.4%	9.6%
Lignoceric acid (C24:0)	5.4%	10.9%
Cholestadiene	5.0%	6.4%
Cholestane	11.0%	7.0%
Cholesterol	24.2%	14.6%

Table 3.3 (Continued...) Summary of metabolites of lipids in percentages from oocyst walls prepared from 10^6 *E. tenella* sporulated and unsporulated oocysts (A), *E. maxima* sporulated and unsporulated oocysts (B) and *E. tenella* unsporulated oocysts from Stotish *et al.* (1978) (C). S/O = sporulated oocysts. U/O = unsporulated oocysts. Metabolites for fatty acids in blue and pink represent high and low abundances, respectively. Metabolites for nonsaponifiable lipids in green represent high abundance. Area highlighted in grey represents the metabolites absent from GC and MS profile but detected from Stotish *et al.* (1978).

C. *E. tenella* from Stotish *et al.* (1978)	
Samples / Lipids	Walls from U/O
Palmitic acid (C16:0)	2.8%
Stearic acid (C18:0)	11.4%
Oleic acid (C18:1)	10.8%
Linoleic acid (C18:2)	1.1%
Behenic acid (C22:0)	-
Lignoceric acid (C24:0)	-
Cholestadiene	-
Cholestane	-
Cholesterol	5.1%
Docosanol	6.3%
Tetracosanol	1.7%
hexacosanol	31.3%
Octacosanol	2%
Triacosanol	6.8%
Myristate	1.1%
Phospholipids	19.4%

The carbohydrate content of *E. tenella* sporulated oocyst walls was very similar to that of sporulated oocyst walls of *E. maxima* (Table 3.4 A and B), the carbohydrate content being made up of 4.3-5% mannose, 33.7-37.4% galactose and 58.3-61.3% glucose. Likewise, the carbohydrate profile of unsporulated oocyst walls of *E. tenella* was similar to that of unsporulated oocyst walls of *E. maxima* but quite different to that of the sporulated walls, being dominated by galactose (62.3%-67.6%), followed by glucose (26-27.9%) and mannose (6.4-9.8%). The carbohydrate composition of unsporulated oocysts of *E. tenella* reported by Stotish *et al.* (1978) was, however, very different; they reported that the carbohydrate profile of the wall was 79.6% glucose and 11% hexosamine (which was not detected in the GC and MS analysis reported here), and only 7.2% galactose and 2.2% mannose (Table 3.4 C).

Table 3.4 Summary of metabolites of carbohydrates in percentages from oocyst walls prepared from 10^6 *E. tenella* sporulated and unsporulated oocysts (A), *E. maxima* sporulated and unsporulated oocysts (B) and *E. tenella* unsporulated oocysts from Stotish *et al.* (1978) (C). S/O = sporulated oocysts. U/O = unsporulated oocysts.

A. *E. tenella* oocyst walls % of metabolites (w/w)		
Samples / Carbohydrates	Walls from S/O	Walls from U/O
Mannose	4.3%	9.8%
Galactose	37.4%	62.3%
Glucose	58.3%	27.9%
B. *E. maxima* oocyst walls		
Samples / Carbohydrates	Walls from S/O	Walls from U/O
Mannose	5%	6.4%
Galactose	33.7%	67.6%
Glucose	61.3%	26%
C. *E. tenella* from Stotish *et al.* (1978)		
Samples / Carbohydrates	Walls from S/O	Walls from U/O
Mannose	Not Done	2.2%
Galactose	Not Done	7.2%
Glucose	Not Done	79.6%
Hexosamine	Not Done	11.0%

3.6 Discussion

The TEM data presented in this chapter confirms that bleaching strips off the outer wall of oocysts of *E. tenella* and *E. maxima* (there was a single sample that was an exception to this and this bilayered sample of sporulated oocyst walls of *E. tenella* proved useful in subsequent analyses) (Figure 3.6). This finding is in agreement with several other reports (Monné and Hőnig, 1954; Nyberg *et al.*, 1968; Nyberg and Knapp, 1970; Ryley, 1973; Belli *et al.*, 2006) but at odds with Stotish *et al.* (1978). However, as will become apparent in this discussion, this is just one of several observations that differ from those of Stotish *et al.*

The TEM analyses conducted here revealed that the oocyst wall purification method described by Stotish *et al.* (1978) does not satisfactorily purify the oocyst walls. Rather, they are heavily contaminated with polysaccharide granules from the internal contents of the oocyst (especially the unsporulated oocyst). Fortunately, treatment of the oocyst wall samples with alpha-amylase effectively removed these amylopectin granules (Figures 3.4 and 3.5) allowing confidence in subsequent analyses of the various oocyst wall preparations.

GC and MS analyses of oocyst walls of *E. tenella* and *E. maxima* indicated very clearly that they are primarily made up of protein (greater than 90%) with relatively small amounts of lipid and carbohydrate (Table 3.1). The composition of the oocyst walls of both species was very similar, whether sporulated or unsporulated, though there was perhaps slightly more protein (and, resultingly, proportionally less carbohydrate and lipid) in the sporulated oocyst walls. This may reflect the presence of sporocyst walls, which were occasionally seen in the sporulated oocyst wall samples (see Figure 3.6 A) and, if so, indicates that the composition of the sporocyst wall is slightly different to that of the oocyst wall. Surprisingly, the presence of both the outer and inner layer of the oocyst wall (as in the *E. tenella* sporulated oocyst wall sample) did not greatly affect the overall composition of the wall, indicating that both layers are chemically similar, even though their relative electron opacities are different, as indicated by the TEM images (Figure 3.6).

All of the above results are at odds with those of Stotish *et al.* (1978), who reported much lower protein content and much higher quantities of carbohydrate and lipid in the unsporulated oocyst wall of *E. tenella.* These differences could conceivably be due to host factors such as diet, age and genotype, or parasite genotype. This has not been studied. However, given the magnitude of the differences observed between the data presented here and that of Stotish *et al*, this seems unlikely. The discrepancies can almost certainly be ascribed to contamination of the walls with the internal contents of the oocyst, as the TEM images in this thesis clearly document the presence of large numbers of amylopectin granules in the samples prepared following the method described by Stotish *et al.* The high levels of glucose reported by Stotish *et al.* – much higher than detected by the GC and MS analyses reported here – support this contention as amylopectin is a polymer of glucose monomers joined by alpha-1, 4 linkages (Ryley *et al.*, 1969; Ryley, 1973).

The amino acid analyses (both those reported in this thesis and those reported by Stotish *et al.* in 1978) held no surprises. All twenty amino acids were detected and, within the limits of analysis possible with these samples, five of the more abundant amino acids were roughly correlated with their predicted abundance if they had originated from Emam56 and EmGam82. Of particular note in this regard, is the fact that these two pro-proteins are cleaved into much smaller peptides (of 8, 10, 12 and ~30 kDa) and incorporated into the oocyst wall by dityrosine bonding, a chemical reaction that gives the oocyst wall its characteristic blue autofluorescence (Belli *et al.,* 2003b; 2006). Thus, the proline-rich C-termini of the gametocyte proteins are expected to be less apparent in the oocyst wall, an expectation borne out by the relative change in abundance in Ala and Pro seen in truncated recombinant version of EmGam56, which lacks the proline-rich tail, compared with the full length EmGam56 (Table 3.2).

The lipid composition of the oocyst walls of *E. tenella* and *E. maxima* was very similar for all the samples that contained the inner wall only. However, a distinct difference was obvious in the bilayered sample available for analysis – specifically, it contained much higher levels of oleic acid. This is the only documentable major metabolic difference

found between the outer oocyst wall and the inner oocyst wall thus far. Only small differences in the lipid compositions of sporulated and unsporulated oocyst walls were noticed; specifically, the unsporulated oocyst wall of *E. maxima* had more stearic acid and less cholesterol than the sporulated oocyst wall. This could possibly reflect the presence of sporocyst walls in the samples of sporulated oocyst walls and, if so, would be an additional indication that the composition of the sporocyst wall is slightly different to that of the oocyst wall.

The lipid compositions of the oocyst wall samples analysed in this thesis are radically different to those reported by Stotish *et al.* (1978), who failed to detect several of the lipids detected by the sensitive GC plus MS methodology used here. Ironically, Stotish *et al.* also detected several fatty alcohols and phospholipids, as well as hexosamine, none of which were detected in this study. This could reflect the higher stringency of the analyses conducted in this thesis – GC plus MS rules out false positives very effectively – but also probably betrays the fact that the wall samples prepared by Stotish *et al.* were contaminated with internal oocyst contents. The carbohydrate analyses lend support to this contention as Stotish *et al.* reported much higher levels of glucose in their unsporulated oocyst wall samples than were observed here for either *E. tenella* or *E. maxima* – the fact that amylopectin is composed of glucose monomers explains this discrepancy.

The carbohydrate composition of the oocyst walls of both *E. tenella* and *E. maxima* varied between sporulated and unsporulated oocysts, galactose being the dominant carbohydrate in unsporulated oocysts and glucose the dominant one in sporulated oocysts. Whether this reflects the presence of sporocyst walls in the sporulated oocyst wall samples or a fundamental difference between sporulated and unsporulated oocyst walls is not known but sporocyst walls were occasionally seen in sporulated oocyst wall samples (see Figure 3.6 A).

In summary, the key findings of this chapter are that:

- the *Eimeria* oocyst wall is composed mainly of protein, with an amino acid composition that roughly (and tentatively) correlates with that of gametocyte proteins known to be processed and incorporated into the oocyst wall;
- there is very little difference between the oocyst wall composition of the two species of *Eimeria* analysed (*E. tenella* and *E. maxima*);
- there are only slight, if any, differences in the composition of the inner walls of sporulated and unsporulated oocyst walls;
- there are only slight differences in the composition of the outer and inner layers of the oocyst wall.

All of this indicates that the structure of proteins like EmGam56 and EmGam82 will be key to understanding how they are incorporated into the oocyst wall and help to give it its structure and resilience.

Chapter Four

Structural Analysis of EmGam56

4.1 Introduction

The analysis of the composition of the oocyst walls of *Eimeria maxima* and *Eimeria tenella,* presented in Chapter 3, demonstrated that the major component of oocyst walls is amino acid. Furthermore, the amino acid composition of the oocyst wall is remarkably similar to that of the protein EmGam56. This is perhaps not completely unexpected given previous results (eg Belli *et al.,* 2002; 2003b and Ferguson *et al.,* 2003) showing that peptides derived from EmGam56 are incorporated into the oocyst wall, possibly via the formation of bonds between tyrosine residues of the protein to form a matrix of structural proteins (Belli *et al.,* 2006).

The structure of proteins can profoundly affect their function. Even intrinsically unstructured proteins have important functions and, indeed, their inherent flexibility is crucial in some instances. Thus, it has been shown that intrinsically unstructured proteins are involved in important biological functions such as DNA recognition, molecular assembly, protein modification and modulation of affinity of protein binding (Dunker *et al.*, 1998; 2000; 2002; Iakoucheva *et al.*, 2002; Ward *et al.*, 2004), the last point being potentially most important with regard the putative function of derivatives of EmGam56. Thus, in this chapter, the structure of EmGam56 was analysed with particular attention paid to the possibility that it is an intrinsically unstructured protein. The aims of this study included:

[1] bioinformatic analyses using PSIPRED, APSSP2, SSpro, GOR4, HNN and SOPMA to predict fundamental secondary structure of EmGam56;

[2] bioinformatic analysis using FoldIndex© to differentiate classically folded from unfolded domains in EmGam56;

[3] bioinformatic analyses using IUPred, RONN, DISPROT and DisEMBL™ to confirm and enhance predictions of intrinsically unstructured regions within EmGam56;

[4] selection of a region of EmGam56 for CD and NMR analyses to confirm bioinformatic predictions;

[5] expression of a recombinant version of the selected region of EmGam56;

[6] confirmation that the recombinant truncation of EmGam56 is structurally similar to the native protein;

[7] confirmation of the stability of the recombinant protein in different temperature and pH conditions;

[8] analysis of the structure of the truncated recombinant version of EmGam56 by circular dichroism (CD); and

[9] analysis of the structure of the truncated recombinant version of EmGam56 by nuclear magnetic resonance (NMR).

4.2 PSIPRED, APSSP2, SSpro, GOR4, HNN and SOPMA analysis of EmGam56 secondary structure

The protein sequence of EmGam56 was submitted to a variety of web servers including PSIPRED, APSSP2, SSpro, GOR4, HNN and SOPMA for secondary structure prediction as described in Chapter 2, Section 2.2.7.1 The relative percentages of predicted α-helices, β-sheets and random coils are summarized in Table 4.1 and the position of each of these structures is detailed in Table 4.2. A diagrammatic representation of the predicted secondary structure of EmGam56 by one program, PSIPRED, is presented as Figure 4.1. Whilst each program predicted slightly different secondary structures, the same general patterns were apparent in all the predictions. Thus, the range of predicted percentage of α-helices was 28-43%, β-sheets was 1-11% and random coils were predicted to account for 52-70% of the secondary structure of EmGam56. Overall, therefore, the results of bioinformatics analyses predict that EmGam56 contains mostly random coils and α-helices with a relatively low level of β-sheets.

4.3 FoldIndex© analysis of EmGam56 secondary structure

The high level of random coils predicted for EmGam56 by PSIPRED, APSSP2, SSpro, GOR4, HNN and SOPMA was further investigated using the program, FoldIndex©, which predicts if a given protein sequence is intrinsically unfolded. This program assigns value between -1 and 1 where values below zero indicate unfolded, unstructured regions (in red in Figure 4.2) and above zero indicate classically folded or structured regions (in green in Figure 4.2). FoldIndex© analysis of the amino acid sequence of EmGam56 confirmed that it contains several unfolded or unstructured regions (with FoldIndex below zero), most especially, amino acid sequences 38-75, 100-137, and 205-324, which agrees broadly with the predicted positioning of random coils by PSIPRED, APSSP2, SSpro, GOR4, HNN and SOPMA.

Table 4.1 Summary of secondary structure predictions for EmGam56 by PSIPRED, APSSP2, SSpro, GOR4, HNN and SOPMA.

Secondary structure predictors	Predicted percentages of secondary structure of EmGam56	References
PSIPRED	α-helices: 42.44 % β-sheets: 0.63 % random coils: 56.93 %	Jones, 1999; McGuffin *et al.*, 2000
APSSP2	α-helices: 28.27 % β-sheets: 2.11 % random coils: 69.62 %	Raghava, 2002
SSpro	α-helices: 37.19 % β-sheets: 3.36 % random coils: 59.45 %	Cheng *et al.*, 2005
GOR4	α-helices: 34.66 % β-sheets: 10.71 % random coils: 54.62 %	Garnier *et al.*, 1996
HNN	α-helices: 34.66 % β-sheets: 3.78 % random coils: 61.55 %	Guermeur, 1997
SOPMA	α-helices: 37.61 % β-sheets: 5.04 % (β-turns: 5.25 %) random coils: 52.10 %	Geourjon and Deléage, 1995

Table 4.2 Relative positions of α-helices, β-sheets and random coils within the amino acid sequence of EmGam56 as predicted by PSIPRED, APSSP2, SSpro, GOR4, HNN and SOPMA

	PSIPRED	APSSP2	SSPro	GOR4	HNN	SOPMA
Predicted	4-15	5-15	3-14	6-14	4-15	1-4
amino acid	34-41					36-37
position	65-101	64-102	64-130	64-104	43-104	65-105
within	107-126	110-128	"	110-131	111-130	111-135
EmGam56 of	135-139					
α-helices	145-174	147-174	145-182	146-173	146-182	146-159
						164-173
		178-181	"	175-184		176-182
	180-182		195-214	186-191	186	185-188
	189-214	197-214		193-226	197-213	196-214
	219-225	219-225			219-225	219-225
	235-240			235-238	237-240	238-240
	258-269					269
	273-287					
	307-327		316-328	318-324	316-327	317-328
			349-352			349-353
		363-367	358-367		359-368	359-368
			381-385	382-386	381-384	382-385
		419-421				
Predicted				30-31		
amino acid				39-41		
position				53-58		
within		136-138		135-139	136-138	136-139
EmGam56 of			186-189		187-189	
β-sheets	247-249	248-249	246-249	245-249	246-249	246-249
			261-262	261-262		255
				270-272		270
			285-288	285-288	285-288	285-287
				302		293-294
		318-322		309-314	310	308-310
				359-360		
				362-368		
					385	386
				391-393	392-393	392-394
				439-440		

Continued/....

Table 4.2 Continued....

	PSIPRED	APSSP2	SSPro	GOR4	HNN	SOPMA
Predicted	1-3	1-4	1-2	1-5	1-3	
amino acid	16-33	15-63	15-63	15-29	16-63	15-35
position				32-38		38-41
within	42-64	"	"	42-52		44-62
EmGam56 of				58-64		
random coils						106
	102-106	103-109		105-109	105-110	109-110
	127-134	129-135	131-144	132-134	131-135	
	140-144	139-146	"	140-145	139-145	140-145
						160-163
	175-179	175-177		174		
	183-188	182-196	183-185	185	183-185	189
	"	"	190-194	192	190-196	193-195
	215-218	215-218	215-218		214-218	217-218
	226-234	226-247	226-245	227-234	226-236	226-237
	241-246	"	"	239-244	241-245	245
	250-257	250-317	250-260	250-260	250-284	250-254
						257-267
	270-272	"	263-284	263-269		273-284
				273-284		
	288-306	"	289-315	289-301	289-309	288-292
				303-308		295-307
				315-317	311-315	311-316
	328-476	323-362	329-348	325-358	328-358	329-348
	"	"	353-357			354-358
	"	368-418	368-380	361	369-380	369-381
				369-381	386-391	
				387-390		388-390
	"	422-476	386-476	394-438		
				441-476	394-476	395-476

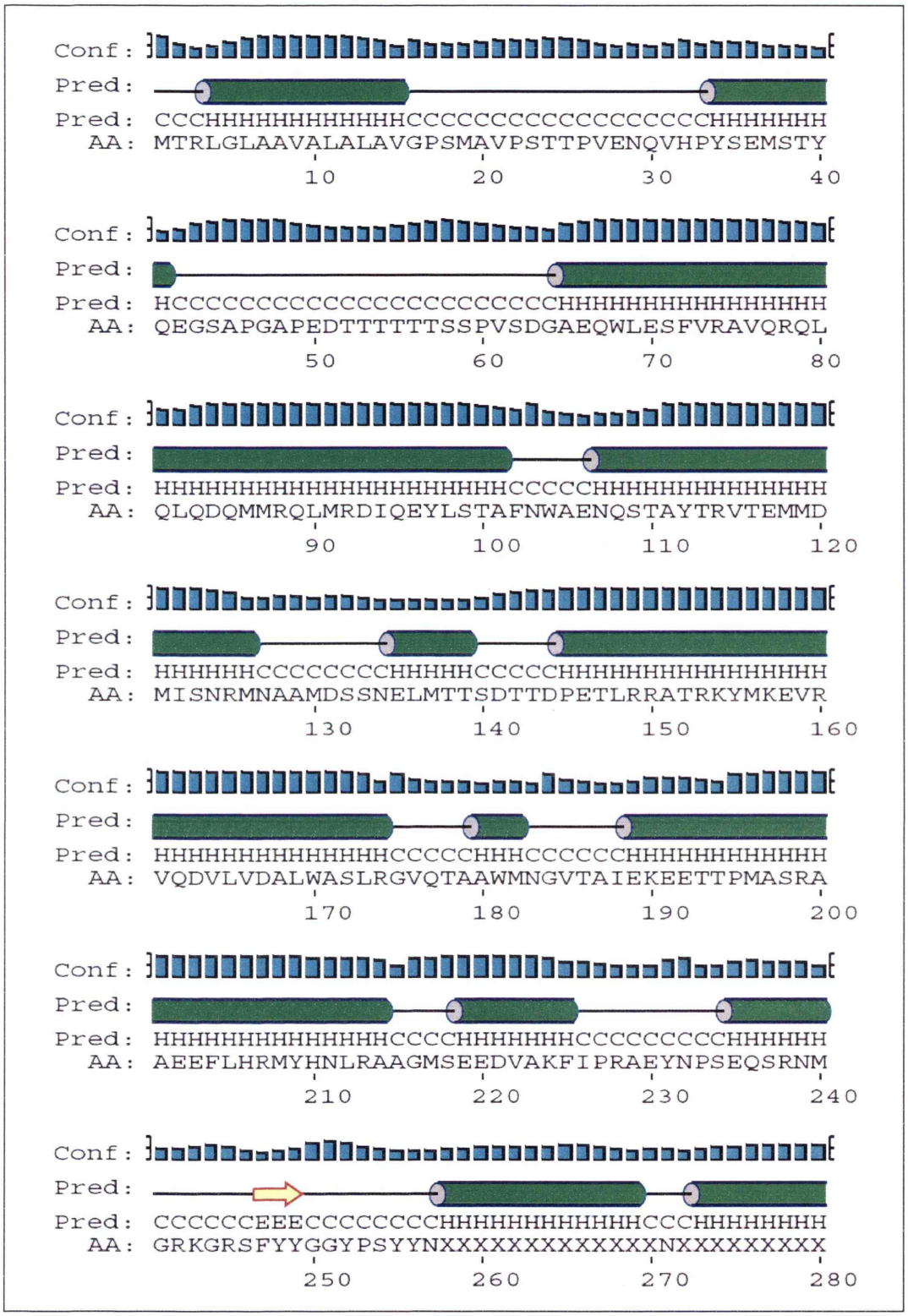

Figure 4.1 Secondary structure prediction of EmGam56 by PSIPRED (Continued…)

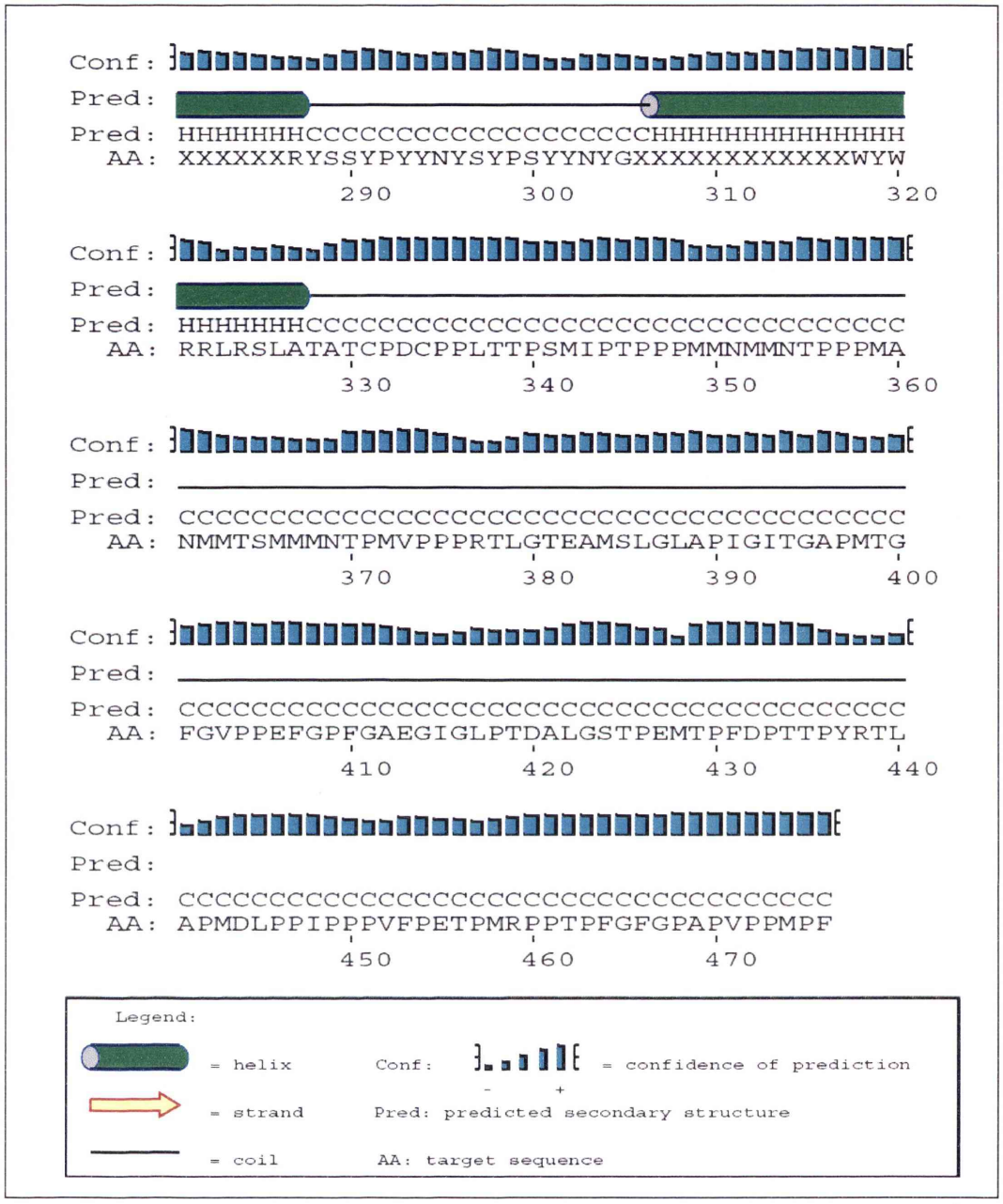

Figure 4.1 Continued. Secondary structure prediction (α-helices in green, β-sheets in yellow, and random coils in black) of EmGam56 by PSIPRED. The protein sequence of EmGam56 (1-476 amino residues) was submitted to the web server, PSIPRED, for secondary structure predictions. The confidence of the prediction assigned to each amino residue is scored from 0 to 1 representing low to high confidence of the secondary structure prediction. The PSIPRED used for this prediction filtered out low complexity regions, likely transmembrane segments and coiled-coil regions. Therefore, regions that were masked out were replaced with X (unknown) residues. X= 258-286 a.a. and 306-317 a.a. (original sequence: SPYYSYSSYPSYYNYSYPSYSYSSYPSYY and SYPYYSYSSYPS, respectively).

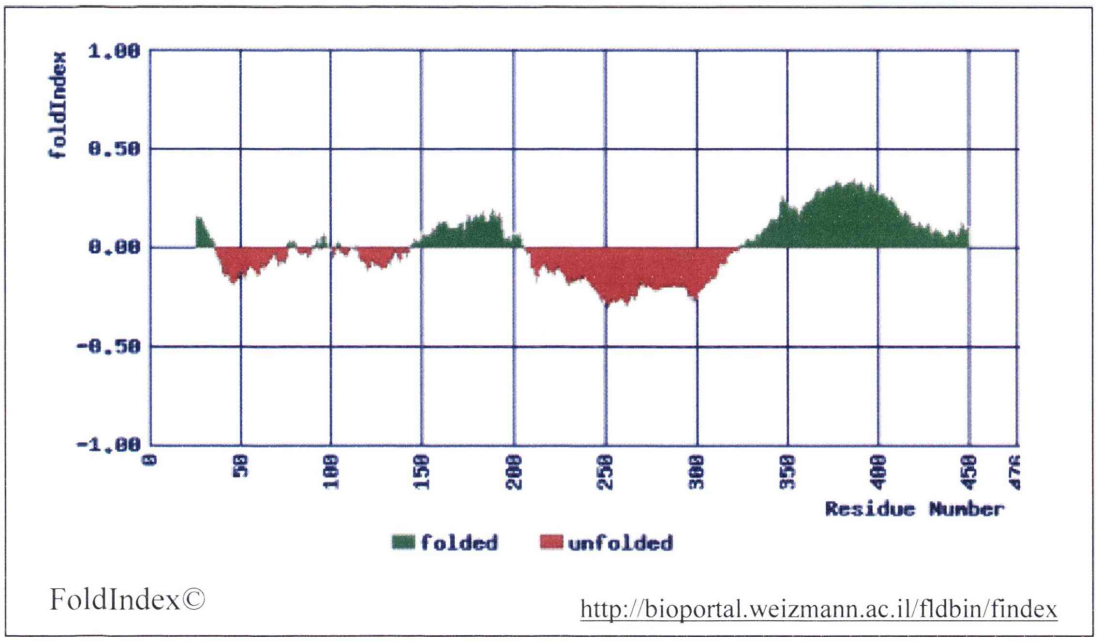

Figure 4.2 FoldIndex© analysis of EmGam56. The following regions were predicted to be disordered: 38-75 a.a., 100-137 a.a. and 205-324 a.a. by FoldIndex© (regions in green and red colour indicate folded and unfolded regions, respectively).

4.4 IUPred, RONN, DISPROT and DisEMBL™ analyses for disorder within the secondary structure of EmGam56

PSIPRED, APSSP2, SSpro, GOR4, HNN, SOPMA and FoldIndex© analyses indicated strongly that EmGam56 contains extensive regions of disorder within its amino acid sequence. Thus, these analyses were extended through use of the programs, IUPred, RONN, DISPROT and DisEMBL™, which are specifically designed to highlight areas that are disordered or intrinsically unstructured. Briefly, the amino acid sequence of EmGam56 was imported into windows of various web servers and submitted for disorder/unstructured predictions as described in Chapter 2, Section 2.2.7.2. The presentation of results varied between web servers but, in general, the x-axis of the graphs represented amino residues of the protein and y-axis indicated the disorder tendency or disorder probability. Predicted disordered regions greater than 30 amino residues are considered to be "long" regions of disorder and less than 30 amino residues is considered to be region of "short" disorder. The scale and threshold for disorder prediction also varied from each program due to the difference in definition of disorder proteins and methods adopted for disorder prediction (see Chapter 2, Table 2.2 for details).

IUPred predicts that EmGam56 contains disordered regions from 20-65 a.a., 124-156 a.a., and 410–467 a.a. (Panel A, Figure 4.3). The higher the score on the y-axis, the higher the likelihood for disorder in that region. For example, the region from 20–60 a.a. within EmGam56 was predicted to be more likely to be disordered than that of the other predicted disordered regions (from 120-150 a.a. and 410-468 a.a) since the score of disorder tendency was higher (Panel A, Figure 4.3). RONN analysis predicts that EmGam56 contains disordered regions from 18-70 a.a., 128-150 a.a., 185-198 a.a., 214-245 a.a., 323-350 a.a. (Panel B, Figure 4.3). DISPROT (VSL2; Obradovic *et al.*, 2005) predicts that EmGam56 contained regions of disorder throughout the entire protein except the following small regions: 5-16 a.a, 89-102 a.a., 156-188 a.a., and 203-211 a.a. (Panel C, Figure 4.3). Thus, once again, as for the predictions by IUPred and RONN, regions centred around amino acids ~50 and ~135 and the C-terminus of EmGam56 are predicted to be largely unstructured. Finally, DisEMBL™ also predicts that EmGam56 contains several regions of disorder (Figure 4.4), which can be further defined by three parameters: (1) disordered by loops/coils: 15-64 a.a., 129-146 a.a., 187-196 a.a., 214-318 a.a., 326-476 a.a.; (2) disordered by hot-loops: 15-24 a.a., 130-147 a.a., 229-243 a.a., 466-473 a.a.; and (3) disordered by Remark-465 (missing coordinates in X-ray structure): 38-63 a.a.. Regions fulfilling all these three criteria are considered to be the most likely to be disordered - no sequence of EmGam56 fell into this category but several regions fulfilled two of the criteria, including regions from 15-24 a.a., 38-63 a.a., 129-146 a.a., 229-243 a.a., and 466-473 a.a. (Figure 4.4).

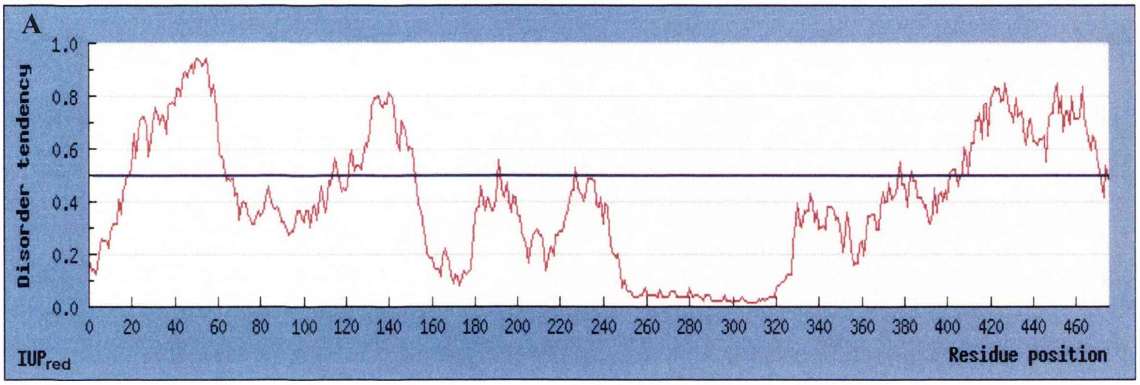

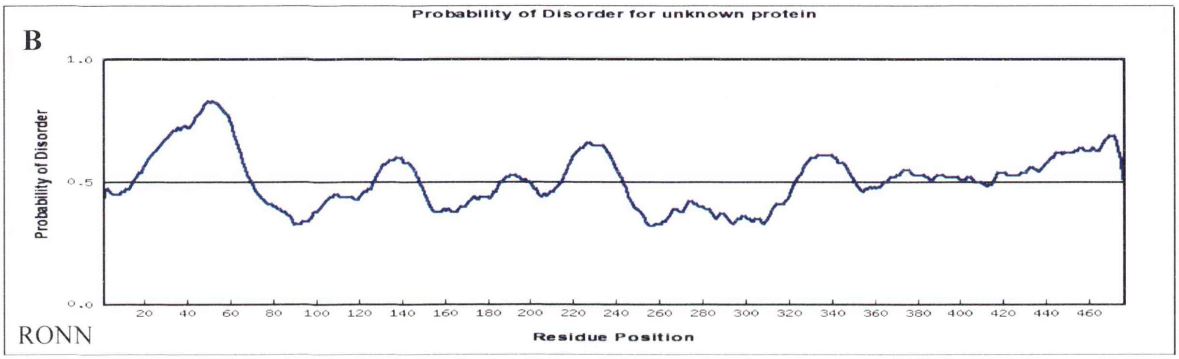

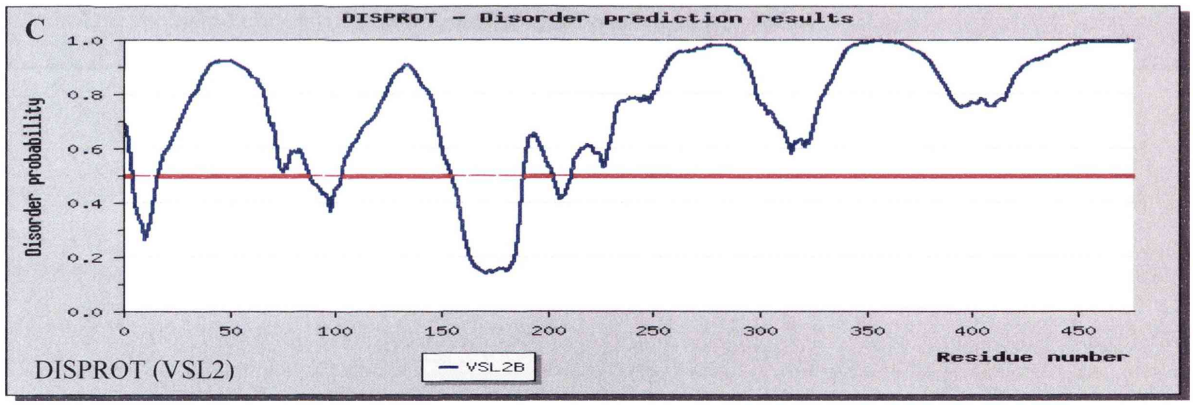

(1- 476 a.a.)

Figure 4.3 Disorder predictions for EmGam56 by IUPred, RONN and DISPROT. The following regions are predicted to be disordered: 20-65 a.a., 124-156 a.a., and 410-467 a.a. by IUPred (Panel A); 18-70 a.a., 128-150 a.a., 185-198 a.a., 214-245 a.a. and 323-350 a.a. by RONN (Panel B); 1-4 a.a., 17-88 a.a., 103-155 a.a., 189-202 a.a. and 212-476 a.a. by DISPROT (VSL2) (Panel C).

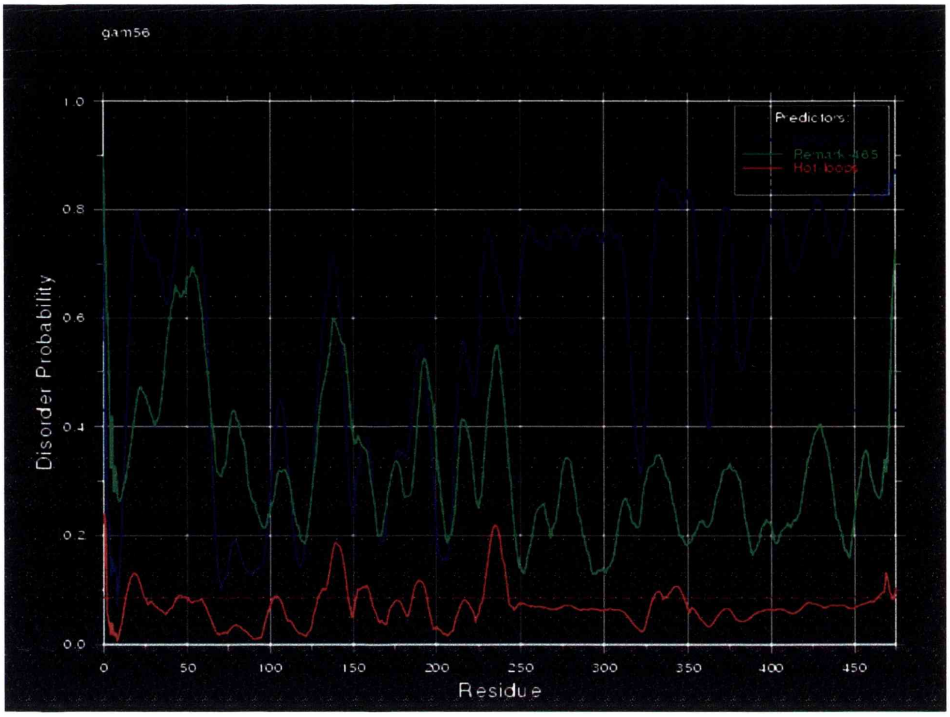

Figure 4.4 Disorder prediction for EmGam56 by DisEMBL™. The following regions were predicted to be disordered: 15-24 a.a., 38-63 a.a., 129-146 a.a., 229-243 a.a. and 466-473 a.a. - these can be further defined by three different parameters: (1) disordered by loops/coils (blue): 15-64 a.a., 129-146 a.a., 187-196 a.a., 214-318 a.a. and 326-476 a.a.; (2) disordered by hot-loops (red): 15-24 a.a., 130-147 a.a., 229-243 a.a. and 466-473 a.a.; (3) disordered by Remark-465 (ie, missing coordinates in X-ray structure, green): 38-63 a.a..

4.5 Generation of a truncated recombinant EmGam56

The region from amino acids 102-225 of EmGam56 was selected for biochemical analyses to confirm the predictions of disorder obtained from the various bioinformatic analyses. This region was chosen for several reasons: first, the full-length protein is too large for structural analysis by NMR, which ideally should take place on proteins of not more than 100 amino acids (Feng, ZP, Zhang X and Norton RS, personal communication); second, this region contains areas predicted to possess classical secondary structures and unstructured regions (versus, for example the tyrosine-rich region and C-terminus of EmGam56, which are predicted to be dominated by random coils), allowing rational evaluation of the accuracy of the bioinformatic predictions; and, third, repeated efforts to produce recombinants of the sequence for amino acids 1-102 failed consistently. Moreover, structural predictions by PSIPRED, APSSP2, DISpro, GOR4, HNN and SOPMA for the peptide from amino acids 102-225 confirmed the predictions for this region when it was

analysed as part of the full-length protein (apart from some slight variations at the N-terminal of the peptide). The pET101 vector was chosen to generate the recombinant protein for structural analyses since it contains a 3' histidine tag, which minimises the possibility of structural change when translation occurs in bacterial cells (Studier *et al.*, 1990; Shiryaev *et al.*, 2006). Furthermore, recombinant proteins arising from this vector have relatively smaller molecular weight than, for example, pTrcHisb constructs (Studier and Moffatt, 1986; Champion™ pET Directional TOPO® Expression Kit, version G, Instruction Manual, Invitrogen™).

DNA fragments coding for amino acids 102-225 were PCR amplified from the parent construct, *56pET25b*, using specific primer sets as shown in Chapter 2, Figure 2.1. The parent construct containing DNA fragment encoding amino acids 24-338 (corresponding to 172-1127 bp of *EmGam56* gene) has been previously generated in an expression vector, pET25b, by Dr Sabina Belli (Institute for the Biotechnology of Infectious Diseases, University of Technology, Sydney). The truncated construct is designated *pETEmGam56.102-225*, the postscript referring to the amino acid sequence within the native EmGam56 protein. The parent construct was included in the experiments as a positive control. Amplification of *56pET25b* was seen on a 1 % agarose gel (Lane 2, Figure 4.5) indicating the success of DNA amplifiction by PCR, with the expected 975 bp fragment seen. The expected 379 bp fragment corresponding to *pETEmGam56.102-225* amplified from *56pET25b* (Lane 1, Figure 4.5) was also seen clearly on a 1% agarose gel.

The PCR product of *pETEmGam56.102-225* was then gel purified to eliminate contaminants such as non-specific PCR products, primer dimers (hairpin), and remaining primers, prior to DNA cloning. The DNA fragment was excised from agarose gels and recovered using a QIAquick® gel extraction kit as described in Chapter 2, Section 2.2.8.3. The DNA fragment was then cloned in frame with the expression vector and competent bacteria were transformed with the recombinant constructs as described in Chapter 2, Section 2.2.8.4 and 2.2.8.5. Ampicillin-resistant transformants from LB Amp plates were then selected to undergo colony PCR using vector specific primers or primers designed as described in Chapter 2, Section 2.2.8.6. An example of colony PCR products from recombinant constructs generated in pET101 is shown in Figure 4.6. In all colonies

selected, the correct sized insert of 379 bp was amplified from *pETEmGam56.102-225* (Figure 4.6).

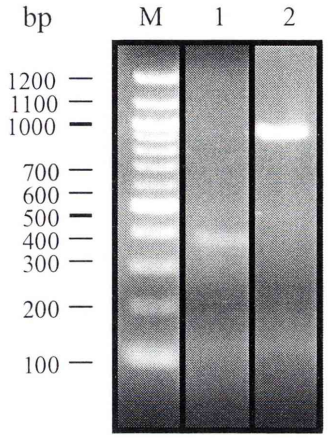

Figure 4.5 Analysis of PCR products of *pETEmGam56.102-225* by agarose gel electrophoresis. DNA fragments were amplified by PCR, products separated on a 1% agarose gel and visualized by staining with ethidium bromide. M= 100 bp DNA ladder; Lane 1= *pETEmGam56.102-225* (379 bps); Lane 2= *56pET25b* (975 bp) using *56pET25b* as DNA template.

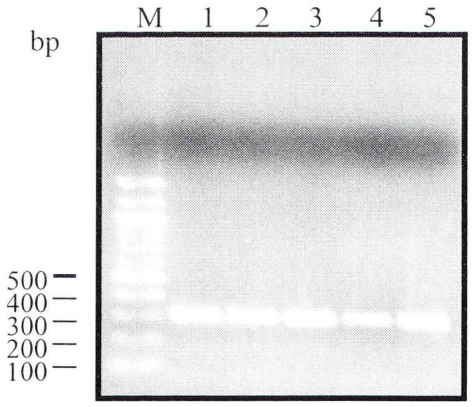

Figure 4.6 Analysis of the colony PCR products of *pETEmGam56.102-225* by agarose gel electrophoresis. Colony PCR products from *pETEmGam56.102-225* were separated on a 1% agarose gel and visualized by staining with ethidium bromide. M= 100 bp DNA ladder; Lane 1-4= amplification of *pETEmGam56.102-225* using designed primers, KM5 and KM12.

DNA sequencing was carried out to ensure the insert was in frame with the start codon of the vector. Plasmid DNA from selected clones of the recombinant construct was isolated and sent to AGRF for automated DNA sequencing as described in Chapter 2, Section 2.2.8.7 and 2.2.8.8. DNA was sequenced in both the forward and reverse directions using vector specific primers; T7 and T7term for pET101 (see Chapter 2, Table 2.3). Sequences of the inserts were aligned to the full-length gene (*EmGam56*) using the software AssemblyLIGN™, which confirmed that the sequence of inserted DNA in *pETEmGam56.102-225* was 100% identical to the full length gene (Figure 4.7).

The DNA sequences were translated into amino acid sequences using ExPASy (Expert Protein Analysis System; Gasteiger *et al.*, 2003), which confirmed that the DNA fragment was cloned in frame with the start codon (ATG) of pET101 (Figure 4.7). The predicted molecular weight and theoretical isoelectric point of the construct is 17.7 and 8.10, respectively.

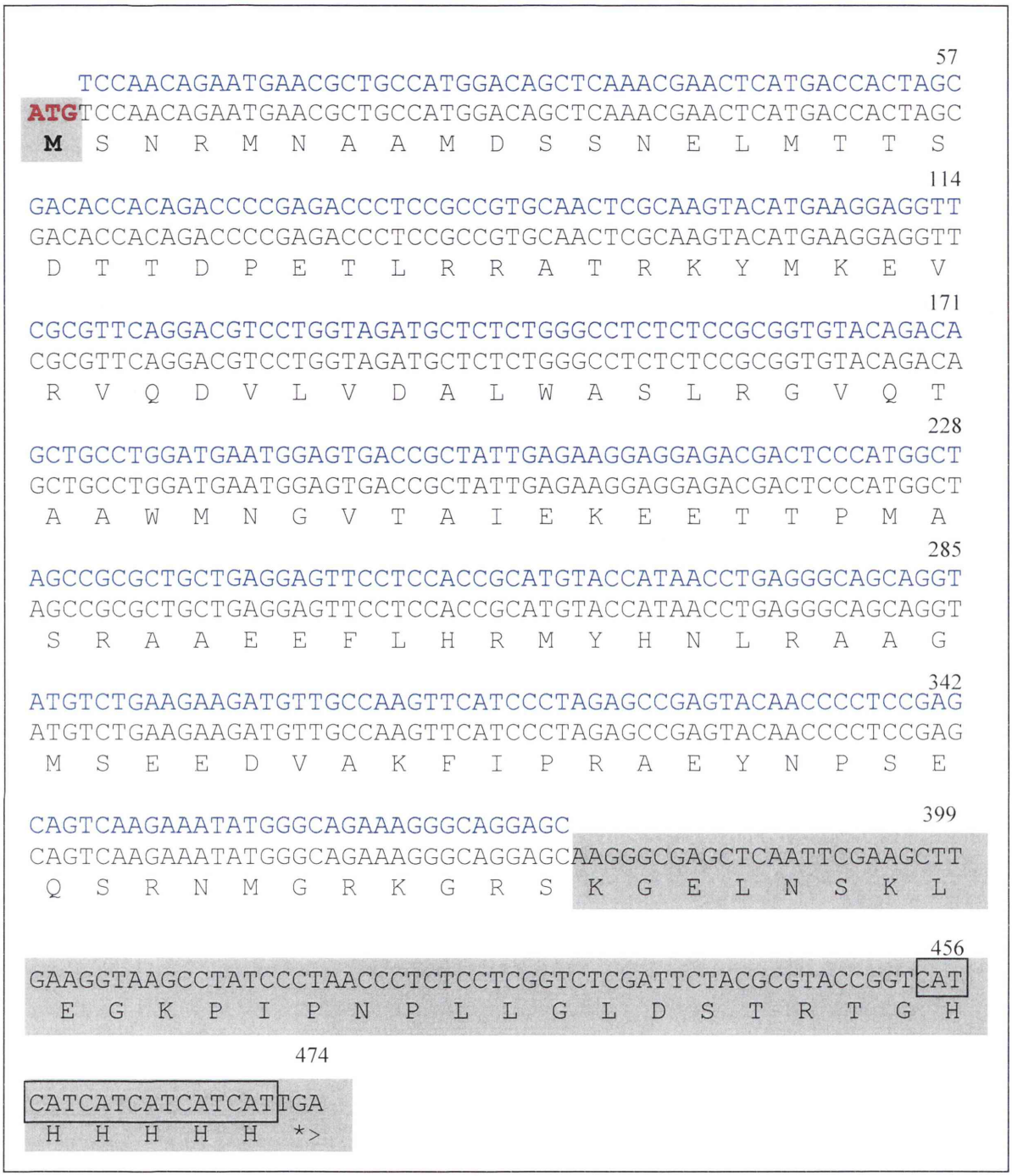

Figure 4.7 DNA and amino acid sequences of *pETEmGam56.102-225*. The DNA sequence was obtained from AGRF by automated DNA sequencing and the resultant predicted amino acid sequence was generated using the web server - ExPASy (Gasteiger *et al.*, 2003). The predicted initiator methionine (ATG) is presented in bold. The DNA sequence in blue represents *pETEmGam56.102-225*, whilst that in black is the confirmed sequence of the same region from the full-length *EmGam56*. The sequences corresponding to pET101 are shaded in grey. The six consecutive histidine residues in pET101 are boxed. *= the stop codon (TGA), the site where termination of translation occurs.

4.6 Expression and purification of recombinant pETEmGam56.102-225

Transformed *E. coli* cells containing the recombinant construct were chemically induced with 1 mM IPTG to express pETEmGam56.102-225, as described in Chapter 2, Section 2.2.9. The induced and uninduced bacterial lysates were then analysed by SDS-PAGE, followed by immunoblotting using mouse anti-pentahis antibodies (the antibodies recognize five histidine residues in series fused 3' to the inserted gene in pET101). The parent construct and the recombinant protein markers were also analysed on gel (r56 served as a positive control for protein expression).

Expression of pETEmGam56.102-225 was seen on immunoblots probed with anti-pentahis antibodies. A band of the expected size was detected indicating that the constructs expressed well (Lane 2, Figure 4.8). Several protein bands other than expected 17.7 kDa were, however, detected; these are assumed to be the degraded products of pETEmGam56.102-225. The band with molecular weight slightly larger than 17.7 kDa detected on the blot could be the aggregated pETEmGam56.102-225. There were faint bands detected from the uninduced sample representing, possibly, background (Lane 1, Figure 4.18).

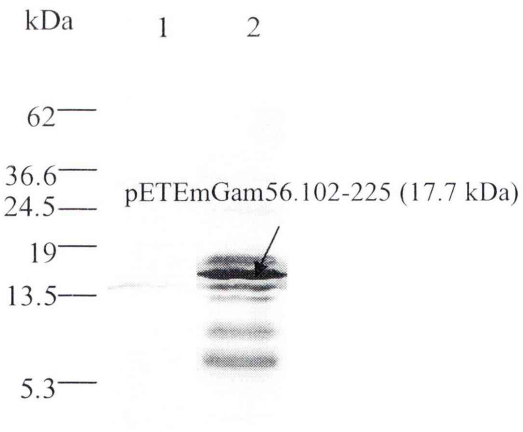

Figure 4.8 Immunoblot analysis of the expression of pETEmGam56.102-225. The recombinant construct was induced with 1 mM IPTG at 30°C for 3 hrs, transferred to PVDF membrane and probed with mouse anti-pentahis antibodies. Lane 1 and 2= bacterial lysates of uninduced and induced pETEmGam56.102-225, respectively.

The recombinant protein was purified using HiTrap™ chelating HP column as described in Chapter 2, Section 2.2.10. pETEmGam56.102-225 was purified and fractions from each step of the purification were analysed by SDS-PAGE, followed by immunoblotting using mouse anti-pentahis antibodies to monitor the purification. Bands representing pETEmGam56.102-225 were detected from the following fractions: before sonication, after sonication, supernatant and pellet of bacterial lysate, fraction collected from flow-through and fraction washed with 150 mM imidazole, and purified pETEmGam56.102-225 fractions (Lane 1, 2, 3, 4, 5, 6, 8, 9 and 10, respectively, Figure 4.9). Detection of pETEmGam56.102-225 from the pellet of bacterial lysate, fraction collected from flow-through, and fraction washed with 150 mM imidazole (Lane 5, 6 and 8, respectively, Figure 4.9) indicated the loss of the proteins during the purification procedure.

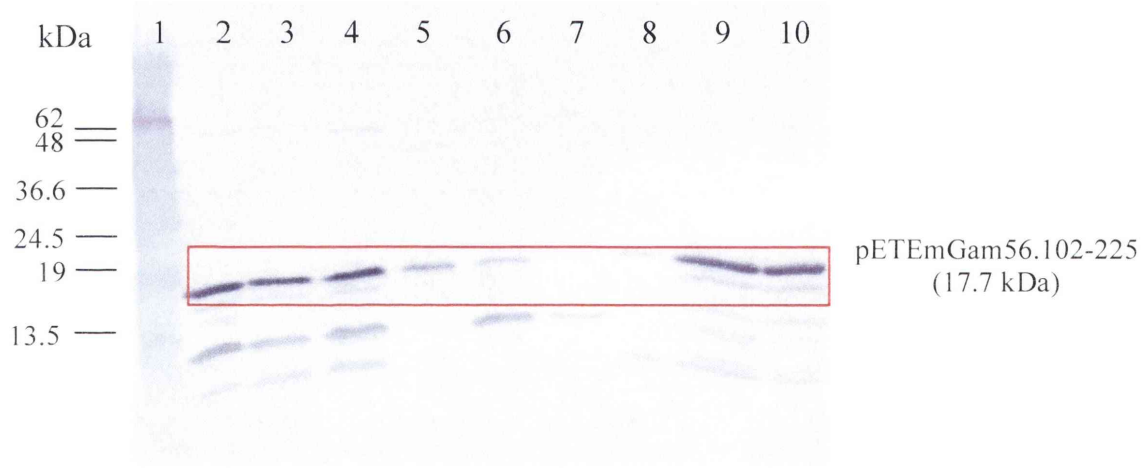

Figure 4.9 Immunoblot analysis of purified pETEmGam56.102-225 fractions. An aliquot from each step of purification was analysed by SDS-PAGE, followed by immunoblotting using mouse anti-pentahis antibodies as described in Chapter 2, Section 2.2.12 and 2.2.14. Lane 1= pre-stained protein ladder; Lane 2= before sonication; Lane 3= after sonication Lane 4= supernatant of bacterial lysate of pETEmGam56.102-225; Lane 5= pellet of bacterial lysate of pETEmGam56.10-225; Lane 6= fraction collected from flow-through; Lane 7= fraction washed with 20 mM imidazole; Lane 8= fraction washed with 150 mM imidazole; Lane 9-10= purified pETEmGam56.102-225 fraction e2 (0.5 µg) and e3 (0.7 µg), respectively. Boxed area represents pETEmGam56.102-225, with a molecular weight of 17.7 kDa.

Two smaller bands (~ 5 and 10 kDa) were also seen from the fractions before sonication, after sonication, supernatant of bacterial lysate, and flow-through (Lane 2, 3, 4 and 6, respectively, Figure 4.9); these likely represent degraded products of pETEmGam56.102-225, since they reacted with the anti-pentahis antibody. The degradation likely occurred during expression in bacterial cells since these proteins were detected from the fraction before sonication. Total yield from this purification was 0.47 µg per ml culture (23.7 µg from 50 ml culture).

4.7 Optimisation of expression of pETEmGam56.102-225

Expression of pETEmGam56.102-225 was optimized to enhance the yield as well as the purity in order to satisfy the conditions required for structural analysis by NMR. Optimal expression conditions for pETEmGam56.102-225, such as temperature for induction, induction time, and IPTG concentration were investigated to enhance expression level as well as to prevent degradation.The transformed bacteria containing *pETEmGam56.102-225* were induced with 1 mM IPTG or 0.1 mM IPTG at 25°C or 30°C for 0, 0.5, 1, 2 or 3 hours. The negative control samples included in this experiment were grown under the same conditions without IPTG. Bacterial lysates were loaded onto 18% polyacrylamide gels and electrophoresed under reducing conditions as described in Chapter 2, Section 2.2.12. The expressed proteins were stained with Coomassie blue and analysed by immunoblotting using mouse anti-pentahis antibodies.

Expression of pETEmGam56.102-225 was seen in the induced bacterial lysates after 1 hour induction onwards on a Coomassie blue stained gel (Lane 4-6, Panel A, Figure 4.10) whereas, in the uninduced samples (Lane 7-10, Panel A, Figure 4.10), pETEmGam56.102-225 was not seen. The fact that pETEmGam56.102-225 was detected on a Coomassie blue-stained gel indicated the expression level of pETEmGam56.102-225 was reasonably high. Bands corresponding to pETEmGam56.102-225 were recognised by anti-pentahis antibodies (Panel B, Figure 4.10). The expression level increased when the induction time increased from 0.5 to 3 hours (Lane 3-6, Panel B, Figure 4.10). Protein bands other than pETEmGam56.102-225 (in the range of 5 to 13 kDa) were also detected from the induced bacterial lysates (Lane 3-6, Panel B, Figure 4.10) representing the degraded products of pETEmGam56.102-225.

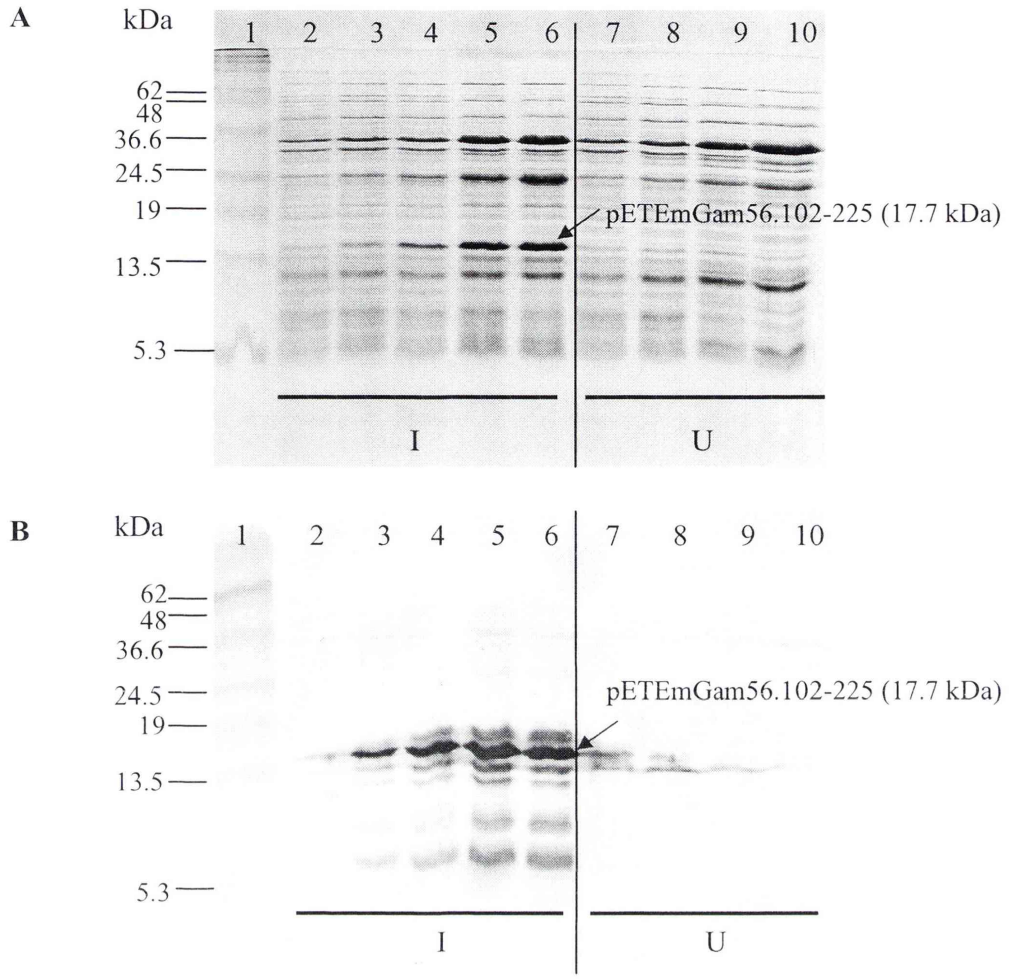

Figure 4.10 Coomassie blue staining (A) and immunoblot analysis (B) of pETEmGam56.102-225 expression from bacterial culture induced with 1 mM IPTG at 30°C. Bacterial lysates were analysed by SDS-PAGE, followed by staining with Coomassie blue or immunoblotting using mouse anti-pentahis antibodies. Lane 1= pre-stained protein ladder; Lane 2-6= bacterial lysates induced with 1 mM IPTG at 30°C for 0, 0.5, 1, 2 and 3 hrs, respectively; Lane 7-10= samples grown without IPTG at 30°C for 0.5, 1, 2 and 3 hrs, respectively. I= constructs with IPTG induction. U= constructs without IPTG induction.

Expression of pETEmGam56.102-225 was also analysed in transformed bacteria induced with 1 mM IPTG at the lower temperature of 25°C. Decreasing the temperaure decreased the level of expression. The intensity of the bands representing pETEmGam56.102-225 on Coomassie blue stained gels decreased (Lane 5 and 6, Panel A, Figure 4.11) and less degradation of pETEmGam56.102-225 appeared on the immunoblot (Lane 3-6, Panel B, Figure 4.11) in comparison to that of 30°C (Panel B, Figure 4.10). The expression level of pETEmGam56.102-225 increased as the induction time increased from 0.5 to 3 hours (Lane 3-6, Panel B, Figure 4.11) whereas in the uninduced bacterial lysates, pETEmGam56.102-225 was not detected (Lane 7-10, Panel B, Figure 4.11), suggesting that the promoter of pET101 vector was tightly regulated under these expression conditions.

Expression of pETEmGam56.102-225 was also seen when the concentration of IPTG was reduced to 0.1 mM. Protein bands representing pETEmGam56.102-225 were seen on a Coomassie blue stained gel (Lane 5 and 6, Panel A, Figure 4.12) as well as the immunoblot probed with anti-pentahis antibodies (Lane 4-6, Panel B, Figure 4.12). The expression level seemed to be lower than that of 1 mM IPTG (Figure 4.11) when the concentration of IPTG was decreased to 0.1 mM (Figure 4.12). However, decreasing IPTG did not significantly prevent the degradation of pETEmGam56.102-225. Protein bands other than pETEmGam56.102-225 recognized by anti-pentahis antibodies (Lane 5 and 6, Figure 4.12) were an indication of degradation of the protein.

A summary of pETEmGam56.102-225 protein expression is presented in Table 4.3. It seemed that the transformed bacteria induced with 1 mM IPTG at 25°C for 3 hours would satisfy the criteria for an enhanced expression level with less degradation of pETEmGam56.102-225. Therefore, for subsequent purifications, the recombinant proteins were purified from the culture under this optimal condition (induced with 1 mM IPTG at 25°C for 3 hours).

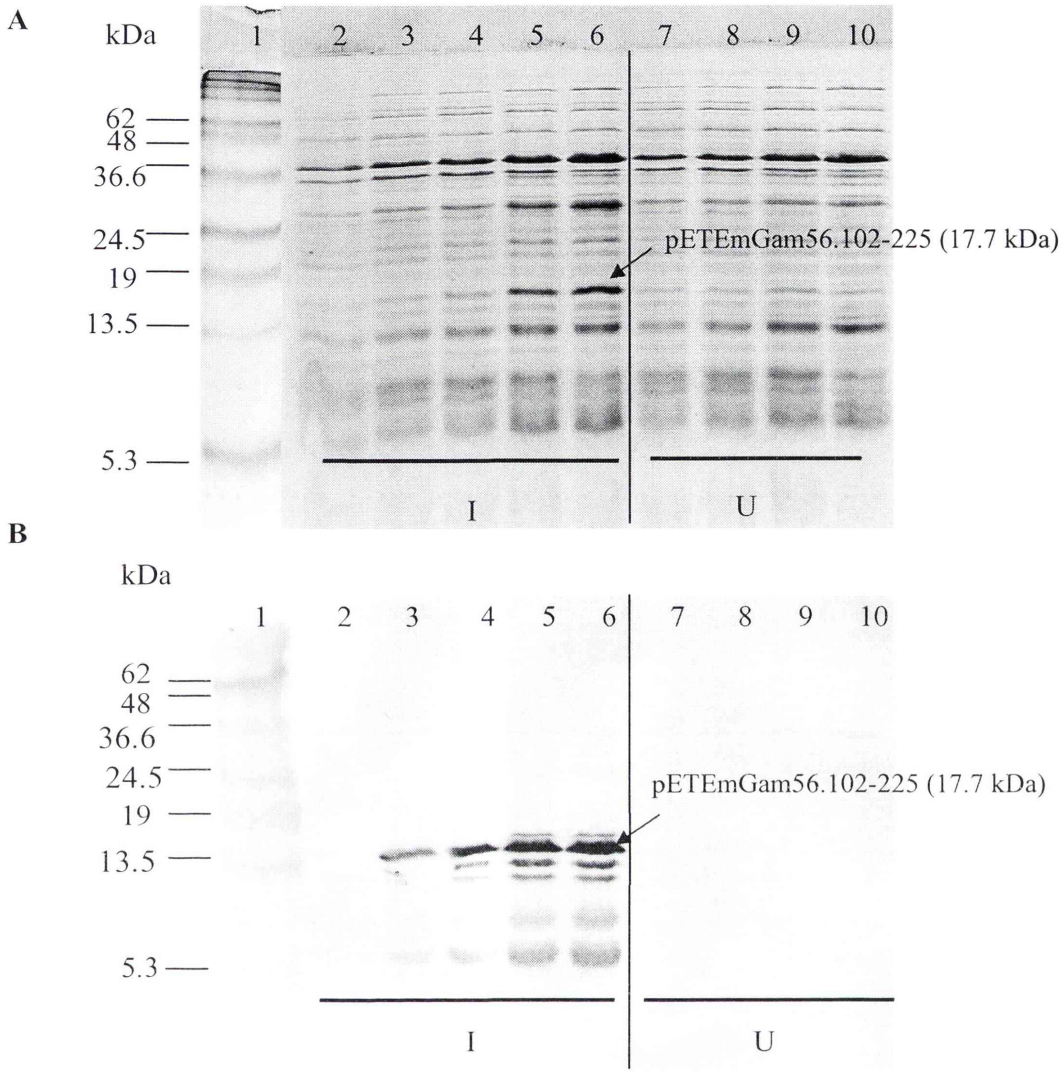

Figure 4.11 Coomassie blue staining (A) and immunoblot analysis (B) of pETEmGam56.102-225 expression from bacterial culture induced with 1 mM IPTG at 25°C. Bacterial lysates were analysed by SDS-PAGE, followed by staining with Coomassie blue or immunoblotting using mouse anti-pentahis antibodies. Lane 1= pre-stained protein ladder; Lane 2-6= bacterial lysates from pETEmGam56.102-225 induced with 1 mM IPTG at 25°C for 0, 0.5, 1, 2 and 3 hrs, respectively; Lane 7-10= samples grown at 25°C without IPTG for 0.5, 1, 2 and 3 hrs, respectively; I= constructs with IPTG induction. U= constructs without IPTG induction.

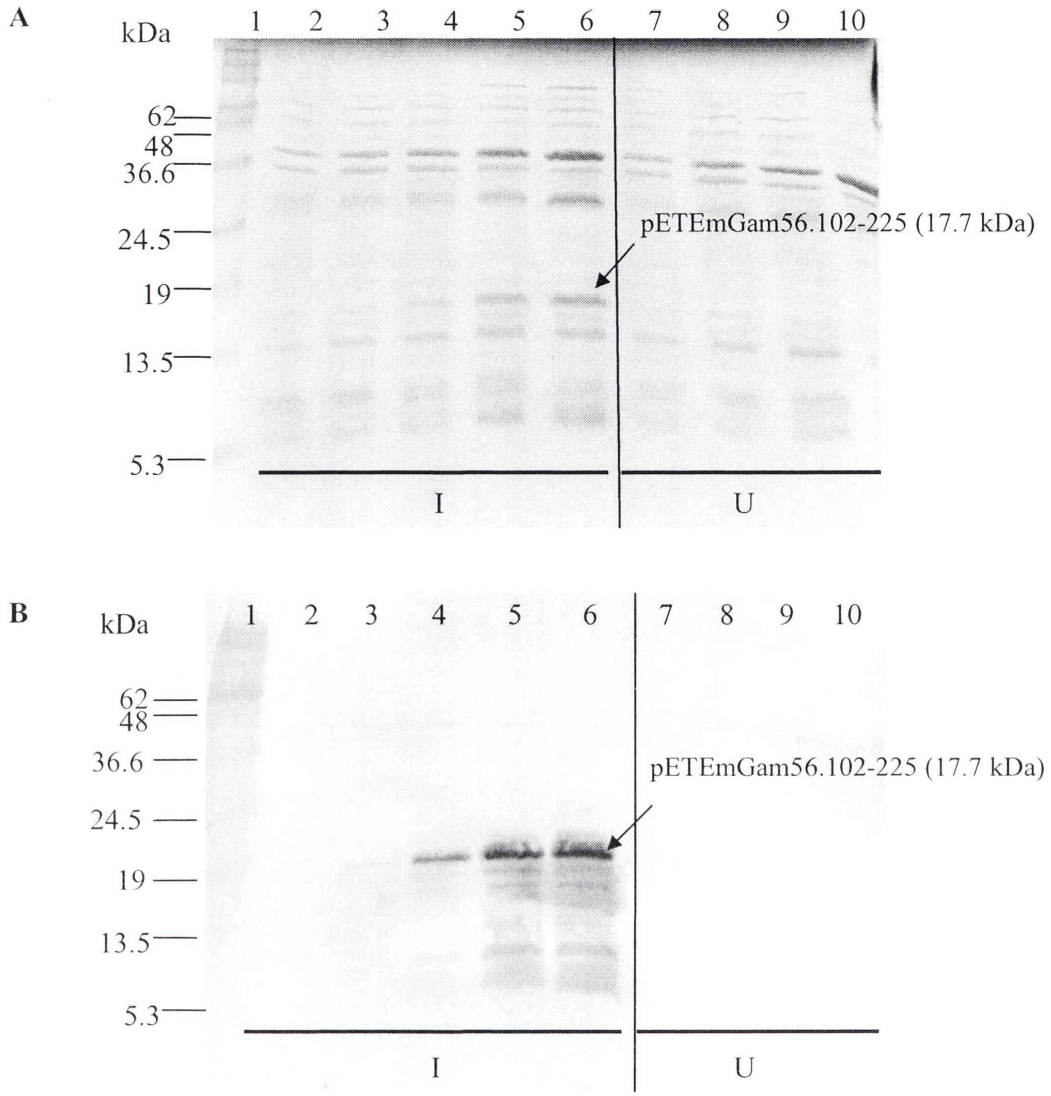

Figure 4.12 Coomassie blue staining (A) and immunoblot analysis (B) of pETEmGam56.102-225 expression from bacterial culture induced with 0.1 mM IPTG at 25°C. Bacterial lysates were analysed by SDS-PAGE, followed by staining with Coomassie blue or immunoblotting using mouse anti-pentahis antibodies. Lane 1= pre-stained protein ladder; Lane 2-6= bacterial lysates induced with 0.1 mM IPTG at 25°C for 0, 0.5, 1, 2 and 3 hrs, respectively; Lane 7-10= samples were grown without IPTG at 25°C for 0.5, 1, 2 and 3 hrs, respectively. I= constructs with IPTG induction. U= constructs without IPTG induction.

		Expression level	Protein degradation	
Temperature	25°C	++	++	✓
	30°C	+++	+++	
IPTG concentration	0.1 mM	++	++	
	1 mM	+++	++	✓
Time points (induction time)	0.5 hrs	+	+	
	1 hrs	++	++	
	2 hrs	+++	+++	
	3 hrs	++++	+++	✓

Table 4.3 Summary of pETEmGam56.102-225 expression under different conditions. Area with a tick indicates a better condition for protein expression in consideration of protein degradation. + to ++++ indicates low to high expression level.

The recombinant protein, pETEmGam56.102-225 was purified from 450 ml bacterial culture prepared under the optimal conditions (ie, induced with 1 mM IPTG at 25°C for 3 hours) and fractions containing pETEmGam56.102-225 were eluted in 500 mM imidazole as described in Chapter 2, Section 2.2.10. The purified fractions were analysed by SDS-PAGE, followed by staining with Coomassie blue. Bands representing pETEmGam56.102-225 were seen on a Coomassie blue stained gel (Lane 2-9, Figure 4.13). However, the purified fractions were still contaminated with higher molecular weight bacterial proteins. The yield from this purification was 4.56 μg per ml of culture (2.052 mg of purified proteins from 450 ml culture). The purification was repeated under the same conditions to produce enough pETEmGam56.102-225 for subsequent structural analyses.

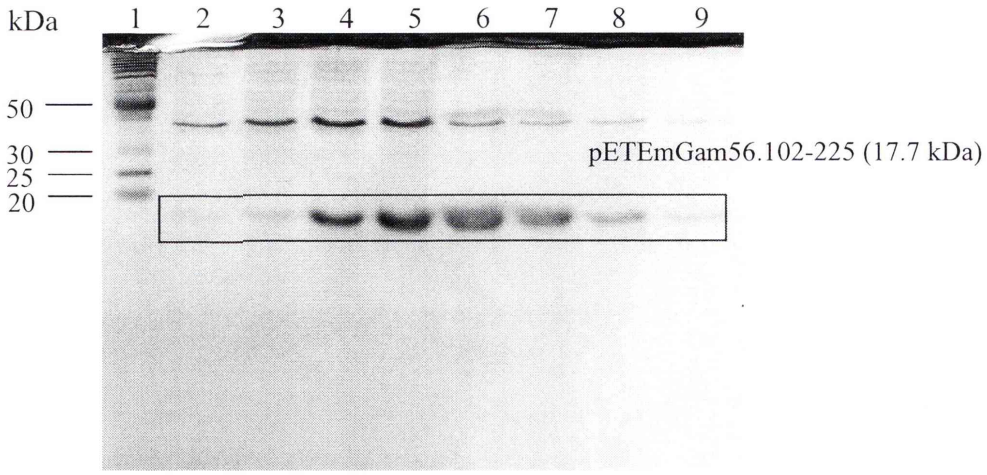

Figure 4.13 SDS-PAGE analysis of purified pETEmGam56.102-225 fractions from culture induced with 1 mM IPTG at 25°C for 3 hours. The purified fractions were analysed by SDS-PAGE, followed by staining with Coomassie blue. Lane 1= protein ladder; Lane 2–9= purified pETEmGam56.102-225 in fractions e1 (1.5 μg), e2 (2.5 μg), e3 (3.1 μg), e4 (3.3 μg), e5 (3.3 μg), e6 (2.9 μg), e7 (2.3 μg) and e8 (1.6 μg), respectively. The area highlighted in box represents the 17.7 kDa pETEmGam56.102-225 protein.

Since the purified fractions of pETEmGam56.102-225 were still contaminated with bacterial proteins, which could interfere with subsequent structural analyses, further purification of pETEmGam56.102-225 was attempted using anion-exchange chromatography. Prior to purification, pETEmGam56.102-225 was desalted using a PD10 column and then loaded onto an anion-exchange column. The column was prepared from DEAE cellulose anion exchange resin and equilibrated in 40mM Tris-HCl at pH 7.4, as described in Chapter 2, Section 2.2.11. An aliquot from each step was saved to monitor the purification. The proteins were eluted with a gradient of 100-600 mM NaCl in 40 mM Tris-HCl, pH 7.4, at a flow rate of 0.5 ml/min. Fractions were collected in four 0.5 ml aliquots for each concentration of NaCl. The purified fractions were analysed by SDS-PAGE, followed by silver staining as described in Chapter 2, Section 2.2.13. Bands representing pETEmGam56.102-225 were seen on the silver stained gels (Lane 7-14, Figure 4.14). No pETEmGam56.102-225 was seen from the following fractions: 100 mM (Lane 3-6, Figure 4.14), 400 mM (Lane 17-20, Figure 4.14), 500 mM (Lane 21-24, Figure 4.14) and 600 mM NaCl in 40 mM Tris-HCl pH 7.4 (Lane 25-18, Figure 4.14). The purity of pETEmGam56.102-225 fractions was enhanced since the purified fractions (Lane 7-14, Figure 4.14) contained less contaminant in comparison to that of the proteins before purification (Lane 15, Figure 4.14).

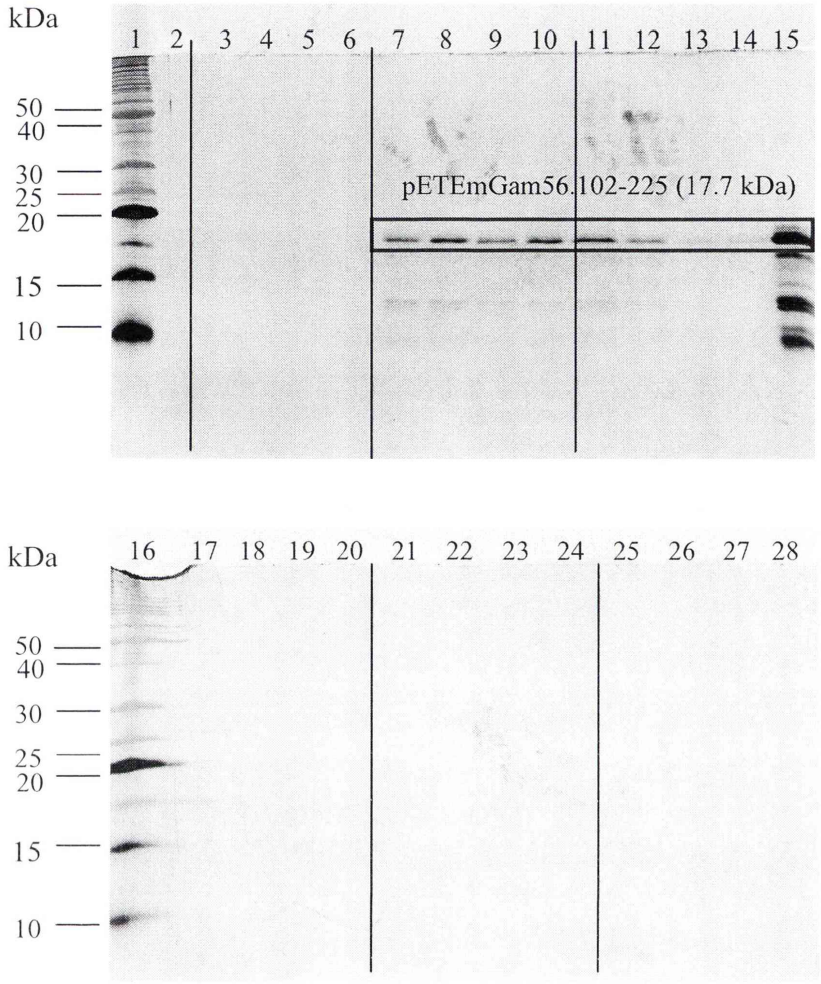

Figure 4.14 SDS-PAGE analyses of purified pETEmGam56.102-225 proteins by anion-exchange chromatography. pETEmGam56.102-225 was purified and eluted with a gradient of 100–600 mM NaCl in 40 mM Tris-HCl pH 7.4 at a flow rate of 0.5 ml/min. The purified fractions were analysed by SDS-PAGE, followed by staining with silver stain. Lane 1 and 16= protein ladder; Lane 2= flow-through; Lane 3-6= fractions eluted in 100 mM NaCl/Tris-HCl; Lane 7-10= purified pETEmGam56.102-225 fractions in 200 mM NaCl/Tris-HCl; Lane 11-14= purified pETEmGam56.102-225 fractions in 300 mM NaCl/Tris-HCl; Lane 15= before purification; Lane 17–20= fractions eluted in 400 mM NaCl/Tris-HCl; Lane 21-24= fractions eluted in 500 mM NaCl/Tris-HCl; Lane 25-28= fractions eluted in 600 mM NaCl/Tris-HCl.

However, smaller protein bands with a molecular weight of ~10 and 12 kDa were still present in the purified fraction; these could be the degraded products of pETEmGam56.102-225, as the fact that these smaller proteins co-purified with pETEmGam56.102-225 from the anion-exchange column suggested they have similar ionic properties.

Although the purity was enhanced slightly with this purification, the recovery was low (~12%) and, therefore, purification using anion-exchange column was not sufficiently efficient to produce the large amounts of pETEmGam56.102-225 proteins with high purity (1-2 mg of pETEmGam56.102-225 with a single band on a protein gel) required for structural analysis by NMR. Therefore, the purified pETEmGam56.102-225 from Figure 4.13 was desalted and buffer exchanged in 50 mM sodium phosphate buffer, pH 6.8. pETEmGam56.102-225 was then concentrated up to ~1.5 mg/ml using a centricon, in preparation for structural analyses by CD and NMR. Protein precipitation occurred after concentration of the recombinant protein. The supernatant and pellet of the concentrated pETEmGam56.102-225 were analysed by SDS-PAGE, followed by immunoblotting using mouse anti-r56 antibodies.

Bands representing pETEmGam56.102-225 were seen from the supernatant (Lane 1, Panel A, Fig. 4.15) as well as in the pellets of concentrated proteins (Lane 2, Panel A, Figure 4.15). However, protein bands other than pETEmGam56.102-225 (with molecular weights of ~ 38 and 65 kDa) were also detected on the gel; these represent contaminating bacterial proteins (Lane 3, Figure 4.15). Smaller bands with molecular weights of ~6 and 12 kDa detected from the supernatant were the degraded products of pETEmGam56.102-225 (Lane 2, Panel A, Figure 4.15), since mouse anti-recombinant 56 kDa antibodies not only recognized pETEmGam56.102-225 but also these two proteins (Lane 1, Panel B, Figure 4.15). The supernatants of the concentrated pETEmGam56.102-225 were selected for subsequent structural analyses.

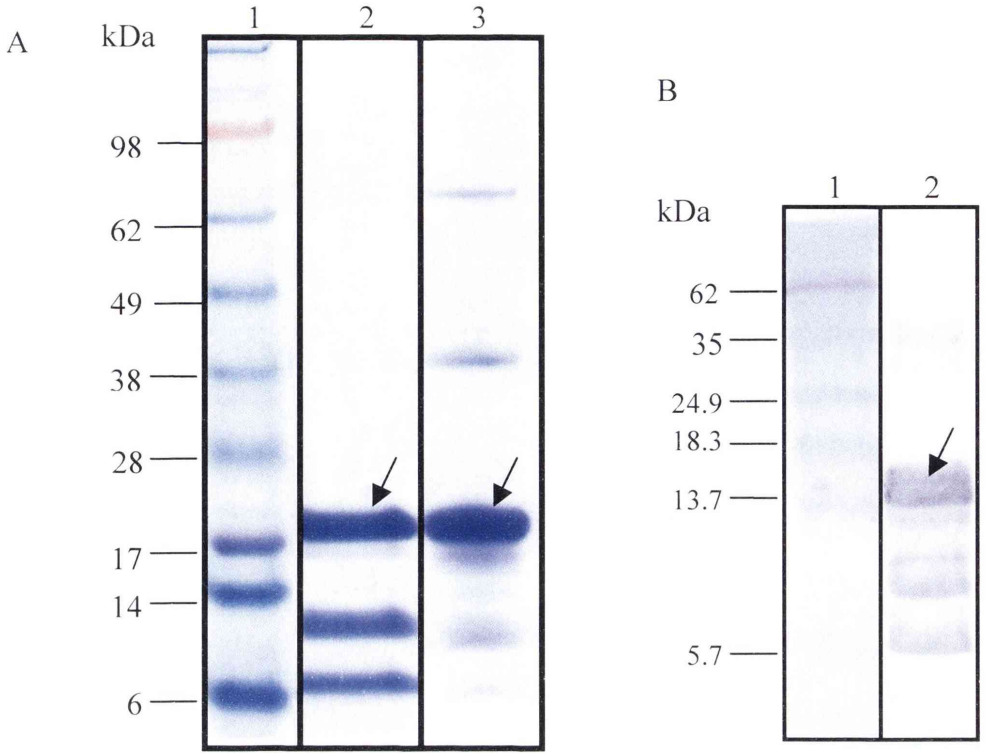

Figure 4.15 SDS-PAGE (A) and immunoblot analysis (B) of concentrated pETEmGam56.102-225. pETEmGam56.102-225 was concentrated up to ~1.5 mg/ml. Supernatants and pellets were analysed by SDS-PAGE, followed by staining with Coomassie blue (Panel A) or immunoblotting using mouse anti-recombinant 56 kDa antibodies (Panel B). Lane 1= SeeBlue® Plus 2 pre-stained protein ladder (panel A) or pre-stained protein ladder (Panel B); Lane 2 (Panel A and B) = supernatants of concentrated pETEmGam56.102-225; Lane 3 (Panel A) = pellets of concentrated pETEmGam56.102-225. Arrows indicate pETEmGam56.102-225 with a molecular weight of 17.7 kDa.

4.8 Recognition of pETEmGam56.102-225 by antibodies that recognise native EmGam56

As a means to provide an indication that the recombinant pETEmGam56.102-225 was structurally similar to the native EmGam56, its reactivity with anti-recombinant 56 kDa or anti-APGA antibodies was analysed by ELISA. Both of these antibodies are known to react strongly with the native EmGam56 protein (Belli *et al.,* 2003a, Ferguson *et al.,* 2003). Briefly, 96 well microtitre plates were coated with the recombinant protein and incubated with chicken anti-recombinant 56 kDa or anti-APGA antibodies (1:100 dilution). The plates were emptied and flushed in wash buffer, followed by incubating with secondary antibodies as described in Chapter 2, Section 2.2.15. Absorbance was read at 405 nm at 10 minutes after addition of substrate. APGA and r56 were included in the experiments as positive controls, with normal chicken serum as a negative control. Chicken anti-recombinant 56 kDa antibodies and anti-APGA antibodies reacted strongly with APGA and r56 and also reacted significantly with pETEmGam56.102-225 (Figure 4.16). The normal chicken serum did not react with any of the proteins.

4.9 The effect of heat treatment and pH on the stability of pETEmGam56.102-225

The stability of pETEmGam56.102-225 under heat treatment and pH change was investigated to provide evidence that it is an intrinsically unstructured protein, since stability under high temperature and extremes of pH are characteristics of intrinsically unstructured proteins (Uversky *et al.*, 1999; Uversky, 2003). Briefly, pETEmGam56.102-225 was boiled for 3, 10, 20, 30 and 40 minutes and analysed by SDS-PAGE and immunoblotting using mouse anti-recombinant 56 kDa antibodies (mouse anti-r56 antibodies). The protein band representing pETEmGam56.102-225 was detected by mouse anti-r56 antibodies reactivity in all the heat-treated samples (samples boiled for 10, 20, 30 and 40 minutes, Lane 3-6, Figure 4.17). This indicated that pETEmGam56.102-225 was stable under heat treatment and that the heat treatment did not abolish epitope binding of the proteins.

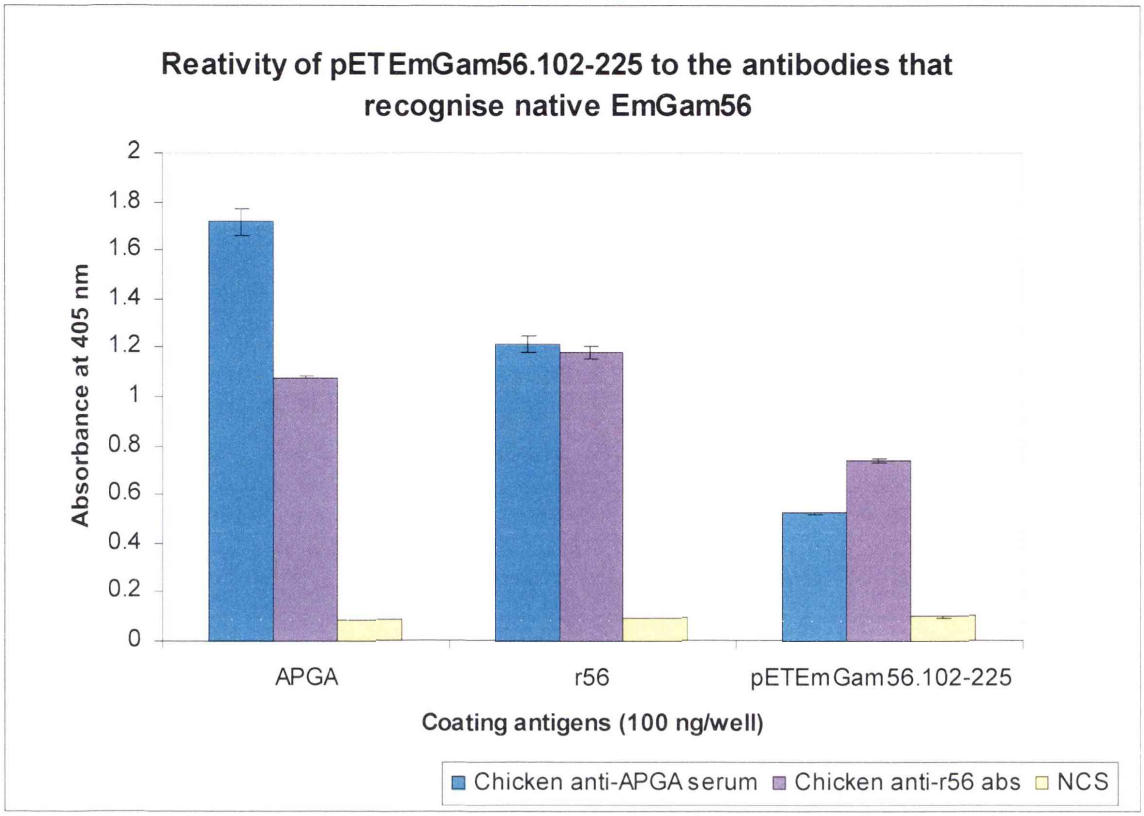

Figure 4.16 Reactivity of pETEmGam56.102-225 with antibodies that recognise native EmGam56. pETEmGam56.102-225 was coated onto a microtitre plate (100 ng/well) and incubated with 100 µl of chicken anti-recombinant 56 kDa antibodies (chicken anti-r56 antibodies, 1:100 dilution) or chicken anti-APGA antibodies (1:100 dilution) as described in Chapter 2, Section 2.2.15. Absorbance was read at 405 nm after 10 minutes incubation at 37°C. APGA and r56 were included in the experiment as positive controls. Negative control serum was normal chicken serum (NCS). Results are the mean ± S.E. for 2-4 repeats of the assay.

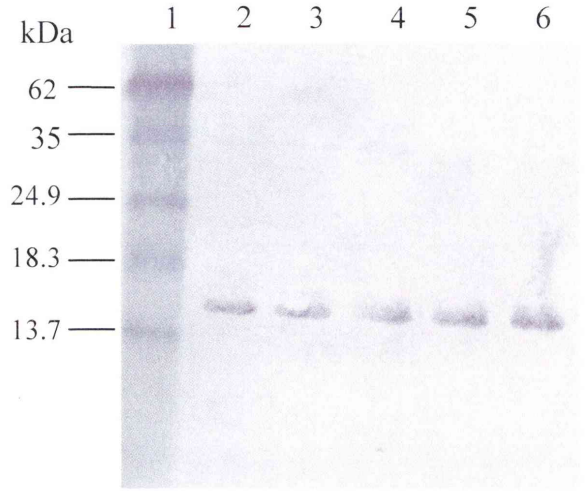

Figure 4.17 Immunoblot analysis of the effect of heat treatment on pETEmGam56.102-225. pETEmGam56.102-225 was boiled for various times and then analysed by SDS-PAGE, followed by immunoblotting using mouse anti-r56 antibodies. Lane 1= pre-stained protein ladder; Lane 2= control sample with boiling for 3 minutes (standard procedure); Lane 3–6= pETEmGam56.102-225, boiled for 10, 20, 30 and 40 minutes, respectively.

The stability of pETEmGam56.102-225 protein was further investigated by change of pH using a strong acid (HCl), a weak acid (citric acid) and a strong base (sodium hydroxide). The pH of pETEmGam56.102-225 was altered by introducing: (1) HCl in a series of different pH including pH 5, pH 3.99, pH 3.01, pH 2 and pH 1.03; (2) citric acid at pH 4; and (3) sodium hydroxide at pH 11. The samples were analysed by SDS-PAGE, followed by immunoblotting using mouse anti-r56 antibodies. Protein bands representing pETEmGam56.102-225 were still detected by mouse anti-r56 antibodies in the sample containing different pH of HCl (Lane 3-7, Figure 4.18); citric acid (Lane 8, Figure 4.18) and sodium hydroxide (Lane 9, Figure 4.18). Therefore, extreme pH range did not affect epitope binding of the protein to mouse anti-r56 antibodies and indicated that pETEmGam56.102-225 is very stable.

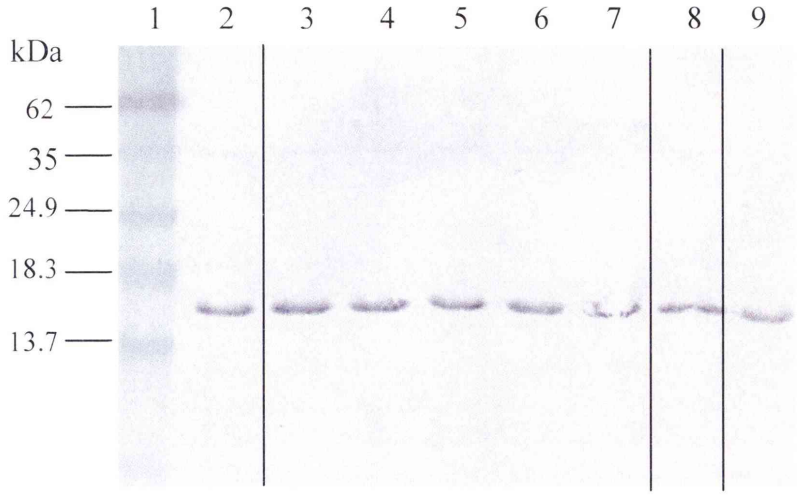

Figure 4.18 Immunoblot analysis of the effect of pH change on pETEmGam56.102.225. The pH of pETEmGam56.102-225 was altered by hydrochloric acid, citric acid and sodium hydroxide. The proteins were analysed by SDS-PAGE, followed by immunoblotting using mouse anti-r56 antibodies. Lane 1= pre-stained protein ladder; Lane 2= negative control sample (pH 7.4); Lane 3-7= pH change by hydrochloric acid at pH 5.1, pH 3.99, pH 3.03, pH 2.09 and pH 1.3, respectively; Lane 8= pH change by citric acid at pH 4; Lane 9= pH change by sodium hydroxide at pH 11.

4.10 Structural analysis of pETEmGam56.102-225 by CD and NMR

The secondary structure of pETEmGam56.102-225 (0.2 mg/ml) was analysed by Far-UV CD (spectral region at 190-250 nm). Prior to the analysis, the protein sample was centrifuged at 12,000 g for 3 minutes, to remove any aggregated matter, and 200 µl of the supernatant was loaded onto a cell with a path length of 1 mm. The spectrum was recorded at a wavelength range of 190 to 260 nm under nitrogen gas at a flow rate of 5 lpm using a spectropolarimeter as described in Chapter 2, Section 2.2.16.

The CD spectrum of pETEmGam56.102-225 was presented as a sum of fractional multiples of the reference spectra (each structure of α-helices, β-sheets and random coils give rise to a characteristic shape, and minima on CD spectrum) for each structural type. A characteristic spectrum of α- helices was observed at wavelengths of 208 nm and 222 nm (area with arrows, Panel A-C, Figure 4.19). The profile of CD spectra from three analyses was consistent at a wavelength of 200 to 260 nm whereas the spectrum at a wavelength below 200 nm was less consistent. Thus, the presence of β-sheets and random coils could not be confirmed by the CD spectra.

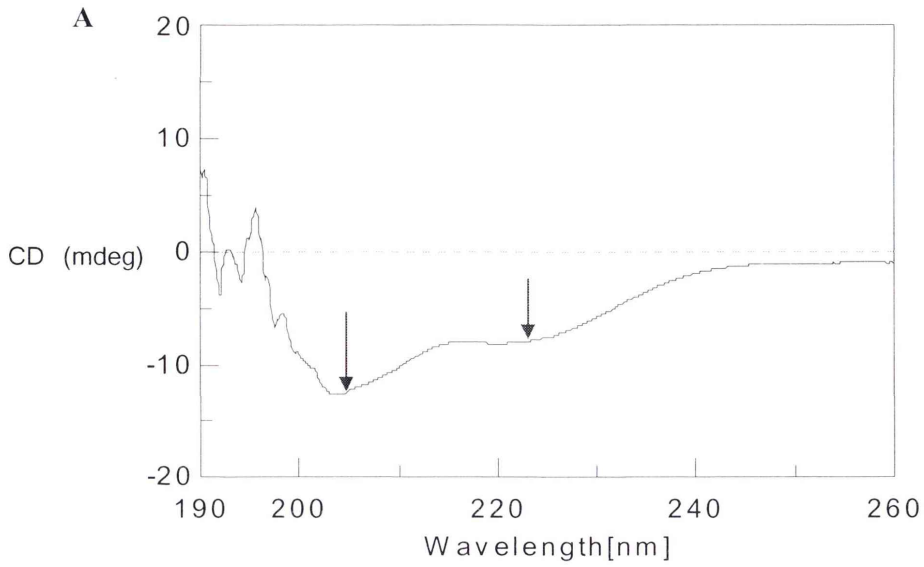

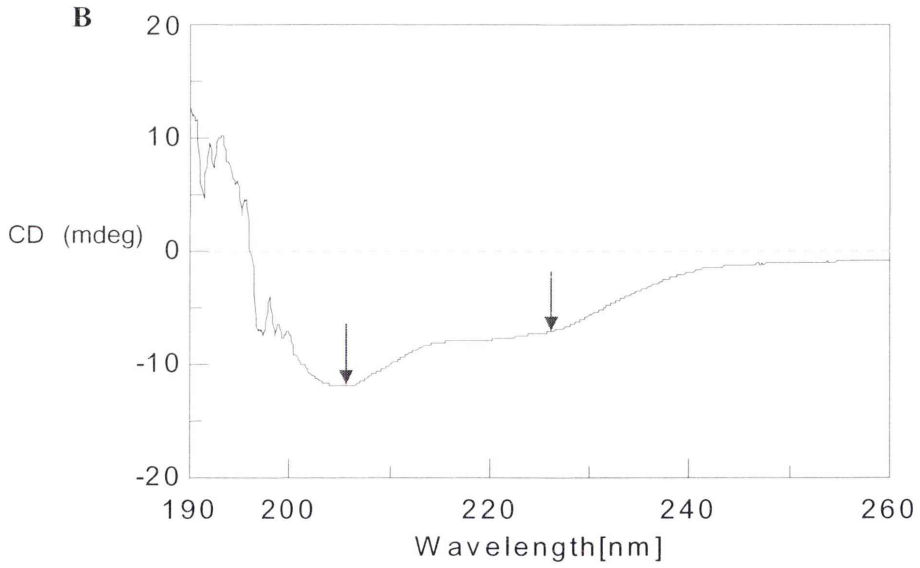

Figure 4.19 CD spectra of pETEmGam56.102-225 (Continued....)

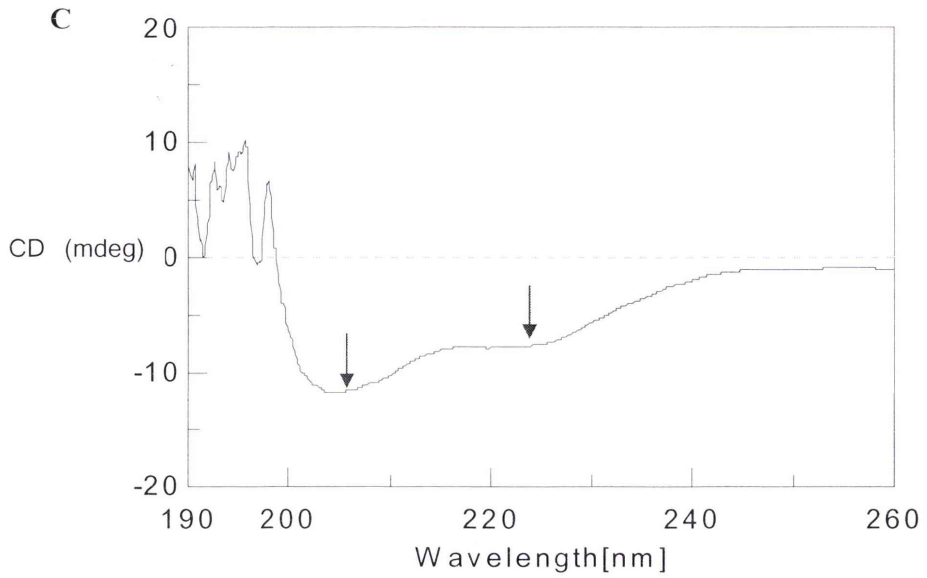

Figure 4.19 CD spectra of pETEmGam56.102-225. pETEmGam56.102-225 (0.2 mg) in 50 mM sodium phosphate buffer pH 6.8 was used for secondary structure analysis by CD. The spectra were recorded at a wavelength range from 190 to 260 nm under nitrogen gas at a flow rate of 5 lpm as described in Chapter 2, Section 2.2.16. Three analyses (Panel A, B and C) were performed and a negative control, 50 mM sodium phosphate buffer pH 6.8, was scanned as a blank (background). Arrows represent characteristic minima of α-helices at wavelengths of 208 nm and 222 nm on CD spectra.

The structural features of pETEmGam56.102-225 were further analysed by 1D-NMR. pETEmGam56.102-225 was desalted and concentrated up to 1.5 mg/ml, D_2O was added to the sample prior to analysis and a spectrum was recorded on a Bruker DRX600 spectrometer at 298 K as described in Chapter 2, Section 2.2.17. The chemical shift of an unstructured protein disperses in a narrow range on 1D-NMR spectrum: the main chain amide proton resonances range usually between 8.0 and 8.5 ppm, and side chain methyl proton resonances rarely shift to less than 0 ppm. The 1D-NMR profile of pETEmGam56.102-225 (Figure 4.20) showed a chemical shift of this recombinant protein dispersed in a narrow region: the main chain amide proton resonances were detected at less than 8.5 ppm, and the methyl proton resonances from the side chains were detected at more than 0.5 ppm, spectra that are characteristic of an intrinsically unstructured protein.

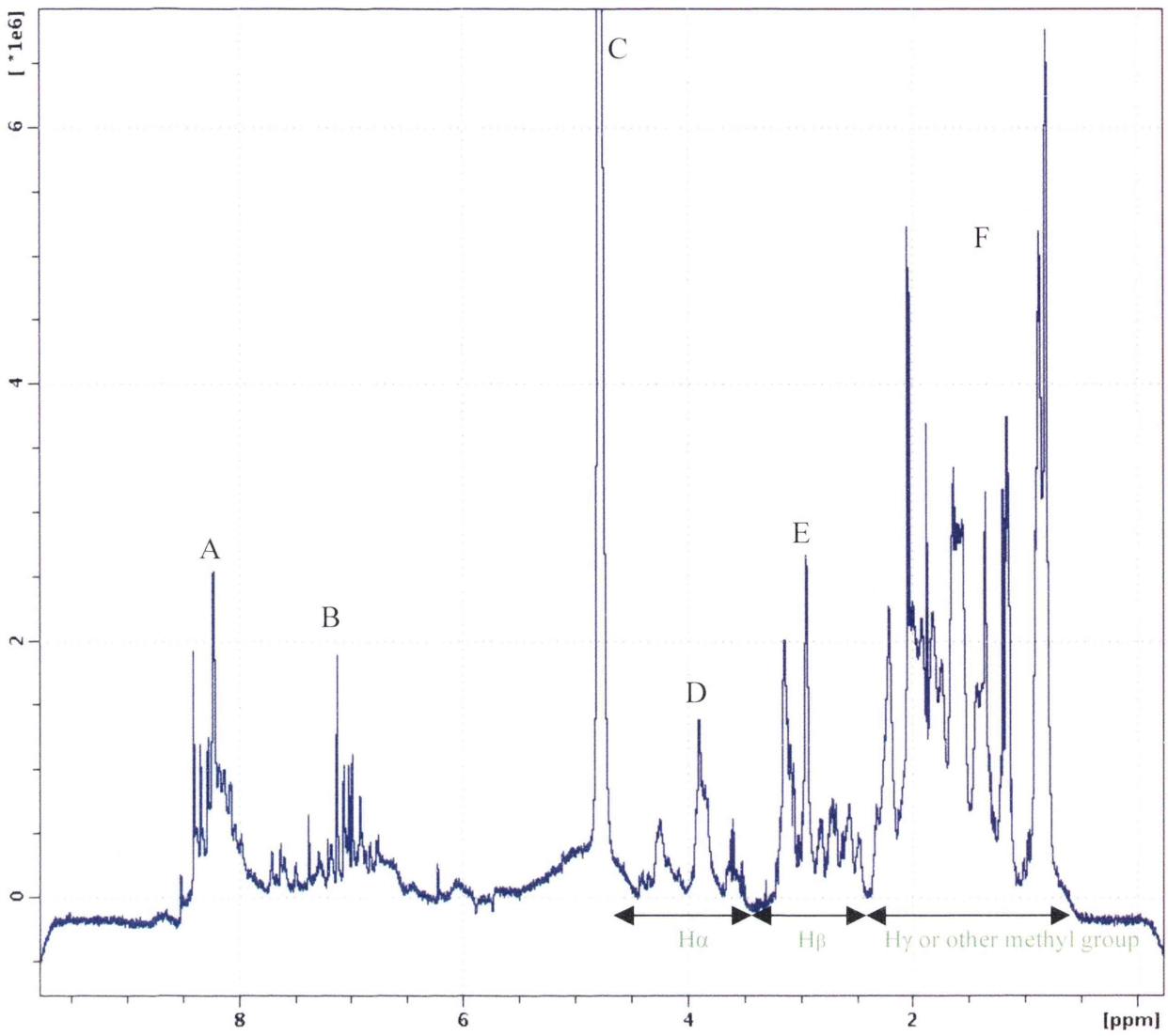

Figure 4.20 1D-NMR spectrum of pETEmGam56.102-225. The supernatant of pETEmGam56.102-225 (1.5 mg/ml) was used for structural analysis by 1D-NMR. Prior to the analysis, D_2O was added to a final concentration of 5% and the spectrum was recorded on a Bruker DRX600 spectrometer at 298 K. A= cross peaks between 8-8.5 ppm representing the proton resonances from the backbone amide (main chain); B= cross peaks between 6.5-7.5 ppm representing the proton resonances either from the side chain amide of Arg, Asn, and Gln or from the aromatic rings (such as Tyr, Trp and Phe); C= the water peak; D, E and F= cross peaks between 3.5-4.5 ppm, 2.5-3.5 ppm, 0.5-2.5 ppm, respectively, usually representing the proton resonances connected to carbons Cα, Cβ, Cγ or other methyl groups of the side chains.

4.11 Discussion

Six different bioinformatics programs – PSIPRED, APSSP2, SSPro, GOR4, HNN and SOPMA – predicted that EmGam56 is dominated by random coils (52-70%), with a significant degree of α-helical structure (28-43%) but relatively little β-sheet structure (1-11%). High level of random coils predicted on EmGam56 reflects its conformational flexibility, which is one of the characteristics of intrinsically unstructured proteins (IUPs). It has been shown that the extended conformation (conformational flexibility) of IUPs facilitates the different conformational requirements for binding modifying enzymes and their receptors - examples are post translational modifications such as phosphorylation (Ruzza *et al.*, 1996) and ubiquitination (Dunten and Cohen, 1989; Cox *et al.*, 2002; Yoshida *et al.*, 2005). In addition, regions of disorder - often found as flexible linkers - function to enable structured or unstructured functional domains to move relative to each other, and to recruit their binding partners which results in an enhanced affinity (with inactivation of voltage-gated ion channels as an example; Armstrong and Bezanilla, 1972).

FoldIndex© confirmed a large percentage of unfolded structure within EmGam56, especially between amino acid sequences 38-75, 100-137, and 205-324, and was, thus, in broad agreement with the predictions by PSIPRED, APSSP2, SSPro, GOR4, HNN and SOPMA, suggesting the consistency of bioinformatic predictions. Disorder proteins (often referred to as "natively unfolded proteins" or "intrinsically unstructured proteins") are defined as proteins that lack a fixed three dimensional structure, either partially or entirely, under physiological conditions (Weinreb *et al.*, 1996; Wright and Dyson, 1999; Uversky *et al.*, 2000). Regions of disorder less than 30 amino residues long are considered to be "short", whereas proteins having regions of disorder more than 30 amino residues are regarded as "long". The results of disorder predictions within EmGam56 varied slightly from one predictor to another due to the difference in methods and criteria used to assign or predict regions of disorder (see Chapter 2, Table 2.2). However, whilst there were differences in detail in the predictions of the different bioinformatics programs, there was consensus that disordered/unstructured/unfolded regions occur around amino acids 15-64, 127-144 and 182-196, as well as towards the C-terminus of the protein, which appears to be dominated by random coils.

Analyses by IUPred, RONN, DISPROT and DisEMBL™, programs designed to identify regions of structural disorder within proteins, confirmed the predictions by PSIPRED, APSSP2, SSPro, GOR4, HNN, SOPMA and FoldIndex©. Based on these predictions, truncated versions of a potential region of disorder can be generated for subsequent structural analyses by a combination of CD and NMR analyses, to confirm the results of the bioinformatics.

To confirm these structural predictions, at least partially, it was decided to generate CD and 1D-NMR spectra of EmGam56. The region from amino acids 102-225 of EmGam56 was selected for these biochemical analyses, for several reasons: first, the full-length protein is too large for structural analysis by NMR, which ideally should take place on proteins of not more than 100 amino acids (Feng, ZP, Zhang X and Norton RS, personal communication); second, this region contains areas predicted to possess classical secondary structures and unstructured regions (versus, for example the tyrosine-rich region and C-terminus of EmGam56, which are predicted to be dominated by random coils), allowing rational evaluation of the accuracy of the bioinformatics predictions; and, third, repeated efforts to produce recombinants of the sequence for amino acids 1-101 failed consistently. This is likely due to the unstructured nature of the recombinant, amino acids 1-101, (which was predicted to be mostly unfolded or unstructured by all disorder predictors used here) given that disorder regions could affect the solubility and/or crystallizability of a whole protein (Oldfield *et al.*, 2005). Alternatively, the recombinant protein may have been toxic and degraded rapidly by proteases of the host resulting in undetectable protein yields (Gupta *et al.*, 1998).

The pET101 vector was chosen to express this recombinant, designated pETEmGam56.102-225, since it contains a 3' histidine tag, which minimises the possibility of structural change when translation occurs in bacterial cells (Studier *et al.*, 1990; Shiryaev *et al.*, 2006) as well as degradation products of the recombinants due to the aim being to produce a single protein band on a gel (in theory, only the full length recombinants would be purified since the histidine tag was located at the 3' end). Furthermore, recombinant proteins arising from this vector have relatively smaller molecular weight than, for example, pTrcHisb constructs (Studier and Moffatt, 1986; Champion™ pET Directional TOPO® Expression Kit, version G, Instruction Manual, Invitrogen™).

The DNA fragments representing *pETEmGam56.102-225* (379 bp) or *56pET25b* (975 bp) were amplified from the parent construct *56pET25b*, indicating the success of DNA amplifiction by PCR. 56pET25b containing a DNA fragment encoding for amino acids 24-338 (corresponding to 172-1127 bp of *EmGam56* gene, see Chapter 2, Figure 2.1) has been previously generated in an expression vector, pET25b, by Dr Sabina Belli (Institute for the Biotechnology of Infectious Diseases, University of Technology, Sydney) and the recombinant proteins arising from the parent construct have been shown to be recognised by antibodies to the recombinant version of EmGam56, anti-r56 antibodies, (unpublished data). Therefore, the construct containing *pETEmGam56.102-225* was generated in a pET101 vector using the parent construct as a positive control. The identity of the recombinant construct was confirmed by DNA sequencing, suggesting the sequence of the insert (*pETEmGam56.102-225*) was 100% identical to the full length gene (*EmGam56*). In addition, it also confirmed that the DNA fragment was cloned in frame with the start codon (ATG) of pET101. The recombinant protein arising from this construct predicted molecular weight and theoretical isoelectric point to be 17.7 and 8.10, respectively.

Unfortunately, the recombinant protein arising from the construct engineered in pET101 was subject to degradation, which likely occurred during expression in bacterial cells since the degraded products were detected by mouse anti-pentahis antibodies before sonication. This is not totally surprising since bacteria possess proteases that lead to degradation of pETEmGam56.102-225. Expression and purification of pETEmGam56.102-225 was then optimised with respect to induction time, temperature, and IPTG concentration as far as possible, the aim being to produce high yields of a single band on a gel, in combat with degradation of pETEmGam56.102-225. Immunoblots of pETEmGam56.102-225 probed with mouse anti-pentahis antibodies revealed that expression level was roughly proportional to an increase of induction time (from 0.5 to 3 hours), temperature (from 25°C to 30°C), or IPTG concentration (from 0.1 mM to 1 mM). However, it seemed that when expression level was enhanced, degradation of pETEmGam56.102-225 was increased. Therefore, the expression condition that best satisfied the criteria for an enhanced expression level with less degradation of pETEmGam56.102-225 was selected to be 1 mM IPTG induction at 25°C for 3 hours.

Immunoblots of concentrated pETEmGam56.120-225 probed with mouse anti-r56 antibodies suggested that the supernatant of the concentrated proteins was still contaminated with two smaller proteins (~6 and 12 kDa; Figure 4.15) representing the degraded products of pETEmGam56.102-225. Never-the-less, the supernatant of the concentrated proteins was used for subsequent structural analyses by CD and NMR due to several reasons: first, an attempt to further purify pETEmGam56.102-225 using anion-exchange column was not successful; second, the presence of contaminants seemed highly unlikely to interfere with the structural analyses due to the fact that they were the degraded products of pETEmGam56.102-225 (ie, since they were derived from the same protein, signals representing the same part of the protein would overlap on the spectrum); third, the pellet from protein concentration contained a number of proteins, possibly bacterial in origin, apart from pETEmGam56.102-225 (Figure 4.15) and, thus, was not suitable for the analyses.

The recombinant protein pTrcEmGam56.102-225 was recognised well by chicken anti-recombinant 56 kDa antibodies by ELISA (Figure 4.16), suggesting that pTrcEmGam56.102-225 contained antigenic determinants that were also present in the recombinant form of EmGam56 (r56). Recognition of pTrcEmGam56.102-225 by chicken anti-APGA serum by ELISA (Figure 4.16) further indicated that pTrcEmGam56.102-225 is antigenic and structurally similar to the native protein (EmGam56). However, the reactivity of pTrcEmGam56.102-225 to these antibodies was lower than that of the positive controls (APGA or r56). This could be due to the fact that epitopes on pTrcEmGam56.102-225 may represent only part of the full complement of antigenic determinants (ie, epitopes might localise not only in the region of amino acids from 102-225 but also in other regions of EmGam56).

Western blot analyses of pETEmGam56.102-225 probed with mouse anti-r56 antibodies (Figure 4.17 and 4.18) demonstrated that extremes of temperature and pH did not affect the structure of pETEmGam56.102-225, giving a strong indication that this protein is intrinsically unstructured, as resistance to these treatments is a characteristic of such proteins (Kim *et al.*, 2000). It has been shown that a purification scheme for an enrichment of unstructured proteins in soluble fractions employs acids (5% PCA in a final concentration) in combination with heat treatment by boiling for 15 minutes (Cortese *et al.*,

2005). This method is based on the nature of intrinsically unstructured proteins (IUPs), which are typically in extended forms and often contain high percentages of charged residues and, thus, do not undergo large-scale structural changes at low pH. Therefore, IUPs are able to maintain solubility under these extreme conditions (Uversky *et al.*, 1999; Uversky, 2003). On the other hand, classically structured proteins are generally sensitive to extreme temperature and pH change since the protonation of negatively charged side chains leads to a charge imbalance that disrupts salt bridges and causes dissociation of subunits and cofactors (Goto *et al.*, 1990; Dill and Shortle, 1991; Fink *et al.*, 1994; Neumann *et al.*, 1998; Haines *et al.*, 2000). This can result in a loss of functions given that some proteins require folding or processing to gain or maintain their functions.

CD is a form of spectroscopy that measures differences in the absorption of left-handed versus right-handed polarized light due to structural asymmetry. CD can be used to determine secondary and tertiary structure of a protein in solution using Far-UV CD (measured at wavelength range from 190-250 nm) and Near-UV CD (measured at wavelength range from 250-350 nm), respectively (Adler *et al.*, 1973; Johnson, 1988). CD analysis confirmed the presence of α-helices within pETEmGam56.102-225 given that the characteristic minima of alpha-helix at a wavelength of 208 nm and 222 nm were seen on CD spectra (Figure 4.19). The spectra were measured in an oxygen-free spectrometer that was filled with pure nitrogen gas at a flow rate of 5 lpm for recording a wavelength range from 190 to 260 nm. The profile of CD spectra was consistent at wavelength range from 200-260 nm, confirming the presence of alpha-helices, whereas the spectra at wavelengths below 200 nm were more ambiguous (Figure 4.19). This is likely due to strong absorption of light by oxygen at wavelengths less than about 200 nm, which, unfortunately meant that the presence of beta sheets within pETEmGam56.102-225 could not be confirmed by CD analysis. This is consistent with the bioinformatics predictions of only low levels of beta sheet. However, unfortunately, CD analysis could also not confirm or refute the presence of random coils in pETEmGam56.102-225. Thus, NMR analyses were conducted.

Nuclear magnetic resonance (NMR) is a phenomenon that occurs when the nuclei of certain atoms are immersed in a static magnetic field and exposed to a second oscillating magnetic field (Wüthrich, 1990). Some nuclei experience this phenomenon, and others do not, depending on whether they possess a property called spin which gives rise to signals

on NMR spectra. 1D-NMR employed here for structural analysis of pETEmGam56.102-225 exploited the magnetic properties of nuclei of the hydrogen protons (^{1}H) of the protein to determine whether pETEmGam56.102-225 was intrinsically unstructured or natively unfolded. 1D-NMR analysis confirmed the presence of random coils within pETEmGam56.102-225, since the chemical shifts of pETEmGam56.102-225 possess signatures representative of intrinsically unstructured proteins. In contrast, in a structured protein, due to the diverse chemical environments caused by classical secondary and tertiary structures, the chemical shifts are dispersed over a large range: the main chain amide proton resonance range is more than 10 ppm and the side chain methyl proton resonance range is less than 0 ppm. In contrast, because the extended conformation of an unstructured protein exposes most residues to similar chemical environments, the major source of chemical shift distinction is eliminated.

Taken together, the bioinformatic and biochemical analyses of EmGam56 indicate an intrinsically unstructured protein. This may be an important feature in the formation of inter-protein bonds and the formation of the oocyst wall (this point will be discussed in more detail in the final discussion chapter of this thesis).

Chapter Five
Peroxidase and peroxide mediated cross-linking of a tyrosine rich protein from the wall forming bodies of the macrogamete of *Eimeria maxima*

5.1 Introduction

The oocyst wall of *E. maxima* is rich in dityrosine and DOPA (Belli *et al.*, 2003b), two molecules involved in the cross-linking of proteins via the amino acid, tyrosine (Aeschbach *et al.*, 1976; Foerder and Shapiro, 1977; Malencik and Anderson, 1996; Burzio and Waite, 2000; Burzio and Waite, 2001). The oocyst wall forms in a regulated fashion from the contents of specialized organelles – wall forming bodies - within the macrogamete stage of the parasite (Ferguson *et al.*, 2003). Two proteins from the macrogamete of *E. maxima*, EmGam56 and EmGam82, have been relatively well characterized and studied and have been shown to be integral to the development of the oocyst wall (Ferguson *et al.*, 2003). Both these proteins are unusually rich in tyrosine and are processed or degrade into smaller proteins of various sizes (Belli *et al.*, 2003b). These smaller proteins are believed to be cross-linked via dityrosine, and possibly DOPA, bonds to help form the oocyst wall and give it its qualities of resistance to chemical and environmental insult (Belli *et al.*, 2005). Dityrosine cross-linking is an oxidative process, normally catalysed by peroxidase(s), and DOPA is, likewise, an oxidative process but catalysed by DOPA oxidase (Marumo and Waite, 1986; Heinecke *et al.*, 1993; Gieseg *et al.*, 1993; Malencik and Anderson, 1996; Michon *et al.*, 1997); both these enzyme activities have been detected specifically in the wall forming bodies and the developing oocyst wall of *E. maxima in situ* in the small intestine (Belli *et al.*, 2003b; 2005; DJP Ferguson, personal communication). However, the idea that the tyrosine-rich proteins, EmGam56, EmGam82 and their derivatives, can actually form suitable dityrosine or DOPA cross-links has not been tested. Thus, the aim of this chapter of research is to show that a truncated recombinant form of EmGam56 can be cross-linked by peroxides in the presence of DOPA oxidase or peroxidase(s).

5.2 Experimental Plan

A truncated recombinant version of EmGam56 – r56 (see Chapter 4 for details) – was used to develop an *in vitro* cross-linking assay (see Chapter 2, Section 2.2.18 for details). Briefly, 5 µg of r56 in 0.1 ml of 0.25 M borate buffer (pH 8.35), was incubated along with peroxide (either H_2O_2 or *tertiary*-butylhydroperoxide – *t*-BHP - at a final concentration of 1%) as substrate, and one of several enzymes, including:

- Catalase (250 kDa, from bovine liver, purchased from Sigma), an antioxidant that activates the decomposition of hydrogen peroxide into oxygen and water;
- DOPA oxidase (119.5 kDa, from mushrooms, purchased from Sigma), a copper-containing oxidase that catalyses oxidation of catechols and cresol and converts tyrosine to L-DOPA or tyramine to dopamine;
- Myeloperoxidase (MPx, a 116 kDa peroxidase from human leukocytes, purchased from Sigma), an enzyme that has cytotoxic actions on bacteria, fungi and tumor cells by catalysing oxidation of hydrogen peroxide resulting in the production of hypochlorous acid;
- Horseradish peroxidase (HRPO, a 40 kDa peroxidase from horseradish, purchased from Fluka 77332); and
- *Arthromyces* peroxidase (APx, a 41 kDa peroxidase from *Arthromyces ramosus,* purchased from Sigma).

Incubations were carried out for various lengths of time and with various concentrations of enzymes, as indicated in the results. The specificity of the effects of the various peroxidases was confirmed by including inhibitors in the incubations including salicylhydroxamic acid (SHA), phenylhydrazine hydrochloride (PH) and 3'-amino-1, 2, 4-triazole (3'AT). SHA is a weak organic acid known to inhibit a number of peroxidases including horseradish peroxidase, *Arthromyces* peroxidase and myeloperoxidase. PH is a potent DOPA oxidase inhibitor; however, it has a much broader spectrum, also inhibiting a wide range of oxidases and peroxidases. 3'AT is a specific inhibitor of catalase but is also known to have inhibitory effects on heme-containing enzymes (Margoliash *et al.*, 1960).

Cross-linking of r56 was assessed in two ways (as described in detail in Chapter 2, Section 2.2.19 and 2.2.20): first, Western blotting (ECL), using specific antibodies to r56, was used to detect the disappearance of the 42 kDa r56 protein band and the appearance of high molecular weight oligomers - dimers, trimers and polymers of r56; and, second, HPLC was used to detect dityrosine and DOPA in the samples.

5.3 Hydrogen peroxide catalyses cross-linking of r56 in the absence of exogenous enzyme

r56 was incubated with 1% H_2O_2. Western blotting revealed the disappearance of the 42 kDa r56 protein band and the appearance of two high molecular weight protein bands, one at ~168 kDa and another very high molecular weight band (Panel A, Figure 5.1). This high molecular weight band was also present in the control incubation but Western blotting did not reveal any significant loss of the original r56 protein in this incubation nor the appearance of the ~168 kDa band. The appearance of this band was observed sporadically during the experiments described throughout this chapter and is likely to represent a background level of spontaneous cross-linking or, more likely given the absence of detection of dityrosine or DOPA by HPLC, aggregation of the recombinant protein under control conditions.

Incubation with 1% *t*-BHP did not have the same effect; there was no disappearance of r56 and no detection of any high molecular weight bands (Panel B, Figure 5.1). HPLC analyses to detect dityrosine and DOPA demonstrated that incubation of r56 with H_2O_2 resulted in the formation of high numbers of dityrosine bonds (~15 mmol/mol *p*-tyrosine; Figure 5.1) but no significant DOPA was detected. *t*-BHP did not cause any formation of dityrosine or DOPA bonds (Figure 5.1).

Catalase was possibly able to partially reverse the effect of H_2O_2, reducing the disappearance of the r56 protein band and reducing the number of dityrosine bonds formed by 28% from 20.36 mmol of dityrosine per mol of *p*-tyrosine to 14.76 (Figure 5.2), though this was not statistically significant. Catalase was also included in incubations with *t*-BHP and had no effect on the Western blot profile of r56; there was no disappearance of the 42 kDa r56 band and no appearance of high molecular weight bands (Figure 5.2). Likewise, catalase plus *t*-BHP had no effect on dityrosine or DOPA formation (Figure 5.2).

Subsequent experiments with various oxidizing enzymes were conducted using *t*-BHP as substrate rather than H_2O_2 because of the latter molecule's propensity to stimulate cross-linking of r56 in the absence of any exogenous co-factors.

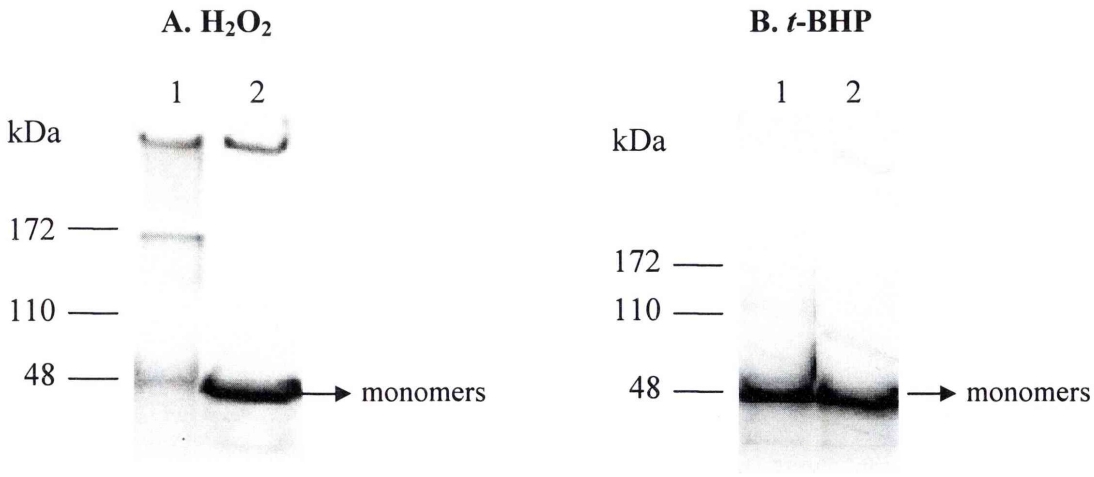

Figure 5.1 ECL analyses of H_2O_2 (A) and *t*-BHP (B) catalyzed r56 crosslinking. Each sample contained 5 μg of r56 proteins with either *t*-BHP or H_2O_2. The samples were incubated at 37°C for 50 minutes, followed by SDS-PAGE and immunoblotting/ECL using mouse anti-r56 antibodies. Components in each sample are indicated in the table below. Arrows indicate r56 proteins with a molecular weight of 42 kDa in monomeric forms.

Lane number		1	2
r56 (5 μg)		+	+
Peroxide (final conc. of 1 %)		+	-
0.25 M sodium borate buffer pH 8.35		+	+
Dityrosine* (mmol/mol of p-tyrosine)	*t*-BHP	0.256+/-0.153	0.251+/-0.184
	H_2O_2	15.357 +/-1.057	0.251 +/-0.184
DOPA* (mmol/mol of p-tyrosine)	*t*-BHP	0.70 +/- 0.43	1.91 +/- 0.70
	H_2O_2	0.00+/-0.00	1.91 +/- 0.70

*The levels of dityrosine and DOPA are the mean + standard deviation (n= 4).

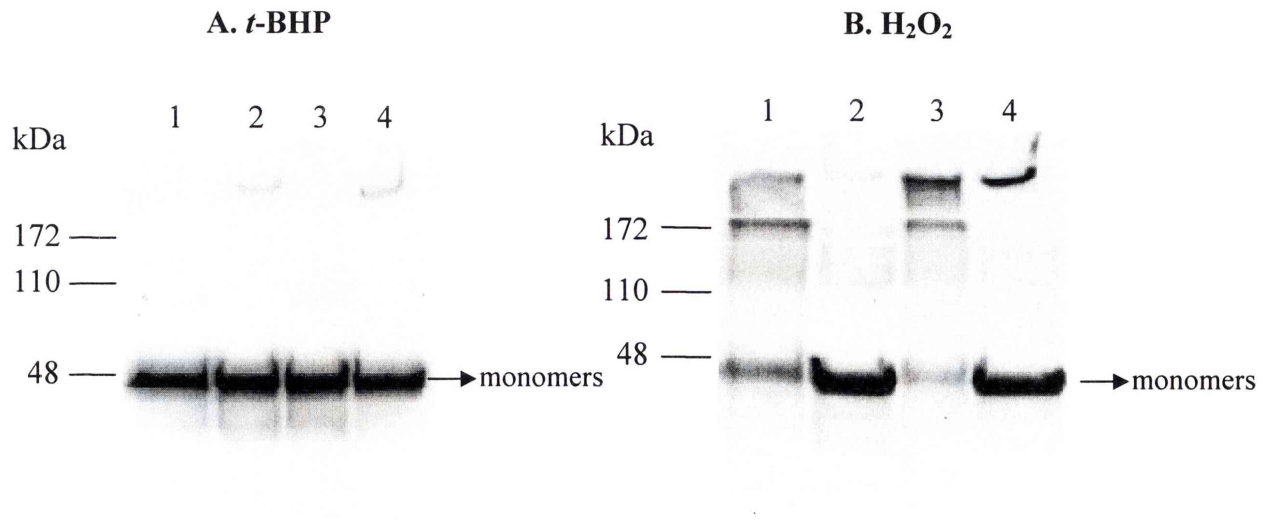

Figure 5.2 ECL analyses of the effect of catalase on r56 crosslinking. Each sample contained 5 μg of r56 and 0.25 μg of catalase with either *t*-BHP or H_2O_2 as a crosslinking agent. The samples were incubated at 37°C for 50 minutes, followed by SDS-PAGE and immunoblotting/ECL using mouse anti-r56 antibodies. Components in each sample are indicated in the table below. Arrows indicate r56 proteins with a molecular weight of 42 kDa in monomeric forms.

Lane number		1	2	3	4
r56 (5 μg)		+	+	+	+
Catalase (0.25 μg)		+	+	-	-
Peroxide (final conc. of 1 %)		+	-	+	-
0.25 M sodium borate buffer pH 8.35		+	+	+	+
Dityrosine* (mmol/mol of p-tyrosine)	*t*-BHP	0.097 +/- 0.091	0.069 +/- 0.023	0.075 +/- 0.031	0.079 +/- 0.017
	H_2O_2	14.755 +/- 3.603	0.069 +/-0.023	20.360 +/-4.784	0.083+/-0.015

*The levels of dityrosine are the mean + standard deviation (n= 4).

5.4 DOPA oxidase does not catalyse cross-linking of r56

Incubation of r56 with DOPA oxidase did not result in any significant formation of dityrosine or DOPA, despite the apparent formation of a high molecular weight protein band (Figure 5.3); as mentioned previously, since HPLC analysis failed to reveal any significant dityrosine or DOPA, this band probably represents low level spontaneous aggregation of r56. The addition of *t*-BHP to the incubation mix did not result in any formation of high molecular weight bands, dityrosine or DOPA (Figure 5.3).

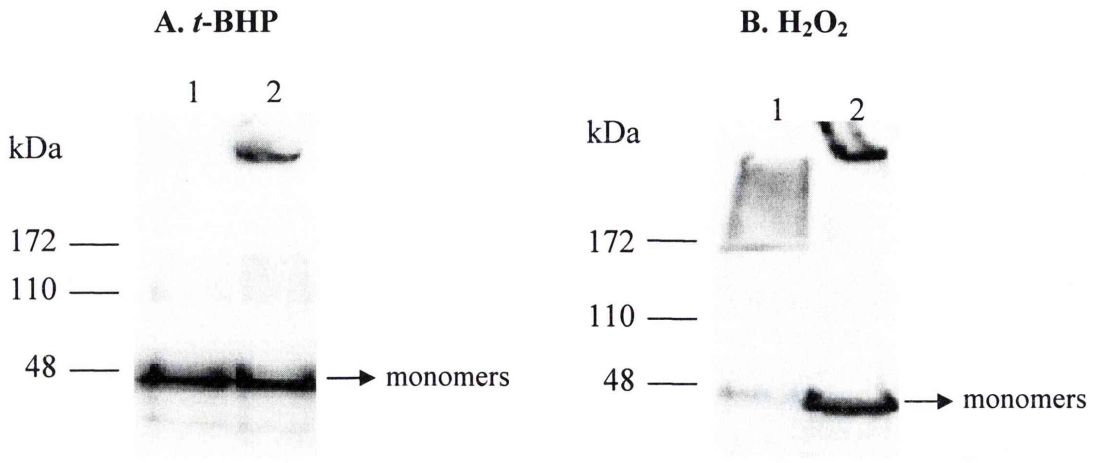

Figure 5.3 ECL analyses of DOPA oxidase catalyzed r56 crosslinking. Each sample contained 5 μg of r56 proteins and 0.25 μg of DOPA oxidase with either *t*-BHP or H_2O_2 as a crosslinking agent. The samples were incubated at 37°C for 50 minutes, followed by SDS-PAGE and immunoblotting/ECL using mouse anti-r56 antibodies. Components in each sample are indicated in the table below. Arrows indicate r56 proteins with a molecular weight of 42 kDa in monomeric forms.

Lane number		1	2
r56 (5 μg)		+	+
DOPA oxidase (0.25 μg)		+	+
Peroxide (final conc. of 1 %)		+	-
0.25 M sodium borate buffer pH 8.35		+	+
Dityrosine* (mmol/mol of p-tyrosine)	*t*-BHP	0.150 +/- 0.076	0.259 +/-0.098
	H_2O_2	14.146 +/- 1.607	0.259 +/-0.098
DOPA* (mmol/mol of p-tyrosine)	*t*-BHP	1.11 +/- 0.33	1.92 +/- 0.71
	H_2O_2	0.00 +/- 0.00	0.98+/-0.280

*The levels of dityrosine and DOPA are the mean + standard deviation (n= 4).

5.5 Myeloperoxidase does not catalyse cross-linking of r56 in the presence of *t*-butylhydroperoxide

Incubation of r56 with MPx did not cause the disappearance of the 42 kDa r56 protein band (Figure 5.4) or the appearance of high molecular weight protein bands that did not also occur in control incubations. Thus, high molecular weight protein bands were not detected in Lane 1, Figure 5.4 and, in addition, the level of dityrosine in Lane 1 (0.30 +/- 0.163 mmol/mol p-tyrosine) was not significantly different from the rest of the samples (0.193 +/- 0.031 mmol/mol p-tyrosine in Lane 2, 0.283 +/- 0.164 mmol/mol p-tyrosine in Lane 3, and 0.484 +/- 0.288 mmol/mol p-tyrosine in Lane 4, Figure 5.4). The band with a molecular weight of greater than 172 kDa is, once again, likely to be aggregated proteins rather than polymers, given the absence of dityrosine in the samples (Figure 5.4).

The MPx-catalysed cross-linking assays were repeated under the same conditions except that incubation time was varied. Thus, incubations of 0, 5, 10, 20, 30, 40, 50 and 60 minutes were carried out (as described in detail in Chapter 2, Section 2.2.18). Varying incubation time did not affect MPx-catalysed formation of high molecular weight protein bands, with the possible exception of the longer incubations. However, as the band seen in the 60 minute incubation is also seen in the 60 minute control incubation, along with similar intensity of detection of the 42 kDa r56 band being apparent in both samples, this is, again, likely due to protein aggregation rather than polymerisation (Figure 5.5). Very similar results were obtained when the concentration of MPx was varied (Figure 5.6); there was no significant decrease in intensity of the 42 kDa r56 protein band and no polymers of this protein were detected.

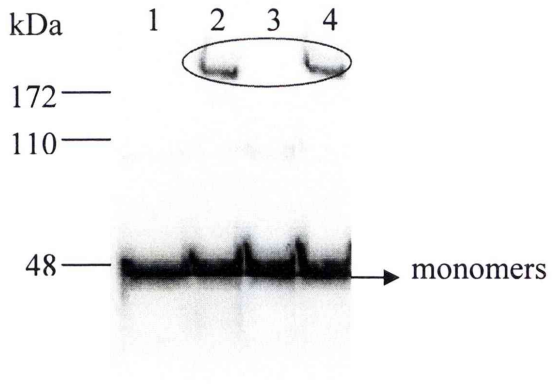

Figure 5.4 ECL analysis of MPx catalyzed r56 crosslinking. Crosslinked samples were prepared and separated on a 12% polyacrylamide gel, followed by transferring proteins to PVDF membrane. High molecular weight oligomers were detected by immunoblotting/ECL using mouse anti-r56 antibodies. Components in each sample are indicated in the table below. Arrow indicates r56 proteins with a molecular weight of 42 kDa in monomeric forms. Circled area represented aggregated r56 proteins.

Lane number	1	2	3	4
r56 (5 μg)	+	+	+	+
MPx (0.25 μg)	+	+	-	-
t-BHP (final conc. of 1 %)	+	-	+	-
0.25 M sodium borate buffer pH 8.35	+	+	+	+
Dityrosine* (mmol/mol p-tyrosine)	0.196 +/- 0.156	0.193 +/- 0.031	0.237 +/- 0.169	0.224 +/- 0.130

*The levels of dityrosine are the mean + standard deviation (n= 4).

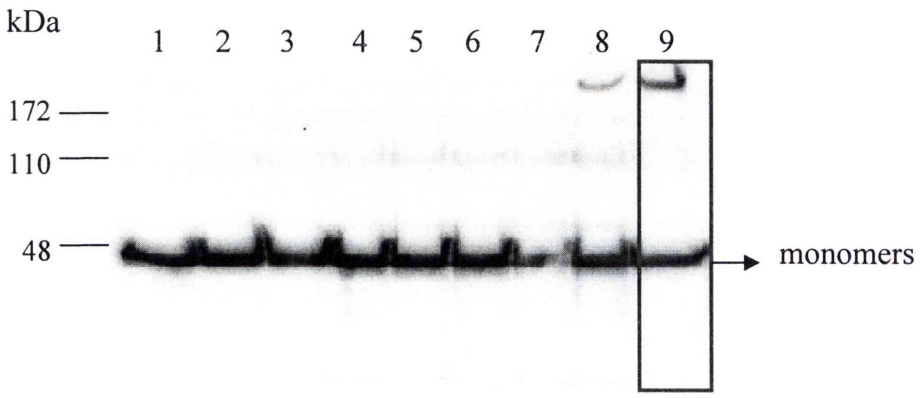

Lane number	1	2	3	4	5	6	7	8	9
Incubation time (mins)	0*	5	10	20	30	40	50	60	60

*Not absolute zero; approximately 5 seconds delayed from zero.

Figure 5.5 ECL analysis of time course on MPx catalyzed r56 crosslinking. Each sample contained 5 μg of r56 proteins, 0.25 μg of MPx and 1% of *t*-BHP. The samples were incubated at 37°C for 0, 5, 10, 20, 30, 40, 50 and 60 minutes (in Lane 1, 2, 3, 4, 5, 6, 7 and 8, respectively). A negative control sample, boxed area in Lane 9, contained r56 proteins only with incubation for 60 minutes. The samples were analyzed by immunoblotting/ECL using mouse anti-r56 antibodies. Arrow indicates monomeric forms of r56 proteins, 42 kDa (monomers).

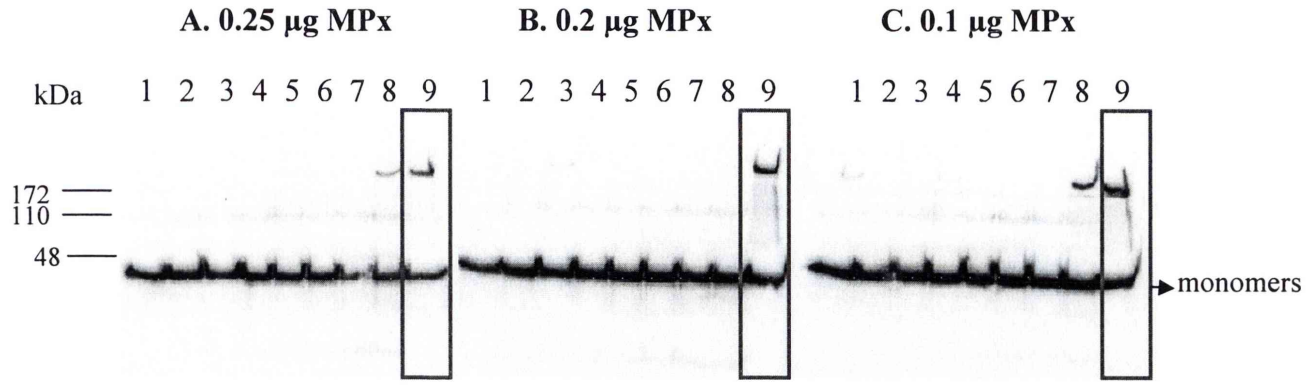

Lane number	1	2	3	4	5	6	7	8	9
r56 (5 μg)	+	+	+	+	+	+	+	+	+
MPx (0.25, 0.2 or 0.1 μg)	+	+	+	+	+	+	+	+	-
t-BHP (final conc. of 1%)	+	+	+	+	+	+	+	+	-
0.25 M sodium borate buffer pH 8.35	+	+	+	+	+	+	+	+	+
Incubation time (mins)	0*	5	10	20	30	40	50	60	60

*Not absolute zero; it was approximately 5 seconds delayed from zero.

Figure 5.6 ECL analyses of r56 crosslinking with varied MPx concentration. Each sample contained 5 μg of r56 proteins and 1% of *t*-BHP but different amount of MPx (0.25 μg in Panel A, 0.2 μg in Panel B and 0.1 μg in Panel C). The samples were incubated at 37°C for 0, 5, 10, 20, 30, 40, 50 and 60 minutes (in Lane 1, 2, 3, 4, 5, 6, 7 and 8, respectively). A negative control sample, boxed area in Lane 9, contained r56 proteins only with incubation for 60 minutes. The samples were analyzed by immunoblotting/ECL using mouse anti-r56 antibodies.

5.6 Horseradish peroxidase catalyses cross-linking of r56 in the presence and absence of exogenous *t*-butylhydroperoxide

Incubation of r56 proteins with HRPO and *t*-BHP caused the disappearance of the 42 kDa r56 protein band and the appearance of a very strong band at a very high molecular weight (Lane 1, Figure 5.7). In the absence of *t*-BHP, HRPO still caused the disappearance of the 42 kDa band but, in addition to the very high molecular weight band, protein bands of ~84 kDa, ~126 kDa and ~168 kDa were also observed (Lane 2, Figure 5.7). In addition, high level of dityrosines (5.422 +/- 0.567 mmol/mol p-tyrosine) were detected in the sample that had both *t*-BHP and HRPO (Lane 1, Figure 5.7); these levels were approximately 5 times higher than those seen in the absence of *t*-BHP (Lane 2, Figure 5.7) and 43 times higher and 39 times higher than the levels of dityrosine seen in the control samples lacking HRPO (Lane 3 and 4, Figure 5.7). The levels of dityrosine seen in the sample containing HRPO but no *t*-BHP (1.171 +/- 0.061 mmol dityrosine/mol *p*-tyrosine) were still significantly higher than levels seen in the control incubations.

The HRPO-catalysed cross-linking assays were repeated under the same conditions, in the presence of *t*-BHP but incubation time was varied. Thus, incubations of 0, 5, 10, 20, 30, 40, 50 and 60 minutes were carried out (as described in detail in Chapter 2, Section 2.2.18). Protein bands of ~84 and ~168 kDa were apparent immediately upon addition of HRPO (Lane 1, Figure 5.8), became more intense after 5 and 10 minutes of incubation, when a very high molecular weight band (>172 kDa) also became apparent (Lane 2 and 3, Figure 5.8). The high molecular weight band became dominant with increasing incubation time and the 42 kDa r56 protein band became less and less intense as incubation time increased. The ~84 and ~168 kDa bands also disappeared with longer incubation time (Lane 4-8, Figure 5.8). Similar results were seen when the concentration of HRPO was varied (Figure 5.9). Thus, with increasing HRPO concentration, the disappearance of the 42 kDa r56 protein band and the appearance of the >172 kDa band was earlier, the high molecular weight band being observable at 5 minutes with 0.25 μg HRPO, 10 minutes with 0.2 μg HRPO but not until 20 minutes with 0.1 μg HRPO. At the same time, the ~84, ~126 and ~168 kDa bands were obvious for longer time in the presence of lower concentrations of HRPO (Figure 5.9).

Inhibitors of peroxidase activity – SHA, PH and 3'AT – all inhibited the formation of higher molecular weight protein bands that reacted with the anti-r56 antibodies (Figure 5.10). Thus, both SHA and PH reduced the disappearance of the 42 kDa r56 protein band and completely prevented formation of the >172 kDa band even at the lowest concentration of inhibitor tested (0.1 mM), though faint bands at ~84 and ~168 kDa could be seen on the Western blots (Figure 5.10, Panels A and B). 3'AT had little effect on the formation of the >172 kDa band at 0.1 mM but progressively inhibited formation of this band, as well as the ~84 and ~168 kDa bands, as the concentration of inhibitor was increased (Figure 5.10, Panel C).

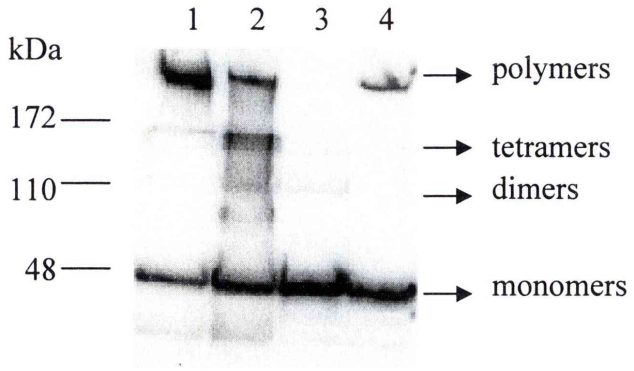

Figure 5.7 ECL analysis of HRPO catalyzed r56 crosslinking. Crosslinked samples were prepared and separated on a 12% polyacrylamide gel, followed by transferring proteins to PVDF membrane. High molecular weight oligomers were detected by immunoblotting/ECL using mouse anti-r56 antibodies. Components in each sample are indicated in the table below. Arrows indicate monomeric forms of r56 proteins, 42 kDa (monomers); polymerized r56 proteins in dimeric forms, ~84 kDa (dimers); in tetrameric forms, ~168 kDa (tetramers); in polymeric forms, greater than 172 kDa (polymers).

Lane number	1	2	3	4
r56 (5 μg)	+	+	+	+
HRPO (0.25 μg)	+	+	-	-
t-BHP (final conc. of 1 %)	+	-	+	-
0.25 M sodium borate buffer pH 8.35	+	+	+	+
Dityrosine* (mmol/mol p-tyrosine)	5.422 +/- 0.567	1.076 +/- 0.077	0.126 +/- 0.046	0.140 +/- 0.012

*The levels of dityrosine are the mean + standard deviation (n= 4).

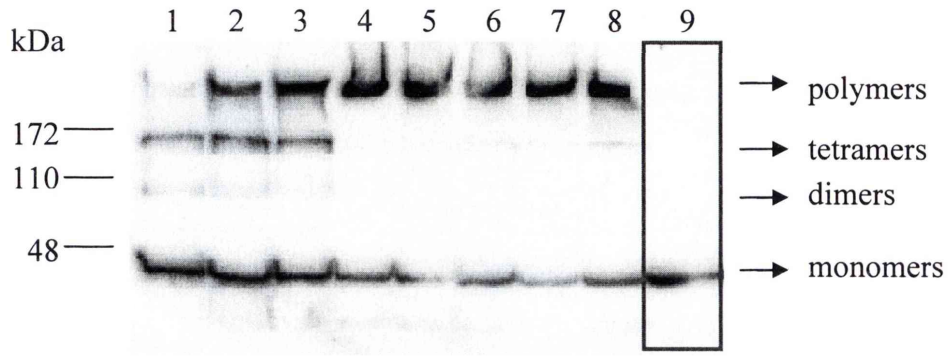

Lane number	1	2	3	4	5	6	7	8	9
Incubation time (mins)	0*	5	10	20	30	40	50	60	60

*Not absolute zero; approximately 5 seconds delayed from zero.

Figure 5.8 ECL analysis of time course on HRPO catalyzed r56 crosslinking. Each sample contained 5 μg of r56 proteins, 0.25 μg of HRPO and 1% of *t*-BHP. The samples were incubated at 37°C for 0, 5, 10, 20, 30, 40, 50 and 60 minutes (in Lane 1, 2, 3, 4, 5, 6, 7 and 8, respectively). A negative control sample, boxed area in Lane 9, contained r56 proteins only with incubation for 60 minutes. The samples were analyzed by immunoblotting/ECL using mouse anti-r56 antibodies. Arrows indicate monomeric forms of r56 proteins, 42 kDa (monomers); polymerized r56 proteins in dimeric forms, ~84 kDa (dimers); in tetrameric forms, ~168 kDa (tetramers); in polymeric forms, greater than 172 kDa (polymers).

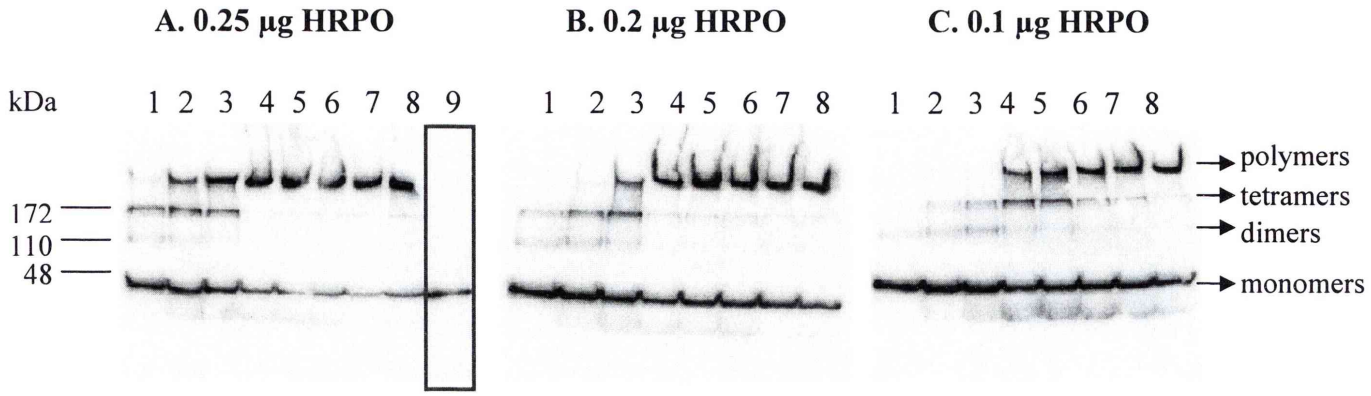

HRPO concentration	0.25 µg	0.2 µg	0.1 µg
High molecular weight oligomers	+++	++	+
Monomers	+	++	+++

Lane number	1	2	3	4	5	6	7	8	9
r56 (5 µg)	+	+	+	+	+	+	+	+	+
HRPO (0.25, 0.2 or 0.1 µg)	+	+	+	+	+	+	+	+	-
t-BHP (Final conc. of 1%)	+	+	+	+	+	+	+	+	-
0.25 M Sodium borate buffer pH 8.35	+	+	+	+	+	+	+	+	+
Incubation time (mins)	0*	5	10	20	30	40	50	60	60

*Not absolute zero; it was approximately 5 seconds delayed from zero.

Figure 5.9 ECL analyses of r56 crosslinking with varied HRPO concentration. Each sample contained 5 µg of r56 proteins and 1% of *t*-BHP but different amount of HRPO (0.25 µg in Panel A, 0.2 µg in Panel B and 0.1 µg in Panel C). The samples were incubated at 37°C for 0, 5, 10, 20, 30, 40, 50 and 60 minutes (in Lane 1, 2, 3, 4, 5, 6, 7 and 8, respectively). A negative control sample, boxed area in Lane 9, contained r56 proteins only with incubation for 60 minutes. The samples were analyzed by immunoblotting/ECL using mouse anti-r56 antibodies.

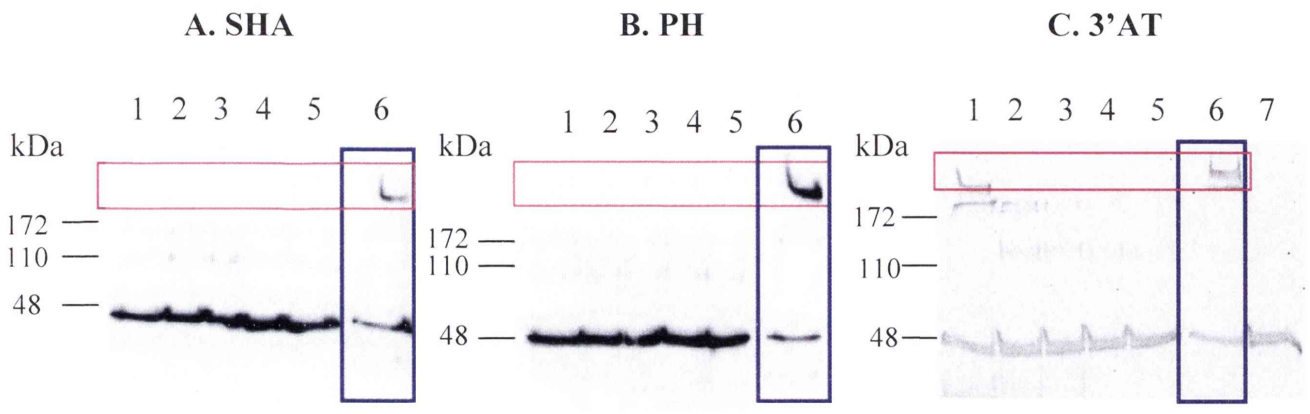

Lane number	1	2	3	4	5	6	7
r56 (5 μg)	+	+	+	+	+	+	+
HRPO (0.25 μg)	+	+	+	+	+	+	-
t-BHP (final conc. of 1%)	+	+	+	+	+	+	-
0.25 sodium borate buffer pH 8.35	+	+	+	+	+	+	+
Concentration of inhibitors (mM)	0.1	0.5	1	1.5	2	-	-

Figure 5.10 ECL analyses of HRPO catalyzed r56 crosslinking in the presence of inhibitors. Each sample contained 5 μg of r56 proteins, 0.25 μg of HRPO and 1% of *t*-BHP with different inhibitors (salicylhydroxamic acid in Panel A, phenylhydrazine hydrochloride in Panel B, 3'-amino-1, 2, 4-triazole in Panel C). The concentration of the inhibitors varied from 0.1 mM, 0.5 mM, 1 mM, 1.5 mM to 2 mM (in Lane 1, 2, 3, 4 and 5, respectively). The samples were incubated at 37°C for 50 minutes. The inhibitors were absent from the negative controls, boxed area in Lane 6 (Panel A, B and C) and Lane 7 (Panel C, containing r56 proteins only). The samples were analyzed by immunoblotting/ECL using mouse anti-r56 antibodies. Boxed area in red colour indicates the disappearance or fade out of polymers.

5.7 *Arthromyces* peroxidase catalyses cross-linking of r56 in the presence and absence of exogenous *t*-butylhydroperoxide

Incubation of r56 proteins with APx and *t*-BHP caused the disappearance of the 42 kDa r56 protein band and the appearance of bands at ~168 kDa and at a very high molecular weight (Lane 1, Figure 5.11). In the absence of *t*-BHP, APx still caused the disappearance of the 42 kDa band, albeit to a lesser extent, and also catalysed formation of the ~168 and >172 kDa bands (Lane 2, Figure 5.11). In addition, high levels of dityrosine (3.295 +/- 0.161 mmol dityrosine/mol *p*-tyrosine) were detected in the sample that had both *t*-BHP and APx (Lane 1, Figure 5.11) and almost comparable levels were seen in the sample containing APx but no *t*-BHP (2.296 +/- 0.299 mmol dityrosine/mol *p*-tyrosine); these levels were approximately 20 times higher and 15 times higher, respectively, than the levels of dityrosine seen in the control samples lacking APx (eg, Lane 3, Figure 5.11).

The APx-catalysed cross-linking assays were repeated under the same conditions, in the presence of *t*-BHP but incubation time was varied. Thus, incubations of 0, 5, 10, 20, 30, 40, 50 and 60 minutes were carried out (as described in detail in Chapter 2, section 2.2.18). Protein bands of ~84, ~168 and >172 kDa were apparent immediately upon addition of APx (Lane 1, Figure 5.12), and became increasingly intense with increasing incubation time (Lane 2-8, Figure 5.12). However, in contrast to similar incubations with HRPO, the 42 kDa r56 protein band remained readily detectable over the different incubation periods. Similar results were seen when the concentration of APx was varied (Figure 5.13). Thus, the ~84 and ~168 kDa bands were more obvious at higher concentrations of APx (ie, 0.25 and 0.2 μg versus 0.1 μg; Panels A and B versus Panel C, Figure 5.13). Indeed, in the presence of only 0.1 μg APx, only the >172 kDa band was seen and not the ~84 and ~168 kDa bands. Again, the 42 kDa r56 protein band was readily observable at all APx concentrations and over all incubation times; however, formation of high molecular weight bands was inversely proportional to the apparent amount of 42 kDa r56 protein remaining in the assays at the end of the experiment. Thus, for example, more high molecular weight bands are observed in the presence of high concentrations of APx (Panel A, Figure 5.13), where less 42 kDa protein is apparent, versus the case for 0.1 μg APx (Panel C, Figure

5.13), where high molecular weight bands are less intensely detected and more 42 kDa protein remains.

Inhibitors of peroxidase activity – SHA, PH and 3'AT – all inhibited the formation of higher molecular weight protein bands that reacted with the anti-r56 antibodies (Figure 5.14). Thus, all three inhibitors reduced the appearance of the ~168 kDa protein band and almost completely prevented formation of the >172 kDa band even at the lowest concentration of inhibitor tested (0.1 mM). Faint bands at ~84 kDa could be seen on the Western blots for all inhibitors (Figure 5.14).

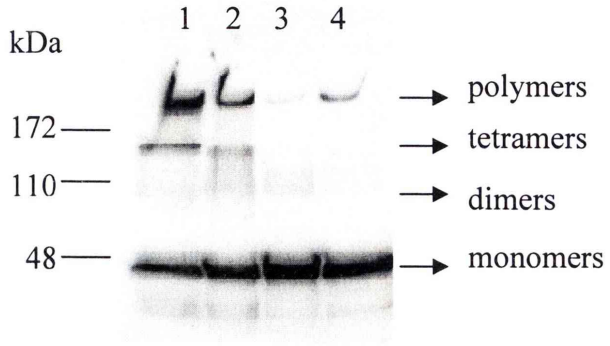

Figure 5.11 ECL analysis of APx catalyzed r56 crosslinking. Crosslinked samples were prepared and separated on a 12% polyacrylamide gel, followed by transferring proteins to PVDF membrane. High molecular weight oligomers were detected by immunoblotting/ECL using mouse anti-r56 antibodies. Components in each sample are indicated in the table below. Arrows indicate monomeric forms of r56 proteins, 42 kDa (monomers) and polymerized r56 proteins in dimeric forms, ~84 kDa (dimers); in tetrameric forms, ~168 kDa (tetramers); in polymeric forms, greater than 172 kDa (polymers).

Lane number	1	2	3	4
r56 (5 μg)	+	+	+	+
APx (0.25 μg)	+	+	-	-
t-BHP (final conc. of 1 %)	+	-	+	-
0.25 M sodium borate buffer pH 8.35	+	+	+	+
Dityrosine* (mmol/mol p-tyrosine)	3.295 +/- 0.161	2.296 +/- 0.299	0.161 +/- 0.052	0.196 +/- 0.184

*The levels of dityrosine are the mean + standard deviation (n= 4).

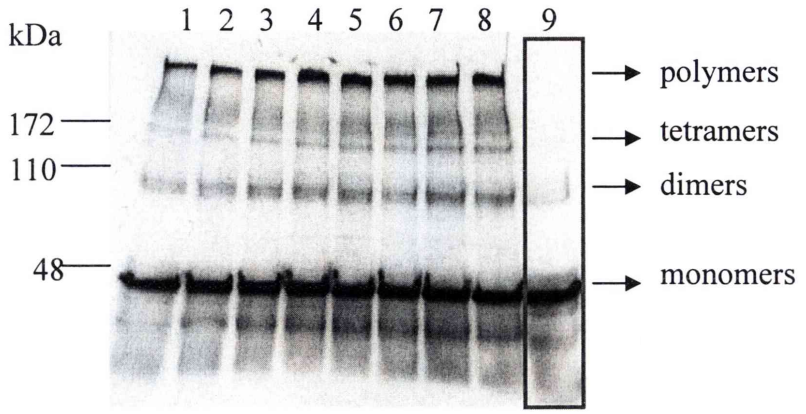

Lane number	1	2	3	4	5	6	7	8	9
Incubation time (mins)	0*	5	10	20	30	40	50	60	60

*Not absolute zero; approximately 5 seconds delayed from zero.

Figure 5.12 ECL analysis of time course on APx catalyzed r56 crosslinking. Each sample contained 5 μg of r56 proteins, 0.25 μg of APx and 1% of *t*-BHP. The samples were incubated at 37°C for 0, 5, 10, 20, 30, 40, 50 and 60 minutes (in Lane 1, 2, 3, 4, 5, 6, 7 and 8, respectively). A negative control sample, boxed area in Lane 9, contained r56 proteins only with incubation for 60 minutes. The samples were analyzed by immunoblotting/ECL using mouse anti-r56 antibodies. Arrows indicate monomeric forms of r56 proteins, 42 kDa (monomers); polymerized r56 proteins in dimeric forms, ~84 kDa (dimers); in tetrameric forms, ~168 kDa (tetramers); in polymeric forms, greater than 172 kDa (polymers).

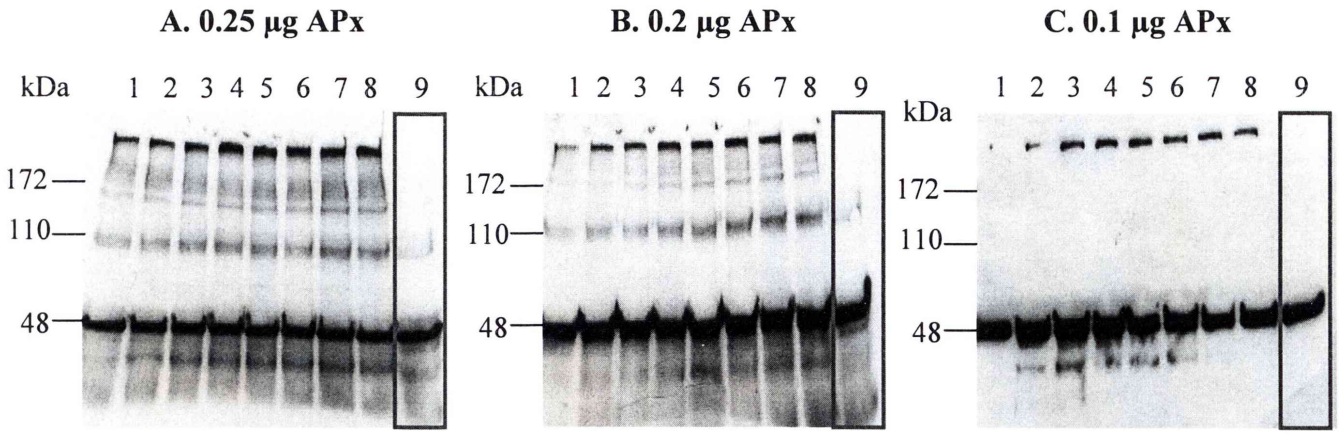

APx concentration	0.25 µg	0.2 µg	0.1 µg
High molecular weight oligomers	+++	++	+
Monomers	+	++	+++

Lane number	1	2	3	4	5	6	7	8	9
r56 (5 µg)	+	+	+	+	+	+	+	+	+
APx (0.25, 0.2 or 0.1 µg)	+	+	+	+	+	+	+	+	-
t-BHP (final conc. of 1%)	+	+	+	+	+	+	+	+	-
0.25 M sodium borate buffer pH 8.35	+	+	+	+	+	+	+	+	+
Incubation time (mins)	0*	5	10	20	30	40	50	60	60

*Not absolute zero; it was approximately 5 seconds delayed from zero.

Figure 5.13 ECL analyses of r56 crosslinking with varied APx concentration. Each sample contained 5 µg of r56 proteins and 1% of *t*-BHP but different amount of APx (0.25 µg in Panel A, 0.2 µg in Panel B and 0.1 µg in Panel C). The samples were incubated at 37°C for 0, 5, 10, 20, 30, 40, 50 and 60 minutes (in Lane 1, 2, 3, 4, 5, 6, 7 and 8, respectively). A negative control sample, boxed area in Lane 9, contained r56 proteins only with incubation for 60 minutes. The samples were analyzed by immunoblotting/ECL using mouse anti-r56 antibodies.

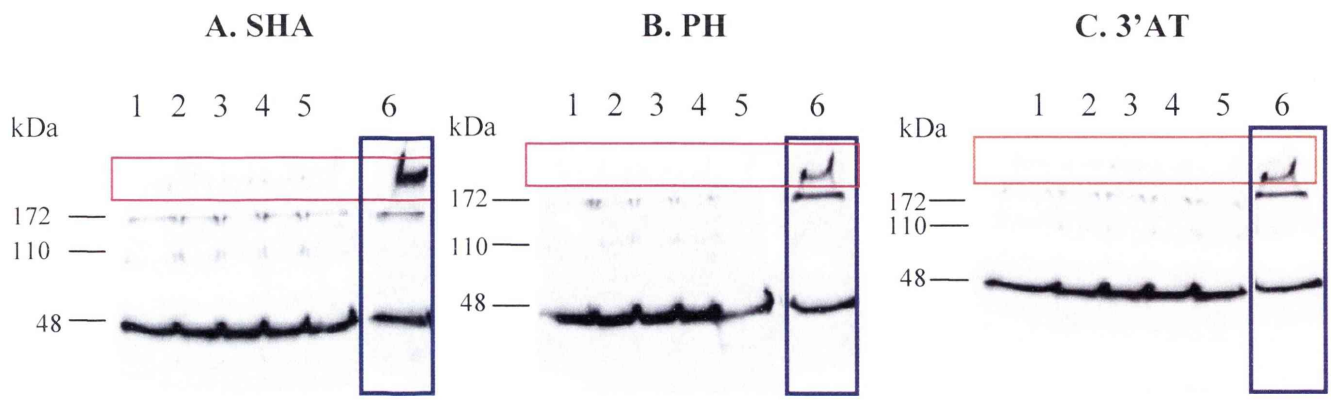

Lane number	1	2	3	4	5	6
r56 (5 μg)	+	+	+	+	+	+
APx (0.25 μg)	+	+	+	+	+	+
t-BHP (final conc. of 1%)	+	+	+	+	+	+
0.25 sodium borate buffer pH 8.35	+	+	+	+	+	+
Concentration of inhibitors (mM)	0.1	0.5	1	1.5	2	-

Figure 5.14 ECL analyses of APx catalyzed r56 crosslinking in the presence of inhibitors. Each sample contained 5 μg of r56 proteins, 0.25 μg of APx and 1% of *t*-BHP with different inhibitors (salicylhydroxamic acid in Panel A, phenylhydrazine hydrochloride in Panel B, 3'-amino-1, 2, 4-triazole in Panel C). The concentration of the inhibitors varied from 0.1 mM, 0.5 mM, 1 mM, 1.5 mM to 2 mM (in Lane 1, 2, 3, 4 and 5, respectively). The samples were incubated at 37°C for 50 minutes. The inhibitors were absent from negative control samples, boxed area in Lane 6. The samples were analyzed by immunoblotting/ECL using mouse anti-r56 antibodies. Area boxed in red colour indicates the disappearance or fade out of polymers.

5.8 Catalase reverses the *Arthromyces* peroxidase-catalysed crosslinking of r56 in the absence of *t*-butylhydroperoxide

The formation of high molecular weight protein bands in the presence of APx (and HRPO) but in the absence of *t*-BHP, indicates that some peroxide may be present endogenously in the incubation mix and used by these enzymes to catalyse dityrosine cross-linking. Therefore, r56 was pretreated with catalase (0.05 mg/ml, final concentration), which was shown in Section 5.3 to not affect the cross-linking assay itself. The assay was then carried out as described above. The presence of catalase inhibited the formation of high molecular weight protein bands in the presence of APx but absence of *t*-BHP (Lane 2, Figure 5.15), though an ~82 kDa band was detected faintly. A characteristic band of high molecular weight (>172 kDa) was observed in the presence of both APx and *t*-BHP, as well as bands of ~84 kDa and ~168 kDa (Lane 1, Figure 5.15). The apparent level of 42 kDa r56 protein was also reduced in this sample but unaffected in the APx plus catalase incubation (Lane 2, Figure 5.15) and in the control incubations (Lane 3 and 4, Figure 5.15). A high molecular weight band was observed in the control incubations but, given the lack of diminution of intensity of the 42 kDa band, is assumed, again to be aggregated protein rather than cross-linked protein.

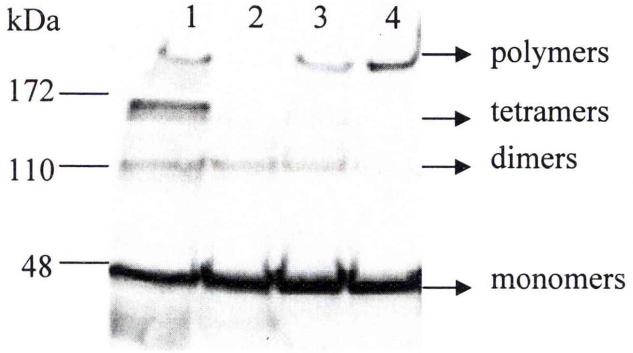

Lane number	1	2	3	4
r56 (5 μg) pre-treated with catalase	+	+	+	+
APx (0.25 μg)	+	+	-	-
t-BHP (final conc. of 1 %)	+	-	+	-
0.25 M sodium borate buffer pH 8.35	+	+	+	+

Figure 5.15 ECL analysis of peroxide scavenger on APx catalyzed r56 crosslinking. r56 proteins were pre-treated with catalase to a final concentration of 0.05 mg/ml at 37°C for 50 minutes, followed by a crosslinking assay using APx and *t*-BHP. Crosslinked samples were separated on a 12% polyacrylamide gel, followed by transferring proteins to PVDF membrane. High molecular weight oligomers were detected by immunoblotting/ECL using mouse anti-r56 antibodies. Arrows indicate monomeric forms of r56 proteins, 42 kDa (monomers) and polymerized r56 proteins in dimeric forms, ~84 kDa (dimers); in tetrameric forms, ~168 kDa (tetramers); in polymeric forms, greater than 172 kDa (polymers).

5.9 Discussion

This study has clearly demonstrated that cross-linking of the *E. maxima* macrogamete protein, EmGam56, is easily induced *in vitro.* Thus, in the presence of *t*-BHP plus peroxidases from either horseradish or *Arthromyces,* the formation of dimers, tetramers and larger polymers of r56 (a 42 kDa truncated version of EmGam56) was readily detected by Western blotting (ECL), and the presence of dityrosines in these polymers was confirmed by HPLC analysis. Interestingly, however, significant formation of DOPA was not detected in the polymers and, furthermore, DOPA oxidase failed to catalyse cross-linking of r56 *in vitro.* This is seemingly at odds with data from the oocyst wall showing the presence of DOPA in that structure (Belli *et al.,* 2003b), and the observation of DOPA oxidase in wall forming bodies and the developing oocyst wall of *E. maxima* (DJP Ferguson, personal communcation), however, the DOPA in oocyst walls could conceivably result from cross-linking of other tyrosine-rich peptides derived from EmGam56 or EmGam 82 or other, as yet unidentified, proteins from the wall forming bodies of the macrogametes of *E. maxima.*

Intriguingly, H_2O_2 was able to induce a high level of cross-linking of r56, even in the absence of exogenous peroxidase or DOPA oxidase, an effect that could be partially reversed by catalase, which converts H_2O_2 to oxygen and water. This cross-linking was associated with formation of dityrosine (as measured by HPLC) but not DOPA, confirming the apparent lack of a role for DOPA in cross-linking of r56. This result indicates that cross-linking of tyrosine-rich proteins to help form the oocyst wall of *Eimeria* parasites is theoretically possible in the absence of oxidative enzymes. This may help explain observations from the 1980s and 1990s that host-generated free oxygen radicals are associated temporally with apparent elimination of *Eimeria* parasites in a murine model of infection (Ovington *et al.,* 1990), yet stimulants of oxygen radical generation by macrophages actually enhance oocyst excretion in infected mice (Smith and Ovington, 1996), and scavengers of oxygen radicals, such as butylated hydroxyanisole, which can inhibit intestinal worm expulsion by rodents (Smith and Bryant, 1988), cause decreased oocyst excretion by infected mice (personal communication of unpublished data by E. Rose, K.S. Ovington and N.C. Smith); all of these results – which were extremely puzzling at the time they were obtained - can now be explained by the oxidative-dependency of

chemical reactions leading to polymerization of proteins that are key structural elements in oocyst wall formation in *Eimeria* parasites.

Intriguing, and possibly significant, as the results with H_2O_2 are, they made assessment of a possible role for peroxidases in cross-linking of EmGam56 experimentally impossible. Fortunately, *t*-BHP, an apparently much milder oxidant than H_2O_2, does not induce cross-linking of r56 by itself, allowing development of a sensitive, effective assay to assess cross-linking of r56 *in vitro*. In this assay, the combination of *t*-BHP and peroxidases from horseradish or *Arthromyces* proved highly effective at inducing polymerization of r56. Again, this cross-linking was accompanied by formation of dityrosine but not DOPA. Surprisingly, significant, though less, cross-linking of r56, coupled with dityrosine formation, was seen with both these peroxidases even in the absence of an exogenous peroxide substrate. Addition of catalase to these incubations inhibited this cross-linking, indicating that it was, in fact, due to the presence of (probably, very low levels of) endogenous peroxide. This should perhaps not be totally surprising since the recombinant r56 protein is purified from bacteria and several bacteria (such as *Pneumococci, Streptococci, Lactobacilli,* and *Escherichia coli*; McLeod and Gordon, 1922; Dahiya and Speck, 1968; Wheater *et al.*, 1952; Nishiyama *et al.*, 2001) are able to generate hydrogen peroxide in culture. This observation is an important one, however, as it – together with the observation of the effectiveness of H_2O_2 alone at inducing cross-linking – demonstrates the high level of "susceptibility" this tyrosine-rich protein has for forming dityrosine cross-links and, furthermore, underscores the apparent high efficiency of *Eimeria* at harnessing this reaction to generate the protective oocyst wall.

In contrast to HRPO and APx, MPx, a peroxidase of vertebrate animals, did not catalyse cross-linking or dityrosine or DOPA formation. This is a potentially important result, as it seems to rule out involvement of host peroxidase in the catalysis of oocyst wall formation in *Eimeria.* MPx is known to be involved in the formation of protein cross-links in mammalian systems. Thus, although MPx is best known for its cytotoxic actions on bacteria, fungi and tumor cells by catalysing oxidation of hydrogen peroxide, forming hypochlorous acid, it also functions in cross-linking of immune complexes and inactivates chemotactic factors (Clark *et al.*, 1975; Clark and Szot, 1982; Odell and Segal, 1988;

Uesugi *et al.*, 1998). In addition, it has been shown that MPx is able to catalyse dityrosine mediated protein cross-linking of calmodulin (Malencik and Anderson, 1996). Moreover, it has been shown that dityrosine cross-linking of BSA can be achieved only when MPx, hydrogen peroxide, and L-tyrosine are present in the reaction (Heinecke *et al.*, 1993). The fact that MPx does not mediate r56 cross-linking is likely, therefore, to be due to substrate specificity. MPx appears to need free L-tyrosine to promote a significant level of dityrosine cross-linking in proteins (Heinecke *et al.*, 1993) because its active site is buried in the centre of the protein, accessible only by a narrow hydrophobic solvent channel (Davey and Fenna, 1996). Thus, MPx requires low molecular weight intermediates such as L-tyrosine to convey oxidizing equivalents from its heme group to its targets (Heinecke, 2002).

Both HRPO and APx catalysed cross-linking in an extremely rapid and specific (as indicated by the inhibitory effects of SHA, PH and 3'AT) manner. Both are well known as inducers of dityrosine bridges; for example, APx is able to catalyse dityrosine cross-linking of calmodulin (Malencik and Anderson, 1996) and this cross-linking occurs rapidly (it takes 20 seconds to reach maximum increase in apparent dityrosine fluorescence), and it has been shown that peptides can be cross-linked to form dityrosine dimers *in vitro* when HRPO, oxygen, and hydrogen peroxide are present (Aeschbach *et al.*, 1976). In addition, it has been reported that HRPO can catalyse dityrosine cross-linking of a recombinant CUT-2, a component of cuticlin, from nematode *C. elegans*, *in vitro* (Lassandro *et al.*, 1994), which is a particularly significant result since cuticle formation in nematodes is quite analogous to the proposed process of oocyst wall formation in *Eimeria* (Belli *et al.*, 2005). Moreover, in contrast to MPx, HRPO can directly oxidise protein-bound tyrosine residues because the heme group of HRPO is exposed and readily accessible to relatively large substrates (Gross and Sizer, 1959; Deits *et al.*, 1984).

HRPO and APx are from a plant and a fungus, respectively, and their effectiveness as agents promoting cross-linking and dityrosine formation of r56 is tantalising given the significant plant-like characteristics possessed by *Eimeria* and related apicomplexan parasites. For example, it has been reported that *E. tenella* possesses a mitochondrial genome and a newly discovered "plant-like" genome which is probably acquired from an ancestor, an algal cell containing a chloroplast (Shirley, 1997). In addition, Ryley *et al.*

(1969) suggested that coccidia have energy reserves similar to that of plants rather than animals and the best example is storage polysaccharides (alpha-1, 4-linked, alpha-1, 6-branched glucose polymers) also known as amylopectin in apicomplexan parasites such as *Eimeria*, *Toxoplasma*, and *Crytosporidium* (Ryley *et al.*, 1969; Coppin *et al.*, 2003; Harris *et al.*, 2004). Moreover, genes encoding aquaporins have been found in *T. gondii*, *E. tenella*, *P. falciparum*, *P. berghei*, *P. yoelii*, *P. chabaudi* and *P. knowlesi* (Hansen *et al.*, 2002; Pavlovic-Djuranovic *et al.*, 2003; Beitz, 2005). (Aquaporins belong to a major intrinsic protein superfamily of integral plasma membrane channel proteins whose genes are of bacteria or plant origin). The coccidian aquaporins (*Toxoplasma* and *Eimeria*) are the closest to tonoplast intrinsic proteins (water specific membrane protein) from plants, *A. thaliana*, based on protein sequence similarity, in contrast, *Plasmodium* aquaporins are the closest to bacterial proteins, *E. coli* GlpF, glycerol facilitator, (Maurel *et al.*, 1993; Beitz, 2005). Furthermore, the apicoplast in *T. gondii* is thought to be an algae-derived plastid-like organelle, contains many plant-like or plant specific metabolic pathways which are absent from mammalian cells (Roos *et al.*, 1999; Wilson, 2002; Gleeson, 2000; Maréchal and Cesbron-Delauw, 2001). Examples are synthesis of (1) fatty acid (enzymes for fatty acid synthesis belong to type II pathway which is commonly found in plastid of plants, algae and bacteria; Waller *et al.*, 1998); (2) isoprenoid (a lipid pathway utilizing a number of enzymes specifically found in apicoplast and the pathway is also characteristic of plants, algae and bacteria; Seeber, 2003); (3) enzymes for shikimate pathway (found in *T. gondii*, *P. falciparum*, *C. parvum* that is essential for synthesis of folate, ubiquinone, and aromatic amino acids in algae, and plants; Roberts *et al.*, 1998); (4) calcium release channels and calcium-dependent kinases, commonly found in plants, also present in apicomplexan parasites (Nagamune and Sibley, 2006); and (5) structural proteins, tubulin (Stockkermans *et al.*, 1996).

Even though APx and HRPO belong to different classes within the plant peroxidase superfamily (class II and class III for APx and HRPO, respectively), these two enzymes do resemble each other with respect to kinetic and structural properties (Lukat *et al.*, 1989; Welinder, 1992; Farhangrazi, *et al.*, 1994; Abelskov *et al.*, 1997). Thus, any hunt for the endogenous peroxidase(s) of *Eimeria* – whether genomic or biochemical - should,

logically, focus on plant- or fungal-like enzymes, rather than utilising mammalian sequences or characteristics.

In summary, the research conducted in this chapter has demonstrated that:

- Cross-linking of a truncated version of EmGam56 (r56) occurs readily in the presence of a powerful oxidant, H_2O_2, even in the absence of peroxidase, raising the possibility that it may be a spontaneous chain of events in the infected intestine;
- DOPA oxidase does not catalyse cross-linking of r56 and no DOPA is seen in H_2O_2-catalysed or peroxidase-catalysed polymers of r56;
- Peroxidases of plant (HRPO) or fungal (APx) origin, but not peroxidase of vertebrates (MPx), catalysed cross-linking and dityrosine formation in the presence of a mild peroxide (*t*-BHP) in a highly efficient, rapid manner, suggesting that searches for peroxidases in *Eimeria* should focus on plant-like enzymes rather than animal homologues; and
- The efficiency of cross-linking of r56 parallels the *in situ* efficiency with which *Eimeria* produces its protective oocyst wall (discussed in more detail in the concluding chapter of this thesis).

Chapter Six
General Discussion

Coccidian parasites, which include the genera *Toxoplasma, Neospora, Hammondia, Isospora, Sarcocystis* and *Eimeria,* amongst others, share many features. For example, like all Apicomplexa, their lifecycle includes asexual spore stages (sporozoites and merozoites) that possess a phylum-defining feature, the apical complex of organelles, associated with cell invasion. An additional defining feature of the Coccidia is the oocyst; coccidian parasites are transmitted from host to host by accidental ingestion of oocysts that contaminate food or water. Oocysts are remarkably hardy and able to persist in the environment for prolonged periods of time. The "soft-bodied" parasites are safely encapsulated inside a unique structure, the oocyst wall.

The oocyst wall is extremely robust. It is resistant to mechanical and chemical damage; breaking oocysts for laboratory studies requires prolonged, high-speed vortexing with glass beads, and oocysts are routinely cleaned with bleach and stored in the harsh oxidant, potassium dichromate, or the mineral acid, sulphuric acid (Dubey *et al.,* 1970; Shirley, 1995; Schares *et al.,* 2005). The wall is also resistant to proteolysis and impermeable to water-soluble substances, including many detergents and disinfectants (Monné and Hönig, 1954; Ryley, 1973). This contributes to the difficulty experienced in attempting to exclude oocysts from, for example, poultry houses. The oocyst wall is, however, permeable to some small molecules and lipid-soluble substances, ammonia and methyl bromide being two of the best known (Monné and Hönig, 1954; Ryley, 1973; Kuticic and Wikerhauser, 1996).

The oocyst wall is essentially consistent in structure across different species of coccidian parasites (Belli *et al.,* 2006) but it is the oocyst wall of *Eimeria* that has been best studied, probably because of the relative ease of acquiring large numbers of oocysts of the parasites of this genus. When first formed, oocysts are enclosed in a loose membranous structure, called the outer veil (Ferguson *et al.,* 2000; 2003). However, this veil is shed as the oocysts mature so that oocysts recovered from faeces no longer have an outer veil. The oocyst wall itself is bi-layered. The electron dense outer layer, formed from the contents of WFB1 (see Chapter 1), is variable in size across different genera; for example, it can be ~200 nm thick in *E. maxima* (Ferguson *et al.,* 2003) but only 20-40 nm thick in *T. gondii* (Ferguson *et al.,* 1975; 2000). The

electron luscent inner layer, formed from the contents of WFB2, is more consistent, being around 40 nm thick in most genera studied (Belli *et al.,* 2006). The two layers do not seem to be tightly fused and can be separated relatively easily (Monné and Hönig, 1954); bleach treatment, for instance, usually strips the outer layer away from the inner layer.

As discussed in detail in Chapter 3 of this thesis, the biochemical composition of the oocyst wall has proven controversial and difficult to ascertain. However, the metabolic analyses carried out for this thesis provide compelling evidence that both the outer and inner layers of the wall of *Eimeria* species are more than 90% protein, with low levels of lipids (range from 1.4% to 7.6%), and only very small amounts of carbohydrates (range from 0.3% to 2.0%). It seems likely that previous analyses were confounded by the presence of polysaccharide granules and other "contaminants" from the internal contents of the oocysts, reflecting inadequate purification of the oocyst walls (see Chapter 3 for detailed discussion). This observation is an important one as it implies that understanding the structure and characteristics of oocyst wall proteins - the major building blocks of the oocyst wall - will provide an insight into how the oocyst wall is formed and, potentially, identify vulnerabilities for attack by chemical or immunological agents either within the chicken and prior to oocyst wall formation or in the floor litter of poultry houses.

There are only a small number of oocyst wall proteins that have been identified and characterized, mostly from *Eimeria* species. Stotish *et al.* (1978) believed that the protein content of the oocyst wall was predominantly, if not solely, a repeating subunit of ~10 kDa, based on their detection of only a single band on SDS-PAGE gels. Karim *et al.* (1996) made similar conclusions when describing a monoclonal antibody to a single 12 kDa protein band of the oocyst wall of *E. tenella*; the antibody reacted with macrogametocytes, as well as the inner wall of oocysts, and crossreacted with *E. maxima.* Eschenbacher *et al.* (1996) discovered 14 kDa oocyst wall proteins in *E. tenella* and *E. acervulina,* noting that these proteins were characterized by an abundance of amino acids that contain hydroxyl groups in their side-chains, especially serine, tyrosine and threonine. Based on this, they resurrected the idea, first proposed

by Monné and Hönig (1954), and reiterated by Pittilo and Ball (1980), that the oocyst wall contained quinone-tanned protein.

Studies on the macrogametocyte stage of *Eimeria* have yielded valuable information about oocyst wall proteins. Mouafo *et al.* (2002) reported that a monoclonal antibody raised against the macrogametocytes of *E. tenella,* reacted with three proteins of 23, 25 and 30 kDa, in the inner layer of the oocyst wall, in addition to an antigen of 51 kDa in the macrogametocytes. In parallel, detailed studies on the 56 and 82 kDa proteins from the macrogametocytes of *E. maxima* (EmGam56 and EmGam82) demonstrated conclusively (by N-terminal amino acid sequencing and Western blotting) that a series of oocyst wall proteins of 8, 10, 12 and 33 kDa were all derived from these two precursor proteins (Belli *et al.,* 2003b; Figure 6.1). Like the 14 kDa proteins described by Eschenbacher *et al.* (1996), these proteins are tyrosine-rich. It seems likely that the 10, 12 and 14 kDa proteins described by Stotish *et al.* (1978), Mouafa *et al.* (1996) and Eschenbacher *et al.* (1996), are essentially the same as the 8, 10 and 12 kDa proteins uncovered by Belli *et al.* (2003b) using methods that enabled separation of an apparent single band on an SDS-PAGE gel into three bands. An additional protein of ~29 kDa was also noted but its composition was not defined.

Antibodies to EmGam56 and EmGam82 and to affinity purified gametocyte antigens (APGA) were subsequently used to definitively map the relocation of antigens from WFB1 to the outer layer of the oocyst wall and proteins from WFB2 to the inner layer of the oocyst wall of *E. maxima* (Ferguson *et al.,* 2003). Similar results have subsequently been obtained with both *E. tenella* and *E. acervulina,* demonstrating the conservation of these proteins and the process of wall formation (Belli SI, Ferguson DJP, Slapetova I, Mai K, Flowers SA, Slapeta J, Myska K, Wallach MG and Smith NC, personal communication, manuscript in preparation). Recently, Krücken *et al.* (2008) have confirmed the presence of two *E. tenella* homologues of EmGam56 and, additionally, reported the discovery of a 22 kDa antigen in the macrogametocytes of *E. tenella.* Like the other proteins so far characterized, antibodies to this protein react with WFB2 and the inner layer of the oocyst wall.

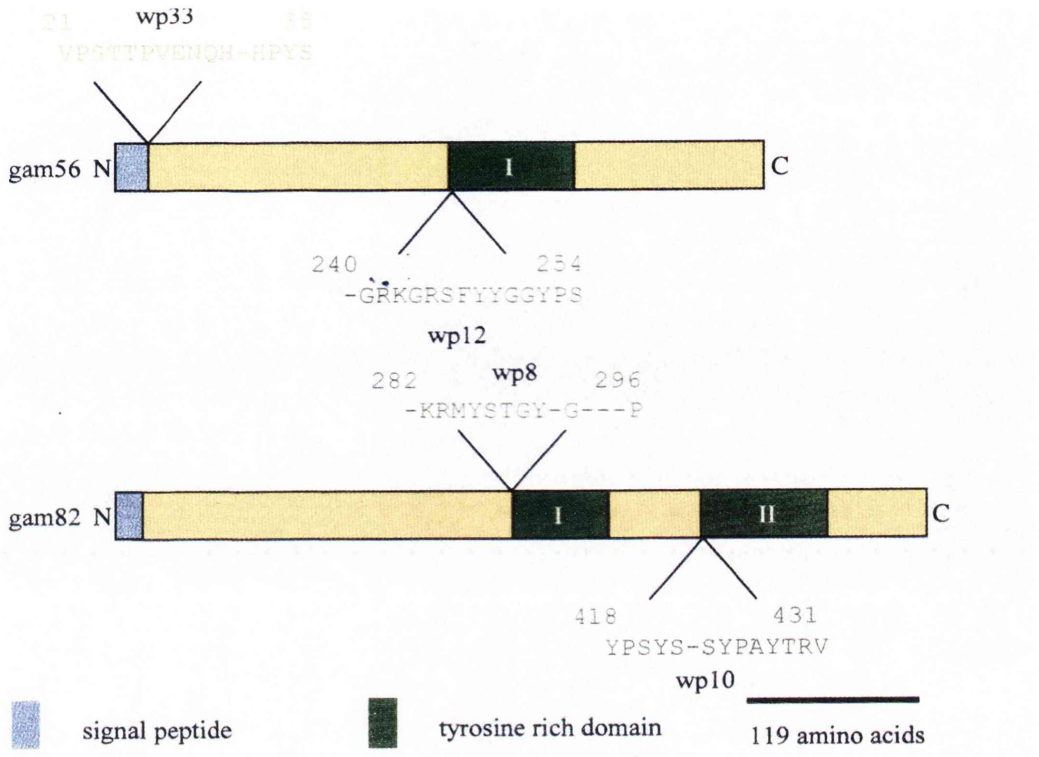

Figure 6.1 N-terminal sequences of oocyst wall proteins in *E. maxima*. Schematic representation of the N-terminal amino acid sequences of oocyst wall proteins, wp8, wp10, wp12 and wp33, mapping them to the gametocyte glycoproteins EmGam56 and EmGam82 (Belli *et al.*, 2003b).

Although this 22 kDa protein does contain some tyrosine residues, it is dominated by histidine and proline residues. It is notable for another reason, namely that its gene is present in extremely high copy number (in contrast to the single copies of the genes for, for example, EmGam56 and EmGam82), indicating that it may be important in oocyst wall formation via a mechanism distinct from that of the tyrosine-rich proteins (discussed below). As yet, no information is available about whether this 22 kDa protein is processed into smaller polypeptides nor how it is incorporated into the oocyst wall, though its involvement in stabilising the oocyst wall via cross-links between histidine and catechols, as seen in insect cuticles (Christensen *et al.*, 1991; Xu *et al.*, 1997; Kerwin *et al.*, 1999), is a distinct possibility (Krücken *et al.*, 2008).

The only other oocyst wall proteins to be documented thus far are the members of the multigene *Cryptosporidium* oocyst wall protein (COWP), a family of large (174-190 kDa), cysteine-rich proteins that localise to the inner wall of the *Cryptosporidium* oocyst (Spano *et al.*, 1997; Templeton *et al.*, 2004). It is thought that COWP forms extensive disulphide bridges and matrices within the oocyst wall (Spano *et al.*, 1997). This would make it quite distinct from the oocyst wall proteins described for *Eimeria* but this fits with the fact that the *Cryptosporidium* oocyst wall, in contrast to those of *Eimeria, Toxoplasma, Neospora, Sarcocystis, Isospora* and *Cyclospora,* which all display the blue autofluorescence characteristic of dityrosine bonds (Belli *et al.*, 2006). A homologue of COWP has been documented in *T. gondii* (Templeton *et al.*, 2004) and, very recently, two apparent homologues have been found in *Eimeria* (Robert Walker, University of Technology, Sydney, personal communication). The role of these proteins in oocyst wall formation in *T. gondii* and *Eimeria* has yet to be investigated.

A model for how the tyrosine-rich wall proteins are incorporated into the oocyst wall of *Eimeria* has been proposed by Belli *et al.* (2006) (Figure 6.2). Briefly, the model proposes that EmGam56 and EmGam82 are precursors that are processed into small tyrosine-rich wall proteins of 8, 10, 12 (sometimes seen as single bands of 10 or 14 kDa, depending on species of parasite and method of analysis) and 33 kDa. It is easy to envisage that this processing is the result of proteolysis by an, as yet, unidentified protease or proteases. The model goes on to propose that the tyrosine-rich proteins are

oxidized, by peroxidase/s and DOPA oxidase/s, and crosslinked via their tyrosine residues to form a matrix that subsequently becomes dehydrated ("tanned") and leads to hardening of the oocyst wall, with its accompanying, notorious resilience.

Having established the dominance of proteins in the oocyst walls of *Eimeria* species, one protein, EmGam56, was chosen for structural and biochemical analysis to further our knowledge about the molecular events that underpin oocyst wall formation. As presented and discussed in Chapter 4, EmGam56 is apparently an intrinsically unstructured protein (IUP). Several lines of evidence support this conclusion: (1) eleven different, well validated, bioinformatic programs predicted that EmGam56 is dominated by random coils (52-70%) with a significant percentage (28-43%) of α-helical structure but relatively little β-sheets (1-11%); (2) CD and 1D-NMR spectra on a defined region of EmGam56, confirmed the broad bioinformatic predictions; and (3) a truncated version of EmGam56 was remarkably resistant to extremes of both temperature and pH.

The finding that EmGam56 is an IUP is intriguing. IUPs are characterised by their lack a fixed three dimensional structure under physiological conditions and may exist in molten globule-like (collapsed) and random coil-like (extended) forms (Weinreb *et al.*, 1996; Wright and Dyson, 1999; Uversky *et al.*, 2000). They have recently become a focus of much interest as they have been shown to be far more common than previously realised (Tompa, 2005). Furthermore, IUPs are involved in critically important biological functions such as DNA recognition, molecular assembly, protein modification, entropic chain activities and modulation of affinity of protein binding (Dunker *et al.*, 1998; Dunker *et al.*, 2002; Iakoucheva *et al.*, 2002; Ward *et al.*, 2004; Vucetic *et al.*, 2005). They are unusually prevalent in apicomplexan genomes (Feng *et al.,* 2006). With regard to EmGam56 and its putative role in oocyst wall formation, two characteristics of IUPs may be particularly relevant, namely their intrinsic susceptibility to proteolysis and their inherent structural flexibility, which enables the assembly of multi-protein complexes, including extracellular matrices (Tompa, 2003).

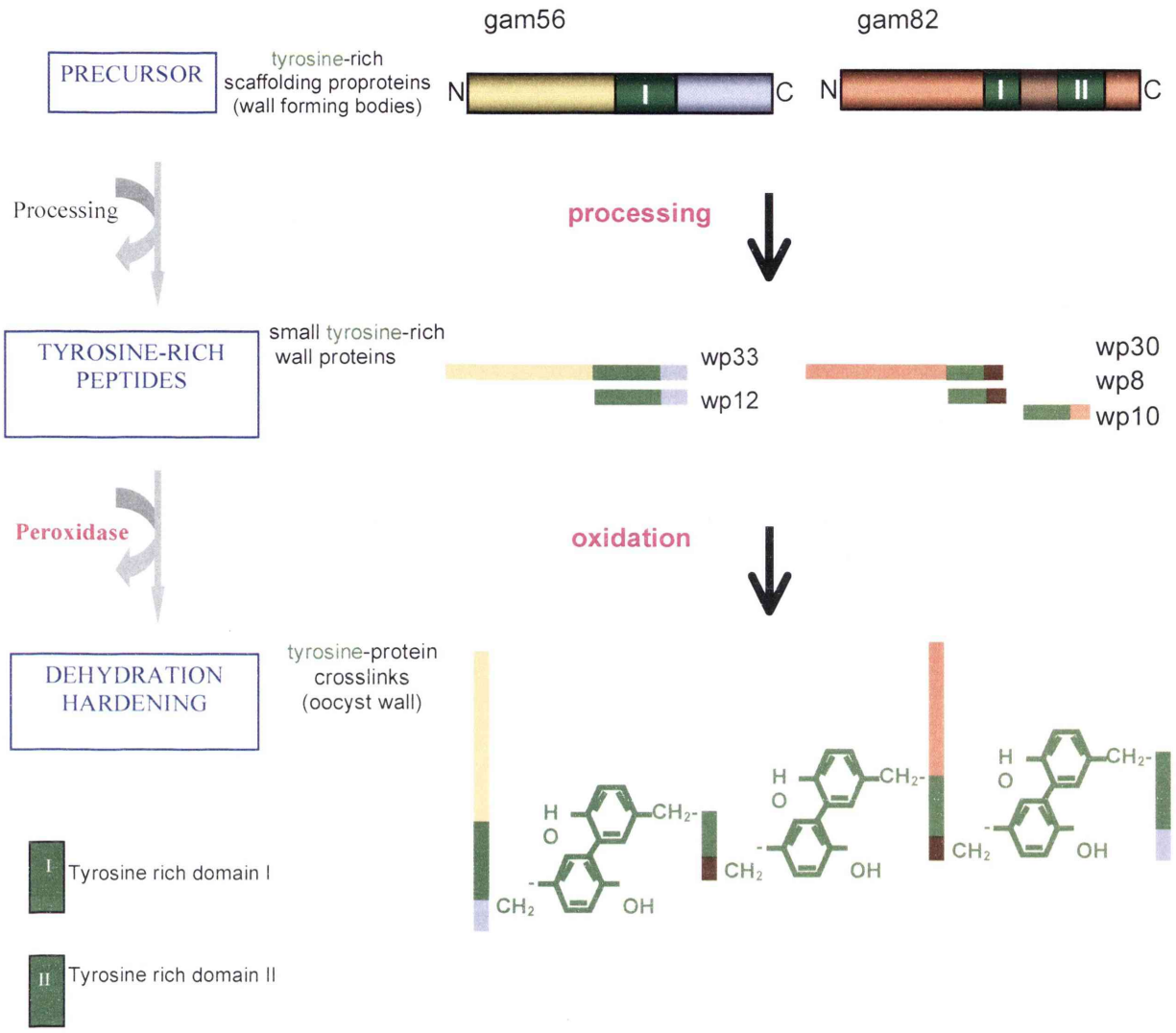

Figure 6.2 Model of oocyst wall formation in *Eimeria* (Belli *et al.*, 2006). EmGam56 and EmGam82, from the macrogametocytes, are precursor proteins that are processed, possibly by an unknown protease, into small tyrosine-rich proteins such as wp12 and wp33 from EmGam56; and wp8, wp10 and wp30 from EmGam82. These wall proteins are then oxidized, presumably by peroxidase/s and/or DOPA oxidase/s, and crosslinked to form the oocyst wall, which subsequently dehydrates and hardens in a process similar to quinone "tanning" or sclerotisation.

As discussed above, EmGam56 is processed into smaller polypeptides that are incorporated into the oocyst wall. These polypeptides are various sizes and are not cleaved from the parent protein at ordinarily predictable protease cleavage sites. This is a prominent feature of IUPs, many of which exhibit extreme proteolytic sensitivity, a feature that allows for extremely rapid turnover (Tompa, 2005). This is an important characteristic for oocyst wall formation, which is known to occur rapidly using molecules that are stored in the WFB of the macrogamtocyte (Belli *et al.,* 2003a). Such a mechanism enables rapid encapsulation of an otherwise fragile stage of the parasite, facilitating its survival in its passage out of the host in the faeces and in the outside world. This provides a rationale for believing that proteases may be integral to the breakdown of EmGam56 and EmGam82. If proven, and the proteases that are responsible for the processing of these two gametocyte proteins are identified, then a totally new class of anticoccidial drug – a specific protease inhibitor (or inhibitors) – is not hard to imagine. Thus, future work directed at identifying proteases from the sexual stages of *Eimeria* is well warranted.

Indeed, it has already commenced and recent work at the University of Technology, Sydney has detected several gametocyte-specific proteases (Katrib M, Ikin R, Sharman P, Slapetova I, Belli SI and Smith NC, personal communication). Included amongst these are several subtilisins, which are particularly interesting with regard to dityrosine bond formation because of their known role in the formation of the cuticle of nematodes. Thus, the assembly of cuticlins and collagens to form the cuticle involves a number of catalytic pathways: (1) collagens are synthesized as proproteins that are cleaved at the N-terminus by a subtilisin-like protease prior to cuticle formation (Thacker *et al.*, 1995; 2000a, b; 2006); (2) the collagens (and cuticlins) are held together by di- and tri-tyrosine crosslinks (Page and Winter, 2003); and (3) dual oxidase is the oxidative enzyme responsible for the generation of the tyrosine crosslinks (Page *et al.,* 2003). Mutations at any one of these steps, result in a deficiency of di- and tri-tyrosine in the cuticle, the formation of a structurally defective cuticle and parasite death (Page *et al.,* 2003). The model of oocyst wall formation presented in Figure 6.2, predicts a very similar picture. Fortunately, the availability of a range of full-length and truncated recombinant versions of EmGam56 and EmGam82, including the ones

described in this thesis and others developed at the University of Technology, Sydney (Dr Sabina Belli, University of Technology, Sydney, personal communication), means that a specific cleavage assay (using these recombinants as substrates) can be readily developed to test the ability of identified proteases to cleave EmGam56 and EmGam82 and produce tyrosine-rich polypeptides.

The presumptive conformational flexibility of EmGam56, and its derivatives improves the chances of crosslinking occurring between different peptides of different sizes, leading to formation of the oocyst wall. There are several examples of IUPs that bind with several different partners and it is even recognised that some complexes simply cannot assemble if their components are rigid structures (Tompa, 2005). In addition, IUPs are involved in regulation, signaling and control pathways where interactions occur with multiple partners with high-specificity and low-affinity thus conferring great functional diversity (Vucetic *et al.*, 2005). In the case of assembly of the oocyst wall, this feature provides two advantages: first, proteins derived from EmGam56 (and presumably EmGam82), are able to undergo protein binding and crosslinking with a variety of different peptides of various sizes as a result of their inherent flexibility; and, second, this inherent flexibility may increase the possibility that tyrosine residues may be readily exposed and accessible for peroxidase and/or DOPA oxidase to catalyse crosslinking of tyrosine-rich wall proteins through formation of dityriosine bridges. As presented and discussed in Chapter 5, cross-linking of a truncated version of EmGam56 (r56) occurs very readily and rapidly in the presence of HRPO or APx and peroxide (*t*-BHP) through formation of dityrosine bridges. There is precedent for the idea that IUPs can increase the accessibility of tyrosine residues - for example, it has been shown that the highly efficient nitration and oxidation of α-synuclein, resulting in the formation of α-synuclein polymers through dityrosine cross-linking, is attributable to the unstructured conformation of the protein, which causes all its tyrosine residues to be exposed in the solvent phase, thereby enhancing the probability for reaction with nitrating agent (Souza *et al.*, 2000).

The possibility that EmGam56 is an IUP and that being an IUP is important for its subsequent processing and dityrosine bonding is a novel concept that may have implications in a variety of biological processes. Dityrosine bonding has been implicated in hardening of a number of biological structural materials from a number of organisms through different phyla. These include such structures as insect cuticular resilin (Andersen, 1964), exoskeletons of the nematodes, *Haemonchus contortus*, *Caenorhabditis elegans* and *Ascaris suum* (Fujimoto, 1975; Fetterer and Rhoads, 1990; Lassandro *et al.*, 1994), ascospore walls from the yeast, *Saccharomyces cerevisiae* (Briza *et al.*, 1986), cell walls of *Candida albicans* (Smail *et al.*, 1995), and the fertilization membrane of sea urchin eggs, *Stronglycocentrotus purpuratus* (Foerder and Shapiro, 1977). The presence of dityrosine in vertebrate animal proteins is also seen in chicken aorta elastin, collagen, and connective tissues from bovines, rats, and cats, and in tissues of normal and diseased humans (LaBella *et al.*, 1968; Amado *et al.*, 1984; Davies *et al.*, 1999). DOPA-containing proteins are also widely distributed in nature and are involved in the synthesis of extraorganismic structural materials such as helminth worm and mosquito eggshells, egg capsules, cocoons, mussel byssal threads and various biological glues and cements (Waite, 1990; Huggins and Waite, 1993). In addition, phenol oxidase activity (catalysing oxidation of DOPA to dopachrome) is detected only in homogenates of female *Trichuris suis* (a parasite inhabiting the intestines of pigs) not males, suggesting that the enzyme is likely to be associated with hardening of eggshell and the eggshell proteins might consist of DOPA-containing proteins (Fetterer and Hill, 1993). With the exception of the finding that the unstructured conformation of α-synuclein may facilitate its polymerization via dityrosine crosslinking, which may be significant in the pathogenesis of Parkinson's Disease (Souza *et al.,* 2000), the potential importance of IUPs in the construction of dityrosine and DOPA matrices has not been considered.

The *in vitro* cross-linking assay described in Chapter 5 enabled the discovery of the finding that plant-like, but not mammalian, peroxidases were able to catalyse the rapid crosslinking of a tyrosine-rich truncation of EmGam56 in the presence of a relatively mild peroxide. Identifying the peroxidases of *Eimeria* should now be a priority research goal because, once identified and validated as playing a crucial role in dityrosine bond

formation during the genesis of the oocyst wall, these peroxidases could be the targets of specific inhibitors that embody a novel class of anticoccidials. This search for *Eimeria* peroxidases should proceed despite the finding that a strong oxidizing agent can initiate cross-linking of a tyrosine-rich truncation of EmGam56 (see Chapter 5 for a full discussion) because peroxidase activity has been detected in tissue sections of *Eimeria* macrogametocytes (Belli *et al.,* 2003a; 2006). To date, efforts to detect peroxidase or DOPA oxidase activity in gametocytes or unsporulated oocysts using standard assays have proven fruitless. This is perhaps not totally surprising since histological activity assays have demonstrated that all the peroxidase (Belli *et al.,* 2006) and DOPA oxidase activity (Prof. David Ferguson, University of Oxford, personal communication) of *Eimeria* is exquisitely localized to the WFB and the still developing oocyst wall. Thus, it appears essential that methods to isolate and purify the WFB be developed and these organelles be used in future assays for peroxidase and DOPA oxidase activity and as a starting point for purification of the native enzymes. Attempts to identify peroxidases and DOPA oxidase in the *E. tenella* genome database have also been unsuccessful to date; however, the database is incompletely annotated at this stage.

The results presented in this thesis indicate that future querying of the *E. tenella* genome database should focus on screening for plant-like peroxidases. Peroxidases are widely distributed throughout bacteria, fungi, plants and vertebrates and they can be divided into two superfamilies: (1) the mammalian peroxidase superfamily such as myeloperoxidase, lactoperoxidase, eosinophil peroxidase, and thyroid peroxidase; and (2) the plant peroxidase superfamily. Within the plant peroxidase superfamily, peroxidases are grouped into one of three classes (Welinder, 1992): Class I are the intracellular prokaryotic peroxidases including chloroplast and cytosol ascorbate peroxidases, yeast cytochrome c peroxidase, and gene duplicated bacterial peroxidases; Class II are extracellular fungal peroxidases such as lignin and manganese-dependent peroxidases from *Phanerochaete chrysosporium*; and Class III are classical secretory plant peroxidases, an example of which is horseradish peroxidase from *Armoracia rusticana.* A summary of functions and characteristics of the peroxidases in each superfamily is shown in Table 6.1.

Within the plant peroxidase superfamily, the structural properties of Class II and III are quite similar but Class I exhibits unique features. Class I peroxidases do not contain any disulphide bridge whereas in Class II and III, disulphide bridges are present and they are implicated in providing a high degree of rigidity to the protein (Banci, 1997). In addition, Class I peroxidases do not contain any carbohydrate, structural calcium ions and endoplasmic reticulum signal sequence, in contrast to the peroxidases in Class II and III, which are glycosylated on the protein surface, contain two structural calcium ions and are routed via the endoplasmic reticulum (Welinder, 1992). The calcium ions play a role in maintaining the structure and biological function of the active site, which is essential for enzymatic activity. For example, Haschke and Friedhoff (1978) found that removal of the calcium ions from plant horseradish peroxidase results in sizable reduction of its enzymatic activity. Thus, it would be surprising if Class I peroxidases were to catalyse cross-linking of dityrosine bond formation between *Eimeria* proteins, though this cannot be definitively ruled out since enzymes from this class were not tested in this study. As stated above, it seems more logical and, potentially, more fruitful to focus on the Class II and III peroxidases, particularly given the several other plant-like characteristics possessed by *Eimeria* (reviewed in the discussion of Chapter 5).

Finally, the research described in this thesis contributes to our understanding of how the anticoccidial vaccine, CoxAbic®, works (Figure 6.3). CoxAbic® is the only commercially available subunit vaccine against any protozoan parasite and, because of the novelty of its application and mode of action, its uptake by poultry farmers has been slower than hoped for (Avner Finger, Abic Ltd, personal communication). Never-the-less, CoxAbic® has now been used around the world in trials involving 177 million broiler chickens and the results from all trials clearly demonstrate that, in all aspects of parasite control, broiler growth, flock health and mortality, the performance of CoxAbic® broilers was similar to that of medicated or live vaccine control groups. Indeed, in most instances, CoxAbic® broilers performed slightly better than flocks reared on prophylactic drugs or live vaccines (Wallach MG, Smith NC, Ashash U and Michael A, manuscript in preparation). CoxAbic® is composed of an affinity purified gametocyte antigen preparation from *E. maxima,* dominated by EmGam56 and EmGam82 (Wallach, 2002). Immunisation of broiler breeder hens with the vaccine stimulates the production of

IgG (sometimes referred to as IgY) antibodies that are transferred to the developing broiler chick via the egg yolk. The results presented in this thesis, together with previous studies on oocyst wall formation (Belli *et al.,* 2003b; Ferguson *et al.,* 2003), are consistent with the hypothesis that the protective antibodies prevent formation of oocysts by either: (a) protecting the full length versions of EmGam56 and EmGam82 from degradation/proteolysis into smaller tyrosine-rich polypeptides destined for incorporation into the oocyst wall; or (b) interfere with the formation of dityrosine cross-links between the tyrosine-rich polypeptides (Figure 6.3). By helping to explain the molecular basis for CoxAbic®'s activity, the research presented in this thesis will directly contribute to the marketability of this novel vaccine.

Table 6.1 Summary of the functions and characteristics of peroxidases in each superfamily

Mammalian peroxidase superfamily	❖ Myeloperoxidase (EC 1.11.1.7): is found in granulocyte and monocytes and plays a role in the H_2O_2-dependent microbicidal system of neutrophils through the oxidation of chloride or thiocyanate to hypochlorite or hypothiocyanite, respectively (Klebanoff, 1991). ❖ Lactoperoxidase (EC 1.11.1.7): is abundant in milk and in other biological fluids such as tears and saliva and plays a host defense role through antimicrobial activity by converting thiocyanate to hypocyanite in an H_2O_2-dependent reaction (Ferrari *et al.*, 1995). ❖ Eosinophil peroxidase (EC 1.11.1.7): a 77 kDa, two subunit enzyme that contributes to 40 % of total specific granule proteins of eosinophils and plays a critical role in killing parasites (Abu-Ghazaleh *et al.*, 1992; Carlson *et al.*, 1985). ❖ Thyroid peroxidase (1.11.1.8): is a membrane-bound, glycosylated hemoprotein involved in biosynthesis of thyroid hormone by catalyzing both iodination and coupling of iodotyrosine residues into the thyroglobulin (Magnusson *et al.*, 1987; Nakamura *et al.*, 1984).
Plant peroxidase superfamily	**Class I: intracellular prokaryotic peroxidases** ❖ Ascorbate peroxidases (EC 1.11.1.11): play a role in removal of H_2O_2 through the oxidation of ascorbate in the chloroplasts and cytosol of plants and in algae and cyanobacteria (Shigeoka *et al.*, 2002). ❖ Yeast cytochrome c peroxidase (EC 1.11.1.5): functions to reduce H_2O_2 generated during aerobic respiratory process by oxidizing cytochrome c in the mitochondrial intermembrane space (Kwan *et al.*, 2003). ❖ Bacterial catalase-peroxidases (1.11.1.6): are heme-containing catalase-peroxidases that exhibit both catalase and peroxidase activities (Welinder, 1991). They degrade H_2O_2 either as a catalase ($2H_2O_2 \rightarrow 2H_2O + O_2$) or as a peroxidase ($H_2O_2 + 2AH \rightarrow 2H_2O + 2A^{\bullet}$) to prevent the formation of highly reactive breakdown products of H_2O_2 (Donald *et al.*, 2003). Examples of such enzymes are catalase-peroxidase from *Burkholderia pseudomallei* and catalase hydroperoxidase I from *Escherichia coli*.

Table 6.1 (Continued...) Summary of the functions and characteristics of peroxidases in each superfamily

Plant peroxidase superfamily	**Class II: extracelluar fungal peroxidases** ❖ Lignin peroxidases (1.11.1.14) and manganese-dependent peroxidase (1.11.1.13): are fungal ligninases responsible for catalyzing the degradation of lignin through oxidation of large polymers, lignin, and inorganic ions, Mn^{2+}, respectively. Examples of such enzymes are found in whit-rot fungus, *Phanerochaete chrysosporium* (Wariishi *et al.*, 1991; Sarkanen *et al.*, 1991). ❖ *Arthromyces* peroxidase (1.11.1.7): is a heme-containing enzyme that catalyzes the oxidation of a variety of compounds such as phenols and ascorbic acids in the presence of hydrogen peroxide. A well known example is peroxidases from *Arthromyces ramosus* (Shinmen *et al.*, 1986).
	Class III: classical secretory plant peroxidases ❖ Plant peroxidases (1.11.1.7): some of these enzymes have a role in the removal of H_2O_2 and oxidation of toxic reductants such as horseradish peroxidase, whilst others might play a part in biosynthesis of lignin, lignification of cell wall, metabolism of plant hormones and/or responses to environmental stress such as oxidative stress and pathogen attack (Hiraga *et al.*, 2001; Kawaoka *et al.*, 2003).

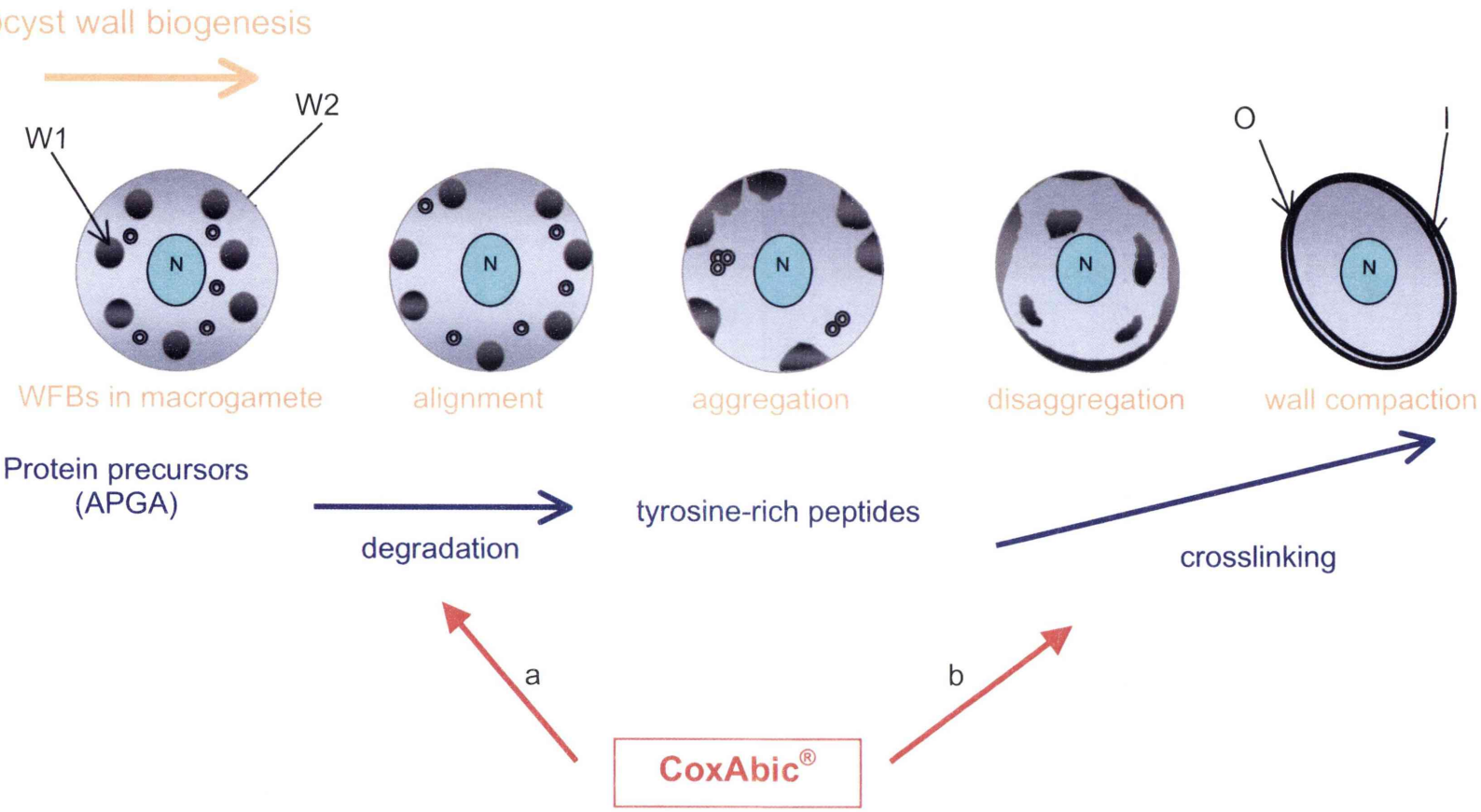

Figure 6.3 Molecular basis of action of CoxAbic®. The vaccine induces production of antibodies that may prevent formation of the oocyst walls by either: (a) blocking degradation/proteolysis of the full length versions of EmGam56 and EmGam82 into smaller tyrosine-rich polypeptides destined for incorporation into the oocyst wall; or (b) interfering with the formation of dityrosine cross-links between the tyrosine-rich polypeptides

Chapter Seven

References

Abelskov, A.K., Smith, A.T., Rasmussen, C.B., Dunford, H.B. and Welinder, K.G. (1997) pH dependence and structural interpretation of the reactions of *Coprinus cinereus* peroxidase with hydrogen peroxide, ferulic acid, and 2,2'-azinobis(3-ethylbenzthiazoline-6-sulfonic acid). *Biochemistry* **36**(31): 9453–9463.

Abu-Ghazaleh, R.I., Dunnette, S.L., Loegering, D.A., Checkel, J.L., Kita, H., Thomas, L.L. and Gleich, G.J. (1992) Eosinophil granule proteins in peripheral blood granulocytes. *Journal of Leukocyte Biology* **52**(6): 611-618.

Adler, A.J., Greenfield, N.J. and Fasman, G.D. (1973) Circular dichroism and optical rotatory dispersion of proteins and polypeptides. *Methods in Enzymology* **27**: 675-735.

Aeschbach, R., Amado, R. and Heukom, H. (1976) Formation of dityrosine cross-links in proteins by oxidation of tyrosine. *Biochimica et Biophysica Acta* **439**(2): 292-301.

Allen, P.C. and Fetterer, R.H. (2002) Recent advances in biology and immunobiology of *Eimeria* species and in diagnosis and control of infection with these coccidian parasites of poultry. *Clinical Microbiology Reviews* **15**(1): 58-65.

Allocco, J.J., Profous-Juchelka, H., Myers, R.W., Nare, B. and Schmatz, D.M. (1999) Biosynthesis and Catabolism of Mannitol Is Developmentally Regulated in the Protozoan Parasite *Eimeria tenella*. *The Journal of Parasitology* **85**(2): 167-173.

Amado, R., Aeschbach, R. and Neukom, H. (1984) Dityrosine: *in vitro* production and characterization. *Methods in Enzymology* **107**: 377-388.

Andersen, S.O. (1964) The crosslinks in resilin identified as dityrosine and trityrosine. *Biochimica et Biophysica Acta* **93**: 213–215.

Armstrong, C. M. and Bezanilla, F. (1977) Inactivation of the sodium channel. II. Gating current experiments. *The Journal of General Physiology* **70**(5): 567-590.

Banci, L. (1997) Structural properties of peroxidases. *Journal of Biotechnology* **53**(2-3): 253-263.

Beitz, E. (2005) Aquaporins from pathogenic protozoan parasites: structure, function and potential for chemotherapy. *Biology of the Cells* **97**(6): 373-383.

Belli, S.I., Lee, M., Thebo, P., Wallach, M., Schwartsburd, S. and Smith, N.C. (2002a) Biochemical characterisation of the 56 and 82 kilodalton immunodominant gametocyte antigens from *Eimeria maxima*. *International Journal for Parasitology* **32**(7): 805-816.

Belli, S.I., Witcombe, D., Wallach, G.M. and Smith, N.C. (2002b) Functional genomic of gam56: characterisation of the role of a 56 kilodalton sexual stage antigen in oocyst wall formation in *Eimeria maxima*. *International Journal for Parasitology* **3**(14): 1727-1737.

Belli, S.I., Wallach, M.G., and Smith, N.C. (2003a) Cloning and characterization of the 82 kDa tyrosine-rich sexual stage glycoprotein, GAM82, and its role in oocyst wall formation in the apicomplexan parasite, *Eimeria maxima*. *Gene* **307**: 201-212.

Belli, S.I., Wallach, M.G., Luxford, C., Davies, M.J. and Smith, N.C. (2003b) Role of tyrosine-rich precursor glycoproteins and dityrosine- and 3,4-dihydroxyphenylalanine-mediated protein cross-linking in development of the oocyst wall in the coccidian parasite *Eimeria maxima*. *Eukaryotic Cell* **2**(3): 456-464.

Belli, S.I., Mai, K., Skene, C.D., Gleeson, M.T., Witcombe, D.M., Katrib, M., Finger, A., Wallach, M.G. and Smith, N.C. (2004) Characterisation of the antigenic and immunogenic properties of bacterially expressed, sexual stage antigens of the coccidian parasite, *Eimeria maxima*. *Vaccine* **22**(31-32): 4316-4325.

Belli, S.I., Walker, R.A. and Flowers, S.A. (2005) Global protein expression analysis in apicomplexan parasites- current status. *Proteomics* **5**(4): 918-924.

Belli, S.I., Smith, N.C. and Ferguson, D.J.P. (2006) The coccidian oocyst: a tough nut to crack! *Trends in Parasitology* **22**(9): 416-423.

Briza P, Winkler, G., Kalchhauser, H. and Breitenbach, M. (1986) Dityrosine is a prominent component of the yeast ascospore wall: a proof of its structure. *The Journal of Biological Chemistry* **261**(9): 4288-4294.

Burzio, L.A. and Waite, J.H. (2000) Cross-linking in adhesive quinoproteins: studies with model decapeptides. *Biochemistry* **39**(36): 11147-11153.

Burzio, L.A. and Waite, J.H. (2001) Reactivity of peptidyl-tyrosine to hydroxylation and cross-linking. *Protein Science* **10**(4): 735-740.

Carlson, M.G. Peterson C.G. and Venge, P. (1985) Human eosinophil peroxidase: purification and characterization. *The Journal of Immunology* **134**(3): 1875-1879.

Challey, J.R. and Jeffers, T.K. (1973) Synergism between 4-hydroxyquinoline and pyridine coccidiostat. *The Journal of Parasitology* **59**(3): 502-504.

Chapman, H.D. (1993) Resistance to anticoccidial drugs in fowl. *Parasitology Today* **9**(5): 159-162.

Chapman, H.D. (1999) The development of immunity to *Eimeria* species in broilers given anticoccidial drugs. *Avian Pathology* **28**(2): 155-162.

Cheng, J., Randall, A.Z., Sweredoski, M.J. and Baldi, P. (2005a) SCRATCH: a protein structure and structural feature prediction server. *Nucleic Acids Research* **33**: w72-76.

Cheng, J., Sweredoski, M. and Baldi, P. (2005b) Accurate prediction of protein disordered regions by mining protein structure data. *Data Mining and Knowledge Discovery* **11**(3): 213-222.

Christensen, A.M., Schaefer, J., Kramer, K.J., Morgan, T.D. and Hopkins, T.L. (1991) Detection of cross-links in insect cuticle by REDOR NMR spectroscopy. *Journal of the American Chemical Society* **113**(18): 6799–6802.

Clark, R.A., Klebanoff, S.J., Einstein, A.B. and Fefer, A. (1975) Peroxidase-H2O2-halide system: Cytotoxic effect on mammalian tumor cells. *Blood* **45**(2): 161-170.

Clark, R.A. and Szot, S. (1982) Chemotactic factor inactivation by stimulated human neutrophils mediated by myeloperoxidase-catalyzed methionine oxidation. *The Journal of Immunology* **128**(4): 1507-1513.

Coppin, A., Dzierszinski, F., Legrand, S., Mortuaire, M., Ferguson, D. and Tomavo, S. (2003) Developmentally regulated biosynthesis of carbohydrate and storage polysaccharide during differentiation and tissue cyst formation in *Toxoplasma gondii*. *Biochimie* **85**(3-4): 353-361.

Cortese, M.S., Baird, J.P., Uversky, V.N. and Dunker, A.K. (2005) Uncovering the unfoldome: enriching cell extracts for unstructured proteins by acid treatment. *Journal of Proteome Research* **4**(5): 1610-1618.

Cox, C.J., Dutta, K., Petri, E.T. Hwang, W.C., Lin, Y., Pascal, S.M. and Basavappa, R. (2002) The regions of securing and cyclin B proteins recognized by the ubiquitination machinery are natively unfolded. *FEBS Letters* **527**(1-3): 303-308.

Cox, F.E.G. (1993) Parasitic protozoa. In: Cox, F.E.G. (Ed.). *Modern Parasitology*; pp1-23, Blackwell Scientific Publication, Oxford.

Dahiya, R.S. and Speck, M.L. (1968) Hydrogen peroxide formation by lactobacilli and its effect on *Staphylococcus aureus*. *Journal of Dairy Science* **51**(10): 1568-1572.

Davey, C.A. and Fenna, R.E. (1996) 2.3 Å resolution X-ray crystal structure of the bisubstrate analogue inhibitor salicylhydroxamic acid bound to human myeloperoxidase:

a model for a prereaction complex with hydrogen peroxide. *Biochemistry* **35**(33): 10967-10973.

Davies, M.J., Fu, S., Wang, H. and Dean, R.T. (1999) Stable markers of oxidant damage to proteins and their application in the study of human disease. *Free Radical Biology and Medicine* **27**(11-12): 1151-1163.

Deits, T., Farrance, M., Kay, E.S., Medill, L., Turner, E.E., Weidman, P.J. and Shapiro, B.M. (1984) Purification and properties of ovoperoxidase, the enzyme responsible for hardening the fertilization membrane of the sea urchin egg. *The Journal of Biological Chemistry* **259**(21): 13525-13533.

Dill, K.A. and Shortle, D. (1991) Denatured states of proteins. *Annual Review of Biochemistry* **60**: 795–825.

Donald, L.J., Krokhin, O.V., Duckworth, H.W., Wiseman, B., Deemagarn, T., Singh, R., Switala, J., Carpena, X., Fita, I. and Loewen, P.C. (2003) Characterization of the catalase-peroxidase KatG from *Burkholderia pseudomallei* by mass spectrometry. *The Journal of Biological Chemistry* **278**(37): 35687-35692.

Dosztanyi, Z., Csizmok, V., Tompa, P. and Simon, I. (2005) IUPred: web server for the prediction of intrinsically unstructured regions of proteins based on estimated energy content. *Bioinformatics* **21**(16): 3433-3434.

Dubey, J.P., Miller, N.L. and Frenkel, J.K. (1970) The *Toxoplasma gondii* oocyst from cat faeces. *Journal of Experimental Medicine* **132**(4): 636-662.

Dunker, A.K., Garner, E., Guilliot, S., Romero, P., Albrecht, K., Hart, J., Obradovic, Z., Kissinger, C. and Villafranca, J.E. (1998) Protein disorder and the evolution of molecular recognition: theory, predictions and observations. *Pacific Symposium on Biocomputing* **3**: 473-484.

Dunker, A.K., Obradovic, Z., Romero, P. Garner, E.C. and Brown, C.J. (2000) Intrinsic protein disorder in complete genomes. *Genome Informatics* **11**: 161-171.

Dunker, A.K., Brown, C.J., Lawson, J.D., Iakoucheva, L.M. and Obradovic, Z. (2002) Intrinsic disorder and protein function. *Biochemistry* **41**(21): 6573-6582.

Dunten, R.L. and Cohen, R.E. (1989) Recognition of modified forms of ribonuclease A by the ubiquitin system. *The Journal of Biological Chemistry* **264**(28): 16739-16747.

Edgar, S.A., Herrick, C.A. and Fraser, L.A. (1944) Glycogen in the life cycle of the Coccidium, *Eimeria tenella*. *Transactions of the American Microscopical Society* **63**(3): 199-202.

Eschenbacher, K.H., Eggli, P., Wallach, M. and Braun, R. (1996) Characterization of a 14 kDa oocyt wall protein of *Eimeria tenella* and *E. acervulina*. *Parasitology* **112**(2): 169-176.

Farhangrazi, Z.S., Copeland, B.R., Nakayama, T., Amachi, T., Yamazaki, I. and Powers, L.S. (1994) Oxidation-reduction properties of Compounds I and II of *Arthromyces ramosus* peroxidase. *Biochemistry* **33**(18): 5647-5652.

Feng, Z.P., Zhang, X., Han, P., Arora, N., Anders, R.F. and Norton, R.S. (2006) Abundance of intrinsically unstructured proteins in *P. falciparum* and other apicomplexan parasite proteomes. *Molecular & Biochemical Parasitology* **150**(2): 256-267.

Ferguson, D.J.P., Hutchison, W.M., Siim, J.C. (1975) The ultrastructural development of the macrogamete and formation of the oocyst wall of *Toxoplasma gondii*. *Acta Pathologica et Microbiologica Scandinavica* **83**(5): 491-505.

Ferguson, D.J.P., Brecht, S. and Soldati, D. (2000) The microneme protein MIC4, or an MIC4-like protein, is expressed within the macrogamete and associated with oocyst wall

formation in *Toxoplasma gondii*. *International Journal for Parasitology* **30**(11): 1203-1209.

Ferguson, D.J.P., Belli, S.I., Smith, N.C. and Wallach, M.G. (2003) The development of the macrogamete and oocyst wall in *Eimeria maxima*: immuno-light and electron microscopy. *International Journal of Parasitology* **33**(12): 1329-1340.

Ferrari, R.P., Laurenti, E., Cecchini, P.I., Gambino, O. and Sondergaard, I. (1995) Spectroscopic investigations on the highly purified lactoperoxidase Fe(III)-heme catalytic site. *Journal of Inorganic Biochemistry* **58**(2): 109-127.

Fetterer, R.H. and Rhoads, M.L. (1990) Tyrosine-derived cross-linking amino acids in the sheath of *Haemonchus contortus* infective larvae. *The Journal of Parasitology* **76**(5): 619-624.

Fetterer, R.H. and Hill, D.E. (1993) The occurrence of phenol oxidase activity in female *Trichuris suis*. *The Journal of Parasitology* **79**(2): 155-159.

Fink, A. L., Calciano, L.J., Goto, Y., Kurotsu, T. and Palleros, D.R. (1994) Classification of acid denaturation of proteins: intermediates and unfolded states. *Biochemistry* **33**(41): 12504-12511.

Fitz-Choy, S.H. and Edgar, S.A. (1989) *Eimeria mitis*: immunogenicity and cross immunity of two isolates. *Avian Diseases* **33**(2): 236-237.

Foerder, C.A and Shapiro, B.M. (1977) Release of ovoperoxidase from sea urchin eggs hardens the fertilization membrane with tyrosine crosslinks. *Proceedings of the National Academy of Sciences of the United States of America* **74**(10): 4214-4218.

Fujimoto, D. (1975) Occurrence of dityrosine in cuticlin, a structure protein from *Ascaris* cuticle. *Comparative Biochemistry and Physiology* **51B**: 205-207.

Garnier, J., Osguthorpe, D.J. and Robson, B. (1978) Analysis of the accuracy and implications of simple methods for predicting the secondary structure of globular proteins. *Journal of Molecular Biology* **120**(1): 97-120.

Garnier, J., Gibrat, J.F. and Robson, B. (1996) GOR method for predicting protein secondary structure from amino acid sequence. *Methods in Enzymology* **266**: 540-553.

Gasteiger, E., Gattiker, A., Hoogland, C., Ivanyi, I., Appel, R.D. and Bairoch, A.(2003) *ExPASy: the proteomics server for in-depth protein knowledge and analysis Nucleic Acids Research* **31**(13):3784-3788.

Geourjon, C. and Deléage, G. (1995) SOPMA: significant improvements in protein secondary structure prediction by consensus prediction from multiple alignments. *Bioinformatics* **11**(6): 681-684.

Gieseg, S.P., Simpson, J.A., Charlton, T.S., Duncan, M.W. and Dean R.T. (1993) Protein bound 3,4-dihydroxyphenylalanine is a major reductant formed during hydroxyl damage to proteins. *Biochemistry* **32**(18): 4780-4786.

Gleeson, M.T. (2000) The plastid in Apicomplexa: what use is it? *International Journal for Parasitology* **30**(10): 1053-1070.

Goto, Y., Calciano, L.J. and Fink, A.J. (1990) Acid-induced folding of proteins. *Proceedings of the National Academy of Sciences of the United States of America*. **87**(2): 573-577.

Gross, A.J. and Sizer, I.W. (1959) The oxidation of tyramine, tyrosine, and related compounds by peroxidase. *The Journal of Biological Chemistry* **234**(6): 1611-1614.

Guermeur, Y. (1997) Combinaison de classifieurs statistiques, Application a la prediction de structure secondaire des proteins.

Gupta, P., Batra, S., Chopra, A.P., Singh, Y. and Bhatnagar, R. (1998) Expression and purification of the recombinant lethal factor of *Bacillus anthracis*. *Infection and Immunity* **66**: 862-865.

Haines, D.C., Sevrioukova, I.F. and Peterson, J.A. (2000) The FMN-binding domain of cytochrome P450μ_β-3: resolution, reconstruction, and flavin analogue substitution. *Biochemistry* **39**(31): 9419-9429.

Hansen, M., Kun, J.F.J., Schultz, J.E. and Beitz, E. (2002) A single, bi-functional aquaglyceroporin in blood-stage *Plasmodium falciparum* malaria parasites. *The Journal of Biological Chemistry* **277**(7): 4874-4882.

Harder, A. and Haberkorn, A. (1989) Possible model of action of toltrazuril: studies on two *Eimeria* species and mammalian and *Ascaris suum* enzymes. *Parasitology Research* **76**(1): 8-12.

Harlow, E. and Lane, D (1988) Immunoblotting, Antibodies: a Laboratory Manual; pp.490-492. Cold Spring Harbor Laboratory Press, Cold Spring Harbor.

Harris, H.R., Adrian, M. and Petry, F. (2004) Amylopectin: a major component of the residual body in *Crytosporidium parvum* oocysts. *Parasitology* **128**(3): 269-282.

Haschke, R.H. and Friedhoff, J.M. (1978) Calcium-related properties of horseradish peroxidase. *Biochemical and Biophysical Research Communications* **80**(14): 1039-1042.

Heinecke, J.W., Li, W., Francis, G.A. and Goldstein, J.A. (1993) Tyrosyl radical generated by myeloperoxidase catalyzes the oxidative cross-linking of proteins. *The Journal of Clinical Investigation* **91**(6): 2666-2872.

Heinecke, J.W. (2002) Tyrosyl radical production by myeloperoxidase: a phagocyte pathway for lipid peroxidation and dityrosine cross-linking of proteins. *Toxicology* **177**(1): 11-22.

Huggins, L.G. and Waite, J.H. (1993) Eggshell formation in *Bdelloura candida*, an ectoparasitic turbellarian of the horseshoe crab *Limulus polyphemus*. *Journal of Experimental Zoology* **265**(5): 549-557.

Iakoucheva, L. M., Brown, C. J., Lawson, J. D., Obradovic, Z. and Dunker, A. K. (2002) Intrinsic disorder in cell-signaling and cancer-associated proteins. *Journal of Molecular Biology* **323**(3): 573-584.

James, S. (1980) Thiamine uptake in isolated schizonts of *Eimeria tenella* and the inhibitory effects of amprolium. *Parasitology* **80**(2): 313-322.

Jeffers, T.K. (1975) Attenuation of *Eimeria tenella* through selection for precociousness. *The Journal of Parasitology* **61**(6): 1083-1090.

Jenkins, M.C. (1998) Progress on developing a recombinant coccidiosis vaccine. *International Journal for Parasitology* **28**(7): 1111-1119.

Jeurissen, S.H.M., Janse, E.M., Vermeulen, A.N. and Vervelde, L. (1996) *Eimeria tenella* infections in chickens: aspects of host-parasite interaction. *Veterinary Immunology and Immunopathology* **54**(1-4): 231-238.

Johnson, W.C. (1988) Secondary structure of proteins through circular dichroism spectroscopy. *Annual Review of Biophysics and Biophysical Chemistry* **17**: 145-166.

Jones, D.J. (1999) Protein secondary structure prediction based on position-specific scoring matrices. *Journal of Molecular Biology* **292**(2): 195-202.

Joyner, L.P. and Norton, C.C. (1973) The immunity arising from continuous low-level infection with *Eimeria tenella*. *Parasitology* **67**(3): 333-340.

Karim, M.J., Basak, S.C. and Trees, A.J. (1996) Characterization and immunoprotective properties of a monoclonal antibody against the major oocyst wall protein of *Eimeria tenella*. *Infection and Immunity* **64**(4): 1227-1232.

Kawaoka, A., Matsunaga, E., Endo, S., Kondo, S., Yoshida, K., Shinmyo, A. and Ebinuma, H. (2003) Ectopic expression of a horseradish peroxidase enhances growth rates and increases oxidative stress resistance in hybrid Aspen. *Plant Physiology* **132**(3): 1177-1185.

Kerwin, L.J., Turecek, F., Xu, R., Kramer, K.J., Hopkins, T.L., Gatlin, C.L. and Yates, J.R. (1999) Mass spectrometric analysis of catechol–histidine adducts from insect cuticle. *Analytical Biochemistry* **268**(2): 229-237.

Klebanoff, S.J. (1991) Myeloperoxidase: occurrence and biological functions. In: Everse, J., Everse, K.E. and Grisham, M.B. (Eds.). *Peroxidases in Chemistry and Biology*; pp1-35. CRC Press, Boca Raton, Florida.

Krücken, J., Hosse, R.J., Mouafo, A.N. Entzeroth, R., Bierbaum, S., Marinovski, P., Hain, K., Greif, G. and Wunderlich, F. (2007) Excystation of *Eimeria tenella* sporozoites impaired by antibody recognizing gametocyte/oocyst antigens GAM22 and GAM56. *Eukaryotic Cell* **7**(2): 202-211.

Kuticic, V. and Wikerhauser, T. (1996) Studies on the effect of various treatments on the viability of *Toxoplasma gondii* tissue cysts and oocysts. *Current Topics in Microbiology and Immunology* **219**: 261-265

Kwon, M., Chong, S., Han, S. and Kim, K (2003) Oxidative stresses elevate the expression of cytochrome c peroxidase in *Saccharomyces cerevisiae*. *Biochimica et Biophysica Acta* **1623**(1): 1-5.

LaBella, F., Waykole, P. and Queen, G. (1968) Formation of insoluble gels and dityrosine by the action of peroxidase on soluble collagens. *Biochemical and Biophysical Research Communications* **30**(4): 333-338.

Laemmli, U.K. (1970) Cleavage of structural protein during the assembly of the head of bacteriophage T4. *Nature* **227**: 880-685.

Lassandro, F., Sebastiano, M., Zei, F. and Bazzicalupo, P. (1994) The role of dityrosine formation in the crosslinking of CUT-2, the product of a second cuticlin gene of *Caenorhabditis elegans*. *Molecular and Biochemical Parasitology* **65**(1): 147-159.

Lee, D.L. and Millard, B.J. (1972) Fine structural changes in *Eimeria tenella*, from infections in chick embryos and chickens, after exposure to the anticoccidial drug robenidene. *Parasitology* **65**(2): 309-316.

Lee, E.H. and Fernando, M.A. (1978) Immunogenicity of a single sporocyst of *Eimeria maxima*. *The Journal of Parasitology* **64**(3): 483-485.

Lee, E.H. (1987) Vaccination against coccidiosis in commercial roaster chickens. *Canadian Veterinary Journal* **28**(7): 434-436.

Levine, N.D. and Ivens, V. (1965) The coccidian parasites (Protozoa, Sporozoa) of rodents. Illinois Biological Monographs 33. Urbana: The University of Illinois Press, USA.

Linding, R., Jensen, L.J., Diella, F., Bork, P., Gibson, T.J. and Russell, R.B. (2003a) Protein disorder prediction: implications for structural proteomics. *Structure* **11**(11): 1453-1459.

Linding, R., Rusell, R.B., Neduva, V. and Gibson, T.J. (2003b) GlobPlot: exploring protein sequences for globularity and disorder. *Nucleic Acids Research* **31**(13): 3701-3708.

Long, P.L. (1972) *Eimeria tenella*: reproduction, pathogenicity and immunogenicity of a strain maintained in chick embryos by serial passages. *Journal of Comparative Pathology* **82**(4): 429-437.

Long, P.L. (1973) Pathology and pathogenicity of coccidial infections. In: Hammond, D.M. and Long, P.L. (Eds.), *The Coccidia*: *Eimeria, Isospora, Toxoplasma and related genera*; pp253-294, University Park Press, Baltimore, London.

Long, P.L., Johnson, J., McKenzie, M.E. Perry, E., Crane, M.S.J. and Murray, P.K. (1986) Immunization of young broiler chickens with low level of infections of *Eimeria tenella*, *E. acervulina* or *E. maxima*. *Avian Parasitology* **15**: 271-278.

Lukat, G.S., Rodgers, K.R., Jabro, M.N. and Goff, H.M. (1989) Magnetic resonance spectral characterization of the heme active site of *Coprinus cinereus* peroxidase. *Biochemistry* **28**(8): 3338-3345.

Magnusson, R.P., Gestautas, J., Taurog, A. and Rapoport, B. (1987) Molecular cloning of the structural gene for porcine thyroid peroxidase. *The Journal of Biological Chemistry* **262**(29): 13885-13888.

Malencik, D.A. and Anderson, S.R. (1996) Dityrosine formation in calmodulin: cross-linking and polymerization catalyzed by arthromyces peroxidase. *Biochemistry* **35**(14): 4375-4386.

Maréchal, E. and Cesbron-Delauw, M.F. (2001) The apicoplast: a new member of the plastid family. *Trends in Plant Science* **6**(5): 200-205.

Margoliash, E., Novogrodsky, A. and Schejter, A. (1960) Irreversible reaction of 3-amino-1:2:4-triazole and related inhibitors with the protein of catalase. *The Biochemical Journal* **74**: 339-348.

Marumo, K. and Waite, J.H. (1986) Optimization of hydroxylation of tyrosine and tyrosine-containing peptides by mushroom tyrosinase. *Biochimica et Biophysica Acta* **872**(1-2): 98-103.

Maurel, C., Reizer, J., Schroeder, J.I. and Chrispeels, M.J. (1993) The vacuolar membrane protein gamma-TIP creates water specific channels in Xenopus oocytes. *The EMBO Journal* **12**(6): 2241-2247.

McConville, M.J., Thomas-Oates, J.E., Ferguson, M.A. and Homans, S.W. (1990) Structure of the lipophosphoglycan from *Leishmania major*. *Journal of Biological Chemistry* **265**(32): 19611-19623.

McDougald, L.R. and Seibert, B.P. (1998) Residual activity of anticoccidial drugs in chickens after withdrawal of medicated feeds. *Veterinary Parasitology* **74**(2-4): 91-99.

McGuffin, L.J., Bryson, K. and Jones, D.T. (2000) The PSIPRED protein structure prediction server. *Bioinformatics* **16**(4): 404-405.

McKenzie, M.E., Conway, D.P., Logan, N.B., Wilkins, C.P. and Chappel, L.R. (1993) Anticoccidial efficacy of semduramycin. 1. Evaluation against field isolates by dose titration in battery tests. *Poultry Science* **72**(11): 2052-2057.

McLaren, D.J. (1969) Observations on the fine structural changes associated with schizogony and gametogony in *Eimeria tenella*. *Parasitology* **59**(3): 563-574.

McLeod, J.W. and Gordon, J. (1922) Production of hydrogen peroxide by bacteria. *Biochemical Journal* **16**(4): 499-506.

Melhorn, H. (Ed.). (1988) Parasitology in focus. Springer, Berlin Heidelberg, New York.

Meyers, P.R., Bourn, W.R., Steyn, L.M., Helden, P.D., Beyers, A.D. and Brown, G.D. (1998) Novel method for rapid measurement of growth of Mycobacteria in detergent-free media. *Journal of Clinical Microbiology* **36**(9): 2752-2754.

Michael, A. (2002) The practical use of a maternal vaccine against coccidiosis. *World Poultry* **18**: 2-3.

Michon, T., Chenu, M., Kellershon, N., Desmadril, M. and Gueguen, J. (1997) Horseradish peroxidase oxidation of tyrosine-containing peptides and their subsequent polymerization: a kinetic study. *Biochemistry* **36**(28): 8504-8513.

Monné, L. and Hönig, G. (1954) On the properties of the shells of coccidian oocysts. *Arkiv för Zoologi* **7**: 251-256.

Mouafo, A.N., Weck-Heimann, A., Dubremetz, J-F. Entzeroth, R. (2002) Monoclonal antibodies specific for the two types of wall-forming bodies of *Eimeria tenella* macrogametes (Coccidia, Apicomplexa). *Parasitology Research* **88**(3): 217-224.

Nagamune, K. and Sibley, L.D. (2006) Comparative genomic and phylogenetic analyses of calcium ATPase and calcium-regulated proteins in the Apicomplexa. *Molecular Biology and Evolution* **23**(8): 1613-1627.

Nakamura, M., Yamazaki, I. Nakagawa, H., Ohtaki, S. and Ui, N. (1984) Iodination and oxidation of thyroglobulin catalyzed by thyroid peroxidase. *The Journal of Biological Chemistry* **259**: 359-364.

Neumann, S., Matthey, U., Kaim, G. and Dimroth, P. (1998) Purification and properties of the F_1F_0 ATPase of *Ilyobacter tartaricus*, a sodium ion pump. *Journal of Bacteriology* **180**(13): 3312-3316.

Nishiyama, Y., Massey, V., Takeda, K., Kawasaki, S., Sato, J., Watanabe, T. and Niimura, Y. (2001) Hydrogen peroxide-forming NADH oxidase belonging to the peroxiredoxin oxidoreductase family: existence and physiological role in bacteria. *Journal of Bacteriology* **183**(8): 2431-2438.

Nyberg, P.A. Bauer, D.H. and Knapp, S.E. (1968) Carbon dioxide as the initial stimulus for excystation of *Eimeria tenella* oocysts. *Journal of Protozoology* **15**(1):144-148.

Nyberg, P.A. and Knapp, S.E. (1970) Effect of sodium hypochlorite on the oocyst wall of *Eimeria tenella* as shown by electron microscopy. *Proceedings of the Helminthological Society of Washington* **37**: 32-36.

Obata, K. (2000) Phylum Apicomplexa: gregarines, coccidian, and related organisms. In: Roberts, L.S. and Janory, J.J. (Eds.). *Functions of Parasitology*; pp.117-139, McGraw Hill, USA.

Obradovic, Z., Peng, K., Vucetic, S., Radivojac, P., Brown, C.J. and Dunker, A.K. (2003) Predicting intrinsic disorder from amino acid sequence. *Proteins*: *Structure, Function, and Genetics* **53**(S6): 566-572.

Obradovic, Z., Peng, K., Vucetic, S., Radivojac, P. and Dunker, A.K. (2005) Exploiting heterogeneous sequence properties improves prediction of protein disorder. *Proteins*: *Structure, Function, and Bioinformatics* **61**(S7): 176-182.

Odell, E.W. and Segal, A.W. (1988) The bactericidal effects of the respiratory burst and the myeloperoxidase system isolated in neutrophil cytoplasts. *Biochimica et Biophysica Acta* **971**(3): 266-274.

Oldfield, C. J., Ulrich, E.J., Cheng, Y., Dunker, A.K. and Markley, J.L. (2005) Addressing the intrinsic disorder bottleneck in structural proteomics. *Proteins: Structure, Function, and Bioinformatics* **59**(3): 444-453.

Ovington, K.S., Smith, N.C. and Joysey, H.S. (1990) Oxygen derived free radicals and the course of *Eimeria vermiformis* infection in inbred strains of mice. *Parasite Immunology* **12**(6): 623-631.

Page, A.P. and Winter, A.D. (2003) *Enzymes Involved in the Biogenesis of the Nematode Cuticle. Advances in Parasitology* **53**: 85-148.

Pavlovic-Djuranovic, S., Schultz, J.E. and Beitz, E. (2003) A single aquaporin gene encodes a water/glycerol/urea facilitator in *Toxoplasma gondii* with similarity to plant tonoplast intrinsic proteins. *FEBS Letters* **555**(3): 500-504.

Pittilo, R.M. and Ball, S.J. (1979) The fine structure of the developing macrogamte of *Eimeria maxima*. *Parasitology* **79**(2): 259-265.

Pittilo, R.M. and Ball, S.J. (1980) The ultrastructural development of the oocyst wall of *Eimeria maxima*. *Parasitology* **81**(1): 115-122.

Prilusky, J., Felder, C.E., Zeev-Ben-Mordehai, T., Rydberg, E.H., Man, O., Beckmann, J.S., Silman, I. and Sussman, J.L. (2005) FoldIndex©: a simple tool to predict whether a given protein sequence is intrinsically unfolded. *Bioinformatics* **21**(16): 3435-3438.

Raghava, G.P.S. (2002) APSSP2: a combination method for protein secondary structure prediction based on neural network and example based learning. CASP5. A-132.

Razmi, G.R. and Kalideri, G.A. (2000) Prevalence of subclinical coccidiosis in broiler-chickens farms in the municipality of Mashhad, Khorasan, Iran. *Preventive Veterinary Medicine* **44**(3-4): 247-253.

Roberts, F., Roberts, C.W., Johnson, J.J., Kyle, D.E., Krell, T., Coggins, J.R., Coombs, G.H., Milhous, W.K., Tzipori, S., Ferguson, D.J., Chakrabarti, D., and McLeod, R. (1998) Evidence for the shikimate pathway in apicomplexan parasites. *Nature* **393**(6687): 801-805.

Rose, M.E. and Long, P.L. (1980) Vaccination against coccidiosis in chickens. In: Taylor, A.E.R. and Muller, R. (Eds.). *Vaccination against parasites*, pp.57-74. Blackwell Scientific, Oxdord, UK.

Roos, D.S., Crawford, M.J., Donald, R.G.K., Kissinger, J.C., Klimczak, L.J. and Striepen, B. (1999) Origin, targeting, and function of the apicomplexan plastid. *Current Opinion in Microbiology* **2**(4): 426-432.

Ruzza, P., Donella-Deana, A., Calderan, A., Filippi, B., Cesaro, L., Pinna, L.A. and Borin, G. (1996) An exploration of the effects of constraints on the phosphorylation of synthetic protein tyrosine kinase peptide substrates. *Journal of Peptide Science* **2**(5): 325-338.

Ryley, J.F., Bentley, M., Manner, D.J. and Stark, J.R. (1969) Amylopectin, the storage polysaccharide of the coccidia *Eimeria brunetti* and *E. tenella*. *The Journal of Parasitology*. **55**(4): 839–845.

Ryley, J.F. (1973) Cytochemistry, physiology, and biochemistry. In: Hammond, D.H. and Long, P.L. (Eds.). *The Coccidia: Eimeria, Isospora, Toxoplasma, and related Genera*; pp.145-181. University Park Press, Baltimore, London.

Salisch, H. (1989) Recent developments in the chemotherapy of parasitic infections of poultry. *World's Poultry Science Journal* **45**: 115-124.

Sambrook, J. and Russell, D.W. (2001) Gel electrophoresis of DNA; Amplification of DNA by Polymerase Chain Reaction. *Molecular Cloning – A laboratory Manual*; pp.5.4-5.51; pp.8.18-8.34. Cold Spring Harbor Laboratory Press, Cold Spring Harbor, New York.

Sarkanen, S., Razal, R.A., Piccariello, T., Yamamoto, E, Lewis, N.G. (1991) Lignin peroxidase: towards a classification of its role *in vivo*. *The Journal of Biological Chemistry* **266**(6): 3636-3643.

Schares, G., Pantchev, N., Barutzki, D., Heydorn, A.O., Bauer, C. and Conraths, F.J. (2005) Oocysts of *Neospora caninum, Hmmondia heydorni, Toxoplasma gondii* and *Hammondia hammondi* in faeces collected from dogs in Germany. *International Journal for Parasitology* **35**(14): 1525-1537.

Schmatz, D.M. (1997) The mannitol cycle in *Eimeria*. *Parasitology* **114**: S81-S89.

Scholtyseck, E., Rommel, A. and Heller, G. (1969) Light and electron microscopic studies of the formation of the oocyst wall in *Eimeria* (*Eimeria perforans*, *E. stiedae* and *E. tenella*) *Zeitschrift für Parasitenkunde* **31**(4): 289-298.

Scholtyseck, E. (1973) Ultrastructure. In: Hammond, D.H. and Long, P.L. (Eds.). *The Coccidia: Eimeria, Isospora, Toxoplasma, and related Genera*; pp.81-144. University Park Press, Baltimore, and Butterworth's, London.

Seeber, F. (2003) Biosynthetic pathways of plastid-derived organelles as potential drug targets against apicomplexa. *Current Drug Targets - Immune, Endocrine & Metabolic Disorders* **3**(2): 99-109.

Shigeoka, S., Ishikawa, T., Tamoi, M., Miyagawa, Y., Takeda, T., Yabuta, Y. and Yoshimura, K. (2002) Regulation and function of ascorbate peroxidase isoenzymes. *Journal of Experimental Botany* **53**(372): 1305 - 1319.

Shinmen, Y., Asami, S., Amachi, T., Shimizu, S. and Yamada, H. (1986) Crystallization and characterization of an extracellular fungal peroxidase. *Agricultural and Biological Chemistry* **50**(1): 247-249.

Shirley, M.W. (1986) New methods for the identification of species and strains of *Eimeria*. In: McDougald, L.R., Long, P.L. and Joyner, L.P. (Eds) *Research in Avian Coccidiosis*, pp.13-35, Athens, Georgia: University of Georgia.

Shirley, M.W. (1995) *Eimeria* species and strains of chickens. In: Eckert, J., Braun, R., Shirley, M.W. and Coudert, P (Eds.). *Biotechnology - Guidelines on techniques in coccidiosis research*; pp.1-51, European Commission, Luxemburg.

Shirley, M.W. (1997) *Eimeria* spp. from the chicken: occurrence, identification and genetics. *Acta Veterinaria Hungarica* **45**(3): 331-347.

Shiryaev, S.A., Ratnikov, B.I., Chekanov, A.V., Sikora, S., Rozanov, D.V., Godzik, A., Wang, J., Smith, J.W., Huang, Z., Lindberg, I., Samuel, M. A., Diamond, M.S. and Strongin, A.Y. (2006) Cleavage targets and the D-arginine-based inhibitors of the West Nile virus NS3 processing proteinase. *Biochemical Journal* **393**(2): 503-511.

Silva, A., Kawazoe, U., Freitas, F.F.T., Gatti, M.S.V., Dolder, H., Schumacher, R.I., Juliano, M.A., Silva, M.J. and Leite, A. (2002) Avian anticoccidial activity of a novel membrane-interactive peptide selected from phage display libraries. *Molecular and Biochemical Parasitology* **120**(1): 53-60.

Smail, E.H., Briza, P., Panagos, A. and Berenfeld, L. (1995) *Candida albicans* cell walls contain the fluorescent cross-linking amino acid dityrosine. *Infection and Immunity* **63**(10): 4078-4083.

Smith, C.K. and Galloway, R.B. (1983) Influence of monensin on cation influx and glycolysis of *Eimeria tenella* sporozoites *in vitro*. *The Journal of Parasitology* **69**(4): 666-670.

Smith, N.C. and Bryant, C. (1989) Free radical generation during primary infections with *Nippostrongylus brasiliensis*. *Parasite Immunology* **11**(2): 147-160.

Smith, N.C., Wallach, M., Miller, C,M.D, Morgenstern, R,, Braun, R, and Eckert, J. (1994a) Maternal transmission of immunity to *Eimeria maxima*: enzyme-linked immunosorbent assay analysis of protective antibodies induced by infection. *Infection and Immunity* **62**(4): 1348-1357.

Smith, N.C., Wallach, M., Miller, C,M.D, Braun, R, and Eckert, J. (1994b) Maternal transmission of immunity to *Eimeria maxima*: western blot analysis of protective antibodies induced by infection. *Infection and Immunity* **62**(11): 4811-4817.

Smith, N.C. and Ovington, K.S. (1996) The effect of BCG, zymosan and Coxiella burnetti extract on *Eimeria* infections. *Immunology and Cell Biology* **74**(4): 346-348.

Snelling, W.J., Lin, Q., Moore, J.E., Millar, B.C., Tosini, F., Pozio, E., James S. G. Dooley, J.S.G. and Lowery, C.J. (2007) Proteomics analysis and protein expression during sporozoite excystation of *Cryptosporidium parvum* (Coccidia, Apicomplexa). *Molecular & Cellular Proteomics* **6**(2): 346-355.

Souza, J.M., Giasson, B.I., Chen, Q., Lee, V.M.-Y. and Ischiropoulos, H. (2000) Dityrosine cross-linking promotes formation of stable α-synuclein polymers. *The Journal of Biological Chemistry* **275**(24): 18344-18349.

Spano, F., Puri, C., Ranucci, L., Putignani, L. and Crisanti, A. (1997) Cloning of the entire COWP gene of *Cryptosporidium parvum* and untrastructural localization of the protein during sexual parasite development. *Parasitology* **114**(5): 427-437.

Stephan, B., Rommel, M., Daugschies, A. and Haberkorn, A. (1997) Studies of resistance to anticoccidials in *Eimeria* field isolates and pure *Eimeria* strains. *Veterinary Parasitology* **69**(1-2): 19-29.

Stokkermans, T.J.W., Schwartzman, J.D., Keenan, K., Morrissette, N.S., Tilney, L.G. and Roos, D.S. (1996) Inhibition of *Toxoplasma gondii* replication by dinitroaniline herbicides. *Experimental Parasitology* **84**(3): 355-370.

Stotish, R.L., Wang, C.C. and Meyenhofer, M. (1978) Structure and composition of the oocyst wall of *Eimeria tenella*. *The Journal of Parasitology* **64**(6): 1074-1081.

Studier, F.W. and Moffatt, B.A. (1986) Use of bacteriophage T7 RNA polymerase to direct selective high-level expression of cloned genes. *Journal of Molecular Biology* **189**(1): 113-130.

Studier, F.W., Rosenberg, A.H., Dunn, J.J. and Dubendorff, J.W. (1990) Use of T7 RNA polymerase to direct expression of cloned genes. *Methods in Enzymology* **185**: 60-89.

Templeton, T.J., Lancto, C.A., Vigdorovich, V., Liu, C., London, N.R., Hadsall, K.Z. and Abrahamsen, M.S. (2004) The *Cryptosporidium* oocyst wall protein is a member of a multigene family and has a homolog in *Toxoplasma. Infection and Immunity* **72**(2): 980-987.

Thacker, C., Peters, K., Srayko, M. and Rose, A.M. (1995) The bli-4 locus of *Caenorhabditis elegans* encodes structurally distinct kex2/subtilisin-like endoproteases essential for early development and adult morphology. *Genes & Development* **9**(8): 956-971.

Thacker, C., Srayko, M. and Rose, A.M. (2000a) Mutational analysis of bli-4/kpc-4 reveals critical residues required for proprotein convertase function in *C. elegans*. *Gene* **252**(1-2): 15-25.

Thacker, C. and Rose, A.M. (2000b) A look at the *Caenorhabditis elegans* Kex2/Subtilisin-like proprotein convertase family. *BioEssays* **22**(6): 545-553.

Thacker, C., Sheps, J.A. and Rose, A.M. (2006) *Caenorhabditis elegans* dpy-5 is a cuticle procollagen processed by a proprotein convertase. *Cellular and Molecular Life Science* **63**(10): 1193-1204.

Thomson, R., Hodgman, T. C., Yang, Z. R. and Doyle, A.K. (2003) Characterizing proteolytic cleavage site activity using bio-basis function neural networks. *Bioinformatics* **19**(14): 1741-1747.

Tompa, P (2003) The functional benefits of protein disorder. *Journal of Molecular Structure (Theochem)* **666-667**: 361-371.

Tompa, P. (2005) The interplay between structure and function in intrinsically unstructured proteins. *FEBS Letters* **579**(15): 3346-3354.

Uesugi, M., Hayashi, T. and Jasin, H.E. (1998) Covalent cross-linking of immune complexes by oxygen radicals and nitrite. *The Journal of Immunology* **161**(3): 1422-1427.

Uversky, V.N., Gillespie, J.R., Millett, I.S., Khodyakova, A.V., Vasiliev, A.M., Chernovskaya, T.V., Vasilenko, R.N., Kozlovskaya, G.D., Dolgikh, D.A., Fink, A.L., Doniach, S. and Abramov, V.M. (1999) Natively unfolded human prothymosin α adopts partially folded collapsed conformation at acidic pH. *Biochemistry* **38**(45): 15009-15016.

Uversky, V.N., Gillespie, J.R. and Fink, A.L. (2000) Why are "natively unfolded proteins unstructured under physiological conditions"? *Proteins: Structure, Function, and Bioinformatics* **41**(3): 415-427.

Uversky, V.N. (2003) A protein-chameleon: conformational plasticity of α-synuclein, a disordered protein involved in neurodegenerative disorders. *Journal of Biomolecular Structure and Dynamics* **21**(2): 211-234.

Vermeulen, A.N. (1998) Progress in recombinant vaccine development against coccidiosis. A review and prospects into the next millennium. *International Journal for Parasitology* **28**(7): 1121-1130.

Vermeulen, A.N., Schaap, D.C. and Schetters, T.P.M. (2001) Control of coccidiosis in chickens by vaccination. *Veterinary Parasitology* **100**(1-2): 13-20.

Vucetic, S., Obradovic, Z., Vacic, V., Radivojac, P., Peng, K., Iakoucheva, L.M., Cortese, M.S., Lawson, J.D., Brown, C.J., Sikes, J.G., Newton, C.D. and Dunker, A.K. (2005) DisProt: a database of protein disorder. *Bioinformatics* **21**(1): 137-140.

Waite, J.H. (1990) The phylogeny and chemical diversity of quinine-tanned glue and varnishes. *Comparative Biochemistry and Physiology*. B, *Comparative Biochemistry* **97**(1): 19-29.

Wallach, M., Pillemer, G., Yarus, S., Halabi, A., Pugatsch, T., and Mencher, D. (1990) Passive immunization of chickens against *Eimeria maxima* infection with a monoclonal antibody developed against a gametocyte antigen. *Infection and Immunity* **58**(2): 557-562.

Wallach, M., Smith, N.C., Miller, C,M.D, Eckert, J. and Rose, M.E. (1994) *Eimeria maxima*: ELISA and western blot analyses of protective sera. *Parasite Immunology* **16**(7): 377-383.

Wallach, M., Smith, N.C., Miller, C.M.D, Eckert, J. and Braun, R. (1995) *Eimeria maxima* gametocyte antigens: potential use in a subunit maternal vaccine against coccidiosis in chickens. *Vaccine* **13**(4): 347-354.

Wallach, M. (1997) The importance of transmission-blocking immunity in the control of infections by apicomplexan parasites. *International Journal for Parasitology* **27**(10): 1159-1167.

Wallach, M. (2002) The development of CoxAbic® a novel vaccine against coccidiosis. *World Poultry* **18**: 24-26.

Waller, R.F., Keeling, P.J., Donald, R.G.K., Striepen, B., Handman, E., Lang-Unnasch, N., Cowman, A.C., Besra, G.S., Roos, D.S. and McFadden , G.I. (1998) Nuclear-encoded proteins target to the plastid in *Toxoplasma gondii* and *Plasmodium falciparum*. *Proceeding of the National Academy of Sciences of the United States of America* **95**(21): 12352-12357.

Wang, C.C. (1975) Studies of mitochondria from *Eimeria tenella* and inhibition of the electron transport by quinolone coccidiostats. *Biochimica et Biophysica Acta* **396**(2): 210-219.

Wang, C.C., Stotish, R.L. and Poe, M. (1975) Dihydrofolate reductase from *Eimeria tenella*: rationalization of chemotherapeutic efficacy of pyrimethamine. *The Journal of Protozoology* **22**(4): 564-568.

Ward, J.J., Sodhi, J.S., McGuffin, L.J., Buxton, B.F. and Jones, D.T. (2004) Prediction and functional analysis of native disorder in proteins from the three kingdoms of life. *Journal of Molecular Biology* **337**(3): 635-645.

Wariishi, H., Valli, K. and Gold, M.H. (1991) *In vitro* depolymerization of lignin by manganese peroxidase of *Phanerochaete chrysosporium*. *Biochemical and Biophysical Research Communications* **176**(1): 269-275.

Weinreb, P. H., Zhen, W., Poon, A. W., Conway, K.A. and Lansbury, P.T. (1996) NACP, a protein implicated in Alzheimer's disease and learning, is natively unfolded. *Biochemistry* **35**(43): 13709-13715.

Welinder, K.G. (1991) Bacterial catalase-peroxidases are gene duplicated members of the plant peroxidase superfamily. *Biochimica et Biophysica Acta* **1080**(3): 215-220.

Welinder, K.G. (1992) Superfamily of plant, fungal and bacterial peroxidases. *Current Opinion in Structural Biology* **2**: 388-393.

Wheater, D.M., Hirsch, A. and Mattick, A.T.R. (1952) Possible identity of lactobacillin with hydrogen peroxide produced by lactobacilli. *Nature* **170**(4328)**:** 623–624.

Williams, R.B. (1992) The development, efficacy and epidemiological aspects of Paracox, a new coccidiosis vaccine for chickens. Harefield: Pitman-Moore Europe.

Williams, R.B. (1994) Safety for the attenuated anticoccidial vaccine "Paracox" in broiler chickens isolated from extraneous coccidial infection. *Veterinary Research Communications* **18**(3) 189-198.

Williams, R.B., Bushell, A.C. Répérant, J.M. Doy, T.G. Morgan, J.H., Shirley, M.W., Yvoré, P., Carr, M.M. and Fremont, Y. (1996) A survey of *Eimeria* species in commercially-reared chickens in France during 1994. *Avian Pathology* **25**(1): 113-130.

Williams, R.B. (1998) Epidemiological aspects of the live anticoccidial vaccines for chickens. *International Journal of Parasitology* **28**(7): 1089-1098.

Williams, R.B. (1999) A compartmentalized model for the estimation of the cost of coccidiosis to the world's chicken production industry. *International Journal for Parasitology* **29**(8): 1209-1229.

Wilson, R.J.M. (2002) Progress with parasite plastids. *Journal of Molecular Biology* **319**(2): 257-274.

Witcombe, D.M., Belli, S.I., Wallach, M.G. and Smith, N.C. (2003) Molecular characterisation of EmTFP250: a novel member of the TRAP protein family in *Eimeria maxima*. *International Journal for Parasitology* **33**(7): 691-702.

Wright, P.E. and Dyson, H.J. (1999) Intrinsically unstructured proteins: re-assessing the protein structure-function paradigm. *Journal of Molecular Biology* **293**(2): 321-331.

Wüthrich, K. (1990) Protein structure determination in solution by NMR spectroscopy. *The Journal of Biological Chemistry* **265**(36): 22059-22062.

Xu, R., Huang, X., Hopkins, T.L. and Kramer, K.J. (1997) Catecholamine and histidyl protein cross-linked structures in sclerotized insect cuticle. *Insect Biochemistry and Molecular Biology* **27**(2): 101-108.

Yang, Z.R., Thomson, R., McNeil, P. and Esnouf, R.M. (2005) RONN: the bio-basis function neural network technique applied to the detection of natively disordered regions in proteins. *Bioinformatics* **21**(16): 3369-3376.

Yoshida, Y., Adachi, E., Fukiya, K., Iwai, K. and Tanaka, K. (2005) Glycoprotein-specific ubiquitin ligases recognize N-glycans in unfolded substrates. *EMBO Reports* **6**(3): 239-244.

Appendices

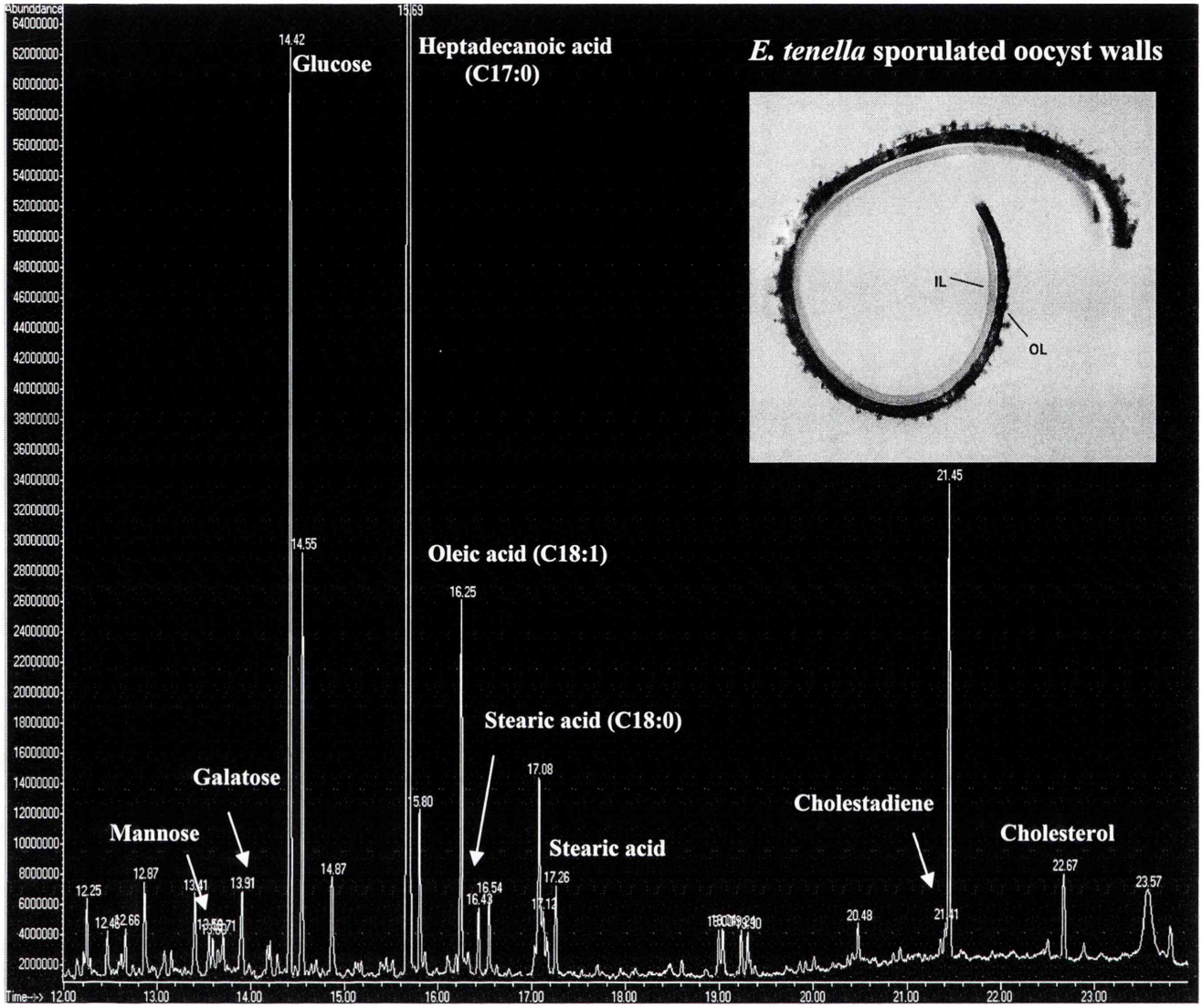

Metabolites	Mannose	Galactose	Glucose	**C17:0**	C18:1	C18:0	Cholestadiene	Cholesterol
RT (mins)	13.56	13.91	14.42	**15.69**	16.25	16.43 17.26	21.41	22.67

Figure A1 GC and MS profile of compositional analysis of *E. tenella* sporulated oocyst walls. The oocyst walls from *E. tenella* bleached sporulated oocysts were hydrolyzed in 0.5M HCl in methanol, followed by evacuation and incubation at 80°C over night as described in Chapter 2, Section 2.2.5. Carbohydrate and lipid contents of the oocyst walls were analysed by GC and MS with heptadecanoic acid served as a control for this analysis. RT= retention time.

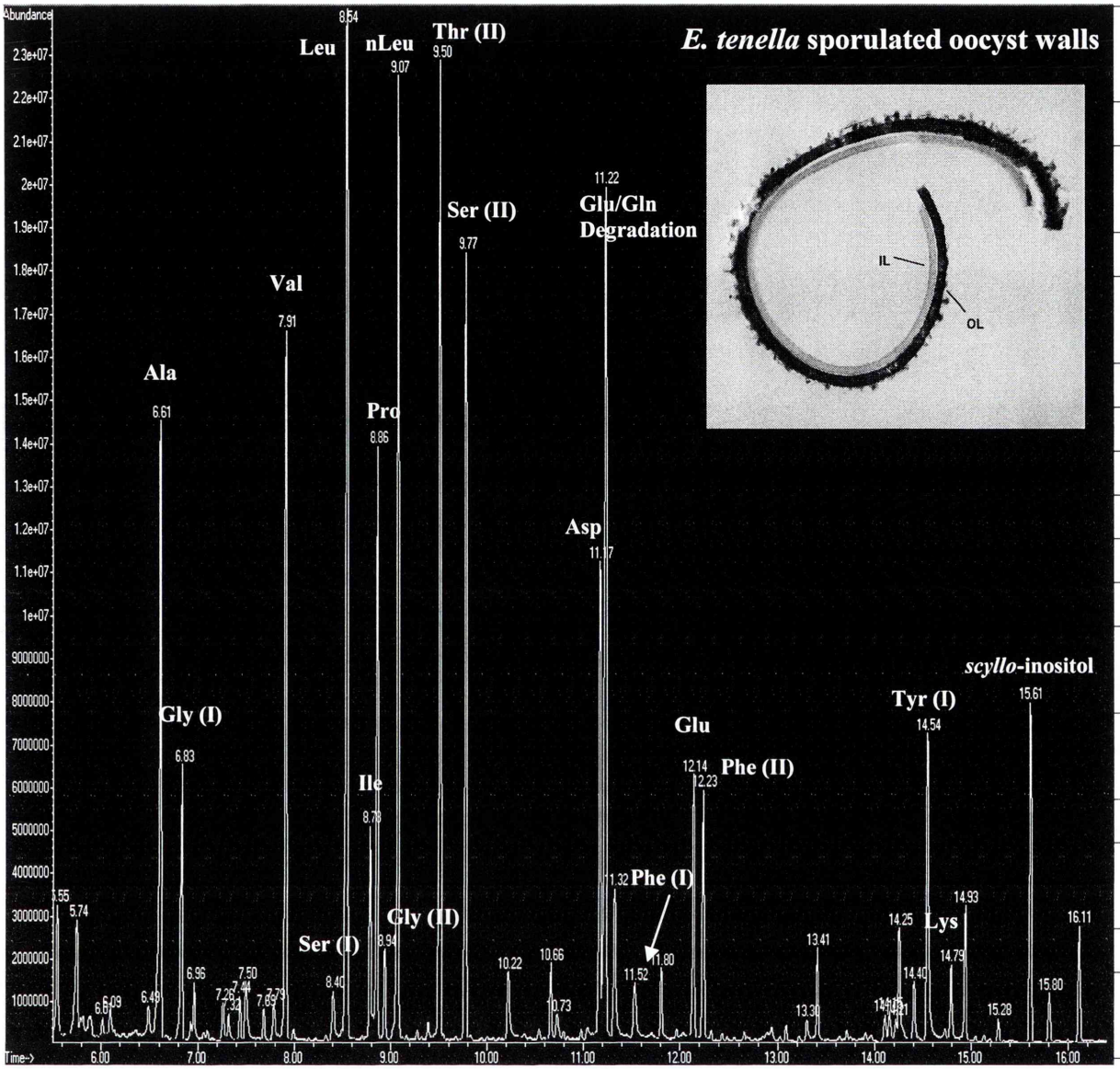

Amino acids	RT (mins)
Ala	6.61
Gly (I)	6.83
Gly (II)	8.94
Val	7.91
Ser (I)	8.4
Ser (II)	9.77
Leu	8.54
Ile	8.78
Pro	8.86
nLeu	**9.07**
Thr	9.50
Asp	11.17
Glu/ Gln	11.22
Phe (I)	11.52
Phe (II)	12.23
Glu	12.14
Tyr (I)	14.54
Tyr (II)	14.93
Lys	14.79
Scyllo-inositol	**15.61**

Figure A2 GC and MS profile of amino acid composition of oocyst wall proteins from *E. tenella* sporulated oocyst walls. The oocyst walls from *E. tenella* bleached sporulated oocysts were hydrolyzed in 6N HCl (acid hydrolysis), followed by evacuation and incubation at 110°C over night as described in Chapter 2, Section 2.2.5. The amino composition of the oocyst walls was analysed by GC and MS with norleucine (nleu) and *scyllo*-inositol served as internal controls for this analysis. RT= retention time.

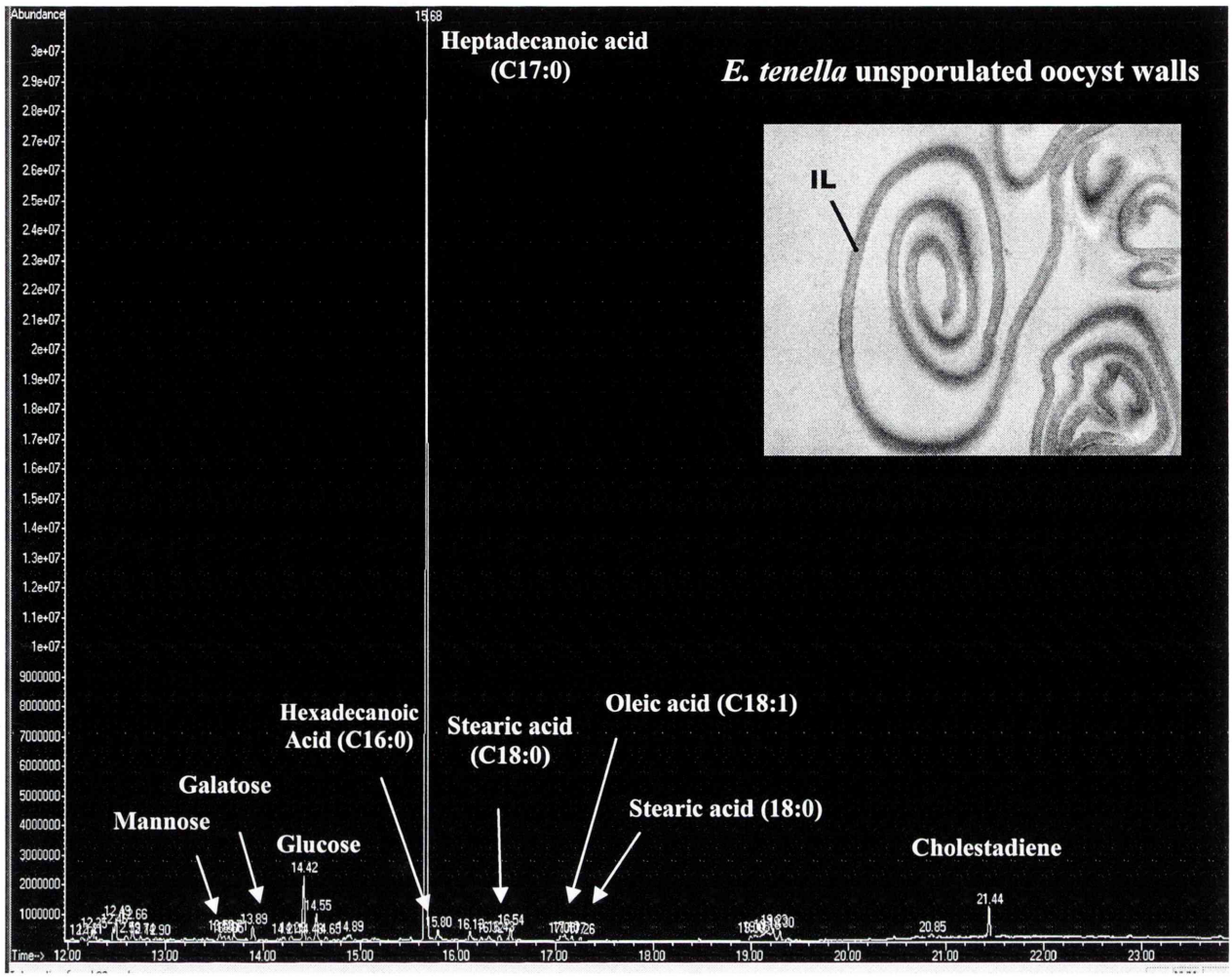

Metabolites	Mannose	Galactose	Glucose	**C17:0**	C16:0	C18:0	C18:1	Cholestadiene	Cholesterol
RT (mins)	13.56	13.89	14.42	**15.68**	15.80	16.43 17.26	17.10	21.44	22.67

Figure A3 GC and MS profile of compositional analysis of *E. tenella* unsporulated oocyst walls. The oocyst walls from *E. tenella* bleached unsporulated oocysts were hydrolyzed in 0.5M HCl in methanol, followed by evacuation and incubation at 80°C over night as described in Chapter 2, Section 2.2.5. Carbohydrate and lipid contents of the oocyst walls were analysed by GC and MS with heptadecanoic acid served as a control for this analysis. RT= retention time.

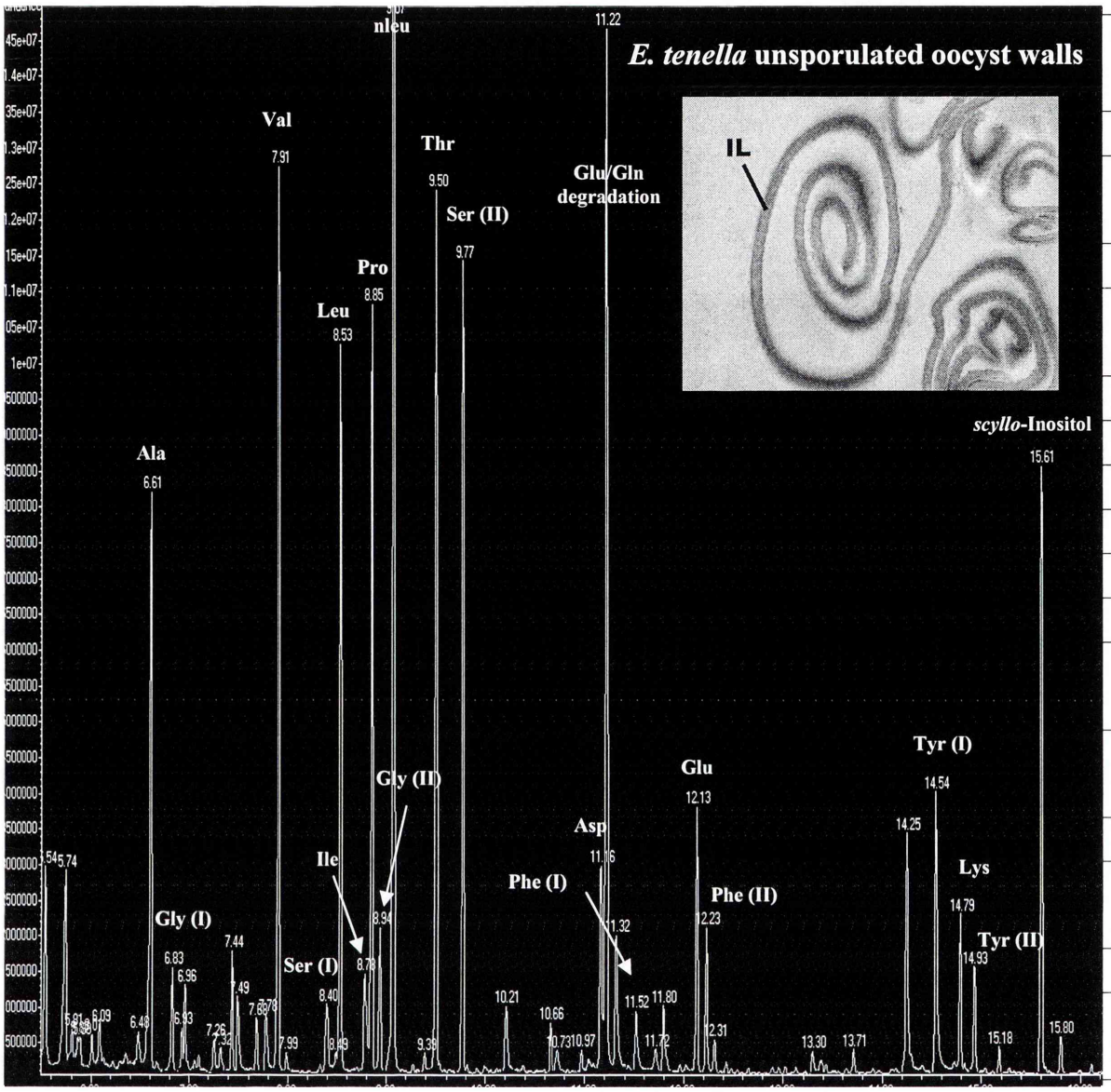

Amino acids	RT (mins)
Ala	6.61
Gly (I)	6.83
Gly (II)	8.94
Val	7.91
Ser (I)	8.40
Ser (II)	9.77
Leu	8.53
Ile	8.78
Pro	8.85
nleu	**9.07**
Thr	9.50
Asp	11.16
Glu/ Gln	11.22
Phe (I)	11.52
Phe (II)	12.23
Glu	12.13
Tyr (I)	14.54
Tyr (II)	14.93
Lys	14.79
***Scyllo*-inositol**	**15.61**

Figure A4 GC and MS profile of amino acid composition of oocyst wall proteins from *E. tenella* unsporulated oocyst walls. The oocyst walls from *E. tenella* bleached unsporulated oocysts were hydrolyzed in 6N HCl (acid hydrolysis), followed by evacuation and incubation at 110°C over night as described in Chapter 2, Section 2.2.5. The amino composition of the oocyst walls was analysed by GC and MS with norleucine (nleu) and *scyllo*-inositol served as internal controls for this analysis. RT= retention time.

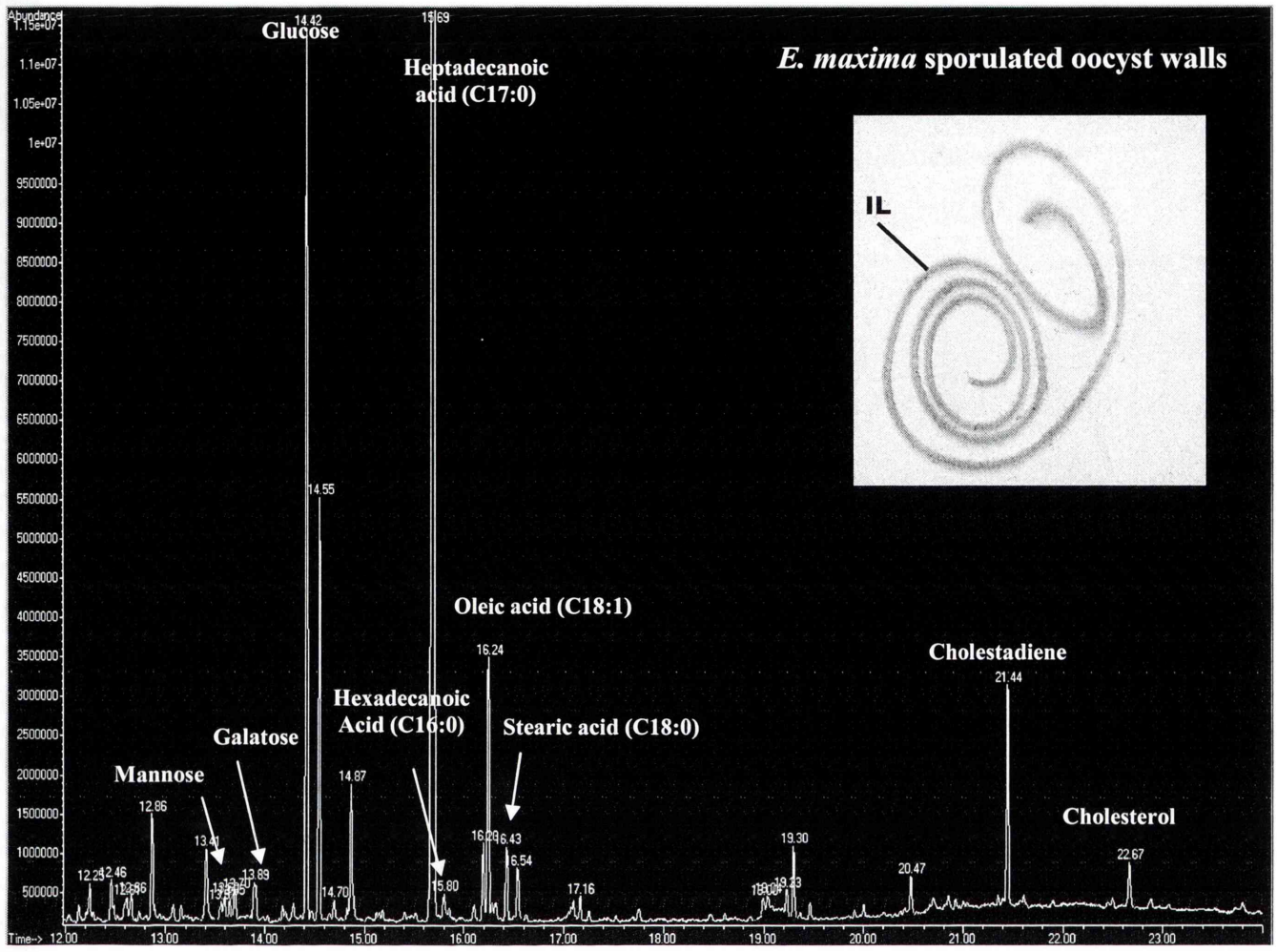

Metabolites	Mannose	Galactose	Glucose	**C17:0**	C16:0	C18:1	C18:0	Cholestadiene	Cholesterol
RT (mins)	13.56	13.89	14.42	**15.69**	15.80	16.24	16.43	21.44	22.67

Figure A5 GC and MS profile of compositional analysis of *E. maxima* sporulated oocyst walls. The oocyst walls from *E. maxima* bleached sporulated oocysts were hydrolyzed in 0.5M HCl in methanol, followed by evacuation and incubation at 80°C over night as described in Chapter 2, Section 2.2.5. Carbohydrate and lipid contents of the oocyst walls were analysed by GC and MS with heptadecanoic acid served as a control for this analysis. RT= retention time.

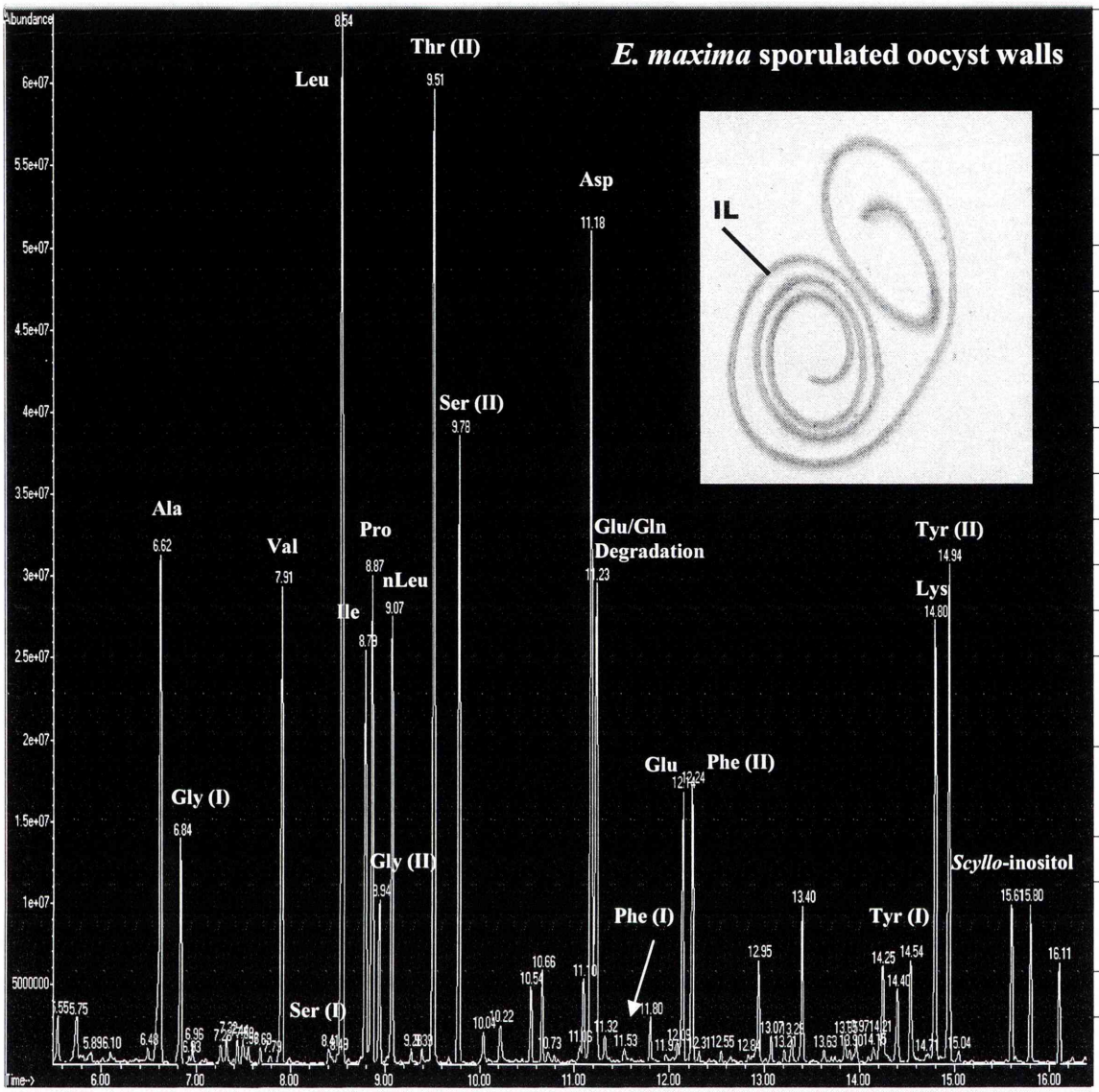

Amino acids	RT (mins)
Ala	6.62
Gly (I)	6.84
Gly (II)	8.94
Val	7.91
Ser (I)	8.41
Ser (II)	9.78
Leu	8.54
Ile	8.78
Pro	8.87
nleu	**9.07**
Thr	9.51
Asp	11.18
Glu/ Gln	11.23
Phe (I)	11.53
Phe (II)	12.24
Glu	12.14
Tyr (I)	14.54
Tyr (II)	14.94
Lys	14.80
***Scyllo*-inositol**	**15.61**

Figure A6 GC and MS profile of amino acid composition of oocyst wall proteins from *E. maxima* sporulated oocysts. The oocyst walls from *E. maxima* bleached sporulated oocysts were hydrolyzed in 6N HCl (acid hydrolysis), followed by evacuation and incubation at 110°C over night as described in Chapter 2, Section 2.2.5. The amino composition of the oocyst walls was analysed by GC and MS with norleucine (nleu) and *scyllo*-inositol served as internal controls for this analysis. RT= retention time.

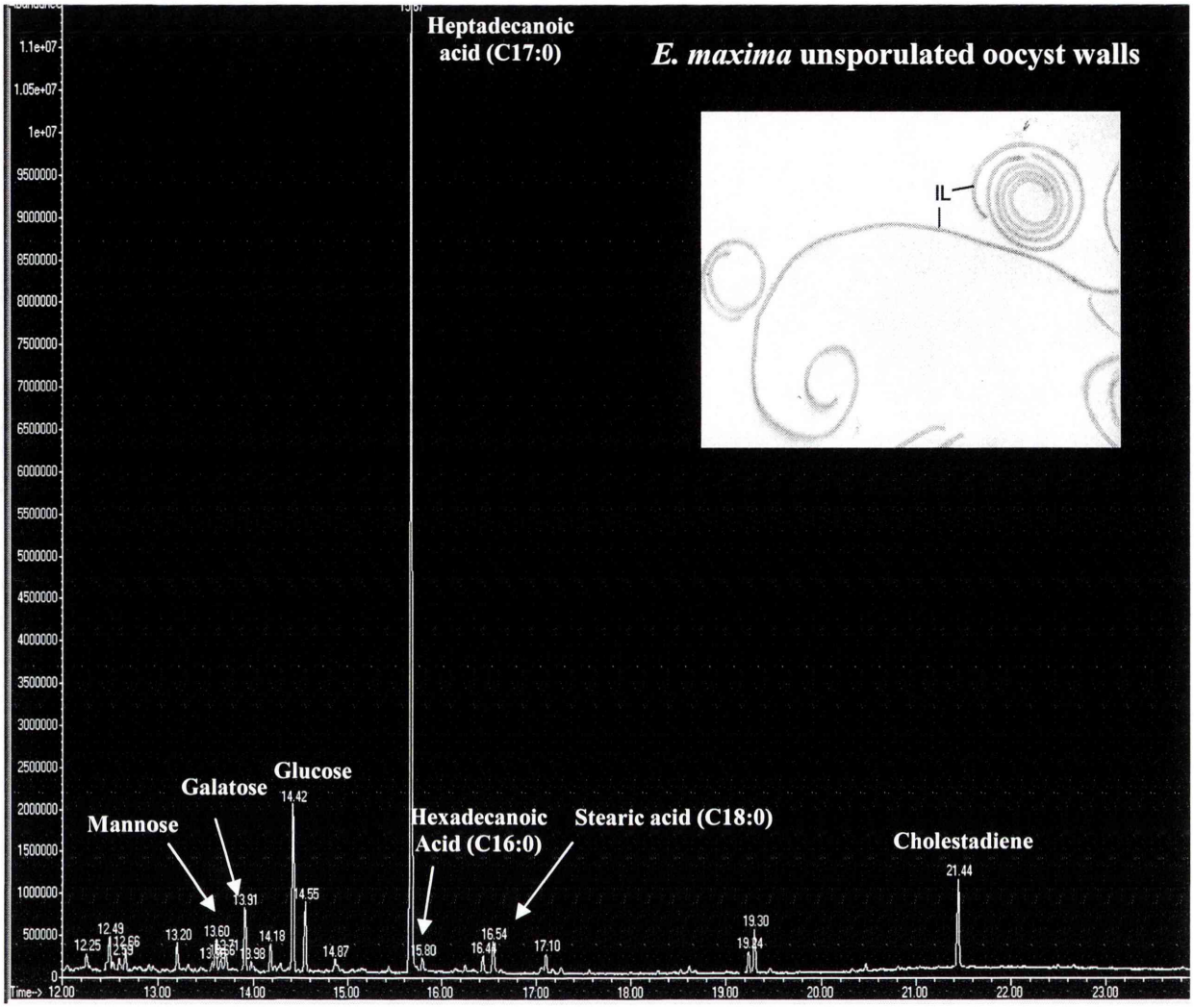

Metabolites	Mannose	Galactose	Glucose	**C17:0**	C16:0	C18:1	C18:0	Cholestadiene	Cholesterol
RT (mins)	13.56	13.91	14.42	**15.69**	15.80	16.24	16.43	21.44	22.67

Figure A7 GC and MS profile of compositional analysis of *E. maxima* unsporulated oocyst walls. The oocyst walls from *E. maxima* bleached unsporulated oocysts were hydrolyzed in 0.5M HCl in methanol, followed by evacuation and incubation at 80°C over night as described in Chapter 2, Section 2.2.5. Carbohydrate and lipid contents of the oocyst walls were analysed by GC and MS with heptadecanoic acid served as a control for this analysis. RT= retention time.

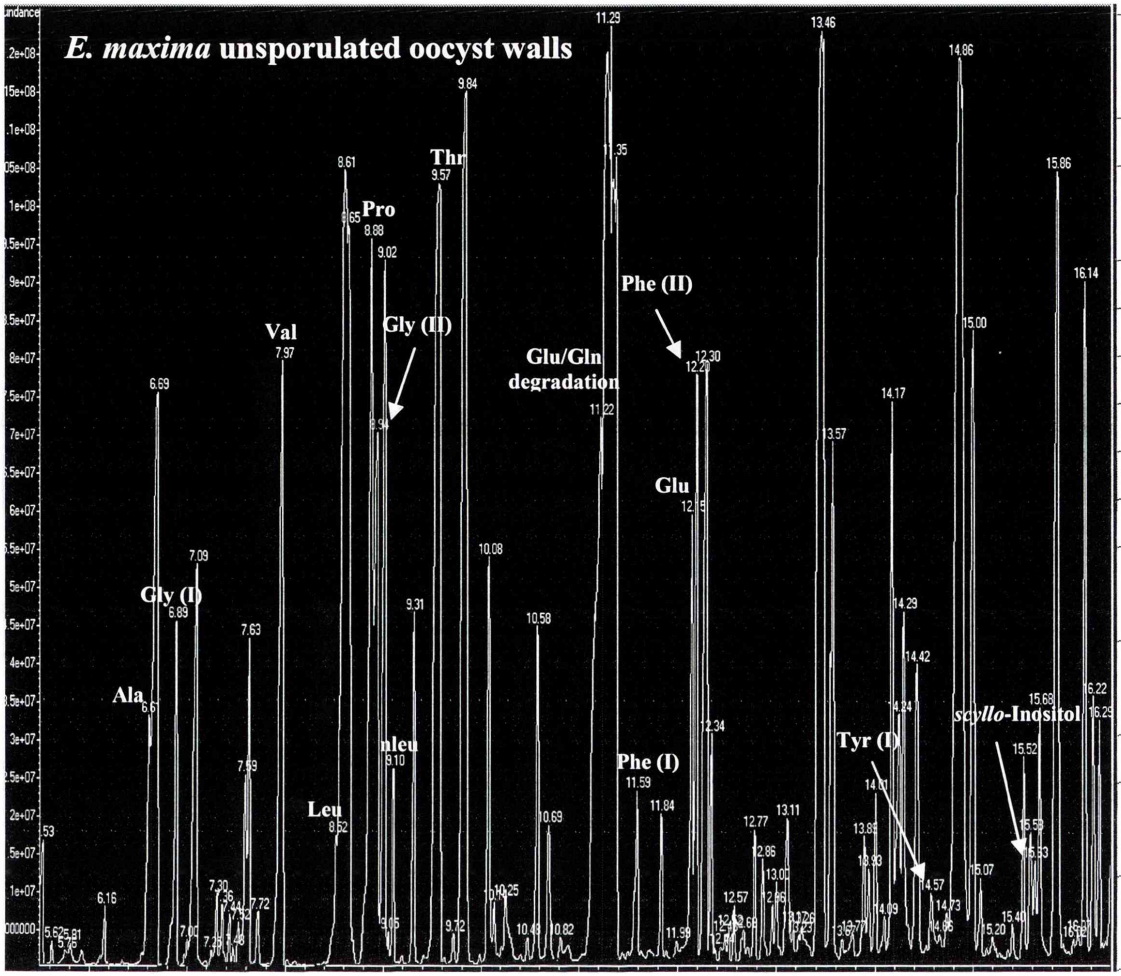

Amino acids	RT (mins)
Ala	6.61
Gly (I)	6.89
Gly (II)	8.94
Val	7.97
Leu	8.52
Ile	8.78
Pro	8.88
nleu	**9.10**
Thr	9.57
Glu/ Gln	11.22
Phe (I)	11.59
Phe (II)	12.20
Glu	12.15
Tyr (I)	14.54
Tyr (II)	14.94
***Scyllo*-inositol**	**15.63**

Figure A8 GC and MS profile of amino acid composition of oocyst wall proteins from *E. maxima* unsporulated oocysts. The oocyst walls from *E. maxima* bleached unsporulated oocysts were hydrolyzed in 6N HCl (acid hydrolysis), followed by evacuation and incubation at 110°C over night as described in Chapter 2, Section 2.2.5. The amino composition of the oocyst walls was analysed by GC and MS with norleucine (nleu) and *scyllo*-inositol served as internal controls for this analysis. RT= retention time.

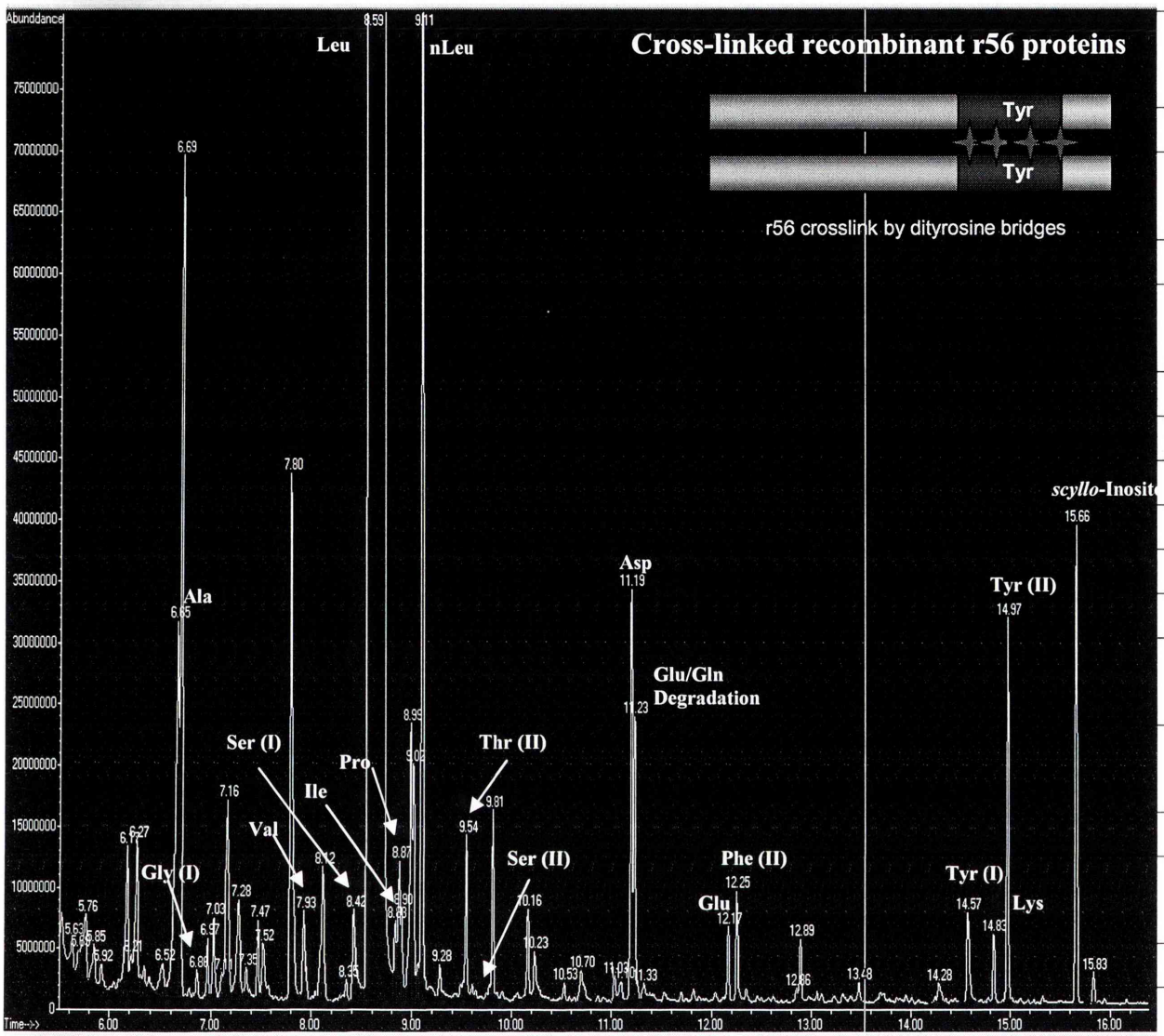

Amino acids	RT (mins)
Ala	6.61
Gly (I)	6.83
Gly (II)	8.94
Val	7.93
Ser (I)	8.42
Ser (II)	9.77
Leu	**8.59**
Ile	8.78
Pro	8.87
nleu	9.07
Thr	9.54
Asp	11.19
Glu/ Gln	11.23
Phe (I)	11.52
Phe (II)	12.25
Glu	12.17
Tyr (I)	14.57
Tyr (II)	14.97
Lys	14.83
***Scyllo*-inositol**	**15.66**

Figure A9 GC and MS profile of amino acid composition of crosslinked recombinant r56 proteins. The crosslinked r56 proteins were prepared as described in Chapter 2, Section 2.2.18 and hydrolyzed in 6N HCl (acid hydrolysis), followed by evacuation and incubation at 110°C O/N as described in chapter 2, section 2.2.5. The amino composition of the crosslinked r56 proteins was analysed by GC and MS with norleucine (nleu) and *scyllo*-inositol served as internal controls for this analysis. RT= retention time.